Development and Calibration of the Cosmogenic ^{36}Cl Surface Exposure Dating Method and Its Application to the Chronology of Late Quaternary Glaciations

by

Marek G. Zreda

Dissertation

submitted in partial fulfillment of the requirements

for the degree of

Doctor of Philosophy

in Hydrology

New Mexico Institute of Mining and Technology

1994

This dissertation is accepted on behalf of the faculty of the Institute by the following committee

Adviser

25 April 1994

Date

Acknowledgments

The following individuals and organizations contributed to the presented research in a variety of ways. Many special thanks are due to my family, Grazyna and Magda, for the continuous support over the years. Fred Phillips, Ronald Dorn, John Wilson, Robert Bowman and John Hawley supervised the study. Their help was important in setting the directions and their critical comments improved the quality of the dissertation. Field work was both productive and enjoyable in the company of Ronald Dorn, Debbie Elliott-Fisk, Terry Swanson, Fred Phillips, Andrew Bach, Oliver Chadwick, Robert Hall, Stewart Smith, George Smith, Andrew Campbell, Cynthia Kruger, Randy Roberts, John England and Rod Smith. The laboratory analyses of ^{36}Cl were possible with the help of David Elmore, Peter Kubik, Pankaj Sharma and their institutions, University of Rochester and Purdue University. Lynn Brandvold and the New Mexico Bureau of Mines and Mineral Resources helped with the sample preparation and analyses of major and trace elements. The financial support was provided by the National Science Foundation; the grant numbers are acknowledged at chapter ends.

Abstract

The development of the cosmogenic ^{36}Cl surface exposure dating method and its applications in Quaternary geochronology form this dissertation. Using 31 independently dated samples, I calculated the production rates of ^{36}Cl from its three main target elements. The sea-level and high-latitude effective production rates due to spallation of ^{39}K and ^{40}Ca are 7520 and 2900 atoms ^{36}Cl per year per mole K and Ca, respectively, and the effective thermal neutron production rate is 313,500 neutrons per kg of rock per yr. The average absolute deviation associated with these production rates is $\sim 9\%$. The precision and accuracy of the method, established by the comparison of the ^{36}Cl method with other dating techniques, are adequate for most geochronological applications. The reported production parameters are valid for geomorphically stable landforms; erosion and other postdepositional surficial processes may affect the production rates and require quantification.

The second part of the dissertation focuses on applications of the cosmogenic ^{36}Cl method to dating late Quaternary glacial, glaciofluvial and pluvial deposits from the western United States. Five glaciated valleys in the Sierra Nevada, White Mountains and Wind River Range contain deposits of several glaciations. Because of the obliterative nature of glacial deposition processes, local glacial chronologies are always fragmentary and thus inadequate for paleoclimatic interpretations. It was therefore necessary to develop a synthesized, regional chronology, based on the five local chronologies. This chronology suggests generally synchronous glaciations with major advances at 150, 90-

110, 60-70, and 14-20 ky and minor ones, found at only one location each, at 45 and 26 ky. With these data, two important problems concerning the Wisconsin glaciations are addressed: one- or two-phase glacier development and extent of early vs. late Wisconsin glaciation. First, the glacial development during the Wisconsin proceeded in two phases. The substantial ice buildup at the beginning of the cycle (90-110 and perhaps 60-70 ky) was followed by a long period of warmer, but occasionally glacial conditions (e.g., 45 ky), and finally by the second expansion of glaciers at the end of the cycle (14-20 ky). Second, the extent of early Wisconsin glaciers (90-110 ky) was larger than that of the so called late Wisconsin maximum ($\sim$20 ky). These results support a rapid transition from the interglacial to full glacial state followed by a long relaxation period with progressively less severe environmental conditions. These glacial ages are correlative with the ^{36}Cl dated glaciofluvial terraces from the Wind River Range, pluvial lake shorelines from Panamint and Death Valleys, and the global ^{18}O record.

Table of contents

Acknowledgments i

Abstract ii

Table of contents iv

List of tables xii

List of figures xiv

1. Introduction 1

Problems with the chronology of the terrestrial glacial record 2

Organization 6

References 7

2. Surface exposure dating by cosmogenic chlorine-36 accumulation 10

Abstract 10

Introduction 11

Spatial distribution of cosmogenic chlorine-36 production 13

Accumulation of *in situ* chlorine-36 in surficial materials 17

Factors affecting cosmogenic ^{36}Cl buildup 23

Erosion 23

Temporary and/or partial cover 25

Chemical weathering 26

Change of position 27

Change of geometry 28

Change of the incident cosmic ray intensity 29

References 29

3. Cosmogenic chlorine-36 production rates in terrestrial rocks 34

Abstract 34

Introduction 35

Major production reactions for ^{36}Cl in minerals at the surface of the earth 36

Accumulation of in situ produced ^{36}Cl in geological materials 38

Methods 40

Sample collection 40

Chemical analyses 44

Sample preparation and isotopic analysis of ^{36}Cl 45

Results and discussion 47

Production rates 47

Spatial variability of the cosmogenic nuclide production rates . . . 56

Test of the production parameters 64

Miscellaneous considerations 65

Summary 68

References 70

Appendix - description of sampling sites 78

4. Cosmogenic chlorine-36 production rates in terrestrial rocks: An extended calibration 80

Abstract 80

Introduction 80

Samples 82

Results and discussion 85

Summary 91

References 92

5. Cosmogenic ^{36}Cl accumulation in unstable landforms: II. Monte Carlo simulations and experimental observations on eroding moraines 95

Abstract 95

Introduction 97

Statistics of cosmogenic ^{36}Cl data distributions 99

Gradual exposure model - theoretical development 108

Gradual exposure model - comparison with data 121

Sample collection and preparation 122

Analytical results and comparison with model calculations 126

Summary and conclusions 131

References 133

Appendix A 137

Appendix B 139

6. Cosmogenic ^{36}Cl dating of a young basaltic eruption complex, Lathrop Wells, Nevada 140

Abstract 140

Introduction 141

Eruptive deposits of the Lathrop Wells volcanic area 142

Surface exposure dating by cosmogenic ^{36}Cl accumulation 145

Experimental methods 147

Sample collection 147

Sample preparation and analyses 148

Determination of ^{36}Cl ages 149

References cited 157

7. Age and geomorphic history of Meteor Crater, Arizona, from cosmogenic ^{36}Cl and rock varnish ^{14}C 160

Abstract 160

References 170

8. Glacial chronology of the eastern White Mountains, California-Nevada by the cosmogenic ^{36}Cl method 174

Introduction 175

Cosmogenic ^{36}Cl dating of moraines 178

Samples 182

Results and discussion 183

Glacial deposits at Chiatovitch Creek 183

Chiatovitch Cirque (Qcc) 183

Late Middle Creek (Qmc2) 184

Early Middle Creek (Qmc1) 188

Late Perry Aiken (Qpa2) 188

Early Perry Aiken (Qpa1) 189

Indian (Qi) 190

Dyer (Qd) 191

Other glacial deposits in the White Mountains 192

Conclusions 194

References 198

9. Cosmogenic ^{36}Cl chronology for glacial deposits in the eastern Sierra Nevada, California 201

Abstract 201

Introduction 202

Stratigraphy of glacial sequences 203

Glacial chronology 205

Chlorine-36 dating results and discussion 207

Bloody Canyon 209

Tioga (QTi) 211

Tenaya (QTe) 215

Tahoe (QTay and QTao) 217

Mono Basin (QMB) 217

Little McGee Creek 218

Neoglacial (NG) 219

Hilgard (H) 225

Early Hilgard (EH) 225

Late Tioga (LTi) 227

Tioga (Ti) 229

Early Tioga (ETi) 229

Tahoe (Ta) 230

"Sherwin" (SH1 and SH2) 230

Bishop Creek 231

Shreve 233

Little Egypt (LE) 233

Sand Canyon (SC) 240

Buttermilk (BU) 241

Bishop (BIS) 241

Coyote (CO) 242

Tungsten Hills (YTH and TH) 243

Birch (BIR) 243

Other samples 244

Conclusions 245

References 253

10. Cosmogenic ^{36}Cl chronology for glacial deposits at Bull Lake, eastern Wind River Range, Wyoming 258

Abstract 258

Introduction 258

Samples 260

Results and discussion 260

Pinedale moraines 265

Bull Lake moraines 267

Sacagawea Ridge moraine 268

Outwash terraces 268

Discussion and summary 269

References 271

11. Cosmogenic ^{36}Cl ages of late Pleistocene shorelines in Panamint and Death Valleys, California 274

Abstract 274

Introduction 275

Methods 276

Model for dating shorelines in presence of inherited ^{36}Cl 277

Shoreline ages 280

Death Valley 280

5-m shoreline 282

Beatty beach bar 282

Blackwelder shoreline 283

Panamint Valley 284

579-m shoreline 284

1st prominent shoreline (I) 285

2nd prominent shoreline (H) 285

3rd prominent shoreline (Gale) 286

2nd shoreline above Gale (E) 286

Uplift rate 287

Summary and conclusions 288

References 290

12. Summary of conclusions 292

Appendix A: Laboratory procedures 297

Appendix B: Geochemical data 302

Author index 310

Geographic index 312

Subject index 314

List of tables

Table 2.1. Scaling formulation for elevation and geomagnetic latitude. 14

Table 2.2. Cosmogenic reactions leading to production of ^{36}Cl. 15

Table 2.3. Thermal neutron absorption cross sections 21

Table 3.1. Relative importance of major reactions producing ^{36}Cl 39

Table 3.2. Geochemistry of calibration samples 48

Table 3.3. Location and production parameters for calibration samples 49

Table 3.4. Production rates due to spallation of ^{40}Ca 56

Table 3.5. Geochemistry of boulders from Mauna Kea, Hawaii 58

Table 3.6. Varnish (^{14}C and cation-ratio) and ^{36}Cl ages of Mauna Kea boulders 59

Table 3.7. Geochemistry of the altitude transect samples 62

Table 3.8. Scaling factors for the altitude transect samples 63

Table 3.9. Locations, scaling factors and ^{36}Cl ages for the Tioga samples 66

Table 4.1. Locations and published dating results for the calibration samples. . 83

Table 4.2. Absolute deviations between ^{36}Cl and independent ages 86

Table 4.3. Production rates of thermal neutrons and of ^{36}Cl 88

Table 5.1. Cosmogenic ^{36}Cl ages calculated from weighted AMS data 102

Table 5.2. Analytical and natural components of the total variance of ^{36}Cl ages 104

Table 5.3. Cosmogenic ^{36}Cl ages calculated from single cycles 105

Table 5.4. Nested analysis of variance for the cosmogenic ^{36}Cl dates 106

Table 5.5. Comparison of variances calculated for four nested experiments . . . 108

Table 5.6. Measured $^{36}Cl/Cl$ ratios and apparent boulder ages 123

Table 5.7. Empirical data for three soil samples from Bishop Creek 125

Table 6.1. ^{36}Cl surface-exposure ages for samples from Lathrop Wells 150

Table 7.1. Chemical and ^{36}Cl data for ejected material at Meteor Crater 166

Table 7.2. AMS Radiocarbon analyses of varnish from Meteor Crater 167

Table 8.1. Glacial chronostratigraphy for the White Mountains 176

Table 8.2. ^{36}Cl ages for samples from Chiatovitch Creek. 185

Table 9.1. Surface ages for samples from Bloody Canyon 212

Table 9.2. ^{36}Cl ages for samples from Little McGee Creek 221

Table 9.3. ^{36}Cl ages for samples from Bishop Creek 234

Table 9.4. Comparison of ^{36}Cl chronologies 246

Table 10.1. ^{36}Cl ages of samples from the Bull Lake area 262

Table 10.2. Correlation of cosmogenic ^{36}Cl glacial chronologies 270

Table 11.1. Surface ages for samples from Panamint and Death Valleys 281

List of figures

Fig. 2.1. Distribution of thermal and fast neutrons in the shallow subsurface . 17

Fig. 2.2. Buildup of cosmogenic ^{36}Cl in the surface in rocks. 20

Fig. 3.1. Chlorine extraction apparatus 46

Fig. 3.2. Thermal neutron stopping rate in rocks at the surface of the earth . . . 52

Fig. 3.3. Production of ^{36}Cl due to spallation of ^{39}K. 53

Fig. 3.4. Production of ^{36}Cl due to spallation of ^{40}Ca 55

Fig. 3.5. Measured versus theoretical $^{36}Cl/Cl$ for the calibration samples. 57

Fig. 3.6. Comparison of observed data with theoretical scaling factors 61

Fig. 4.1. General location map for the samples COM92 from Idaho 82

Fig. 4.2. Comparison of ^{36}Cl with independent ages for the calibration samples 89

Fig. 4.3. Average absolute deviation as a function of production rates. 90

Fig. 5.1. Schematics of the three-level nested analysis of variance 100

Fig. 5.2. Relationship between landform age and fraction of the total variance 103

Fig. 5.3. Conceptual model of soil erosion and gradual exposure of boulders . 109

Fig. 5.4a. Dependence of cosmogenic ^{36}Cl production rates 112

Fig. 5.4b. Chlorine-36 accumulation paths and resulting apparent ages 113

Fig. 5.4c. Dependence of ages on initial depth and chemical composition 115

Fig. 5.5. Distribution of apparent surface exposure ages 117

Fig. 5.6. Apparent coefficient of variation vs. mean apparent age 119

Fig. 5.7a. Distribution of ^{36}Cl ages for 26 samples from Bishop Creek 126

Fig. 5.7b. Observed vs. modeled distribution of ^{36}Cl ages 128

Fig. 5.8. Relationship between boulder size and measured ^{36}Cl age. 129

Fig. 6.1. Geologic map of Lathrop Wells volcanic center 144

Fig. 6.2. ^{36}Cl ages of samples from Lathrop Wells. 152

Fig. 6.3. Cumulative distributions of ^{36}Cl ages and $^{40}Ar/^{39}Ar$ and K/Ar ages . . 155

Fig. 7.1. Carbon-14 and chlorine-36 sample locations at Meteor Crater 163

Fig. 8.1. Study areas in the eastern White Mountains 179

Fig. 8.2. Glacial deposits at Chiatovitch Creek 180

Fig. 8.3. ^{36}Cl ages for the glacial deposits in the Chiatovitch Creek basin 184

Fig. 9.1. Study areas in the eastern Sierra Nevada, California 208

Fig. 9.2. Late Pleistocene glacial deposits at Bloody Canyon 210

Fig. 9.3. Cosmogenic ^{36}Cl exposure ages for moraines at Bloody Canyon 215

Fig. 9.4. Glacial deposits at Little McGee Creek 220

Fig. 9.5. Distribution of exposure ages at Little McGee Creek 226

Fig. 9.6 Glacial deposits at Bishop Creek 232

Fig. 9.7. Distribution of exposure ages for moraines from Bishop Creek 240

Fig. 10.1. Glacial deposits at Bull Lake, Wind River Range, Wyoming 261

Fig. 10.2. Age distributions for moraines in the Bull Lake area 265

Fig. 11.1. Study areas in Panamint and Death Valleys, California 278

Fig. 11.2. Vertical offset vs. shoreline age for shorelines at Pleasant Canyon . 287

1. Introduction

Past climate changes is a problem of global scope. While much has been learned from marine indicators of global climate changes, less is known about the continental record. The marine ^{18}O record is a proxy for the global ice volume, and thus average global temperature, without regard to spatial variability and as such is not indicative of climatic conditions at any specific location. The key to understanding regional and local climatic changes lies in terrestrial landforms, such as moraines and paleolake shorelines, which contain records of local climatic fluctuations. However, until recently, the information contained in these sediments has not been available because of lack of reliable techniques to date landforms. In this work, I use a new surface exposure dating technique to resolve this problem. The method is based on accumulation of cosmogenic ^{36}Cl in surficial rocks and permits direct dating of geomorphic surfaces. The research presented herein has two aspects. The first part focuses on further development of the cosmogenic ^{36}Cl dating method. A new calibration based on 31 samples from the Craters of the Moon, Idaho; Meteor Crater, Arizona; Wales, Great Britain; Hawaii; and Banks Island and Inuvik, the last two in the Canadian Arctic); is developed and factors that may influence cosmogenic ^{36}Cl ages are discussed. The second part of this work addresses changes in climatic conditions which are recorded in terrestrial sediments at various locations on the northern hemisphere during the Late Pleistocene (approximately the last 250 thousand years). The studied glacial and glacially-related deposits include moraines in three valleys in the eastern Sierra Nevada, California; four valleys in the eastern White Mountains, California/Nevada border; and four locations in the eastern Wind

River Range, Wyoming.

Problems with the chronology of the terrestrial glacial record

Fingerprints of Pleistocene climatic changes can be found in both marine and terrestrial deposits. The buildup of glacier ice not only removes water from the oceans, but also enriches the ocean in heavy oxygen (^{18}O) by locking up isotopically lighter water in the ice. The change in the ^{18}O content of the oceans from full-glacial to interglacial conditions depends on the amount of water in the ice and the isotopic composition of this water. Therefore, oxygen isotope content of marine microfossils (often benthic *Foraminifera*) provide a record of past fluctuations in the global ice volume (Emiliani, 1955; Berger, 1981), which is a proxy for the global climate. The standard marine isotopic record (Shackleton and Opdyke, 1973, 1976; Imbrie et al., 1984; Martinson et al., 1987) is of limited temporal resolution because the isotopic composition of the ocean water lags the environmental change by long and generally only approximately known time (Mix and Ruddiman, 1984), due to the large size of the global ocean. In addition, the isotopic composition of sea water is not only a function of the global ice volume, but also local environmental conditions, such as salinity, evaporation rate, carbonate dissolution rate, and influx of fresh water from the adjacent continents. Despite these limitations, the marine isotopic record is a remarkable result which has been a heart of many paleoclimatic studies for more than 30 years.

In contrast to the global nature of the marine ^{18}O record, the terrestrial paleoclimatic record is geographically confined. The most direct paleoclimatic inferences can be obtained from proxy sources that involve only the physical environment (Barry, 1983). These sources include, among others, moraines, which are an evidence of the past ice extent and thus of cold climates, and paleolake shorelines, which are indication of past hydrologic budget which, in turn, is a function of climatic conditions. Both moraines and paleolake shorelines are created by local geomorphic processes which usually respond abruptly and linearly to environmental changes. Since they are very prominent evidence of glacial/interglacial cycles, their proper understanding will have important paleoclimatic implications. The critical information regarding timing, duration and extent of glaciations lies in precise chronologies of these landforms. These surfaces, however, are not tractable by the standard dating techniques because they are composed of geomorphically redistributed material; attempts to date these materials would yield the time of mineral formation rather than the time of the landform construction. To overcome this deficiency, a new method for the direct dating of landforms using in situ accumulation of cosmogenic ^{36}Cl in minerals exposed at the surface of the earth has been developed (Phillips et al., 1986, 1990; Zreda et al., 1990, 1991).

There is a large body of literature related to Pleistocene global environmental changes; this literature has been recently reviewed by Broecker and Denton (1989). While the marine ^{18}O climatic record has been familiar for many years (e.g. Emiliani, 1955; Imbrie et al., 1984; Martinson et al., 1987), its continental counterpart has

remained obscure. As a result, no precise correlations have been established between continental glacial stratigraphy and the marine isotopic stratigraphy. One of the major unresolved questions in Pleistocene paleoclimatology has been whether the marine glacial ^{18}O record is in phase with and has similar amplitude to the changes in climatic conditions indicated by the terrestrial record. The results obtained from studies of the Owens River lake system, Great Basin, western United States indicate that although there is a strong similarity regarding cyclicity of climatic changes between the marine and the paleolake records, there are also significant differences in the amplitude of the cycles (Smith, 1984; Bishoff et al., 1985; Jannik et al., 1991). These differences are attributed to both local geographic conditions and global climatic patterns at mid-latitudes. Similar observations and paleoclimatic inferences were made based on the continuous record of ^{18}O in a calcitic vein, deposited from groundwater, in Ash Meadows, the southern Great Basin, Nevada, where a systematic difference in timing of key glacial/interglacial periods between the global ^{18}O and the local record was found (Winograd et al., 1988).

Other key controversies in the last glacial cycle are: (1) whether glacial advances proceeded in one phase or in two phases separated by a period of decreased ice volume and (2) whether buildup of ice was progressive with culmination at the end of the glacial cycle or it was abrupt at the beginning of the cycle followed by a long relaxation period. These controversies may, however, result from stratigraphic and chronologic misclassification and miscalibration (Schlüchter, 1990). The marine record indicates progressively more extensive global (continental) ice, accumulating during a two-phase

advance extending from standard isotope stage 5d to 4 and then from 3 to 2, with a warmer period characterized by 30% decrease in the global ice volume (Shackleton and Opdyke, 1973). In contrast, as suggested by Phillips et al. (1990), the early advances of small, mountain glaciers seem to be the most extensive. This controversy can be addressed through development of precise terrestrial glacial chronologies at various locations and their correlation with each other and with the marine ^{18}O record. Establishment of terrestrial glacial records is now possible by using our new surface exposure dating technique based on cosmogenic ^{36}Cl accumulation in surficial rocks.

In conclusion, the marine and terrestrial paleoclimatic records are inconsistent. This inconsistency may be a result of either (1) a significant difference between different environments which results in different responses to climatic changes or (2) inexact chronologies and incomplete correlations between the oceanic and continental record which results in wrong paleoclimatic interpretations. Both problems are addressed in this work by development of detailed glacial chronologies and their inter-regional correlations. The research described herein is unique in its attempt to date and correlate previously undatable geomorphic surfaces which contain records of past climatic conditions. It yields insights into the nature of the response of alpine glaciers, continental ice sheets, and paleolake systems to major climatic forcing in the Late Pleistocene.

Organization

This dissertation has an unconventional structure. It is a collection of ten chapters, each of which is a separate unit presented in a format of a journal article. There are two major reasons for choosing this format. Firstly, it facilitates preparation of manuscripts for submission to scientific journals. About half of these chapters have already been published, while the remaining ones will require only minor preparation before submission for publication. Secondly, it is convenient for readers interested in only one aspect of the work; these readers will find all necessary information within the chapter of interest. The subjects covered in this work include the fundamentals of ^{36}Cl dating method, calibration, initial applications, and development of glacial and pluvial chronologies and their correlations.

Chapter 2 describes production and accumulation of cosmogenic ^{36}Cl in surficial materials and discusses factors influencing surface ages. Determination of production rates of ^{36}Cl from its three major target elements, ^{35}Cl, ^{39}K and ^{40}Ca, is presented in chapters 3 and 4. Erosion, a major geological process affecting ^{36}Cl ages, is discussed in detail in chapter 5. A model of ^{36}Cl accumulation in boulders on eroding moraines is developed and used to quantify erosion of soil matrix. The initial applications to date late Pleistocene landforms are described in chapters 6 and 7; these samples are from geomorphically well understood contexts and were also used to assess the accuracy and precision of the method. The remaining chapters focus on the chronology of late

Pleistocene environmental changes. Cosmogenic ^{36}Cl chronologies for glacial deposits in mountains of the western United States are established in chapters 8, 9 and 10. Finally, chapter 11 describes the results of dating ancient shorelines in the Great Basin. Glacial and pluvial records are correlated with each other and with the marine ^{18}O record of the global paleoclimate.

References

Barry, R. G., 1983, Late-Pleistocene climatology, In: Late-Quaternary Environments of the United States, H. E. Wright, Jr., editor, Vol. 1: The Late Pleistocene, S. C. Porter, editor, pp. 390-407, University of Minnesota Press, Minneapolis.

Berger, W. H., 1981, Oxygen and carbon isotopes in foraminifera: an introduction, Paleogeography, Paleoclimatology, Paleoecology 33, 3-7.

Bishoff, J. L., R. J. Rosenbauer and G. I. Smith, 1985, Uranium-series dating of sediments from Searles Lake, California: documentation of differences between land and sea climate records, Science 227, 1222-1224.

Broecker W.S. and G.H. Denton, 1989, The role of ocean-atmosphere reorganizations in glacial cycles, Geochimica et Cosmochimica Acta 53, 2465-2501.

Emiliani, C., 1955, Pleistocene temperatures, Journal of Geology 63, 538-578.

Imbrie J., J. D. Hays, D. Martinson, A. McIntyre, A. Mix, J. Morley, N. Pisias, W. Prell and N. J. Shackleton, 1984, The orbital theory of Pleistocene climate: support from a revised chronology of the marine ^{18}O record, In: Milankovitch and

Climate, Part 1, A. L. Berger et al., eds., pp. 269-305, D. Reidel, Dortrecht.

Jannik, N. O., F. M. Phillips, G. I. Smith and D. Elmore, 1991, A ^{36}Cl chronology of lacustrine sedimentation in the Pleistocene Owens River system, Geological Society of America Bulletin 103, 1146-1159.

Martinson D.G. et al., 1987, Age dating and the orbital theory of the ice ages: Development of a high-resolution 0 to 300,000-yr chronostratigraphy, Quaternary Research 27, 1-29.

Mix, A. C. and W. F. Ruddiman, 1984, Oxygen-isotope analyses and Pleistocene ice volumes, Quaternary Research 21, 1-20.

Phillips F.M. et al., 1986, The accumulation of cosmogenic chlorine-36 in rocks: A method for surface exposure dating, Science 231, 41-43.

Phillips F.M., M.G. Zreda, S.S. Stewart, D. Elmore, P.W. Kubik and P. Sharma, 1990, A cosmogenic chlorine-36 chronology for glacial deposits at Bloody Canyon, Eastern Sierra Nevada, California, Science 248, 1529-1532.

Schlüchter, C., 1990, The last glacial cycle - what do we know from continental glacial records?, Palaeogeography, Palaeoclimatology, Palaeoecology (Global and Planetary Change Section) 82, 69-72.

Shackleton, N. J. and N. D. Opdyke, 1973, Oxygen isotope and paleomagnetic stratigraphy of equatorial Pacific core V28-238: oxygen isotope temperatures and ice volumes on a 10^5 and 10^6 year scale, Quaternary Research 3, 39-55.

Shackleton, N. J. and N. D. Opdyke, 1976, Oxygen isotope and paleomagnetic stratigraphy of Pacific core V28-239, Late Pliocene to Latest Pleistocene,

Geological Society of America, Memoir 145, 449-464.

Smith, G. I., 1984, Paleohydrologic regimes in the southwestern Great Basin, 0-3.2 my ago, compared with other long records of "global" climates, Quaternary Research 22, 1-17.

Winograd, I. J., B. J. Szabo, T. B. Coplen and A. C. Riggs, 1988, A 250,000-year climatic record from the Great Basin vein calcite: implications for Milankovitch theory, Science 242, 1275-1280.

Zreda M.G., F.M. Phillips and S.S. Smith,, 1990, Cosmogenic ^{36}Cl dating of geomorphic surfaces, New Mexico Institute of Mining and Technology, Hydrology Report 90-1.

Zreda M.G., F.M. Phillips, D. Elmore, P.W. Kubik, P. Sharma and R.I. Dorn, 1991, Cosmogenic ^{36}Cl production rates in terrestrial rocks, Earth and Planetary Science Letters 105, 94-109.

2. Surface exposure dating by cosmogenic chlorine-36 accumulation

Marek G. Zreda and Fred M. Phillips

Geoscience Department, New Mexico Tech, Socorro, NM 87801

Abstract

The cosmogenic ^{36}Cl accumulation method is a recently developed surface exposure dating technique that allows direct dating of construction time of geomorphic surfaces. Chlorine-36 is produced in materials exposed at the surface of the earth at a rate proportional to the cosmic-ray intensity and to concentrations of three main target nuclides for ^{36}Cl formation, ^{35}Cl, ^{39}K, and ^{40}Ca. Since the production rates of ^{36}Cl from the three target nuclides are known, measured concentration of cosmogenic ^{36}Cl in a surficial rock can be used to calculate how long a surface has been exposed to cosmic radiation and thus the time of its construction can be determined. Because ^{36}Cl is a long-lived radionuclide (half-life of 301,000 years), the method can be used to date landforms constructed during the last million years, and because of the ubiquitous nature of chlorine, it is applicable to surfaces constructed out of materials of essentially any chemical composition.

Accepted for publication in: Dating in Surface Context, C. Beck (ed.), University of New Mexico Press, 1994; modified for the purpose of this work.

Buildup of cosmogenic ^{36}Cl in terrestrial rocks depends on production rates and radioactive decay. In rocks at the surface, buildup is fastest during the initial period of exposure, decreases with time, and eventually reaches steady state when cosmogenic production equals radioactive decay. This idealized buildup pattern may be severely influenced by surficial geological processes which result in calculated apparent ages that differ from the landform age. Erosion and gradual exposure at the surface result in variable production rates and usually, but not always, lead to underestimated apparent ages. Intense chemical weathering may lead to mixing of chlorine in the rock, which contains cosmogenic ^{36}Cl, with meteoric chlorine, which has its own ^{36}Cl content, and thus to departure from the ideal buildup curve. Partial and temporal shielding result in overestimated apparent ages because of reduction in the cosmic-ray intensity. These and other factors controlling buildup are considered and appropriate corrections applied to calculate reliable ^{36}Cl surface exposure ages.

Introduction

Earth scientists have long understood factors that influence formation of landforms and realized that landforms contain valuable information about surficial processes and geological conditions prevailing at the time of their construction. For instance, moraines form under cold climatic conditions; therefore, dating of glacial moraines, which results in establishment of glacial chronologies, yields useful data about changes in local climatic conditions in the past and aids in understanding of the nature of the global climate

changes. Similarly, the ages of terrestrial impact craters yield important information on meteorite fluxes, and dating of fault scarps gives quantitative information about tectonic activity. Landforms are, however, intrinsically difficult to numerically date because they are generally made of preexisting geological materials and classical radiometric techniques would measure the age of the rock or mineral formation rather than the age of geomorphic redistribution. Geomorphic surfaces are thus usually not amenable to the standard dating techniques. The last decade has seen development of alternative dating techniques that can measure how long an object has been exposed at the surface of the earth - surface exposure dating methods. They include methods based on *in situ* accumulation of cosmogenic nuclides (^{36}Cl, ^{26}Al, ^{10}Be, ^{3}He, and ^{14}C) in surficial rocks, accumulation of organic matter in desert varnish, and physico-chemical changes in rock-forming minerals due to weathering processes. In this chapter, we describe the cosmogenic ^{36}Cl buildup method and its applications to dating of late Pleistocene landforms.

Chlorine-36 is produced by cosmic rays that interact with several nuclides, predominantly ^{35}Cl, ^{39}K, and ^{40}Ca. In materials exposed at the surface of the earth, cosmogenic ^{36}Cl is produced at a rate proportional to the local cosmic-ray intensity and to the concentrations of the three target nuclides. The concentration of ^{36}Cl can thus be used as a measure of the length of time a material has been exposed to cosmic radiation (Davis and Schaeffer 1955; Phillips et al. 1986). The very low concentrations of ^{36}Cl can now be routinely measured using accelerator mass spectrometry (Elmore et al. 1979;

Elmore and Phillips 1987). The half-life of 301,000 years makes ^{36}Cl suitable for dating groundwater, geomorphic surfaces, and anthropogenic constructions in the time range from a few thousand years up to about one million years. The ubiquitous character of chlorine and its conservative nature are important attributes that allow the use of the cosmogenic ^{36}Cl buildup method to establish surface exposure time of rocks that originated in various environments and have very wide range of chemical compositions.

We present in this chapter a state-of-the-art description of the cosmogenic ^{36}Cl buildup method. We start with a description of the spatial distribution of cosmic radiation in the atmosphere and the top five meters of solid materials. In the next section we characterize mechanisms and rates of cosmogenic ^{36}Cl production and formulate equations of accumulation of ^{36}Cl in rocks exposed at the surface of the earth and in the shallow subsurface. In the following section, we present two case studies to demonstrate applicability of the ^{36}Cl method to dating geomorphic surfaces. Finally, we examine possible effects of erosion, weathering, and shielding on ^{36}Cl buildup dating and discuss practical aspects of the cosmogenic ^{36}Cl accumulation method.

Spatial distribution of cosmogenic chlorine-36 production

The intensity of cosmic radiation at the surface of the earth is modulated by the earth's magnetic field and by the interactions with atmospheric nuclei. As a result of these processes, the highest intensity is at high geomagnetic latitudes and at high

elevations. Cosmic-ray neutron measurements at a variety of latitudes and elevations have been used by Lal (1991) to formulate a cubic polynomial equation that allows calculation of present-day cosmic-ray intensity at any location relative to any other location (Table 2.1).

Table 2.1. Scaling formulation for elevation and geomagnetic latitude in the form of a series of cubic polynomials ($y=a+bx+cx^2+dx^3$), where x is the elevation above sea level in km and y is the scaling factor, fitted to the observed thermal neutron data of Lal (1991).

Geomagnetic latitude	a	b	c	d
0	0.5790	0.4482	0.1723	0.0359
10	0.5917	0.4415	0.1944	0.0363
20	0.6691	0.4764	0.2320	0.0435
30	0.8217	0.6910	0.1712	0.0822
40	0.9204	0.8849	0.2487	0.1031
50	0.9865	1.0298	0.2992	0.1333
60-90	1.0000	1.0889	0.3105	0.1382

Cosmic rays, despite strong attenuation in the atmosphere, reach the surface of the earth, interact with the nuclei of the minerals in the shallow subsurface, and produce cosmogenic nuclides. Three types of cosmic-ray particles produce most of the ^{36}Cl: secondary fast neutrons (Yokoyama et al. 1977), thermal neutrons (Davis and Schaeffer 1955; Fabryka-Martin 1988; Phillips et al. 1986), and negative slow muons (Fabryka-Martin 1988; Zreda et al. 1990; Zreda et al.,1991); their relative importance is presented in Table 2.2.

Neutrons form the major part of the reactive cosmic-ray flux at high (mountain) elevations. Fast secondary neutrons have high energies (1 to 30 MeV) and are responsible for spallation reactions of ^{39}K and ^{40}Ca. They are attenuated both in the atmosphere (Lal 1987; Zreda et al. 1991) and solid materials (Kurz 1986; Lal 1987) according to $exp(1/\lambda_n)$ where the attenuation length, λ_n, for the fast component is from 150 to 160 g/cm^2 (Kurz 1986; Lal 1987; Zreda et al. 1991).

Table 2.2. Relative contribution of major cosmogenic reactions leading to production of ^{36}Cl in the top 100 g/cm^2 in examples of terrestrial rocks (granites, basalts, carbonates, and shales) at sea level and high geomagnetic latitudes (from Zreda et al. 1990, modified after Fabryka-Martin 1988).

Reaction type	Notation	% of total ^{36}Cl
Spallation of K and Ca	$^{39}K(n,2n2p)^{36}Cl$ $^{40}Ca(n,2n3p)^{36}Cl$	16-80
Thermal neutron activation of Cl	$^{35}Cl(n,\gamma)^{36}Cl$	11-80
Negative muon capture by Ca	$^{40}Ca(\mu^-,\alpha)^{36}Cl$	0-10

Thermal neutrons (energies below 0.025 eV) are formed from the fast neutrons that collide with atoms in the atmosphere or within a rock mass and lose energy. In contrast to the spallation component, distribution of these neutrons in the subsurface cannot be described by a simple exponential term because of the air-ground boundary effect (O'Brien et al. 1978; Yamashita et al. 1966). The macroscopic thermal neutron absorption cross-section of the atmospheric gases is much higher than that of the common crustal rocks. Therefore, neutrons that are produced in the top several centimeters of the rock mass have propensity to escape out of the rock and into the air above it, where they

are absorbed by nitrogen atoms. This leads to relative depletion of thermal neutrons in the uppermost part of the rock mass. The distribution of thermal neutrons in the top 100 g/cm^2 of a concrete block was measured by Fabryka-Martin et al. (1991) who reported a maximum at the depth of about 45 g/cm^2 (18 cm). Below this depth, the intensity of thermal neutrons decreases exponentially at a rate similar to that for the fast component. Figure 2.1 shows the behavior of the two main components of cosmic radiation, fast and thermal neutrons, in the shallow subsurface (0 to 1000 g/cm^2).

At sea level, the negative muon stopping rate is comparable to the neutron flux and in very calcic rocks slow muon capture by ^{40}Ca becomes a significant cosmogenic ^{36}Cl production reaction (Jha and Lal 1982; Lal and Peters 1967; Rama and Honda 1961). The slow negative muons can penetrate deeper due to their lower reactivity (attenuation length, λ_m of 247 g/cm^2, Conversi 1950; Rossi 1952), and dominate cosmogenic production of ^{36}Cl at depths below about three m of water equivalent (mwe). They can be captured by the nucleus of ^{40}Ca, which results in production of ^{36}Cl. The production from negative muon capture is uncertain and therefore it is lumped together with that due to spallation of ^{40}Ca (Zreda et al. 1990; Zreda et al. 1991).

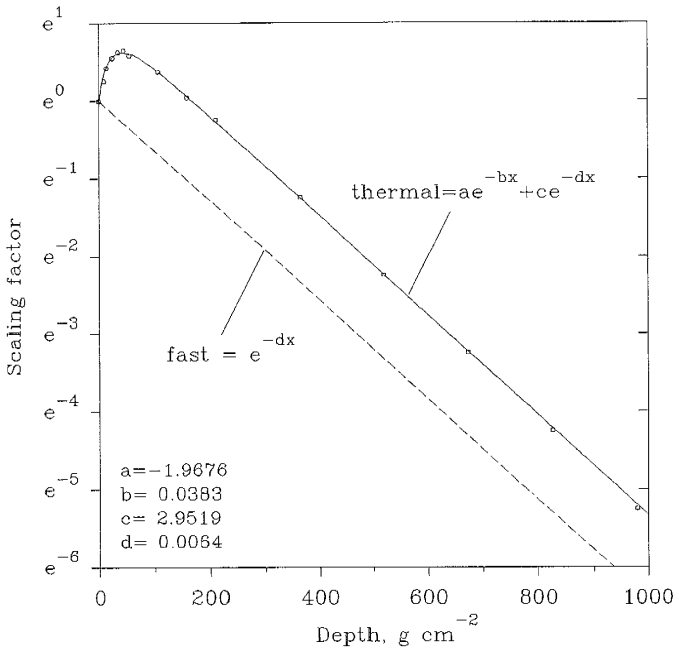

Fig. 2.1. Distribution of thermal (solid line) and fast neutrons below the surface. Circles are measured thermal neutron intensities (Fabryka-Martin et al. 1991), squares are calculated values based on attenuation length of 156 g/cm^2. The distribution of thermal neutrons may vary with chemical composition.

Accumulation of *in situ* chlorine-36 in surficial materials

In the idealized case in which a surface is suddenly exposed to cosmic rays and remains in constant position, cosmogenic ^{36}Cl accumulation is a function of the local cosmic-ray intensity, the chemical composition of the sample, and the exposure time. Chlorine-36 is produced at a rate P and radioactively decays at a rate proportional to its abundance and its decay constant λ_{36}. Its accumulation with time is described by a linear first order ordinary differential equation

$$\frac{dN_{36}}{dt} = P - \lambda_{36} N_{36} \quad (1)$$

which has the solution (Bentley et al. 1986)

(2) $$N_{36} = \frac{P}{\lambda_{36}}\left(1 - e^{-\lambda_{36} t}\right)$$

where N_{36} is the number of atoms of ^{36}Cl and t is the exposure time. For a given chemical composition of material, the production rate P is constant and can be expressed as the sum of the rates of the spallation and thermal neutron activation reactions

(3) $$P = \psi_{Ca} C_{Ca} + \psi_K C_K + \phi_n \frac{\sigma_{35} N_{35}}{\Sigma \sigma_i N_i}$$

where ψ_{Ca} and ψ_K are the production rates due to spallation of Ca and K per unit concentration of Ca and K, C_{Ca} and C_K are the concentrations of Ca and K, ϕ_n is the thermal neutron absorption rate per unit mass of rock, σ_{35} is the thermal neutron absorption cross section for ^{35}Cl, N_{35} is the number of atoms of ^{35}Cl, σ_i is the thermal neutron absorption cross section for every element i in the rock matrix and N_i is the number of atoms of element i. The production parameters in equation (3) are for rocks on the land surface at sea level and at high geomagnetic latitudes. For materials from other locations, the production rates have to be scaled according to Table 2.1 for elevation and latitude (scaling factor *EL*) and according to Figure 1 for depth below the surface (scaling factor *D*). It is also convenient to express the concentration of ^{36}Cl in terms of the ratio of ^{36}Cl to the total Cl because this is the quantity actually measured by accelerator mass spectrometry. The solution to the above differential equation thus becomes

$$R_{36} = ELD\frac{\psi_{Ca}C_{Ca} + \psi_K C_K + \phi_n \frac{\sigma_{35}N_{35}}{\Sigma\sigma_i N_i}}{\lambda_{36}N_{Cl}}\left(1 - e^{-\lambda_{36}t}\right) \quad (4)$$

In this equation R_{36} is the $^{36}Cl/Cl$ ratio after subtraction of background radiogenic ^{36}Cl that is formed in rocks due to neutrons derived from decay of uranium and thorium (Andrews et al. 1989; Bentley et al. 1986; Feige et al. 1968; Kuhn et al. 1984) and N_{Cl} is the number of chlorine atoms per unit mass of rock. In commonly-used geochemical units, the concentrations of Ca and K are in weight percents of CaO and K_2O, the production rates due to spallation are in atoms of ^{36}Cl per weight percent of oxide per kg of rock per year, and the thermal neutron absorption rate is in neutrons per kg of rock per year (Phillips et al. 1986; Zreda et al. 1991). Buildup of cosmogenic ^{36}Cl in rocks with approximately equal production rates due to spallation and thermal neutron activation is graphed in Figure 2.2. The sample is exposed at the surface since the landform formation. The buildup rate of ^{36}Cl is fastest during the initial period of exposure and decreases with time until the decay rate of ^{36}Cl in the rock asymptotically approaches secular equilibrium with the cosmogenic production rate.

The exposure time is obtained by solving the last equation for t

$$t = \frac{-1}{\lambda_{36}} ln \left[1 - \frac{R_{36}\,\lambda_{36}\,N_{Cl}}{ELD\left[\psi_K C_K + \psi_{Ca}C_{Ca} + \phi_n \frac{\sigma_{35}\,N_{35}}{\Sigma\sigma_i\,N_i}\right]} \right] \quad (5)$$

The error of the exposure time calculation is a combination of (a) analytical errors associated with isotopic and chemical analyses; (b) uncertainties in the production rates; and (c) uncertainties related to the distribution of the cosmic-ray flux in the atmosphere and the shallow subsurface. The analytical error is in the order of five to ten percent and is mainly due to analytical uncertainty of ^{36}Cl measurements by accelerator mass spectrometry; this error is routinely reported as the uncertainty of the age determination (Phillips et al. 1990; Phillips et al. 1991; Zreda et al. 1990; Zreda et al. 1991). The uncertainties in the assessment of the temporal and spatial distribution of the cosmic-ray intensity and also the production rates of cosmogenic ^{36}Cl may add another ten or twenty percent to the estimated error of the exposure time, but these errors have not been systematically evaluated yet.

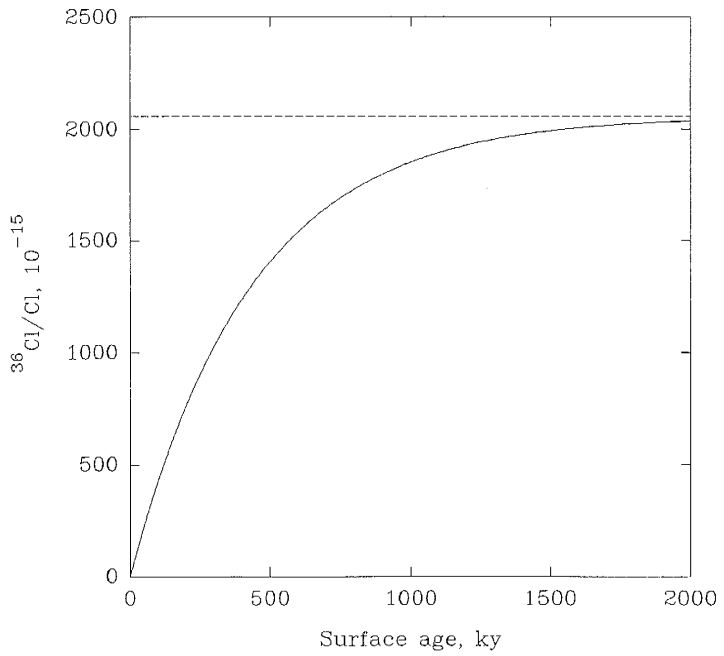

Fig. 2.2. Buildup of cosmogenic ^{36}Cl in rocks instantly exposed at the surface at time t=0 and remaining there without any surficial modification. The buildup curve is steepest at early times and flattens gradually to reach a steady state at times on the order of several half-lives of ^{36}Cl.

The production rate of ^{36}Cl due to the thermal neutron activation of ^{35}Cl can be calculated based on the thermal neutron absorption rate, the concentration of Cl, and the chemical composition of the sample (Davis and Schaeffer 1955; Phillips et al. 1986). Only a limited number of elements with high thermal neutron absorption cross-sections and/or high concentrations (Table 2.3) strongly compete with ^{35}Cl for thermal neutrons; they usually account for more than 98% of the absorbed thermal neutrons (Leavy 1987) and therefore it is not necessary to measure concentrations of all elements.

Table 2.3. Thermal neutron absorption cross sections, σ, of the elements which contribute significantly to the total macroscopic thermal neutron cross section, $\Sigma\sigma N$. The example chemical composition is that of a monzonite.

Element	σ[a] 10^{-24} cm^2	Composition[b] g/kg	N[c] 10^{22}/kg	σN cm^2/kg	% of $\Sigma\sigma N$
Si	0.16	326.70	703	1.125	22.09
Al	0.23	79.40	177	0.407	7.99
Fe	2.55	7.00	7.53	0.192	3.77
Mn	13.3	0.40	0.438	0.058	1.14
Ti	6.1	1.20	1.51	0.092	1.81
Mg	0.063	1.20	3.01	0.002	0.04
Ca	0.43	7.10	10.69	0.046	0.90
Na	0.53	37.10	97.14	0.515	10.11
K	2.1	41.50	64.08	1.346	26.44
P	0.19	0.20	0.389	0.001	0.02
Cl	33.2	0.10	0.170	0.056	1.10
B	759	0.005	0.027	0.205	4.03
Gd	49,000	0.005	0.0019	0.931	18.28
Sm	5,800	0.005	0.0020	0.116	2.28
$\Sigma\sigma N$[d]				5.092	100.00

[a] Thermal neutron absorption cross-sections are from Mughaghab and Garber (1973).

[b] Composition of a monzonite from the White Mountains, California (Zreda et al. 1990).

[c] Number of atoms of the element per kg of rock, based on the composition of the rock.

[d] Macroscopic thermal neutron absorption cross-section of the sample.

The first attempt to use the *in situ* buildup of ^{36}Cl in rocks due to the thermal neutron activation was made by Davis and Schaeffer (1955). However, the analytical instruments in the 1950's were not sufficiently sensitive to measure very small quantities of ^{36}Cl and the idea could not be realized. In addition, the total thermal neutron absorption rate was poorly known at that time. A thermal neutron absorption rate varying from 2×10^5 to 4×10^5 neutrons per kg of rock per year was reported by different investigators (Andrews et al. 1986; Hendricks and Edge 1966; Montgomery and Montgomery 1939; Simpson 1951; Yamashita et al. 1966), but the range was too wide to be useful and needed refinement.

The cross-sections for the spallation processes are not well known and their quantification is difficult. For practical purposes, we assume that the production of ^{36}Cl due to spallation of ^{39}K and ^{40}Ca is proportional to the concentration of the target elements and the respective production rates. The first theoretical estimates of the production rates of ^{36}Cl from ^{39}K and ^{40}Ca were published by Yokoyama et al. (1977). When applied to ^{36}Cl data from late Pleistocene moraines in the Sierra Nevada, they yielded ages much younger than those indicated by independent geological methods. An empirical determination of the effective production rates from these elements was therefore attempted herein.

Factors affecting cosmogenic ^{36}Cl buildup

In the physically and chemically stable environment, accumulation of cosmogenic ^{36}Cl is a function of time alone and by measuring the ^{36}Cl content one can directly obtain the surface exposure age by solving the production equation (3) for time. Implicit assumptions in the above simple model are that the production rate (P) is constant and that R represents only cosmogenic ^{36}Cl, i.e., any meteoric component potentially present in the sample has been removed prior to the analysis. However, postdepositional modifications of landforms and other environmental changes may invalidate these assumptions and corrections to the above model may be necessary. In this section, I explore the issue of environmental factors that may influence the buildup of cosmogenic ^{36}Cl in surficial materials, examine their possible impact on ^{36}Cl dating, and discuss ways of accounting for their effects.

Erosion

Soil erosion and gradual exposure of initially buried boulders (or bedrock) are likely the most common postdepositional processes that severely affect cosmogenic ^{36}Cl ages. The production rates of cosmogenic nuclides vary with depth below the surface. Consequently, on eroding landforms, they also vary in time. As a result of the process of soil erosion and gradual exposure, the apparent ^{36}Cl ages will usually be younger than the true landform age, but can also be older for some combinations of small erosion

depths ($\sim$100 g cm^{-2}) and chemical compositions (high Cl, low K and Ca). One can account for these effects in the following ways: (1) collecting multiple samples (five or more) from each landform; (2) sampling from horizontal surfaces which are less likely to have been modified by erosion; (3) performing statistical analysis of the distribution of apparent ^{36}Cl ages; (4) using soil analysis to assess landform stability. The effects of soil erosion on ^{36}Cl ages are addressed in detail in the next chapter in which I discuss accumulation of ^{36}Cl on eroding glacial landforms.

Stream dissection is similar in its nature to the above, but varies in the extent of the modification. The calculated ^{36}Cl ages are for the erosion episode rather than the landform construction and can be useful in studies of regional geomorphic evolution. Analysis of landform morphology and its position with respect to the streams should be sufficient to exclude it from being sampled for cosmogenic nuclide dating.

Erosion of rock surface has similar effect to the effect of erosion of soil, but the rate is much slower because solid rocks are much more resistant to erosion than are soils. Erosion of rocks with high Cl content may result in slightly overestimated apparent ages; in low Cl rocks, the apparent ages will be younger than the true surface exposure age. The effects of erosion of rock surface can be minimized by selecting surfaces that show indications of zero erosion (e.g., glacial polish or heavy varnish development) or on which erosion can be quantified (e.g., differential erosion of rocks with variable lithology). They can also be accounted for by using a second radionuclide with different

decay constant than that of ^{36}Cl (e.g., ^{10}Be or ^{26}Al).

Spalling of rock surfaces (e.g., due to fire) is similar to erosion of rock surfaces, but it occurs at very "erratic" rate. Depending on the thickness of spalled fragments and frequency of spalling, the apparent age may under or overestimate the true age. This kind of surfaces should be avoided, if possible; if not, multiple samples are necessary to obtain a good estimate of the true surface exposure age.

Temporary and/or partial cover

Snow cover will temporarily reduce the cosmic-ray flux reaching the boulder surface which will (usually) result in underestimation of the true age. This factor is especially important in areas, such as the High Arctic, where snow cover is thick and persists for long periods of time. Sampling from tops of large boulders or other topographic highs from which snow is quickly removed by wind should minimize the effect of snow cover on accumulation of ^{36}Cl.

Volcanic ash, dust, or sand cover temporarily reduces the cosmic-ray flux reaching the rock surface and (usually) results in underestimation of the true age. Sampling from the highest points should again give best results. In addition, examination of the study area for remnants of ash or sand, which should be preserved in topographically lowest zones where the action of wind is not strong enough to remove them, should provide clues

about the presence or absence of such cover in the past.

Vegetation cover temporarily blocks cosmic rays and may lead to underestimation of the true ages. It is considered a minor factor in arid environments, such as climates of the Great Basin; however atmospheric conditions could have been less arid in the past and vegetation may have been different. This effect is very difficult to quantify. Multiple sampling should be a good means of solving this problem.

Chemical weathering

Chemical weathering and preferential loss of ^{36}Cl reduces the accumulated cosmogenic ^{36}Cl and leads to underestimation of the true surface age. Sampling of only relatively unweathered rocks should eliminate this problem.

Chemical weathering and change of bulk macroscopic cross-section for thermal neutron activation may have some effect in samples with high Cl content. Depending on the direction of this change, this process may lead to either overestimation or underestimation of the true age. Sampling of unweathered rocks is again the best way to avoid this problem. One can also back calculate initial chemical composition from the present composition and use a linear model to assess this effect on the dating; however, to do this the mineralogy of the rock must be known.

Chemical weathering and precipitation of secondary minerals will affect the dating because of inclusion of non-cosmogenic ^{36}Cl. This will interfere with the age determination in three ways: (1) by mixing of secondary Cl with primary Cl; (2) by providing new target elements (e.g., Ca in the case of carbonates) for cosmogenic ^{36}Cl production; and (3) by changing the macroscopic thermal neutron absorption cross section. Again, relatively unweathered rocks should help avoid this problem. In the lab, one can attempt separation of the secondary minerals from the original ones; this will work for clay minerals and carbonates, but may fail for some non-separable minerals such as iddingsite replacing olivine.

Change of position

Tectonic activity will lead to change of elevation and thus the cosmic-ray flux reaching the studied surfaces. Tectonic activity may also cause deformation of the landform and destruction of the original surface. The effects of these processes are relatively minor for young surfaces on which we concentrate because of the extremely low rates typical of tectonic uplift. The surface morphology should bear the information about any destructive processes caused by tectonics and thus correct sampling should eliminate this problem.

Isostatic movement will change the elevation and thus the cosmic-ray flux reaching the studied surface. It is usually a minor factor, but may be important in the Canadian

Arctic where some surfaces may have experienced glacial rebound on the order of 100 m in the last 10 ky. Assessment of these effects can be made by using reconstructed isostatic movement rates for the last few tens ky. For older surfaces the cyclicity in the signal due to isostasy is averaged out and the effects on cosmogenic ^{36}Cl buildup should be negligible.

Sea-level changes will result in elevation changes and thus in variable cosmic-ray flux reaching the studied surface. To account for sea-level changes, one can use reconstructed sea levels; for older surfaces this signal is averaged out because of "cyclicity" of changes.

Change of geometry

Geometry change by rolling over will cause exposure of "new" surfaces to cosmic radiation and result in underestimation of the true age. Sampling from more than one surface of the boulder would yield the necessary information to address this problem. It is, however, expensive and therefore not routinely done in surface exposure dating; instead, multiple boulders from the same landform are sampled.

Geometry change by breaking up along vertical fractures leads to the so called "edge effect" which changes the thermal neutron absorption rate. This process may lead to underestimation of the true ages because of diffusion of thermal neutrons out of the rock

and into the atmosphere. To minimize this effect, samples should be collected from centers of large boulders (larger than the attenuation length for thermal neutrons) and from horizontal, flat surfaces.

Change of the incident cosmic ray intensity

Geomagnetic field strength changes (quasi-cyclic) result in changes in the cosmic-ray flux and thus the cosmogenic ^{36}Cl production rates. The two are in phase, but have reversed magnitude, i.e., higher magnetic field strength leads to lower production rates and vice versa. These changes may have significant effect on young surfaces, while for the older ones the variability should be integrated over time and the production rates should converge to the average value. The effects of variable geomagnetic field strength can be assessed using the function of magnetic strength vs. time and corrections for any desired time interval can then be calculated.

References

Andrews, J. N., J.-Ch. Fontes, J.-L. Michelot, and D. Elmore, 1986, In-situ neutron flux, ^{36}Cl production and groundwater evolution in crystalline rocks at Stripa, Sweden. *Earth and Planetary Science Letters* 77: 49-58.

Andrews, J. N., S. N. Davis, J. Fabryka-Martin, J.-Ch. Fontes, B. E. Lehmann, H. H. Loosli, J.-L. Michelot, H. Moser, B. Smith and M. Wolf, 1989, The *in situ*

production of radioisotopes in rock matrices with particular reference to the Stripa Granite. *Geochimica et Cosmochimica Acta* 53: 1,803-1,815.

Bentley, H. W., F. M. Phillips, and S. N. Davis, 1986, Chlorine-36 in the terrestrial environment. In *Handbook of Environmental Isotope Geochemistry, Vol. 2, The Terrestrial Environment, B*, edited by P. Fritz and J.-Ch. Fontes, pp. 427-480. Elsevier, New York.

Conversi, M., 1950, Experiments on cosmic-ray mesons and protons at several altitudes and latitudes. *Physics Reviews* 79: 749-767.

Davis Jr., R., and O. A. Schaeffer, 1955, Chlorine-36 in nature. *Annals of New York Academy of Science* 62: 105-122.

Elmore D., B. R. Fulton, M. R. Clover, J. R. Marsden, H. E. Gove, H. Naylor, K. H. Purser, L. R. Kilius, R. P. Beukins, and A. E. Litherland, 1979, Analysis of ^{36}Cl in environmental water samples using an electrostatic accelerator. *Nature* 277: 22-25.

Elmore, D., and F. M. Phillips, 1987, Accelerator mass spectrometry for measurement of long-lived radioisotopes. *Science* 236: 543-550.

Fabryka-Martin, J.T., 1988, *Production of Radionuclides in the Earth and Their Hydrogeologic Significance, With Emphasis on Chlorine-36 and Iodine-129*. Ph.D. dissertation, University of Arizona. University Microfilms, Ann Arbor.

Fabryka-Martin, J. F., M. M. Fowler and R. Biddle, 1991, Study of neutron fluxes underground. *Isotope and Nuclear Chemistry Division Quarterly Report* October 1 - December 31, 1990, 82-85.

Feige, Y., B. G. Oltman and J. Kastner, 1968, Production rates of neutrons in solids due to natural radioactivity. *Journal of Geophysical Research* 73: 3,135-3,142.

Hendricks, L. D., and R. D. Edge, 1966, Cosmic-ray Neutrons Near the Earth. *Physics Reviews* 145: 1,023-1,025.

Jha, R., and D. Lal, 1982, On cosmic ray produced isotopes in surface rocks. In *Natural Radiation Environment*, edited by K. G. Vohra et al., pp. 629-635. Proceedings of Second Special Symposium on Natural Radiation Environment, Halsted Press.

Kuhn, M. W., S. N. Davis, H. W. Bentley and R. Zito, 1984, Measurements of thermal neutrons in the subsurface. *Geophysical Research Letters* 11: 607-610.

Kurz, M., 1986, Cosmogenic helium in a terrestrial igneous rock. *Nature* 320: 435-439.

Lal, D., 1987, Cosmogenic nuclides produced in situ in terrestrial solids. *Nuclear Instruments and Methods in Physics Research* B29: 238-245.

Lal, D., 1991, Cosmic ray labelling of erosion surfaces: *in situ* production rates and erosion models. *Earth and Planetary Science Letters* 104: 424-439.

Lal, D. and B. Peters B., 1967, Cosmic ray produced radioactivity on Earth. In *Encyclopedia of Physics*, edited by S. Fluegge, *Vol. 46/2, Cosmic Rays II*, edited by K. Sitte, pp. 551-612. Springer-Verlag, Berlin.

Leavy, B.D., 1987, *Surface-exposure Dating of Young Volcanic Rocks Using the in situ Buildup of Cosmogenic Isotopes*. Unpublished Ph.D. dissertation, Geoscience Department, New Mexico Institute of Mining and Technology.

Montgomery, C. G. and D. D. Montgomery, 1939, The intensity of neutrons of thermal

energy in the atmosphere at sea level. *Physics Reviews* 56: 10-12.

Mughaghab, S. F. and D. I. Garber, 1973, *Neutron Cross Sections, Vol. 1, Resonance Parameters*. Brookhaven National Laboratory.

O'Brien, K., H. A. Sandmeier, G. E. Hansen and J. E. Campbell, 1978, Cosmic ray induced neutron background sources and fluxes for geometries of air over water, ground, iron, and aluminum. *Journal of Geophysical Research* 83: 114-120.

Phillips, F.M., B. D. Leavy, N. D. Jannik, D. Elmore and P. W. Kubik, 1986, The accumulation of cosmogenic chlorine-36 in rocks: A method for surface exposure dating. *Science* 231: 41-43.

Rama and M. Honda, 1961, Cosmic-ray-induced radioactivity in terrestrial materials. *Journal of Geophysical Research* 66: 3,533-3,539.

Rossi, B., 1952, *High Energy Particles*, 569 p., Prentice Hall, New Jersey.

Simpson, J. A., 1951, Neutrons produced in the atmosphere by the cosmic radiations, *Physics Reviews*, 83:1,175-1,188.

Yamashita, M., L. D. Stephens, and H. W. Patterson, 1966, Cosmic-ray-produced neutrons at ground level: Neutron production rate and flux distribution. *Journal of Geophysical Research* 71: 3,817-3,834.

Yokoyama, Y., J.-L. Reyss, and F. Guichard, 1977, Production of radionuclides by cosmic rays at mountain altitudes. *Earth and Planetary Science Letters* 36: 44-50.

Zreda, M.G., F. M. Phillips and S. S. Smith, 1990, *Cosmogenic ^{36}Cl Dating of Geomorphic Surfaces*. Hydrology Program Report 90-1, New Mexico Tech.

Zreda, M.G., F. M. Phillips, D. Elmore, P. W. Kubik, P. Sharma and R. I. Dorn,

1991, Cosmogenic ^{36}Cl production rates in terrestrial rocks. *Earth and Planetary Science Letters* 105: 94-109.

3. Cosmogenic chlorine-36 production rates in terrestrial rocks

MAREK G. ZREDA and FRED M. PHILLIPS

Geoscience Department, New Mexico Institute of Mining and Technology, Socorro, NM 87801

DAVID ELMORE

Department of Physics, Purdue University, West Lafayette, IN 47907

PETER W. KUBIK[1] and PANKAJ SHARMA

Nuclear Structure Research Laboratory, University of Rochester, Rochester, NY 14627

RONALD I. DORN

Department of Geography, Arizona State University, Tempe, AZ 85287

[1] Present address: Institut Für Mittelenergiephysik, ETH-Hönggerberg, CH-8093 Zürich, Switzerland

Abstract

Chlorine-36 is produced in rocks exposed to cosmic rays at the earth surface through thermal neutron activation of ^{35}Cl, spallation of ^{39}K and ^{40}Ca, and slow negative muon capture by ^{40}Ca. We have measured the ^{36}Cl content of ^{14}C-dated glacial boulders

---

Published in 1991, Earth and Planetary Science Letters, 105, 94-109.
Additional calibration samples have been analyzed since 1991; the results are reported in Chapter 4.

from the White Mountains in eastern California and in a ^{14}C-dated basalt flow from Utah. Effective, time-integrated production parameters were calculated by simultaneous solution of the ^{36}Cl production equations. The production rates due to spallation are $4,160\pm310$ and $3,050\pm210$ atoms ^{36}Cl yr^{-1} $(mole)^{-1}$ ^{39}K and ^{40}Ca, respectively. The thermal neutron capture rate was calculated to be $(3.07\pm0.24)\times10^5$ neutrons (kg of rock)$^{-1}$ yr^{-1}. The reported values are normalized to sea level and high geomagnetic latitudes. Production of ^{36}Cl at different altitudes and latitudes can be estimated by appropriate scaling of the sea level rates. Chlorine-36 dating was performed on carbonate ejecta from Meteor Crater, Arizona, and late Pleistocene morainal boulders from the Sierra Nevada, California. Calculated ^{36}Cl ages are in good agreement with previously reported ages obtained using independent methods.

Introduction

For many years Quaternary geologists have struggled to assign numerical ages to landforms. Cosmogenic nuclide accumulation has the potential to be useful for measuring the exposure time of landforms and thus for estimating their time of formation. In order to successfully use cosmogenic isotope geochronometers, the isotope production parameters have to be determined with high precision. The objective of this research was to calibrate the cosmogenic ^{36}Cl method by using well-dated or geologically well-constrained rock samples. We report new measurements of the production rates of ^{36}Cl in rocks at the earth's surface. The following sections describe how the experiment

was carried out, point out uncertainties, and give examples of applications.

Cosmogenic nuclide accumulation is a function of exposure time, geographic location, and the abundance of target elements in a sample. Possible applications of cosmogenic ^{36}Cl dating in the earth sciences were first suggested over 30 years ago [1]. However, the geochronological potential of ^{36}Cl could not be fully realized at that time due to lack of sufficiently sensitive analytical techniques. This limitation has recently been overcome for ^{36}Cl by developments in accelerator mass spectrometry (AMS) [2]. However, despite the analytical advances of the last decade, cosmogenic nuclide geochemistry is still in its early stage of development. Presently, only a few cosmogenic isotopes have been applied in geoscience. They include ^{36}Cl ($t_{1/2} = 3.01 \times 10^5$ yrs.), ^{26}Al ($t_{1/2} = 7.05 \times 10^5$ yrs.), ^{10}Be ($t_{1/2} = 1.5 \times 10^6$ yrs.), ^{3}He (stable), and ^{14}C ($t_{1/2} = 5730$ yrs.). The half-lives of these isotopes make them especially valuable dating tools in hydrology, geomorphology, Quaternary stratigraphy and paleogeography, and archaeology.

Major production reactions for ^{36}Cl in minerals at the surface of the earth

Chlorine-36 is produced in rocks exposed at the surface of the earth almost entirely by cosmic-ray induced reactions with ^{35}Cl, ^{39}K, and ^{40}Ca. Cosmic rays are moderated in the atmosphere by interactions with nuclei of atmospheric gases. The major part of the cosmic-ray flux at high (mountain) elevations is neutrons. At sea level, the

negative muon flux is comparable to that of neutrons and slow negative muon capture becomes a significant cosmogenic reaction [3, 4, 5]. Neutrons directly interact with nuclei to produce disintegrations. On the other hand, muons do not produce radionuclides by direct interactions; negative muons fall into the K shell of the atom and may be captured by the nucleus before they decay [3]. The negative muon capture rate exceeds that of neutron at depths below 3 meters of water equivalent (mwe) at sea level [6].

In the top meter of the lithosphere, thermal neutron activation of ^{35}Cl and spallation of ^{39}K and ^{40}Ca are the dominant production mechanisms for ^{36}Cl [7, 8, 9, 10]. Below that depth, the contribution from slow negative muon capture by ^{40}Ca becomes progressively more important [4, 5, 10]. Thermal neutron activation of ^{39}K, negative muon capture by ^{39}K, spallation of Ti and Fe by the high energy component of the cosmic-ray flux, and nuclear reactions involving ^{36}Ar and ^{36}S are relatively insignificant reactions in minerals at the surface of the earth; they are responsible for less than 2% of total in situ produced ^{36}Cl [10] and will not be discussed in our paper. The relative contributions of the dominant production reactions (Table 3.1) depend on chemical composition of rocks.

Accumulation of in situ produced ^{36}Cl in geological materials

The amount of cosmogenic ^{36}Cl accumulated in a given sample after t years of exposure to the cosmic rays and with negligible erosion can be expressed as:

$$R-R_0=\frac{E_n L_n D_n(\psi_K C_K+\psi_{Ca} C_{Ca}+\Psi_n)+E_{\mu^-} L_{\mu^-} \Psi_{\mu^-}}{\lambda N}(1-e^{-\lambda t})$$

where: R = atomic ratio of 36Cl to stable Cl; R_0 = background $^{36}Cl/Cl$ ratio supported by U and Th derived neutrons; ψ_K, ψ_{Ca} = production rates due to spallation of ^{39}K and ^{40}Ca, in atoms per kg of rock per year per unit concentration (w/w) of K or Ca, at sea level and geomagnetic latitudes $\geq 60°$; C_K, C_{Ca} = concentration of K or Ca (w/w); Ψ_n = production rate due to thermal neutron activation of ^{35}Cl, in atoms per kg of rock per year, at sea level and geomagnetic latitudes $\geq 60°$; Ψ_{μ^-} = production rate due to slow negative muon capture by ^{40}Ca, in atoms per kg of rock per year, at sea level and geomagnetic latitudes $\geq 60°$; E, L, D = scaling factors for dependence of cosmic-ray neutron (n) and muon (μ) fluxes on elevation above sea level (E), geomagnetic latitude (L), and depth below surface (D); t = time of exposure, in years; N = stable Cl concentration, in atoms per kg of rock; λ = decay constant for ^{36}Cl (2.30×10^{-6} yr^{-1}).

The scaling factors for neutrons for elevation above sea level (E_n) and geomagnetic latitude (L_n) can be calculated as previously described [4, 15, 7, 11, 12, 14], and for depth below surface (D_n) as $\exp(-d/\Lambda_n)$, where Λ_n of 150-160 g/cm^2 [16, 17] is the mean free path for neutrons. Similar scaling factors have been developed for

muons [18, 19, 20].

The background ratio, R_0, of ^{36}Cl due to neutrons from spontaneous fission and (α,n) reactions is usually small (5×10^{-15} to 5×10^{-14} $^{36}Cl/Cl$) [8, 21], but may become relatively important for rocks with very short exposure times.

Estimation of production rates of ^{36}Cl due to spallation of ^{39}K (ψ_K) and ^{40}Ca (ψ_{Ca}) has been attempted by Yokoyama et al. [7], and production of ^{36}Cl by thermal neutron activation of ^{35}Cl (Ψ_n) described by Davis and Schaeffer [1] and Phillips et al. [22]. Production of ^{36}Cl due to slow negative muons (Ψ_{μ^-}) is significant only at low elevations and in very calcic rocks (Table 3.1). The production rate can be calculated using methods described in Charalambus [23] and references therein. Details of all pertinent calculations can be found in Zreda et al. [24].

Table 3.1. Relative importance of major reactions producing ^{36}Cl in the top 0.5 m of water equivalent (mwe) of the lithosphere at sea level in crustal rocks (modified from [10])

Reaction type	Notation	% of total ^{36}Cl
Spallation of K and Ca	$^{39}K(n,2n2p)^{36}Cl$ $^{40}Ca(n,2n3p)^{36}Cl$	16-80
Thermal neutron activation of Cl	$^{35}Cl(n,\gamma)^{36}Cl$	11-80
Negative muon capture by Ca	$^{40}Ca(\mu^-,\alpha)^{36}Cl$	0.3-10
Thermal neutron activation of K	$^{39}K(n,\alpha)^{36}Cl$	0-2
Negative muon capture by K	$^{39}K(\mu^-,p2n)^{36}Cl$	0-0.4

Methods

In order to calibrate the cosmogenic ^{36}Cl dating technique, several rock samples were collected in the western United States and Hawaii from young glacial moraines and lava flows which had previously been dated by independent methods. Some samples were subjected to mineral separations and minerals with high concentration of specific target elements for ^{36}Cl formation were obtained. The samples were then analyzed for ^{36}Cl and for major and trace elements. Effective production rates of ^{36}Cl from ^{35}Cl, ^{39}K, and ^{40}Ca were calculated. Internal consistency of the calculated parameters was tested by dating several rock samples at various locations.

Sample collection

Useful samples for calibrating cosmogenic ^{36}Cl production rates should be from a well understood geological context, should be precisely dated by independent methods, and should have been in a geomorphically and tectonically stable environment since their exposure to cosmic rays. For these reasons we have selected boulders from glacial moraines in the White Mountains of eastern California and samples from lava flow in central Utah as our reference samples.

The glacial samples were collected from a late Quaternary moraine sequence at Chiatovich Creek in the eastern White Mountains. These moraines are in a regionally

well-understood context [25] and, because of the relatively arid climate, exhibit enough rock varnish development to allow the application of varnish radiocarbon dating [26]. Sample 187 was collected from a small moraine deposited during the Chiatovich Cirque glaciation and has a varnish ^{14}C date of 9.74 ka [27]. The Chiatovich Cirque glaciation is correlated with the Hilgard glaciation in the Sierra Nevada, which has been assigned an early Holocene (or possibly terminal Pleistocene) age [28]. Sample 387 was from a late Middle Creek moraine and has a varnish ^{14}C age of 12.51 ka [27]. The late Middle Creek glaciation in the White Mountains is correlated with the late Tioga phase in the Sierra Nevada [25], which has a ^{14}C date for its termination of 11 ka [28]. Rock varnish on a late Tioga moraine at Pine Creek, in the Sierra Nevada west of the White Mountains, yielded a varnish ^{14}C date of 13.9 ± 0.4 ka [29]. Finally, sample 787 was collected from an early Middle Creek moraine with a varnish ^{14}C age of 17.78 ka [27]. The early Middle Creek is correlated with the early Tioga glaciation in the Sierra Nevada. Carbon-14 dates on materials beneath alluvial sediments correlated with the Tioga glaciation indicate that the glaciation was initiated close to 25 ka [30, 31]. An early Tioga moraine at Pine Creek gave a varnish ^{14}C date of 18.9 ± 0.8 ka [29]. In summary, the varnish ^{14}C dates from the Chiatovich Creek moraines are in good agreement with both conventional ^{14}C dating of the regional glacial sequence and with varnish ^{14}C dates on correlative moraines from a nearby part of the Sierra Nevada. We therefore consider the varnish ^{14}C dates to be reliable enough to use for calibrating the cosmogenic production rate of ^{36}Cl.

Presumably, some finite length of time is required to initiate varnish generation (and thus accumulation of organic carbon) on boulder surfaces. This should result in some time lag between the emplacement of the boulder and the ^{14}C date that would be measured on the basal 10 percent of the varnish. Unfortunately, this time lag is unknown for the White Mountains environment. For sites in the western United States where varnish ^{14}C dates were tested against precise independent chronologies the lag was found to be generally less than 5 percent [26]. Due to the relatively small lag, we have chosen to calibrate to the measured, varnish-^{14}C ages of the moraines. When the varnish lag can be accurately quantified, the ^{36}Cl production rates can be appropriately corrected. At present, the magnitude of the correction would appear to be well within the uncertainty of the calculated production rates. Recent calibration of the ^{14}C time-scale using U/Th dates on corals has indicated that ^{14}C dates in the range 15 to 30 ka underestimate the actual sample ages by 2 to 3 ka [32]. We consider it premature to apply this correction until the ^{14}C calibration has been confirmed. For the present we note that our production rates should give dates in conformity with uncorrected ^{14}C dates from the same time interval.

In order to assure that the sample geometries have remained unchanged since the time of deposition, only large boulders with glacially altered surfaces from young moraines were sampled; all samples were collected from near the centers of the top surfaces using a chisel and a hammer. Another rationale for choosing relatively young glacial deposits was to minimize the influence of any elevation changes due to tectonic

uplift of the White Mountain block. The average Quaternary vertical uplift rate of the White Mountains with respect to sea level has been estimated to be 0.5 mm/yr [33], which is similar to the late Quaternary displacement rate of 0.25 mm/yr of the Sierra Nevada block along the Owens Valley fault zone [34]. This uplift rate is equivalent to an offset of 5-9 m since the deposition time of the two Middle Creek and the Chiatovich Cirque moraines. Displacement of this magnitude does not require any corrections.

The three samples from the White Mountains were subjected to mineral separation in a heavy liquid (sodium metatungstate) and three impure mineral groups were obtained. Potassium-rich microcline yielded information on the production rate due to spallation on ^{39}K, whereas relatively pure quartz, where ^{35}Cl is the major target element for ^{36}Cl, was used to estimate the effective thermal neutron capture rate. Small impurities in microcline and quartz are not critical because chemical composition is accounted for in the production equation. The third mineral separate consisted of plagioclase and heavy minerals which could not be completely decomposed by HF during sample preparation. Therefore, chlorine could not be reliably quantified and these mineral separates have not been used in calibration.

Two additional calibration samples were obtained from the Tabernacle Hill basalt flow in Utah (samples 9353 and 9354). The eruption age is bracketed by ^{14}C-dated organic matter incorporated into volcanic ash below the flow and tufa above [35, 36]; the eruption occurred between 14.3 and 14.5 ka. The dates are consistent with the

intensively-studied Lake Bonneville chronology. These two calcium-rich samples were chosen to provide information on the production rates due to spallation of Ca and neutron activation of ^{35}Cl.

Four boulders, one basaltic and three hawaiitic, from late Pleistocene moraines in Mauna Kea, Hawaii, were analyzed (samples MK-MAKY-16, MK-MAKT-29, MK-MAKO-12, and MK-W-5) to test the proposed geomagnetic latitude correction factors [7, 11, 15]. Five siliceous dolomites from Meteor Crater, Arizona, and several granitic boulders from glacial moraines in the Sierra Nevada, California were dated to test the consistency of the calculated ^{36}Cl production rates. Summaries of these results will be presented in this paper and details elsewhere.

Chemical analyses

Major elements were determined by X-ray fluorescence (XRF) spectrometry on fused disks (calibration samples) and on pressed pellets (remaining samples), with analytical uncertainty better than 2% for all critical elements. Inductively coupled plasma atomic emission spectrometry (ICP-AE) was used to determine boron and selected rare earth element concentrations. Powdered samples were fused with sodium carbonate and dissolved in HCl. Boron and rare earths were separated from the matrix by standard cation-exchange chromatography [37, 38]. Additional analyses for boron and gadolinium were performed using prompt gamma emission spectrometry. Replicate (3

to 5) determinations of chlorine content were performed by using a combination ion selective electrode after decomposition of the rock matrix using hydrofluoric acid in teflon gas-diffusion cells [39, 40]; the analytical uncertainty of chlorine determination was generally better than 5%.

Sample preparation and isotopic analysis of ^{36}Cl

We have developed a wet chemical technique for extraction of Cl from silicate rock [24] and conversion into a form suitable for AMS [41]. The extraction apparatus (Fig. 3.1) was made of teflon because of teflon's resistance to hot HF. An air stream was bubbled through the solution to strip the chlorine as HCl. A 2.2 μm air filter and indicating drierite prevent introduction of particulates and water vapor to the sample. The small tubes before and after the chlorine capture tube were included to prevent sample loss in case of sucking back or overspilling of the capture solution.

The rock sample was ground to a size fraction smaller than the mean phenocryst size of the rock and leached for 24 hours in 18 MΩ deionized water in order to remove any meteoric chloride ions from pores or grain boundaries; basalts were leached for 2 hours in 10% nitric acid to remove any secondary carbonate accumulated in the vesicles. Grinding to much smaller sizes is not advisable because Cl from fluid inclusions can be liberated and removed by leaching. This leaching procedure was found sufficient and no contamination by meteoric Cl was observed. Approximately 100 g of the sample

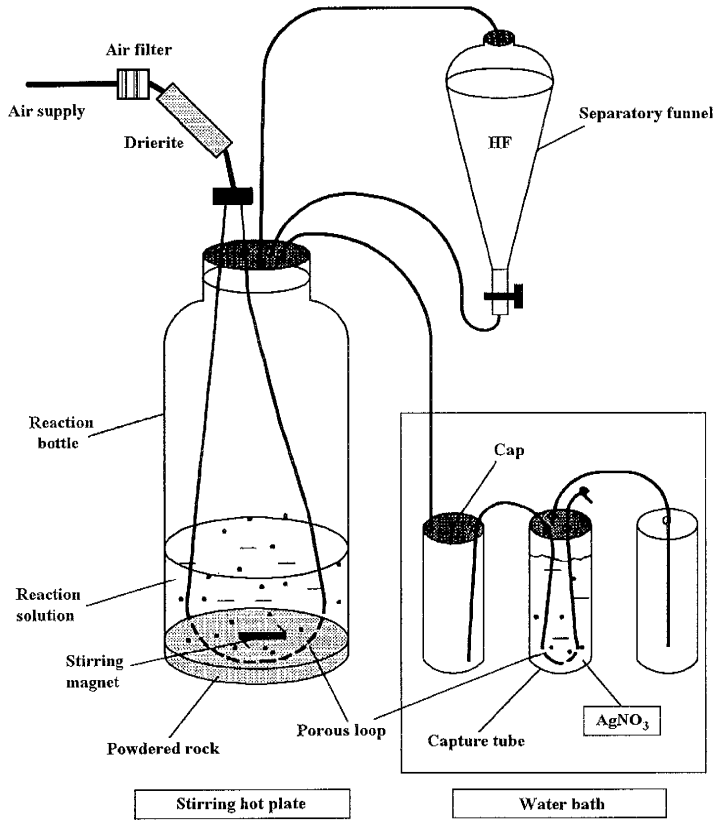

Fig. 3.1. Chlorine extraction apparatus.

were mixed with 100 ml of concentrated HNO_3 and placed in the 1000-ml reaction bottle on a stirring plate. A separatory funnel with 250 ml of concentrated HF and a 50-ml teflon capture tube containing Ag^+ ions in an acidic solution were connected to the reaction bottle. Dry air was supplied through a porous teflon loop at a rate sufficient to cause rapid bubbling, and hydrofluoric acid at a rate slow enough to prevent violent reaction. Chloride ions were liberated from the sample, transported with the air stream as HCl or/and Cl_2, and precipitated in the capture tube as AgCl. The time required for complete decomposition of samples depends on mineralogy and varies from 6 to 12 hours

for silicic and intermediate rocks, respectively. The precipitate was dissolved in NH_4OH and mixed with $BaNO_3$ to remove sulfur; ^{36}S is an interfering isobar which must be minimized prior to AMS measurement. After at least 8 hours any $BaSO_4$ precipitated was removed from the solution by centrifugation or filtration. Near sulfur-free AgCl was recovered by acidifying the remaining base solution, rinsed using deionized water, and placed in an oven at 60° C until it was dry. Small samples (less than 2 mg of AgCl) were mixed with a low-sulfur AgBr binder in proportions not exceeding 3 parts of AgBr to one part of AgCl. The dry samples were loaded into custom-made, low-sulfur tantalum holders.

The samples were analyzed for ^{36}Cl by accelerator mass spectrometry [42] on the tandem Van de Graaff accelerator at the University of Rochester; analytical error was usually better than 10%.

Results and discussion

Production rates

The results of chemical and isotopic analyses are summarized in Table 3.2. Sample locations, correction factors, and calculated parameters are presented in Table 3.3; geographical longitude is to the east of Greenwich.

Table 3.2. Geochemistry of calibration samples

Sample ID	SiO_2 (%)	TiO_2 (%)	Al_2O_3 (%)	Fe_2O_3 (%)	MgO (%)	CaO (%)	MnO (%)	Na_2O (%)	K_2O (%)	P_2O_5 (%)	Cl (ppm)	B (ppm)	Gd (ppm)	$^{36}Cl/Cl$ (10^{-15})
187-Bulk	76.00	0.21	13.80	1.22	0.14	0.21	0.03	4.26	5.44	0.02	130	2.6	4.9	473±74
187-Quartz	84.90	0.04	10.20	0.35	0.18	0.14	0	4.60	3.61	0	125	2.6	2.7	493±48
187-Microcline	70.30	0.02	17.00	0.32	0	0.16	0	5.34	7.80	0	130	0.9	0.9	616±61
387-Quartz	94.80	0.02	3.99	0.27	0.10	0.26	0.01	2.27	0.37	0	101	0	1.26	342±32
387-Microcline	69.70	0.01	18.10	0.28	0	0.22	0.01	5.57	8.78	0	142	0	0.96	856±101
787-Bulk	76.50	0.21	14.00	13.50	0.12	0.49	0.02	4.83	5.43	0.05	160	6.3	4.7	595±74
787-Quartz	92.50	0.05	4.67	0.35	0.16	0.25	0	2.60	0.54	0	135	1.8	0.8	344±26
9353	47.91	1.31	14.03	10.22	6.81	10.93	0.16	2.06	0.86	0.46	94	10	5.4	244±16
9354	46.13	1.42	14.84	11.65	6.75	10.69	0.17	2.37	0.78	0.42	111	10	5.7	226±15

Major elements were measured by XRF spectrometry on pressed pellets (analytical error < 2%), B and Gd by ICP-AE and prompt gamma emission spectrometry. Total Cl was measured by ion selective electrode (analytical error <5%). Chlorine-36 was measured by AMS.

Table 3.3. Location and calculated production parameters for calibration samples[a]

Sample ID	Altitude (km)	Latitude °N	Longitude °E	ELD_n	ELD_μ	$\frac{\sigma_{35}N_{35}}{\Sigma\sigma_i N_i}$	^{14}C age (ka)	Production rate due to activation of Cl[d]	Production rate due to spallation of K[c,d]	Production rate due to spallation of Ca[d]
187-Bulk	3.750	37.46	241.40	12.45	3.80	0.01416	9.74[b]	3852	4012	-
187-Quartz	3.750	37.46	241.40	12.45	3.80	0.01361	9.74[b]	5452	-	-
187-Microcline	3.750	37.46	241.40	12.45	3.80	-	12.51[b]	-	6675	-
387-Quartz	3.700	37.46	241.40	12.13	3.74	0.01061	12.51[b]	3362	-	-
387-Microcline	3.700	37.46	241.40	12.13	3.74	-	12.51[b]	-	8906	-
787-Bulk	3.275	37.47	241.42	9.511	3.27	0.01677	17.78[b]	4740	4078	-
787-Quartz	3.275	37.47	241.42	9.511	3.27	0.01415	17.78[b]	4027	-	-
9353	1.445	38.94	247.48	2.965	1.76	-	14.4±0.1	-	-	5561 (4719)
9354	1.445	38.94	247.48	2.965	1.76	-	14.4±0.1	-	-	6177 (5380)

[a] Production rates are for sea level and high geomagnetic latitudes. Only values for samples used in calculations are shown (see text for details).

[b] Estimated uncertainty is less than 10% [27].

[c] The first values refer to probability 0.005 of reaction with muons yielding ^{36}Cl and the values in parentheses refer to probability 0.15 (see text for details).

[d] Atoms ^{36}Cl per kg of rock per year.

Production rates due to the different mechanisms discussed below were obtained by solving the production equation for the parameters: Ψ_K ($=\psi_K C_K$), Ψ_{Ca} ($=\psi_{Ca} C_{Ca}$), and Ψ_n (defined earlier). For each production mechanism, we used only those samples in which this particular mechanism contributed approximately half or more to total ^{36}Cl production. By doing this, we minimized propagation of errors associated with other production mechanisms. The samples used for calculation of parameters for different mechanisms are indicated in the last three columns of Table 3.3.

A computer algorithm for iterative solution of an overdetermined system of linear equations was developed. First, the production rates due to thermal neutron capture Ψ_n were calculated for each of the five samples for which thermal neutron capture is the major reaction leading to formation of ^{36}Cl (samples 187-Bulk, 187-Quartz, 387-Quartz, 787-Bulk, and 787-Quartz), and the individual values (per unit neutron capture probability) were averaged. The mean value was then used in solving the appropriate equations for the total production rates due to spallation of K, Ψ_K (samples 187-Bulk, 187-Microcline, 387-Microcline, and 787-Bulk). Again, the individual values (per unit concentration of K_2O) were averaged, and the mean value was used for solving the last two equations (samples 9353 and 9354) for the remaining parameter - the total production rates due to spallation of Ca, Ψ_{Ca}. The procedure was repeated until no significant change in calculated mean values was observed; the convergence was achieved after less than 8 iterations. The program was run with several different sets of initial values of the three unknowns to check the uniqueness of the solution; for all initial conditions the final

values of Ψ_K, Ψ_{Ca}, and Ψ_n were identical.

The values of total production rates due to thermal neutron activation of ^{35}Cl (Ψ_n) obtained in the final iteration step (Table 3.3, column 9) were plotted (Fig. 3.2) versus the capture probability terms calculated for each sample (Table 3.3, column 7). A straight line of the form

$$\Psi_n = \phi_n \frac{\sigma_{35} N_{35}}{\Sigma \sigma_i N_i}$$

(where σ is the thermal neutron absorption cross-section of element i, N is the atomic concentrations of element i, subscript 35 refers to ^{35}Cl, and subscript i to all other elements in the sample [22]) was fitted to the data using a least squares algorithm; the resulting slope was our best estimate for the time-integrated thermal neutron capture rate.

The calculated thermal neutron absorption rate (ϕ_n) of $(3.07 \pm 0.24) \times 10^5$ neutrons per kg of rock per yr is in fairly good agreement with measured values at different locations. The reported values of the thermal neutron flux range from 10^{-3} to 2×10^{-3} n cm^{-2} s^{-1} [43, 44, 45, 46, 47] which is equivalent to a capture rate of 2×10^5 to 4×10^5 n kg^{-1} yr^{-1}. The variability among them can be explained by analytical uncertainty in the thermal neutron measurements, which can be as high as 50 % [46]. This error arises mainly from uncertainty of the energy distribution and anisotropic properties of the thermal neutron fluxes. The anisotropic properties of the neutron flux may be a source of an additional error introduced during conversion from the flux units (n cm^{-2} yr^{-1}) to

the capture rate units (n kg^{-1} yr^{-1}). This may underestimate converted values by about 15 (ϕ_n) at sea level and geomagnetic latitudes higher than 60°.

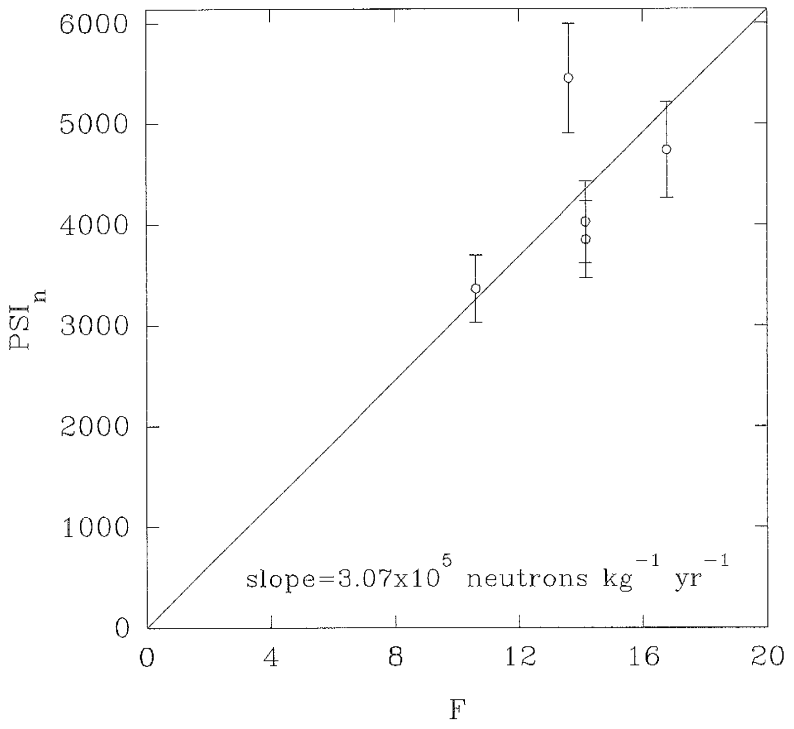

Fig. 3.2. Thermal neutron stopping rate in rocks at the surface of the earth. Horizontal axis shows ^{36}Cl produced per one thermal neutron; vertical axis represents total ^{36}Cl production rate by neutron activation of ^{35}Cl; slope of the fitted line is equal to the thermal neutron production rate. Error bars are calculated based on 10% uncertainty in varnish ^{14}C ages [27]. F = $\sigma_{35}N_{35}/\Sigma\sigma N\times 10$; $PSI_n = \Psi_n$ in text.

The production rates due to spallation of K and Ca were obtained using the same technique. The total production rates (Ψ_K and Ψ_{Ca}) from each of the two target elements obtained in the final iteration (Table 3.3, columns 10, 11) were plotted (Fig. 3.3, 3.4) versus the respective concentrations of K_2O and CaO (Table 3.2). Straight lines of the form $\Psi_K=\psi_K C_K$ and $\Psi_{Ca}=\psi_{Ca}C_{Ca}$ were fitted and our best estimates of production rates (ψ_K, ψ_{Ca}) at sea level and high geomagnetic latitudes were obtained. % [46]. It should be stressed that the measured, present-time fluxes may not be representative for the past

conditions because of possible major changes in the earth's magnetic field strength [48] and the galactic cosmic ray flux. Our calculated value represents the effective, sea-level, high-latitude thermal neutron production rate time-integrated over the last 10-18 ka.

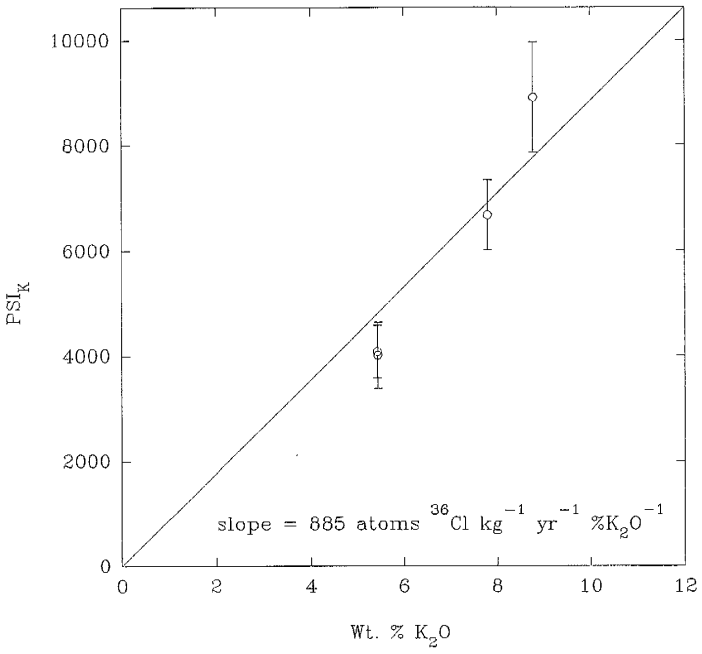

3.3. Production of ^{36}Cl due to spallation of ^{39}K. The slope of the line is equal to the production rate ψ_K of ^{36}Cl from ^{39}K. Error bars are calculated based on 10% uncertainty in varnish ^{14}C ages [27]. $PSI_K = \Psi$ in text.

The production rate due to spallation of potassium (ψ_K) is 4,160 $\pm$ 310 atoms ^{36}Cl (mole K)$^{-1}$ yr^{-1} (885$\pm$65 atoms ^{36}Cl (kg of rock)$^{-1}$ yr^{-1} (% K_2O)$^{-1}$). This value is smaller than that obtained by Yokoyama et al. [7] by a factor of four. About one half of this discrepancy can be accounted for by using different scaling factors for elevation above sea level. Using scaling proposed by Yokoyama et al. [7], our experimental production rates will increase by approximately a factor of two. However, we argue against using this scaling formulation later in this article (section 3.2). Another possible explanation of the discrepancy in the production rates is that the production rates of Yokoyama et al. [7] were theoretically calculated using the excitation functions for ^{36}Cl production given

by Reedy and Arnold [49] for lunar conditions. These conditions, however, may not be applicable on the surface of the earth because of atmospheric moderation and magnetic field effects. The model of Reedy and Arnold [49] assumes that ^{36}Cl is produced evenly over the entire cosmic-ray energy spectrum which is not valid for earth surface conditions because energetically different components of the cosmic radiation are moderated at different rates. Similar discrepancies between theoretically calculated and experimentally derived production rates for ^{3}He [36, 50] and ^{10}Be [51] have been explained by the lack of availability of excitation functions for the nuclides' formation from their target elements. Our calculated value is an experimentally derived, effective terrestrial production rate reported for ^{36}Cl due to spallation of ^{39}K.

Calcium is a target element for ^{36}Cl formation in two different cosmogenic reactions: spallation and negative muon capture. Production due to negative slow muon capture was calculated using the formulation of Charalambus [23] and two different values for probability of reaction ^{40}Ca(μ,α)^{36}Cl: 0.15 [23] and 0.005 [52, cited by 10]. Both probabilities are theoretically calculated and need to be verified experimentally. If the real value of this probability were close to 0.005, the muon term could be safely omitted in the production equation, for production at the earth surface, because its contribution to ^{36}Cl production would be only about 1 % of that of spallation of ^{40}Ca. If, on the other hand, its value were 0.15, the production rate due to negative muon capture by ^{40}Ca would be as high as 14 % of that of spallation of ^{40}Ca and this reaction would have to be treated quantitatively. These figures are valid at sea level; at higher

elevations the muon contribution decreases because of the longer attenuation length for muons than for neutrons. The calculated production rates due to spallation of ^{40}Ca for the two values of the above probability are presented in Table 3.4. They differ by 14% and, since spallation of ^{40}Ca usually accounts for no more than 50% of total ^{36}Cl production, the introduced total uncertainty should be smaller than 7 %.

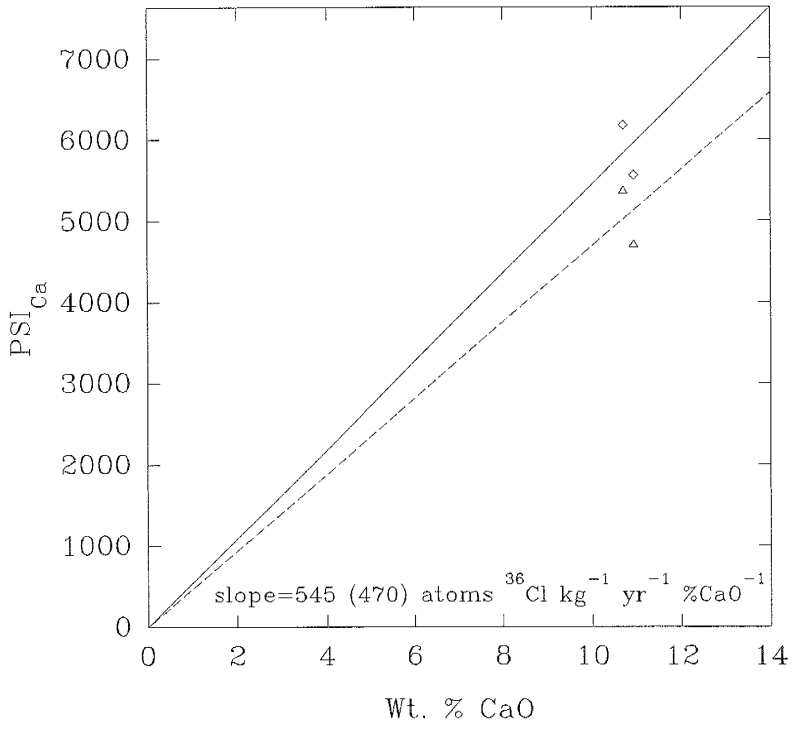

Fig. 3.4. Production of ^{36}Cl due to spallation of ^{40}Ca for different values of contribution of muons: solid line and rhombs are for probability 0.005 of the muon-induced reaction leading to ^{36}Cl formation, dashed line and triangles are for probability 0.15. The slopes of the lines represent the production rates ψ_{Ca} of ^{36}Cl from ^{40}Ca. Error bars are smaller than the symbols used. $PSI_{Ca} = \Psi_{Ca}$ in text.

Both figures are considerably lower than the previously published value of 5,600 atoms of ^{36}Cl per year per mole of Ca [7]. The same factors that affect potassium spallation may account for this discrepancy. The calculated values may have to be adjusted in the future when more accurate estimates for the probability of reaction

$^{40}Ca(\mu,\alpha)^{36}Cl$ are available. Until then, since the reactions involving muons are not of critical importance for most surface samples, the slow negative muon component can be omitted in the production equation and the higher of the two reported values for spallation of calcium used.

Table 3.4. Production rates due to spallation of ^{40}Ca for different contributions of slow negative muons to ^{36}Cl production

Probability of reaction leading to formation of ^{36}Cl due to slow muons (see text)	Production rate due to spallation of ^{40}Ca	
	(atoms ^{36}Cl (mole Ca)$^{-1}$ yr^{-1})	(atoms ^{36}Cl (kg rock)$^{-1}$ (%CaO)$^{-1}$ yr^{-1})
0.005	3040±210	545±40
0.15	2620±180	470±35

Theoretical $^{36}Cl/Cl$ values for the calibration samples, calculated using our production rates, were plotted versus the measured values (Fig. 3.5). The slope of the resulting line is very close to 45°, which indicates internal consistency of the calculated production parameters.

Spatial variability of the cosmogenic nuclide production rates

For samples from altitudes and latitudes differing from those of the calibration location, appropriate scaling factors have to be applied. Previously published altitude/latitude gradients [7, 11, 15] differ by as much as 100 %; for each of these

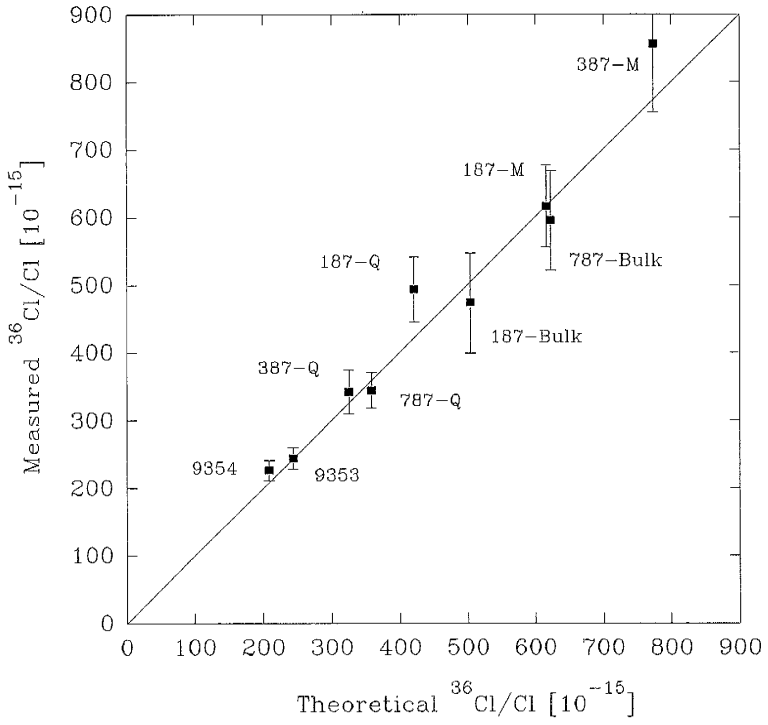

Fig. 3.5. Comparison of measured versus theoretically predicted ^{36}Cl/Cl for the calibration samples. Theoretical ratios were calculated using previously published ages and the production parameters calculated earlier in this paper. For mineral separates, the macroscopic absorption cross-sections ($\Sigma\sigma_i N_i$) of the associated bulk rocks were used. Error bars reflect analytical uncertainties in AMS measurements of ^{36}Cl.

gradients, the calculated production parameters for ^{36}Cl are different. In order to address the problem of the uncertain cosmic ray flux gradients, we used these different production parameters and the corresponding scaling factors to date a set of samples from Mauna Kea, Hawaii. To test the latitudinal dependence (L_n) of the production rates, we collected four basaltic and hawaiitic boulders (Table 3.5) from late Pleistocene moraines at elevations similar to the calibration elevation, but at differing geomagnetic latitude. Chlorine-36 buildup ages calculated using the geomagnetic correction factors of

Table 3.5. Geochemistry of boulders from late Pleistocene moraines, Mauna Kea, Hawaii

Sample ID	SiO_2 (%)	TiO_2 (%)	Al_2O_3 (%)	Fe_2O_3 (%)	MgO (%)	CaO (%)	MnO (%)	Na_2O (%)	K_2O (%)	P_2O_5 (%)	Cl (ppm)	B (ppm)	Gd (ppm)	$^{36}Cl/Cl$ (10^{-15})
MK-MAKO-12	54.93	2.37	17.98	9.85	2.04	6.82	0.19	5.44	1.99	1.04	49	10	3.0	1121 ± 82
MK-MAKY-16	51.90	2.37	18.80	10.00	1.90	6.72	0.20	5.61	2.04	0.96	84	9	5.2	708 ± 30
MK-MAKT-29	52.90	2.22	18.00	9.47	1.51	6.22	0.20	5.97	2.12	0.95	45	10	4.9	1110 ± 36
MK-W-5	46.88	4.65	17.64	14.96	4.72	9.39	0.18	3.91	0.99	0.76	45	10	5.0	2991 ± 111

Major elements were measured by XRF spectrometry on pressed pellets (analytical error $< 2\%$), B and Gd by ICP-AE and prompt gamma emission spectrometry. Total Cl was measured by ion selective electrode (analytical error $< 5\%$). Chlorine-36 was measured by AMS.

Yokoyama et al. [7] and Lingenfelter [11] exceeded the corresponding ^{14}C ages by as much as 50 %, whereas the geomagnetic latitude dependence of Lal [15] yielded ages almost identical with those obtained by the varnish ^{14}C method (Table 3.6) [54].

Table 3.6. Varnish (^{14}C and cation-ratio) and ^{36}Cl ages of boulders from late Pleistocene moraines, Mauna Kea, Hawaii

Sample ID	$(ELD)_n$[a]	Varnish age (ka)	^{36}Cl age[b] (ka)
MK-MAKO-12	7.01	21.5±0.2[c]	20.3±1.5
MK-MAKY-16	7.32	18.3±0.2[c]	18.9±0.8
MK-MAKT-29	9.26	14.4±0.1[c]	14.7±0.5
MK-W-5	5.67	68.0±5.0[d]	63.0±2.3

[a] Calculated according to the altitude/latitude dependence of Lal [15].

[b] Calculated using the production equation solved for t.

[c] Varnish ^{14}C age [54]; reported uncertainty reflects AMS measurement error only; the true uncertainty is estimated as ± 10% [54].

[d] Varnish cation-ratio age [54].

We tested the altitude dependence (E_n) in a similar fashion, using eleven samples collected from glacial moraines and two lava flows (Table 3.7) at altitudes ranging from 0.38 km to 4.05 km (Table 3.8). Dates obtained using the K/Ar method were used for the flows, with one exception. Sample MK-MAK-IF-15 is from the same flow as samples MK-AT2M-21 and MK-AT2M-23; the flow has a K/Ar age of 33±12 ka [54]. However, a varnish ^{14}C sample from MK-MAK-IF-15 yielded a date of 22.9±0.2 ka. This discrepancy can be explained by the position of the MK-MAK-IF-15 sample a few meters in front of a large moraine from the most recent glacial advance on Mauna Kea.

This moraine (sample MK-MAKY-16) yielded a varnish ^{14}C date of 18.3±0.2 ka and a ^{36}Cl date of 18.9±0.8 ka. We believe that the early advance of this glacial pulse overrode the outcrop sampled and removed the surface of the flow.

All samples used for the altitude dependence (E_n) have the same geomagnetic latitude and therefore the variability in the calculated scaling factors is attributed to the altitude alone. The theoretical and experimental altitude transect curves calculated as least squares exponential fits are presented on Fig. 3.6. Again, the $^{36}Cl/Cl$ ratios calculated from the altitude dependences of Yokoyama et al. [7] and Lingenfelter [11] agree poorly with the data. They tend to diverge from the true scaling factor significantly. On the other hand, the curve based on the altitude dependence of Lal [15] is in excellent agreement with the curve fitted to the experimental data points. The average difference between the two is smaller than 8 %, which is well within analytical uncertainty of the cosmogenic ^{36}Cl buildup method.

The exponential fit to the data allowed calculation of an attenuation length of 152 g cm^{-2} for neutrons in the atmosphere at elevations from 0.38 to 4.05 km (987 to 624 g cm^{-2}) and at 20° N geographic latitude. This value is in concordance with the value of 156 g cm^{-2} calculated for the exponential fit to the altitudinal scaling values of Lal [15]. This agreement indicates that cosmogenic ^{36}Cl production rates can be corrected for geomagnetic latitudes and elevations differing from the calibration latitude. In cosmogenic nuclide buildup applications, we recommend using the polynomial fits to

nuclear disintegration rate data developed by Lal [15].

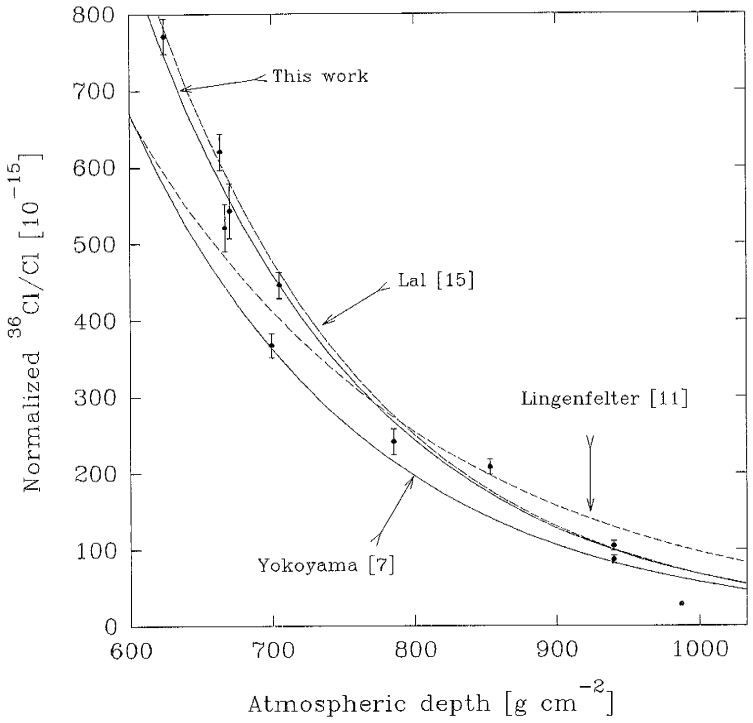

Fig. 3.6. Comparison of observed data (circles and rhombs) with theoretically calculated [7, 11, 15] altitudinal scaling factors; experimental curve was constructed for samples indicated by circles. Error bars reflect uncertainties in age determinations.

It must be noted here that the calculated scaling factors integrate changes in the earth's magnetic field strength and the intensity of the cosmic ray flux during the last 20-60 ka. The very good agreement between the present-day and the time-integrated distributions of the cosmic ray intensity implies either (a) that the flux varied little during the past 60 ka or (b) that the present-day flux is equal to the average flux over the past 60 ka. Knowledge of the time distribution of the cosmic ray flux will have important implications for calibration of the ^{14}C time-scale [32].

Table 3.7. Geochemistry of the altitude transect samples

Sample ID	SiO_2 (%)	TiO_2 (%)	Al_2O_3 (%)	Fe_2O_3 (%)	MgO (%)	CaO (%)	MnO (%)	Na_2O (%)	K_2O (%)	P_2O_5 (%)	Cl (ppm)	$^{36}Cl/Cl$ (10^{-15})
MK-MAK-IF2-15	51.24	2.63	16.10	11.20	3.37	6.56	0.21	4.20	1.56	0.55	124	532±32
MK-AT2M-21	52.38	2.45	15.84	10.87	3.40	6.62	0.21	4.29	1.48	0.68	137	501±22
MK-AT2B-23	52.95	2.48	16.14	10.92	3.26	6.39	0.21	4.48	1.63	0.71	44	750±53
MK-AT3M-25	51.48	2.69	15.09	11.44	3.43	6.94	0.21	4.61	1.60	0.60	188	171±9
MK-AT3M-26	49.67	2.83	16.06	11.63	3.65	6.92	0.21	3.95	1.43	1.13	296	164±10
MK-AT3T-28	51.00	2.95	15.11	12.09	4.23	7.04	0.21	3.87	1.47	0.68	209	365±17
MK-AT3B-30	52.42	2.70	15.95	11.43	3.43	6.71	0.20	4.40	1.51	0.64	53	134±11

Major elements were measured by XRF spectrometry on pressed pellets (analytical error < 2%), B and Gd by ICP-AE and prompt gamma emission spectrometry. Total Cl was measured by ion selective electrode (analytical error <5%). Chlorine-36 was measured by AMS.

Table 3.8. Theoretical [15] and experimental scaling factors for the altitude transect samples, Mauna Kea, Hawaii.

Sample ID	Sample origin	Age (ka)	Altitude (km)	Latitude °N	Longitude °E	$^{36}Cl/Cl$[d] (10^{-15})	
						Theoretical[d]	Experimental[e]
MK-MAKO-12	moraine	21.5±0.2[a]	3.500	19.849	204.493	578±58	543±36
MK-MAKY-16	moraine	18.3±0.2[a]	3.584	19.843	204.492	605±61	620±24
MK-MAKT-29	moraine	14.4±0.1[a]	4.054	19.825	204.521	780±78	771±23
MK-W-5	moraine	68.0±5.0[b]	3.109	19.777	204.521	462±34	446±17
MK-MAK-IF2-15	mugearite flow	22.9±0.2[a]	3.536	19.847	204.493	591±59	521±31
MK-AT2M-21	mugearite flow	33±12[c]	3.170	19.848	204.496	479±174	367±16
MK-AT2B-23	mugearite flow	33±12[c]	2.256	19.879	204.467	275±100	241±17
MK-AT3M-25	mugearite flow	55±7[c]	0.792	19.850	204.258	101±13	87±5
MK-AT3M-26	hawaiite flow	55±7[c]	0.792	19.850	204.210	101±13	105±6
MK-AT3T-28	hawaiite flow	55±7[c]	1.585	19.795	204.317	177±22	208±10
MK-AT3B-30	mugearite flow	55±7[c]	0.380	19.898	204.224	72±10	28±2

[a] Varnish ^{14}C age [54]; reported uncertainty reflects AMS measurement error only; the true uncertainty is estimated as ± 10% [54].

[b] Varnish cation-ratio age [54].

[c] Calculated from two K-Ar ages reported by Wolfe et al. [53].

[d] This uncertainty is due to uncertainty in age determination (column 3); ± 10% uncertainty in varnish ^{14}C ages was used.

[e] Normalized to chemical composition of sample MK-MAK-IF2-15. The experimental data points are also plotted on Fig. 3.6.

Test of the production parameters

In an effort to test the ^{36}Cl production rates determined using the White Mountain and Tabernacle Hill Flow samples, we have used these production rates to calculate the ages of two geomorphic surfaces of well-known or relatively well-constrained ages: (a) carbonate boulders ejected during the meteorite impact at Meteor Crater, Arizona and (b) boulders from a Tioga-age moraine in the Sierra Nevada, California.

Five dolomite samples from Meteor Crater, Arizona, were analyzed and the time of the meteorite impact calculated [55]. The mean age of 49.7 ± 0.85 ka is in spectacular agreement with the ages of 49.0 ± 3.0 ka obtained from thermoluminescence studies of shock-metamorphosed minerals [56] and of 49.2 ± 1.7 obtained using cosmogenic $^{26}Al/^{10}Be$ pair [57]. Varnish ^{14}C studies of the same material yielded "dead radiocarbon" which supports our results; low activity of ^{14}C results from decay and not from contamination by ancient carbonate carbon. The ^{36}Cl data are very consistent. Four out of five samples yielded almost identical ages, with standard deviation smaller than analytical uncertainty of the individual AMS measurements. The single anomalously young sample can be interpreted as being partially shielded by loose material or as having rolled over. This suite of samples indicates that given favorable geological conditions, such as low erosion rates in arid environments, the cosmogenic ^{36}Cl buildup method gives reliable and accurate exposure ages. It also shows that by appropriate scaling of the sea level production rates, the ^{36}Cl buildup method can be applied at

different elevations.

Four samples (Table 3.9) were obtained from a Tioga-age moraine at Bloody Canyon in the Mono Basin. The glacial geology of Bloody Canyon has been described by Sharp and Birman [58], Burke and Birkeland [59], and Gillespie [60]. Details of sample location and analytical results are given in [24] and [61]. Previous investigations of the sampled moraine indicate that its position is close to, or at, the maximum limit of the Tioga moraines. As described above, the Tioga advance is known to have occurred in the interval 25 ka to 11 ka, with the maximum in the earlier part of this interval [29, 31, 62, 63]. A limiting minimum varnish ^{14}C date of 18.9 ka was obtained for the maximum Tioga advance at Pine Creek [29]. The average (from 3 of the 4 ^{36}Cl buildup dates) of 21.2 ± 1.6 ka is in excellent agreement with this chronology. Although the Bloody Canyon results are not completely independent of the ^{36}Cl buildup calibration samples (because they are from correlative glacial deposits) the fact that appropriate ages are obtained for geographically distant samples offers considerable support for the validity of the new production parameters.

Miscellaneous considerations

Effective production rates of cosmogenic nuclides may be affected by partial or/and temporal shielding of the target surface from the cosmic rays. Partial shielding occurs near topographic features which block a part of the incident flux. The required

Table 3.9. Locations, scaling factors and ^{36}Cl ages for the Tioga samples, Bloody Canyon, California (modified from [61]).

Sample ID	Elevation (km)	Latitude °N	Longitude °E	$(ELD)_n$	$\Sigma\sigma_i N_i$ (cm^2/kg)	$^{36}Cl/Cl$ (10^{-15})	Boulder age (ka)	Moraine age (ka)
BC-86-1-Ti	2.38	37.9	240.8	5.56	4.97	1770±136	22.9	21.2±1.6
BC-86-2-Ti	2.38	37.9	240.8	5.56	4.06	402±17	12.0[a]	
BC-86-3-Ti	2.38	37.9	240.8	5.56	4.88	536±39	19.6	
BC-86-5-Ti	2.38	37.9	240.8	5.56	5.24	455±22	21.2	

[a] This boulder age was not used to calculate the moraine age.

correction ($F(\Theta)$) is a function of the slope (Θ) of a line connecting the top of the feature and the sampling site, and can be expressed as $(\sin\Theta)^{2.3}$ [51]. The production rates should be multiplied by ($F(\Theta)$) averaged over all horizontal directions (2π). This correction is usually small and approaches 15% for angles close to 45°. For all our samples the correction was smaller than 1.0 % and was therefore neglected.

Snow cover or volcanic ash can temporarily attenuate the cosmic-ray flux reaching rock surfaces. Nishiizumi et al. [51] have calculated that in the Sierra Nevada as much as 10 % decrease in nuclide production could have occurred on horizontal surfaces. In order to minimize this effect we sampled the tops of high boulders that should be rapidly swept free of snow or ash by the wind. The White Mountains are in the rain shadow of the Sierra Nevada and receive much less precipitation than the Sierra Nevada does [64]. Therefore, the effect of attenuation of the cosmic rays due to snow cover is considered to be negligible for all our calibration samples collected in the White Mountains.

The excellent agreement between varnish ^{14}C and ^{36}Cl ages indicate that snow or volcanic ash cover have also a negligible influence on the Mauna Kea samples. The Hawaiian samples were collected at locations where snow cover was unlikely to develop and persist for long periods of time, and away from places where volcanic tephra was observed to be present. They yielded ^{36}Cl ages nearly identical to the varnish ^{14}C ages (Table 3.6). Although temporal attenuation of the cosmic ray flux by snow or volcanic ash was not a problem in our study area it should not be overlooked; in all locations

where any covering material is significantly thick and persists for long periods of time, appropriate corrections for additional attenuation of the cosmic rays should be made.

Summary

Cosmogenic chlorine-36 buildup in rocks exposed at the surface of the earth was investigated and the production rates due to individual reactions quantified. Effective production rates due to spallation of ^{39}K and ^{40}Ca are $4,160 \pm 310$ and $3,050 \pm 210$ atoms ^{36}Cl per yr per mole ^{39}K and ^{40}Ca, respectively. These values, although considerably lower than those previously calculated, have been tested and appear to be valid for late Pleistocene conditions. An effective thermal neutron capture rate of $(3.07 \pm 0.24) \times 10^5$ neutrons per kg of rock per yr compares well with the present-day measured values.

Production of ^{36}Cl due to negative muon capture was investigated using two previously reported values of probability of the reaction leading to ^{36}Cl formation. The maximum sea-level production rate due to this process is less than 14% of that of spallation of calcium. This proportion becomes negligibly small at high (mountain) altitudes.

The latitudinal and altitudinal distribution of cosmic-ray intensity of Lal [15] is supported by agreement obtained between the ^{36}Cl buildup and ^{14}C and K/Ar dates. The new production rates were applied to dating rocks of various ages and at various

geomagnetic latitudes and elevations. The results are in excellent agreement with ages obtained by other means. They show that the cosmogenic ^{36}Cl dating method can be successfully applied for samples at differing geomagnetic latitudes and elevations by appropriate scaling of the reported sea-level rates.

The cosmogenic ^{36}Cl dates compare well with the ages obtained using different dating methods. Consistent production rates of ^{36}Cl were obtained using samples collected at different locations and independently dated by both varnish ^{14}C and classical ^{14}C techniques. The ^{36}Cl ages of the glacial moraines in the Sierra Nevada compare well with ^{14}C-dated organic material below and above correlative glacial sequences. Finally, cosmogenic ^{36}Cl dating of the impact at Meteor Crater yielded ages almost identical to the age obtained from independent studies. These results strengthen our confidence in the calculated production parameters and indicate that the cosmogenic ^{36}Cl geochronology can be successfully applied in the earth sciences.

Acknowledgements

This research was supported by the National Science Foundation grants EAR-8603440, SES-8901437, PHY-8515908, and PHY-8818281. We thank S.S. Smith and D. Elliott-Fisk for help in sample collection, E. Wolfe for help in sample collection and helpful comments, T. Cerling for supplying the Tabernacle Hill samples, L. Brandvold and the New Mexico Bureau of Mines and Mineral Resources for use of

laboratory facilities, W.X. Chavez Jr. for help in the mineral separations, S. Tullai-Fitzpatrick, R.T.D. Teng, and B.G. Jones for help during ^{36}Cl measurements, and D. Lal and T. Swanson for helpful discussions and comments.

References

1 R. Davis, Jr. and O.A. Schaeffer, Chlorine-36 in nature, Ann. N. Y. Acad. Sci. 62, 105-122, 1955.

2 D. Elmore and F.M. Phillips, Accelerator mass spectrometry for measurements of long-lived radioisotopes, Science 236, 543-550, 1987.

3 Rama and M. Honda, Cosmic-ray-induced radioactivity in terrestrial materials, J. Geophys. Res. 66 (10), 3533-3539, 1961.

4 D. Lal and B. Peters, Cosmic ray produced radioactivity on earth, in: Encyclopedia of Physics, S. Fluegge, ed., Vol. 46/2, Cosmic Rays II, K. Sitte, ed., pp. 551-612, Springer-Verlag, Berlin, Heidelberg, New York, 1967.

5 R. Jha and D. Lal, On cosmic ray produced isotopes in surface rocks, in: Natural Radiation Environment, K.G. Vohra et al., eds., Proc. Second Special Symp. on Natural Radiation Environment, pp. 629-635, Halsted Press, 1982.

6 D. Lal, Cosmogenic nuclides produced in situ in terrestrial solids, Nucl. Inst. Meth. Phys. Res. B29, 238-245, 1987.

7 Y. Yokoyama, J.-L. Reyss and F. Guichard, Production of radionuclides by cosmic rays at mountain altitudes, Earth Planet. Sci. Lett. 36, 44-50, 1977.

8 H.W. Bentley, F.M. Phillips and S.N. Davis, Chlorine-36 in the terrestrial environment, in: Handbook of Environmental Isotope Geochemistry, Vol. 2, The Terrestrial Environment, B.P. Fritz and J.-Ch. Fontes, eds., pp. 422-480, Elsevier, New York, 1986.

9 B.D. Leavy, Surface-exposure dating of young volcanic rocks using the in situ buildup of cosmogenic isotopes, 197 pp., Ph.D. dissertation, New Mexico Institute of Mining and Technology, 197 pp., 1987.

10 J.T. Fabryka-Martin, Production of radionuclides in the earth and their hydrogeologic significance, with emphasis on chlorine-36 and iodine-129, 400 pp., Ph.D. dissertation, University of Arizona, 1988.

11 R.E. Lingenfelter, Production of carbon 14 by cosmic-ray neutrons, Rev. Geophys. 1, 35-55, 1963.

12 D.C. Rose, K.B. Fenton, J. Katzman and J.A. Simpson, Latitude effect of the cosmic ray nucleon and meson components at sea level from the Arctic to the Antarctic, Canadian J. Phys. 34, 968-984, 1956.

13 M. Merker, E.S. Light, H.J. Verschell, R.B. Mendell and S.A. Korff, Time dependent world-wide distribution of atmospheric neutrons and of their products, 1. Fast neutron observations, J. Geophys. Res. 78, 2727-2740, 1973.

14 H. Moraal, M.S. Potgieter, P.H. Stoker and A.J. van der Walt, Neutron monitor latitude survey of cosmic ray intensity during the 1986/1987 solar minimum, J. Geophys. Res. 94 (A2), 1459-1464, 1989.

15 D. Lal, Cosmic ray tagging of erosion surfaces: *in situ* production rates and erosion

models, Submitted to Earth Planet. Sci. Lett.

16 D. Lal, Production of 3He in terrestrial rocks, Chem. Geology (Isotope Geosc. Section) 66, 89-98, 1987.

17 M. Kurz, In situ production of terrestrial cosmogenic helium and some applications to geochronology, Geochim. Cosmochim. Acta 50, 2855-2862, 1986.

18 M. Conversi, Experiments on cosmic-ray mesons and protons at several altitudes and latitudes, Phys. Rev. 79, 749-767, 1950.

19 B. Rossi, High Energy Particles, 569 pp., Prentice Hall, New Jersey, 1952.

20 H. Bilokon, G. Cini Castagnoli, A. Castellina, B. D'Ettore Piazzoli, G. Mannocchi, E. Meroni, P. Picchi and S. Vernetto, Flux of the vertical negative muons stopping at depths 0.35-1000 hg/cm2, J. Geophys. Res.94, 12, 145-152, 1989.

21 J.N. Andrews, S.N. Davis, J. Fabryka-Martin, J-Ch. Fontes, B.E. Lehmann, H.H. Loosli, J.-L. Michelot, H. Moser, B. Smith and M. Wolf, The in situ production of radio-isotopes in rock matrices with particular reference to the Stripa granite, Geochim. Cosmochim. Acta 53, 1803-1815, 1989.

22 F.M. Phillips, B.D. Leavy, N.D. Jannik, D. Elmore and P.W. Kubik, The accumulation of cosmogenic chlorine-36 in rocks: a method for surface exposure dating, Science 231, 41-43, 1986.

23 S. Charalambus, Nuclear transmutations by negative stopped muons and the activity induced by the cosmic-ray muons, Nucl. Phys. A166, 145-161, 1971.

24 M. G. Zreda, F. M. Phillips and S. S. Smith, Cosmogenic 36Cl dating of geomorphic surfaces, Hydrology Program Rept. 90-1, New Mexico Tech, Socorro,

1990.

25 D.L. Elliott-Fisk, Glacial geomorphology of the White Mountains, California and Nevada: establishment of a glacial chronology, Phys. Geography 8, 299-323, 1987.

26 R.I. Dorn, A.J.T. Jull, D.J. Donahue, T.W. Linick and L.J. Toolin, Accelerator mass spectrometry radiocarbon dating of rock varnish, Geol. Soc. Amer. Bull. 101, 1363-1372, 1989.

27 R.I. Dorn, A.J.T. Jull, D.J. Donahue, T.W. Linick and L.J. Toolin, Latest Pleistocene lake shorelines and glacial chronology in the western Basin and Range province, USA: Insights from AMS radiocarbon dating of rock varnish and paleoclimatic implications, Palaeogeogr., Palaeoclimat., Palaeoecol., In press.

28 D.S. Fullerton, Chronology and correlation of glacial deposits in the Sierra Nevada, California, in: Quaternary Glaciations in the Northern Hemisphere-Report of the International Geological Correlation Programme Project 24, V. Sibrava, D.Q. Bowen and G.M. Richmond, eds., pp. 161-169, Pergamon Press, 1986.

29 R.I. Dorn, B.D. Turrin, A.J.T. Jull, T.W. Linick and D.J. Donahue, Radiocarbon and cation-ratio ages for rock varnish on Tioga and Tahoe morainal boulders of Pine Creek, eastern Sierra Nevada, California, and their paleoclimatic implications, Quaternary Res. 28, 38-49, 1987.

30 L.K. Lebetkin, Late Quaternary activity along the Lone Pine fault, Owens Valley fault zone, California, 85 pp., M.S. Thesis, Stanford University, Stanford, California, 1980.

31 B.F. Atwater, D.P. Adam, J.P. Bradbury, R.M. Forester, R.K. Mark, W.R.

Lettis, G.R. Fisher, K.W. Gobalet and S.W. Robinson, A fan dam for Tulare Lake, California, and implications for the Wisconsin glacial history of the Sierra Nevada, Geol. Soc. Amer. Bull. 97, 97-109, 1986.

32 E. Bard, B. Hamelin, R.G. Fairbanks and A. Zindler, Calibration of the 14C timescale over the past 30,000 years using mass spectrometric U-Th ages from Barbados corals, Nature 345, 405-410, 1990.

33 S.B. Bachman, Pliocene-Pleistocene break-up of the Sierra Nevada-White-Inyo Mountains block and formation of Owens Valley, Geology 6, 461-463, 1978.

34 S.J. Martel, T.M. Harrison and A.R. Gillespie, Late Quaternary vertical displacement rate across the Fish Springs Fault, Owens Valley fault zone, California, Quaternary Research 27, 113-129, 1987.

35 C.G. Oviatt and W.P. Nash, Late Pleistocene basaltic ash and volcanic eruptions in the Bonneville basin, Utah, Geol. Soc. Amer. Bull. 101, 292-283, 1989.

36 T.E. Cerling, Dating geomorphologic surfaces using cosmogenic ^{3}He, Quaternary Res. 33, 148-156, 1990.

37 J.N. Walsh, F. Buckley and J. Baker, The simultaneous determination of the rare-earth elements in rocks using inductively coupled plasma source spectrometry, Chem. Geology 33, 141-153, 1981.

38 J.N. Walsh, Determination of boron at trace levels in rocks by inductively coupled plasma spectrometry, Analyst 110, 959-962, 1985.

39 P.J. Aruscavage and E.Y. Campbell, An ion-selective electrode method for determination of chlorine in geological materials, Talanta 28, 745-749, 1983.

40 H.N. Elsheimer, Application of an ion-selective electrode method to the determination of chloride in 41 international geochemical reference materials, Geostandards Newsletter 11, 115-122, 1987.

41 N.J. Conard, D. Elmore, P.W. Kubik, H.E. Gove, L.E. Tubbs, B.A. Chrunyk and M. Wahlen, The chemical preparation of AgCl for measuring ^{36}Cl in polar ice with accelerator mass spectrometry, Radiocarbon 28, 556-560, 1986.

42 D. Elmore, B.R. Fulton, M.R. Clover, J.R. Marsden, H.E. Gove, H. Naylor, K.H. Purser, L.R. Kilius, R.P. Beukins and A.E. Litherland, Analysis of ^{36}Cl in environmental water samples using an electrostatic accelerator, Nature 277, 22-25, 1979.

43 C.G. Montgomery and D.D. Montgomery, The intensity of neutrons of thermal energy in the atmosphere at sea level, Phys. Rev. 56, 10-12, 1939.

44 J.A. Simpson, Neutrons produced in the atmosphere by the cosmic radiations, Phys. Rev. 83 (6), 1175-1188, 1951.

45 L.D. Hendrick and R.D. Edge, Cosmic-ray neutrons near the earth, Phys. Rev. 145, 1023-1025, 1966.

46 M. Yamashita, L.D. Stephens and H.W. Patterson, Cosmic-ray-produced neutrons at ground level: neutron production rate and flux distribution, J. Geophys. Res. 71, 3817-3834, 1966.

47 J.N. Andrews, J.-Ch. Fontes, J.-L. Michelot and D. Elmore, In-situ neutron flux, ^{36}Cl production and groundwater evolution in crystalline rocks at Stripa, Sweden, Earth and Planet. Sci. Lett. 77, 49-58, 1986.

48 K. O'Brien, Secular variations in the production of cosmogenic isotopes in the earth's atmosphere, J. Geophys. Res. 84, 423-431, 1979.

49 R.C. Reedy and J.R. Arnold, Interaction of solar and galactic cosmic-ray particles with the moon, J. Geophys. Res. 77, 537-555, 1972.

50 M.D. Kurz, Cosmogenic helium in a terrestrial igneous rock, Nature 320, 435-439, 1986.

51 K. Nishiizumi, E.L. Winterer, C.P. Kohl, J. Klein, R. Middleton, D. Lal and J.R. Arnold, Cosmic ray production rates of ^{10}Be and ^{26}Al in quartz from glacially polished rocks, J. Geoph. Res. 94, 17,907-17,915, 1989.

52 A. Wyttenbach, P. Baertschi, S. Bajo, J. Hadermann, K. Junker, S. Katcoff, E.A. Hermes and H.S. Pruys, Probabilities of muon induced nuclear reactions involving charged particle emission, Nucl. Phys. A294, 278-292, 1978.

53 E. W. Wolfe, W. S. Wise and G. B. Dalrymple, The geology and petrology of Mauna Kea Volcano, Hawaii - a study of postshield volcanism, U.S.G.S. Prof. Pap., In press.

54 R.I. Dorn, F.M. Phillips, M.G. Zreda, E.W. Wolfe, A.J.T. Jull, P.W. Kubik and P. Sharma, Glacial chronology of Mauna Kea, Hawaii, as constrained by surface-exposure dating, Accepted for publication in National Geogr. J. Res.

55 F. M. Phillips, M. G. Zreda, S. S. Smith, D. Elmore, P. W. Kubik and R. I. Dorn, Dating the impact at Meteor Crater: Comparison of ^{36}Cl buildup and varnish ^{14}C with thermoluminescence, Submitted to Geochim. Cosmochim. Acta.

56 S.R. Sutton, Thermoluminescence measurements on shock-metamorphosed

sandstone and dolomite from Meteor Crater, Arizona: 2. Thermoluminescence age of Meteor Crater, J. Geoph. Research 90, 3690-3700, 1985.

57 K. Nishiizumi, C.P. Kohl, E.M. Shoemaker, J.R. Arnold, J. Klein, D. Fink and R. Middleton, ^{10}Be-^{26}Al exposure ages at Meteor Crater, Arizona, Submitted to Geochim. Cosmochim. Acta.

58 R.P. Sharp and J.H. Birman, Additions to classical sequence of Pleistocene glaciations, Sierra Nevada, California, Geol. Soc. Amer. Bull. 74, 1079-1086, 1963.

59 R.M. Burke and P.W. Birkeland, Reevaluation of multiparameter relative dating techniques and their application to the glacial sequences along the eastern escarpment of the Sierra Nevada, California, Quaternary Res. 11, 21-51, 1979.

60 A.R. Gillespie, Quaternary glaciation and tectonism in the southern Sierra Nevada, Inyo County, California, 695 pp., Ph.D. dissertation, California Institute of Technology, 1982.

61 F.M. Phillips, M.G. Zreda, S.S. Smith, D. Elmore, P.W. Kubik, and P. Sharma, A cosmogenic chlorine-36 chronology for glacial deposits at Bloody Canyon, Eastern Sierra Nevada, California, Science 248, 1529-1532, 1990.

62 D.P. Adam, Late-Pleistocene and recent palynology in the Sierra Nevada, California, in: Quaternary Palynology, E.J. Cushing, H.E. Wright Jr., eds., pp. 275-281, Yale University Press, New Haven, Connecticut, 1967.

63 L. Mezger and D. Burbank, The glacial history of the Cottonwood Lakes area, southeastern Sierra Nevada, Geol. Soc. Amer. Abstract with Programs 18, 157, 1986.

64 The California Water Atlas, W.L. Kahrl (ed.), pp. 113, California Governor's

Office, 1979.

Appendix - description of sampling sites

Sample 187 - Terminal moraine in Chiatovich Creek, White Mountains. Moderately weathered, fine-to-medium-grained granodiorite boulder, 0.6×0.3×0.6 m, sampled from the top surface. Varnish ^{14}C age is 9.74 ka [27]. Shielding angles of the surrounding valley walls are 10-15° in S, W, and N directions.

Sample 387 - Terminal complex in Chiatovich Creek, White Mountains. Strongly-to-moderately-weathered, medium-grained diorite, largest boulder on the ridge, 6.0×3.6×3.0 m, sampled from flat area on the top, more than 1 m from the edges. Varnish ^{14}C age is 12.51 ka [27]. Shielding angles of the surrounding valley walls are about 10° in S, W, and N directions.

Sample 787 - Maximum terminal moraine at steep drop off in Chiatovich Creek, White Mountains. Weakly-to-moderately-weathered, medium-grained monzonite, 1.2×1.2×0.6 m, sampled from the center of the flat, gently sloping (10° NW) area on the top. Varnish ^{14}C age is 17.78 ka [27]. Shielding angles of the surrounding valley walls are about 10-15° in S, W, and N directions.

Sample MK-MAKO-12 - Older Makanaka moraine close to hawaiite flow and covered by it, Mauna Kea, Hawaii. Basaltic boulder 1.5×1.5×4.0 m, sampled from the top surface, close to the edge. Varnish ^{14}C age is 21.5±0.2 ka [54].

Sample MK-MAKY-16 - Crest of outermost "Younger" Makanaka end moraine on top of hawaiite lava flow, Mauna Kea, Hawaii. Boulder 2 m tall, sampled close to the center of the top surface. Varnish age is 18.3±0.2 ka [54].

Sample MK-MAKT-29 - From about 50 m NE of Cal Tech 7mm observatory (aluminum dome), almost on the top of Mauna Kea, Hawaii. Glacially polished rock, about 1.5 m tall, sampled from the center of the subhorizontal top surface. Varnish ^{14}C age is 14.4±0.1 ka [54].

Sample MKW-5 - Top of the Waihu moraine, Mauna Kea, Hawaii. Rounded, very solid boulder, 2×2×2 m, sampled from the subhorizontal top surface. Cation-ratio age is 68±5 ka [54].

MK-MAK-IF2-15 - Interflow between "older" and "younger" Makanaka, Mauna Kea, Hawaii. 0.75×0.75×0.5 m boulder, sampled from the center of the subhorizontal top surface. Varnish ^{14}C age is 22.9±0.2 ka [54].

MK-AT2M-21 - Same flow as MK-MAK-IF2-15. Sample from the center of a large (10 m) sloping surface (15° slope). K-Ar age is 33±12 ka [53].

MK-AT2B-23 - The bottom of the same flow. Sampled close to the edge of the flow, about 1.3 m above the ground level. K-Ar age is 33 ± 12 ka [53].

MK-AT3M-25 - Puu Kee lava flow, Mauna Kea, Hawaii. Ridge about 2 m tall, sampled at the center of the sloping top surface (20° slope). K-Ar age is 55 ± 7 ka [average of 2 dates reported in 53].

MK-AT3M-26 - Same flow as MK-AT3M-25. Ridge about 1 m tall, sampled from the edge at the top. K-Ar age is 55 ± 7 ka [average of 2 dates reported in 53].

MK-AT3T-28 - Top of the flow about 500 m W of Puu Kee. Ridge about 1 m tall, sampled close to the edge of the subhorizontal top. K-Ar age is 55 ± 7 ka [average of 2 dates reported in 53].

MK-AT3B-30 - Bottom of Puu Kee flow at NW side of Puu, Mauna Kea, Hawaii. Ridge about 1 m tall, sampled far from the edge of the subhorizontal top. K-Ar age is 55 ± 7 ka [average of 2 dates reported in 53].

4. Cosmogenic chlorine-36 production rates in terrestrial rocks: An extended calibration

Abstract

Using 31 samples from well-dated lava flows in Craters of the Moon, Idaho and Tabernacle Hill, Utah, ejected boulders from Meteor Crater, Arizona, and well-constrained glacial samples from Wales, Banks Island, and Inuvik, I have refined the production rates for the cosmogenic ^{36}Cl dating method. I obtained the production parameters by two methods: (1) minimization of the average absolute deviation and (2) least-square solution of the overdetermined system of 31 equations in three unknowns; the results from these two methods are different by less than 10%. The calculated production rates of ^{36}Cl from ^{39}K and ^{40}Ca are 7520 and 2900 atoms ^{36}Cl $year^{-1}$ mol^{-1} K and Ca, respectively and the thermal neutron absorption rate is 313500 neutrons $(kg\ rock)^{-1}$ $year^{-1}$. The average absolute error associated with these parameters is $\sim 9\%$.

Introduction

Production rates of cosmogenic ^{36}Cl determined by Zreda et al. (1991) have been applied to dating glacial moraines (Phillips et al., 1990; Dorn et al., 1991), a meteorite crater (Phillips et al., 1991), and volcanic deposits (Zreda et al., 1993) and yielded ages

that are in reasonably good agreement with independent age estimates. All these studies, except one in Hawaii (Dorn et al., 1991), were performed in the Great Basin area, close to the calibration sites, and evaluation of the production rates at other latitudes was limited to only one location. Consequently, there existed a large margin for error when one attempted to date landforms far from the calibration location and more independently dated samples from different geographic latitudes were necessary to solve this problem.

In addition to spatial (latitudinal) variability of the production rates, there exists temporal variability associated with the changes of the earth magnetic field strength (e.g., Mazaud et al., 1991). These effects are largest at the equator and sea level, and decrease with distance toward the poles and with elevation to become negligible at latitudes $>60°$. For *in situ* cosmogenic studies, one needs to calculate time-integrated production rates and therefore samples of different ages need to be measured.

In this communication, I report measurements of cosmogenic ^{36}Cl in samples collected at latitudes between 20 and 70° and of ages between 2 and 55 ky. These well-dated samples provided a good base for calculating effective production rates of ^{36}Cl from its three main target elements - ^{39}K, ^{40}Ca, and ^{35}Cl - by minimizing the average absolute difference between the ^{36}Cl and the independent age estimates and also by the least square method.

Samples

Thirty-one samples (Table 4.1) were collected from the top 2 cm of rock surfaces using the field criteria described in Zreda et al. (1991). All samples have known ages, determined using conventional ^{14}C, K-Ar, thermoluminescence, and cosmogenic ^{26}Al-^{10}Be; varnish ^{14}C dated samples described in Zreda et al. (1991) have not been used because of a possible difference between varnish and ladform ages. The samples cover geographic latitudes from $\sim 20°N$ (Hawaii) to $> 60°N$ (the Arctic) and elevations from sea level to ~ 1800 m above sea level. Most of the samples (20 samples designated as COM92) come from late Pleistocene lava flows in Idaho (Fig. 4.1).

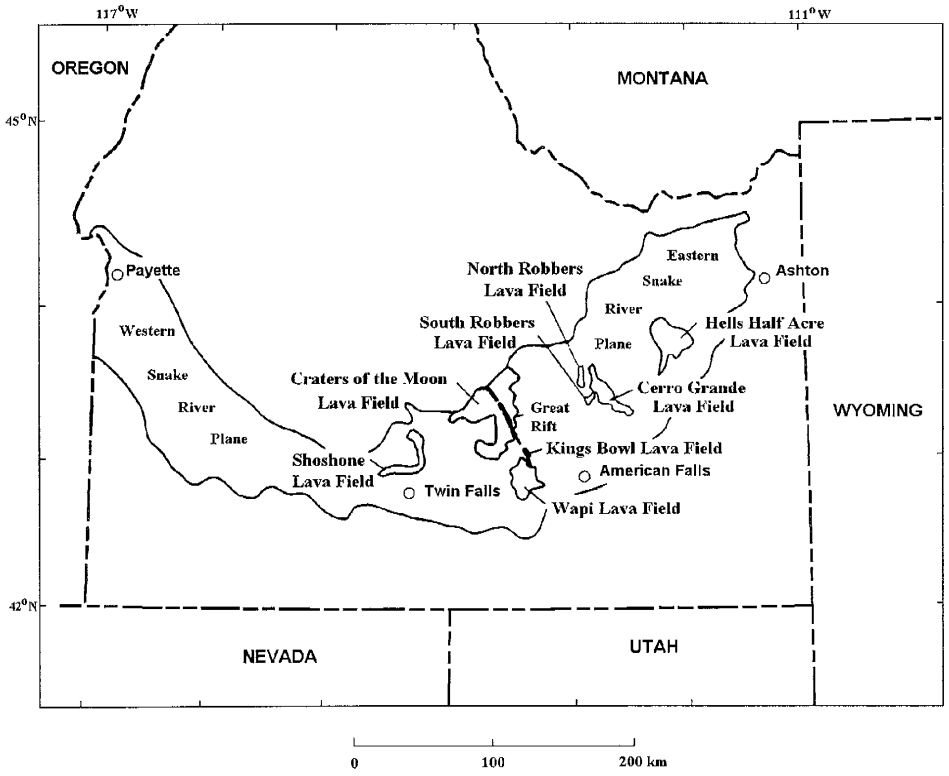

Fig. 4.1. General location map for the samples COM92 from Idaho.

Table 4.1. Locations and previously published dating results for the calibration samples. COM92, CW, BI, IN 9353, and 9354 samples were dated by ^{14}C, MC samples by thermoluminescence and cosmogenic ^{26}Al-^{10}Be, and MK sample by K/Ar.

Sample	Origin	Elevation (m)	Latitude (°N)	Longitude (°W)	ELD	Age (ky)	
						Reported	Calendar
COM92-1	lava flow	1367	43.75	112.20	3.00	5.200	5.7
COM92-2	lava flow	1367	43.75	112.20	3.00	5.200	5.7
COM92-3	lava flow	1367	43.75	112.20	3.00	5.200	5.7
COM92-4	lava flow	1707	43.10	113.05	3.87	15.100	17.7
COM92-5	lava flow	1707	43.10	113.05	3.87	15.100	17.7
COM92-6	lava flow	1707	43.10	113.05	3.87	15.100	17.7
COM92-7	lava flow	1777	43.35	113.05	4.07	2.205	2.2
COM92-8	lava flow	1777	43.35	113.05	4.07	2.205	2.2
COM92-9	lava flow	1777	43.35	113.05	4.07	2.205	2.2
COM92-11	lava flow	1798	43.25	113.25	4.08	7.840	8.8
COM92-12	lava flow	1798	43.25	113.25	4.08	7.840	8.8
COM92-13	lava flow	1798	43.25	113.25	4.08	7.840	8.8
COM92-14	lava flow	1740	43.40	113.00	3.96	12.760	13.7
COM92-15	lava flow	1740	43.40	113.00	3.96	12.760	13.7
COM92-16	lava flow	1740	43.40	113.00	3.96	12.760	13.7
COM92-18	lava flow	1390	43.00	114.40	3.05	10.130	11.4
COM92-19	lava flow	1390	43.00	114.40	3.05	10.130	11.4
COM92-20	lava flow	1402	43.00	114.40	3.08	10.130	11.4
COM92-21	lava flow	1402	43.00	114.40	3.08	10.130	11.4
COM92-22	lava flow	1402	43.00	114.40	3.08	10.130	11.4
CW-3	glacial	375	52	3	1.43	10.5	11.8
CW-7	glacial	375	52	3	1.43	10.5	11.8
BI92-17-BML	glacial	3	75	120	1.00	11.0	12.5
MC-1	meteor crater	1730	35.00	111.00	3.34	49 ± 3	49
MC-3	meteor crater	1700	35.00	111.00	3.27	49 ± 3	49
MC-4	meteor crater	1700	35.00	111.00	3.27	49 ± 3	49

MC-5	meteor crater	1730	35.00	111.00	3.34	49 ± 3	49
IN92-1-BR	glacial	~0	68	135	1.00	13.0	14.8
MK-AT3B-28	lava flow	1585	19.80	155.64	2.17	55 ± 7	55
9353	lava flow	1445	38.94	112.52	2.97	14.4±0.1	16.5
9354	lava flow	1445	38.94	112.52	2.97	14.4±0.1	16.5

Samples COM92-1, 2, 3 are from Hells Half Acre Lava Field, COM92-4, 5, 6 from Little Prairie Flow, COM92-7, 8, 9 from Blue Dragon Flow, COM 11, 12, 13 from Grassy Cone Lava Flow, COM92-14, 15, 16 from Sunset Flow, COM92-18 through 22 from Shoshone Field. They have been dated by conventional ^{14}C by Kuntz et al. (1986) whose ages range from ~2.2 to ~15.5 ky (Table 4.1). Most of these samples have either high Ca or Cl content or both, but some of them also contain up to 2% K_2O. This set should therefore yield the production rates from all three major target elements.

Two other basaltic rocks were collected at Tabernacle Hills, Utah (samples 9353 and 9354); their age is constrained by ^{14}C age of 14.3 ky below and 14.5 ky above the flow (Oviatt and Nash, 1989; Cerling, 1990). One additional lava flow sample comes from Mauna Kea (sample MK-AT3B-28); this lava flow was dated by K/Ar at 55±7 ky (Wolfe et al., unpublished report).

Four samples from ejected boulders at Meteor Crater, Arizona were also used for the calibration. The crater was dated at 49 ky by thermoluminescence (Sutton et al., 1985) and the ^{26}Al-^{10}Be pair (Nishiizumi et al., 1991). These samples have high Ca and

Cl content and almost no K and should therefore be very good for constraining the production rates from Ca and Cl.

To obtain the production rate from ^{39}K, two samples from glacial surfaces in Wales were analyzed. They are granitic boulders containing little Cl and Ca; consequently, most ^{36}Cl has been produced from ^{39}K. The age of these samples has been estimated at 10.5 ky by ^{14}C dating of underlying and overlying sediments (Phillips, personal communication).

The last two samples are from high latitude glacial surfaces at Inuvik (sample IN92-1-BR) and Banks Island (sample BI92-17-BML), in the Canadian High Arctic. Their ages have been estimated at 13 (Rampton, 1988) and 11 ky (Dyke, 1987), respectively, by ^{14}C dates of organic matter in associated sediments.

Results and discussion

The results of chemical and isotopic analyses are reported in Table 4.2. The production rates were calculated using two approaches: least absolute deviations (primary approach) and least squares (secondary method). In the primary approach, the average of absolute differences between the calculated ^{36}Cl ages and the independent age estimates t_{ind} (Table 4.1) was minimized, i.e., the right and left hand sides of the following expressions were compared:

$$(1) \qquad \frac{-1}{\lambda}\ln\left[1-\frac{(R-R_0)\lambda N}{ELD\left[\psi_K C_K+\psi_{Ca}C_{Ca}+\phi_n\frac{\sigma_{35}N_{35}}{\Sigma\sigma_i N_i}\right]}\right] = t_{ind}$$

The secondary method was based on a least-squares Levenberg-Marquardt algorithm and was used to solve the overdetermined system of 31 equations in three unknowns. The equations used were obtained by writing the production equation in the following form:

$$(2) \qquad C_K\psi_K+C_{Ca}\psi_{Ca}+\frac{\sigma_{35}N_{35}}{\Sigma\sigma_i N_i}\phi_n=\frac{(R-R_0)\lambda N}{ELD(1-e^{-\lambda t_{ind}})}$$

Table 4.2. Chemical and isotopic data, calculated ^{36}Cl ages, and absolute deviations between ^{36}Cl ages and independent age estimates for the calibration samples. These absolute deviations are calculated with the three production parameters that produced the smallest average absolute deviation: ϕ_n=313500, ψ_K=1600, and ψ_{Ca}=520.

Sample ID	Cl (ppm)	K_2O (%)	CaO (%)	$\Sigma\sigma N$ ($cm^2\ kg^{-1}$)	$^{36}Cl/Cl$ (10^{-15})	^{36}Cl age (ky)	abs_dev (%)
COM92-1	70	0.73	10.10	7.23	116 ± 8	5.6 ± 0.4	2.479
COM92-2	72	0.70	10.10	7.31	115 ±	5.6 ±	1.009
COM92-3	72	0.67	10.10	7.18	116 ± 5	5.7 ± 0.3	0.009
COM92-4	207	1.65	5.86	9.51	176 ± 17	16.6 ± 1.7	6.394
COM92-5	236	1.65	6.19	10.15	128 ± 6	12.9 ± 0.7	26.969
COM92-6	258	1.68	6.63	10.66	120 ± 8	12.6 ± 0.9	28.585
COM92-7	347	2.24	5.93	11.13	22 ± 4	1.9 ± 0.4	11.965
COM92-8	348	2.26	6.16	11.47	22 ± 2	1.9 ± 0.2	15.748
COM92-9	334	2.31	5.85	11.11	24 ± 2	2.1 ± 0.2	5.395
COM92-11	334	2.10	5.85	10.26	101 ± 10	10.9 ± 1.2	24.043
COM92-12	343	2.09	5.85	10.56	86 ± 4	9.5 ± 0.5	7.700
COM92-13	311	2.09	5.14	9.56	76 ± 7	7.8 ± 0.8	11.751

COM92-14	350	2.03	6.23	11.82	141 ± 9	17.8 ± 1.2	29.587
COM92-15	340	2.09	6.02	10.91	122 ± 12	14.4 ± 1.5	5.011
COM92-16	322	2.00	5.79	11.21	117 ± 7	13.9 ± 0.9	1.188
COM92-18	80	0.84	9.51	7.38	249 ± 16	13.6 ± 0.9	19.039
COM92-19	78	0.77	9.25	7.32	211 ± 19	11.4 ± 1.1	0.405
COM92-20	99	0.84	9.50	7.39	241 ± 18	15.1 ± 1.1	32.730
COM92-21	96	0.88	9.51	7.46	177 ± 18	10.6 ± 1.1	6.877
COM92-22	87	0.88	9.35	7.47	195 ± 9	11.1 ± 0.5	2.993
CW-3	18	3.20	0.03	6.80	403 ± 50	12.9 ± 2.0	9.423
CW-7	6	5.30	0.02	7.20	1511 ± 164	11.6 ± 1.3	2.083
BI92-17-BML	218	0.29	11.60	7.23	44 ± 4	12.5 ± 1.1	0.001
MC-1	143	0.47	21.13	2.26	1462 ± 44	48.5 ± 1.6	1.071
MC-3	217	0.43	29.21	2.61	1280 ± 57	49.3 ± 2.4	0.698
MC-4	132	0.78	23.78	2.70	1469 ± 71	47.3 ± 2.4	3.529
MC-5	259	0.44	28.16	2.46	1207 ± 38	48.8 ± 1.6	0.389
IN92-1-BR	74	0.03	50.50	2.47	421 ± 29	15.7 ± 1.2	12.948
MK-AT3B-28	209	1.47	7.04	7.58	365 ± 17	57.5 ± 2.9	4.635
9353	94	0.86	10.93	6.40	244 ± 16	13.5 ± 0.9	6.244
9354	111	0.78	10.69	6.79	226 ± 15	14.7 ± 1.0	2.087
AVERAGE							8.907

The production rates obtained using these two methods are presented in Table 4.3. The respective values agree within $< 10\%$, which indicates that a sufficient number of samples was used in the calculations and the obtained average values of the production parameters are statistically meaningful. While the values of the thermal neutron absorption cross section (ϕ_n) and the production rate due to spallation of ^{40}Ca (ψ_{Ca}) are virtually the same as in Zreda et al. (1991), the production rate for spallation of ^{39}K (ψ_K) is significantly higher than the value of 885 previously reported (Zreda et al., 1991).

This is likely because the boulders used by Zreda et al. (1991) had ages younger than the moraine age. New samples from that calibration site have higher ^{36}Cl content than those reported by Zreda et al. (1991) and if they had been used by Zreda et al. (1991), they would have resulted in a production rate from ^{39}K close to that reported here.

Table 4.3. Production rates of thermal neutrons (ϕ_n) and of ^{36}Cl from ^{39}K (ψ_K)and ^{40}Ca (ψ_{Ca}).

Production parameter	Absolute deviation method	Least squares method
ϕ_n [neutrons (kg rock)$^{-1}$ y^{-1}]	313500	312600
ψ_K [atoms (kg rock)$^{-1}$ y^{-1} (%K_2O)$^{-1}$]	1600	1450
ψ_{Ca} [atoms (kg rock)$^{-1}$ y^{-1} (%CaO)$^{-1}$]	520	569

The values obtained by the primary method (absolute deviation method) will be used in the future to obtain surface exposure ages. The individual absolute deviations for the final set of production parameters are shown in the last column in Table 4.2; they range from $\sim 0\%$ to $\sim 32\%$ with the average of 8.907%. The internal consistency of these production rates is demonstrated in a plot of ^{36}Cl ages versus the independent age estimates (Fig. 4.2) in which the samples form a straight line with the slope almost exactly 1 and zero intercept.

Samples of all ages are positioned close to the 45° line, which demonstrates that temporal variability in the cosmic-ray flux does not affect greatly time-integrated production rates at these geographic latitudes. Any possible variability of this nature is on the same order as the analytical uncertainty and cannot be seen in this data set. We

therefore conclude that constant, time-integrated production rates can be used in surface-exposure calculations. A similar result was reported by Cerling and Craig (submitted) who measured cosmogenic ^{3}He and found that the maximum temporal variability of the integrated production rate is less than 15% for deposit ages less than 15 ky, and becomes negligible for older surfaces.

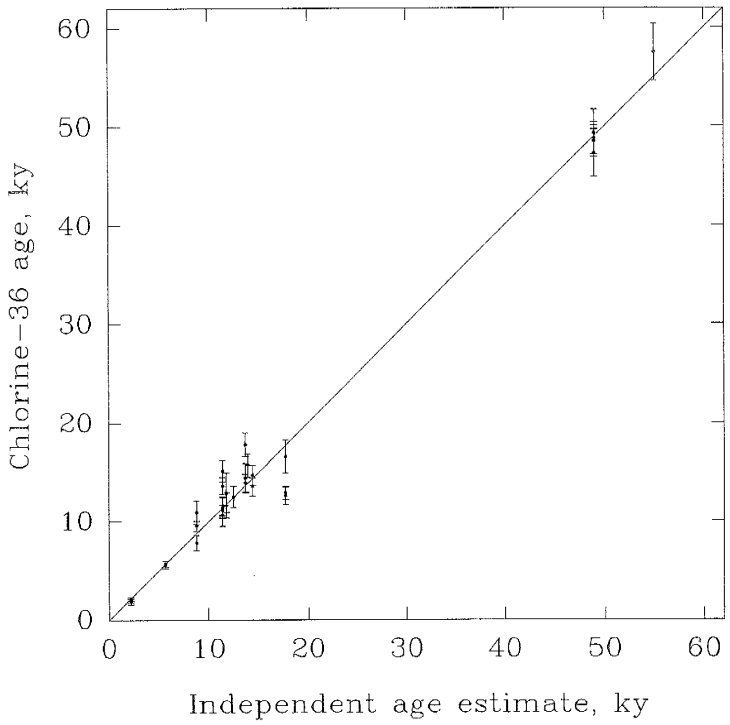

Fig. 4.2. Comparison of ^{36}Cl and independent age estimates for the calibration samples.

The overall error associated with the parameters should be on the same order as the average absolute deviation, i.e., ~9%, but the individual uncertainties may be different for all three production rates. A clue for the individual errors may be obtained from a sensitivity analysis, by examining how fast the absolute deviation changes around its minimum value when the production parameters change. The production rates were changed, one at a time, from 0.5 times to 1.5 times of their optimum values. The

average absolute deviation, divided by the smallest value, was then calculated and graphed in Figure 4.3. The graph for spallation of ^{40}Ca is narrowest of the three, which shows that this production rate is well constrained by the samples and should therefore have small error. On the other hand, the production rate from ^{39}K will have largest error of the three because the minimum value of the absolute deviation is reached more slowly

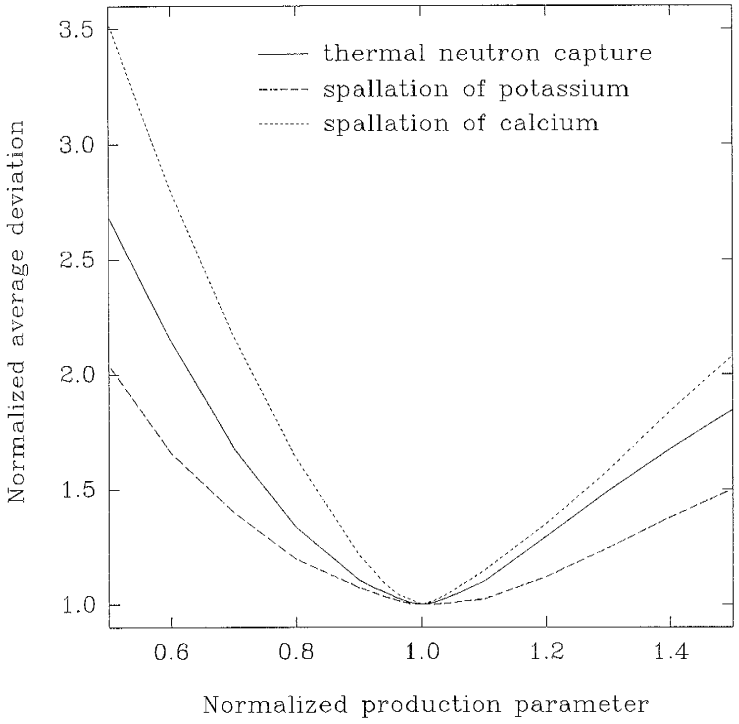

Fig. 4.3. Average absolute deviation as a function of production rates. Each line was calculated by changing the production rate between half and one and a half of its calculated optimum value while keeping the other two production parameters constant. The steepness of the lines around the minimum indicates well-constrained parameters and vice versa. In this case, the production rate from ^{40}Ca is more accurately estimated than that from ^{39}K. Normalized production parameter is the production rate used in the sensitivity analysis divided by the optimum value; the value of 1.0 is for the optimum values of the production rates. Normalized average deviation is the average absolute deviation calculated in the sensitivity analysis divided by the optimum (minimum) value obtained for the optimum production rates; the value of 1.0 reflects the minimum absolute deviation for the optimum production rates.

from both sides of the minimum and the graphed function is widest for this parameter. It is probably due to small number of samples in which spallation of ^{39}K is the major mechanism for cosmogenic ^{36}Cl formation. Only two samples from Wales had high enough concentration of K and these two samples were dominant in calculation of this production rate. In contrast, production rates from ^{35}Cl and ^{40}Ca are based on larger number of samples and are thus better constrained.

Summary

Thirty-one independently dated samples (age from 2 ky through 55 ky) have been analyzed for cosmogenic ^{36}Cl. The production rates from the three main target elements were calculated using minimization of absolute deviations between the ^{36}Cl ages and those obtained by independent means. The thermal neutron absorption cross section (ϕ_n) of 313500 neutrons per kg of rock per year and the production rate from ^{40}Ca (ψ_{Ca}) of 2900 atoms of ^{36}Cl per kg of rock per year per percent CaO are virtually identical to the previous estimates of Zreda et al. (1991). In contrast, the production rate from ^{39}K (ψ_K) of 7520 atoms of ^{36}Cl per kg of rock per year per percent K_2O is significantly higher than previously reported. Difficulties in dating samples used by Zreda et al. (1991) for calculation of this parameter can explain the discrepancy.

The average absolute deviation associated with these production rates is about 9%. The errors of the three individual production parameters are different; the highest

uncertainty should be expected for ψ_K and lower for the other two production rates. Consequently, ^{36}Cl ages of samples with unusually high K content may have larger uncertainty than those of samples with significant contributions from the other two target elements.

The temporal variability of the cosmic-ray flux does not affect the integrated production rates significantly and can therefore be neglected in calculations of surface exposure dating.

References

Cerling, T.E., 1990, Dating geomorphological surfaces using cosmogenic ^{3}He, Quaternary Res. 33, 148-156.

Cerling, T.E. and H. Craig, Cosmogenic ^{3}He production rates from 39°N to 46°N latitude, Submitted to Geochim. Cosmochim. Acta.

Dorn, R.I., F.M. Phillips, M.G. Zreda, E.W. Wolfe, A.J.T. Jull, P.W. Kubik and P. Sharma, 1991, Glacial chronology of Mauna Kea, Hawaii, as constrained by surface-exposure dating, Natl. Geogr. Res. Explor. 7, 456-471.

Dyke, A.S., 1987, A reinterpretation of glacial and marine limits around the northwestern Laurentide Ice Sheet, Can. J. Earth Sci. 24, 591-601.

Kuntz, M.A, E.C. Spiker, M. Rubin, D.E. Champion and R.H. Lefebvre, 1986, Radiocarbon studies of latest Pleistocene and Holocene lava flows of the Snake

River Plain, Idaho: Data, lessons, interpretations, Quaternary Res. 25, 163-176.

Mazaud, A., C. Laj, E. Bard, M. Arnold and E. Tric, 1991, Geomagnetic field control of ^{14}C production over the last 80 ky: Implications for the radiocarbon time-scale, Geophys. Res. Lett. 18, 1885-1888.

Nishiizumi, K., C. P. Kohl, E. M. Shoemaker, J. R. Arnold, J. Klein, D. Fink, and R. Middleton, 1991, ^{10}Be-^{26}Al Exposure Ages at Meteor Crater, Arizona, Geochim. Cosmochim. Acta 55, 2699-2703.

Oviatt, C.G and W.P. Nash, 1989, Late Pleistocene basaltic ash and volcanic eruptions in the Bonneville basin, Utah, Geol. Soc. Amer. Bull. 101, 292-303.

Phillips, F. M., M. G. Zreda, S. S. Smith, D. Elmore, P. W. Kubik and P. Sharma, 1990, Cosmogenic chlorine-36 chronology for glacial deposits at Bloody Canyon, eastern Sierra Nevada, California, Science 248, 1529-1532.

Phillips, F. M., M. G. Zreda, S. S. Smith, D. Elmore, P. W. Kubik, R. I. Dorn and D. Roddy, 1991, Age and geomorphic history of Meteor Crater, Arizona, from cosmogenic ^{36}Cl and rock varnish ^{14}C. Geochim. Cosmochim. Acta 55, 2695-2698.

Rampton, V.N., 1988, Quaternary geology of the Tuktoyaktuk coastlands, Northwest Territories, Geol. Survey Can. Mem. 423, pp. 1-98.

Sutton, S.R., 1985, Thermoluminescence measurements on Shock-metamorphosed sandstone and dolomite from Meteor Crater, Arizona: 2. Thermoluminescence age of Meteor Crater, J. Geophys. Res. 90, 3690-3700.

Wolfe, E.W., W.S. Wise and G.B. Dalrymple, In press (1991), The geology and

petrology of Mauna Kea Volcano, Hawaii - a study of postshield volcanism, U.S.G.S. Prof. Pap.

Zreda, M.G, F.M. Phillips, D. Elmore, P.W. Kubik, P. Sharma and R.I. Dorn, 1991, Cosmogenic chlorine-36 production rates in terrestrial rocks, Earth Planet. Sci. Lett. 105, 94-109.

Zreda, M. G., F. M. Phillips, P. W. Kubik, P. Sharma, and D. Elmore, 1993, Eruption age at Lathrop Wells, Nevada, from cosmogenic ^{36}Cl accumulation, Geology 21, 57-60.

older, the natural variability among boulders becomes the major contributor to the total variance, and eventually the analytical component becomes negligible. This natural boulder-to-boulder variability is due to removal of soil and gradual exposure of boulders at the surface. In the gradual exposure model that we develop, boulder depths below the soil surface change in time. Because the cosmic ray intensity changes with depth, the boulders are subjected to variable production rates of the cosmogenic ^{36}Cl. Each boulder's initial depth and chemical composition are also variable which results in different amounts of the accumulated cosmogenic ^{36}Cl and thus different apparent ages of boulders. The shape of the resulting distribution of the apparent ages and the coefficient of variation depend on the erosion depth, while the first moment is a function of the true surface age and the erosion depth. These properties of the apparent age distributions permit calculation of the surface age, the erosion depth and also the average erosion rate. We tested the model calculations using 26 boulders from a late Pleistocene moraine in Bishop Creek, Sierra Nevada, California. The set exhibited a bi-modal distribution of the ^{36}Cl surface exposure ages. We interpreted the older mode as the result of gradual exposure and the younger one as the result of surficial processes other than soil removal. The 10 samples that constitute the older mode produced a distribution which matches almost exactly the modeled distribution calculated using an age of 85 ky and erosion depth of 570 g cm^{-2}. This age is the same as an independent estimate obtained from cation-ratio studies and the calculated erosion depth is very close to the erosion depth of 600 g cm^{-2} based on a simple analytical erosion model. These results confirm that our statistical model adequately describes effects of soil erosion on

5. Cosmogenic ^{36}Cl accumulation in unstable landforms: II. Monte Carlo simulations and experimental observations on eroding moraines

MAREK G. ZREDA AND FRED M. PHILLIPS

Geoscience Department, New Mexico Tech, Socorro, NM 87801

DAVID ELMORE

Physics Department PRIME Laboratory, Purdue University, West Lafayette, IN 47907

Abstract

Cosmogenic ^{36}Cl surface exposure ages obtained for multiple boulders from single landforms are usually characterized by a variance larger than that of the analytical methods employed. This excessive variability is progressively more profound with increasing age of landforms. We decomposed the total variance into two components, the analytical and natural (geological) variability, using nested analysis of variance. For young landforms, the analytical uncertainty is the dominant component of the total variance associated with the calculated mean landform age. As the surface ages grow

---

In press, Water Resources Research, 1994.

accumulation of cosmogenic ^{36}Cl. The approach can be used to simultaneously obtain the true landform age and the erosion rate from apparent ^{36}Cl ages and therefore may help in evaluation of surface exposure ages of eroding landforms.

Introduction

Landforms are evidence of the diverse geological processes shaping the surface of the earth. Different geomorphic surfaces form under different environmental conditions and these conditions can generally be inferred from detailed studies of the landforms. Analysis of a succession of landforms can provide information about changes of local paleoenvironmental conditions. In many cases, a fundamental goal in paleoenvironmental analysis is to determine the age of landform formation, but until recently few numerical dating tools were available for this purpose. Ideally, with sufficient information from a landform, one could learn not only about its formation time but also about its subsequent geological history.

Numerical dating of geomorphic surfaces has been significantly advanced in the past decade and several new methods have been developed. One of these methods is based on accumulation of cosmic-ray-induced ^{36}Cl in rocks exposed at the surface of the earth (Phillips et al., 1986). The basis of this method in cosmic-ray physics has been described by Davis and Schaeffer (1955), Lal and Peters (1967), Phillips et al. (1986), Fabryka-Martin (1988), and Zreda et al. (1990). This method has been recently

calibrated (Zreda et al., 1991) and applied to dating late Pleistocene moraines (Phillips et al., 1990, 1993), a meteor impact crater (Phillips et al., 1991), and volcanic deposits (Zreda et al., 1993). These studies, although successful, revealed certain limitations of the cosmogenic ^{36}Cl method and inspired further investigations of the underlying mechanisms and assumptions.

Generally, it has been assumed that due to erosion of landforms and successive exposure of fresh material to cosmic radiation, apparent ages calculated using a single cosmogenic nuclide underestimate the true age and therefore constitute only minimum constraining ages. The true construction age can potentially be calculated by using two or more cosmogenic nuclides with distinctly different half-lives, for instance ^{10}Be with $t_{1/2}$ of 1.6 My and ^{26}Al with $t_{1/2}$ of 705 ky. Using this approach, the two nuclide production equations can be solved for the two unknowns, the time of the landform formation and the erosion rate. In this paper, we present an alternative, single-nuclide approach to calculating ages of eroding landforms. It is based on multiple ^{36}Cl age determinations and statistical analysis of the obtained data set. The objectives of this paper are: (1) to optimize sampling and analytical strategy for the cosmogenic ^{36}Cl dating of geomorphic surfaces by examination of sources of errors associated with the apparent age calculation, (2) to evaluate effects of soil erosion on the distribution of ^{36}Cl ages, and (3) to propose a potential method to simultaneously obtain the time of a landform creation and an estimate of the erosion rate and thus the erosion depth.

Statistics of cosmogenic ^{36}Cl data distributions

Phillips et al. (1990) have dated a sequence of moraines at Bloody Canyon, Sierra Nevada, California and nearby Bishop Creek (Phillips et al., 1993) by using cosmogenic ^{36}Cl accumulation in boulders exposed at the surface along moraine crests. The results are supported by ^{14}C and cation-ratio measurements on desert varnish and are consistent with both the marine record of global glaciation based on ^{18}O (Imbrie et al., 1984; Martinson et al., 1987) and continental stable isotope indicators of climatic changes (Winograd et al., 1992). In these studies, detailed investigation of the numerical dates for single surfaces indicates that for young landforms most of the boulders sampled yielded consistent results while only a few gave younger apparent ages. In the case of older surfaces, the data points are distributed approximately evenly between the minimum and maximum values. The authors interpreted the maximum values as the true ages of the landforms, whereas the younger ages as the results of continuing geological degradation of landforms by processes such as soil erosion, boulder surface spalling and erosion, and changing geometry due to rolling of boulders.

Part of the boulder-to-boulder variability may also be due to analytical uncertainty in the ^{36}Cl measurement. The routine accelerator mass spectrometry (AMS) analysis of ^{36}Cl consists of several individual measurements which are combined to yield the final mean ratio $^{36}Cl/Cl$ and the estimated variance. Typically, several consecutive 15-second counting intervals are averaged to yield a cycle mean, two cycles (separated by

measurements on stable chlorine) are combined in a sequence, and two sequences (separated by measurements on standards, blanks, and other samples) are combined in a run. The run value is the final result and is used to calculate the surface exposure age of the boulder. Several boulder ages from a landform surface are then interpreted and the surface age calculated. A nested design (Snedecor and Cochran, 1967) will be used in this paper to decompose the over-all variance into the contributions at each level. A schematic of the nested procedure, with the lowest level (15-second counting intervals) omitted, is presented in Figure 5.1 and the general nested ANOVA table with three levels is in Appendix A. Because both sequences and cycles are associated with analytical

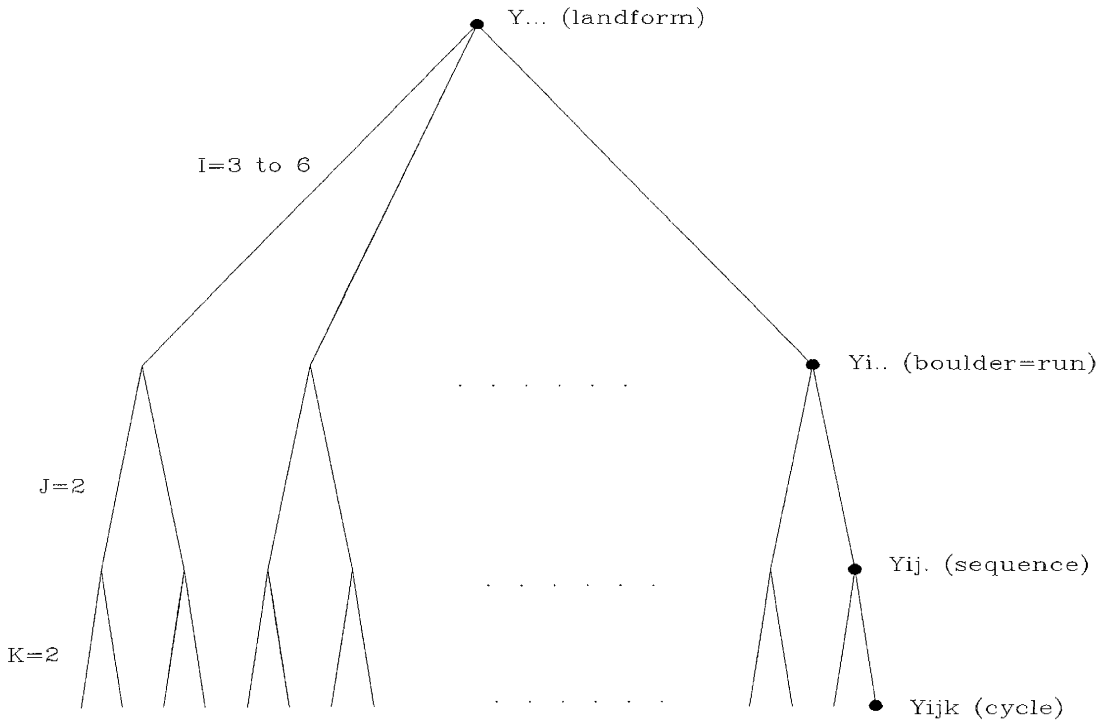

Fig. 5.1. Schematics of the three-level nested analysis of variance used for decomposition of the total variance into analytical and natural components.

uncertainty of AMS measurements, we further simplify the computations by combining them into one level, the "analytical" component of the total variance. The second level, or "geological" component, is due to the natural variability among boulders. The simplified two-level ANOVA layout is presented in Appendix B. In the nested analysis of variance, I is the number of runs (samples), J is the number of sequences, and K is the number of cycles.

For the nested analysis of variance, we used ^{36}Cl AMS data, converted to numerical ages (Table 5.1), for 16 different glacial surfaces in Bishop Creek, Sierra Nevada, California (for dating results, see Phillips et al., 1993). The entries in Table 5.1 represent weighted averages calculated from the lower level (cycles), as shown in Figure 5.1, and they incorporate all variabilities at the two lower levels, cycles and 15-second counting intervals. The nested analysis of variance for each of the 16 surfaces indicates that the two components of the total variance, "geological" and "analytical", are different for moraines of different ages (Table 5.2 and Figure 5.2). We observe a positive correlation between the age of the surface and the boulder-to-boulder variability. For youngest surfaces, this variability is usually relatively small with the major component of the total variance of the calculated cosmogenic ^{36}Cl ages being due to analytical uncertainty of the AMS measurements. As the surfaces become older, an increasing percentage of the total variance is due to the variability between boulders, while the analytical component becomes progressively less important. We attribute the boulder-to-boulder variability to postdepositional processes occurring on the surfaces of

the moraines. The higher variability among boulders from older surfaces is expected because older surfaces have been subjected to degradational processes for longer time.

Table 5.1. Cosmogenic ^{36}Cl ages calculated from weighted AMS data and used for the nested analysis of variance. Two analyses (columns), each of which is from averaging two or more cycles (not shown here), constitute a run. The number of runs varies from three to six and equals the number of boulders collected from each surface. Dashes indicate no sample.

Surface designation	Boulder ages from single sequences, ky					
TA	112	119	91	84	106	105
	119	125	94	97	116	135
PTa1	110	62	80	47	120	---
	121	67	85	52	136	---
SH	28	49	45	115	78	82
	31	53	49	124	87	89
Ti	16	15	13	---	---	---
	18	17	15	---	---	---
Ti2	14	14	13	13	---	---
	16	16	16	16	---	---
PTa3	137	87	97	104	90	132
	158	104	106	112	99	147
PTi1	101	87	62	90	103	---
	109	92	70	100	111	---
PTi7	56	69	72	77	---	---
	61	74	83	88	---	---
PTi6	102	51	71	78	44	---
	108	58	75	83	48	---
PTi4	104	59	49	108	92	---
	114	66	54	120	100	---
PTi3o	118	53	52	105	98	---
	128	58	58	111	103	---
OPB	83	113	88	78	99	---
	91	122	97	85	105	---
PTi5	80	82	73	63	78	---
	87	89	80	67	82	---

PTi8o	62	65	75	68	---	---
	70	71	88	74	---	---
PTi8y	16	16	16	---	---	---
	17	19	17	---	---	---
Ti1y	14	15	15	---	---	---
	16	17	17	---	---	---

We fitted a straight line of the form ax+b and an exponential function of the form $a\text{-}e^{-bx}$ to the data in Figure 5.2. On one hand, the linear fit yielded an intercept of about 0.1 which may represent natural variability of ^{36}Cl content in boulders at the time of deposition. This variability can be explained by the difference in chemical composition of rocks and associated background ^{36}Cl content, previous exposure to cosmic rays in the rock outcrops before incorporating the boulders into moraines, or differences in exposure

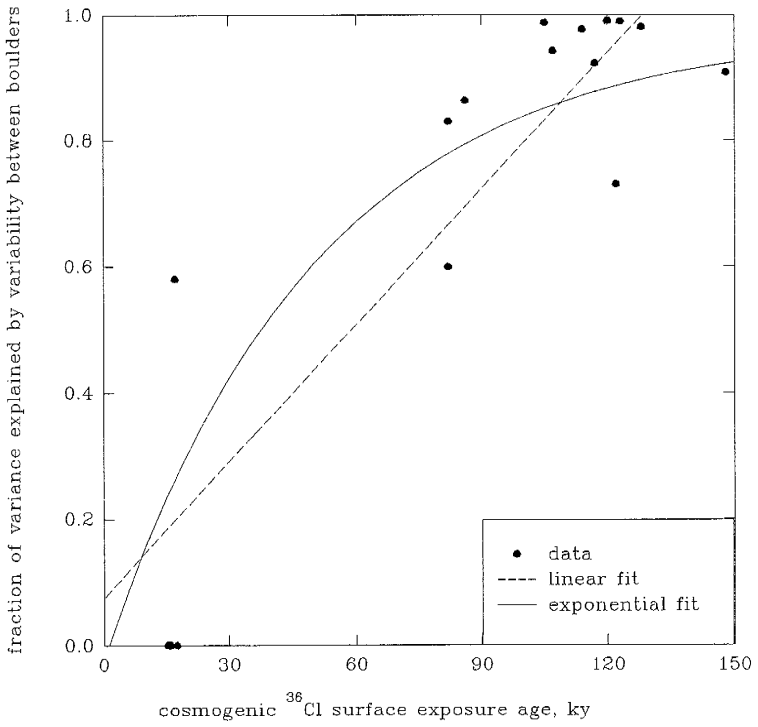

Fig. 5.2. Relationship between landform age and fraction of the total variance explained by natural variability among boulders.

Table 5.2. Analytical (σ^2_S/IJ) and natural (σ^2_R/I) components of the total variance of ^{36}Cl surface exposure ages for moraines from Bishop Creek, Sierra Nevada, California. Nested analysis of variance (Appendix B) was used for variance decomposition.

Surface ID	Age[a] ky	σ^2_S	σ^2_R	Components of variance		
				σ^2_S/IJ (analytical)	σ^2_R/I (natural)	Fraction natural
TA	122	102	138	8.52	23.0	0.730
PTa1	128	45.2	1083	4.52	217	0.980
SH	120	21.0	1064	1.75	177	0.990
Ti	17.1	1.53	1.06	0.256	0.352	0.580
Ti2	15.3	2.65	<0	---	---	0
PTa3	148	98.4	488	8.20	81.3	0.908
PTi1	107	31.7	255	3.17	51.0	0.942
PTi7	82	35.5	89.1	4.56	22.3	0.830
PTi6	105	14.2	529	1.42	106	0.987
PTi4	114	38.2	769	3.82	154	0.976
PTi3o	123	22.2	970	2.22	194	0.989
OPB	117	31.1	185	3.11	37.0	0.922
PTi5	86	17.9	56.5	1.79	11.3	0.863
PTi8o	82	38.1	28.5	4.77	7.12	0.599
PTi8y	17.5	1.91	<0	---	---	0
Ti1y	16	1.46	<0	---	---	0

[a] Oldest age from given surface.

during transport between the source area and the depositional location. On the other hand, the exponential fit goes almost exactly through the origin and better represents the data. It means that boulders on a single moraine do not have any previously accumulated ^{36}Cl and this is in agreement with one of the major assumptions of the cosmogenic ^{36}Cl

method. This model's asymptotic behavior at long exposure age is also preferred to that of the linear model.

These results suggest that for most landforms, the natural variability among collected rock samples is more significant than analytical uncertainty of the AMS measurement. This observation is of importance for future applications of cosmogenic nuclide dating techniques because it can aid in development of better sampling and analytical strategies. The quality of the dating can be improved by minimizing the total variance which can be achieved using detailed statistical analysis of the obtained cosmogenic ^{36}Cl data set.

As an example of variance minimization, we look in a detail at the three-level nested analysis of variance, as shown in Appendix A, executed for moraine TA from Table 5.1. This experiment has six runs (I=6), two sequences in each run (J=2), and

Table 5.3. Cosmogenic ^{36}Cl ages calculated from single cycles in AMS analysis for surface TA from Bishop Creek, Sierra Nevada, California.

Sample ID	Sequence #1		Sequence #2	
	Cycle #1	Cycle #2	Cycle #1	Cycle #2
TA1	118	106	123	115
TA2	120	118	125	126
TA3	91	91	91	97
TA4	80	88	93	101
TA5	95	117	125	103
TA6	101	109	131	139

two cycles in each sequence in each run (K=2); the data are presented in Table 5.3. A linear model of the form

$$Y_{ijk} = \mu + R_i + S_{ij} + C_{ijk} \quad (1)$$

is used in the calculations. In this equation Y_{ijk} is a random variable representing single data points (numbers in Table 5.3), μ is the overall mean (μ=const), R_i, S_{ij}, and C_{ijk} are random variables representing values at the level of run, sequence, and cycle, respectively, with means zero and variances σ_R^2, σ_S^2, and σ_C^2.

Table 5.4. Nested analysis of variance for the cosmogenic ^{36}Cl dates calculated for moraine TA from Bishop Creek, Sierra Nevada, California.

Source	SS	DF	MS	E[MS]
Factor I = run	3810.2	5	762.0	$\sigma_C^2 + 2\sigma_S^2 + 4\sigma_R^2$
Factor J = sequence	1233.3	6	205.5	$\sigma_C^2 + 2\sigma_S^2$
Factor K = cycle	736.5	12	61.4	σ_C^2
TOTAL	5780.0	23	---	---

The results of the three-level nested analysis of variance are in Table 5.4. From the formulas for the expected value of mean squares (last column in Table 5.4), the following variances are calculated: (1) between the cycles: $\sigma_C^2 = 61.4$, (2) between the sequences: $\sigma_S^2 = 72.1$, and (3) between the runs: $\sigma_R^2 = 139.1$. The estimates of the overall mean and the variance associated with this mean are expressed as follows

$$\bar{Y}_{...} = \mu + \bar{R}. + \bar{S}.. + \bar{C}... \quad (2)$$

$$var(\bar{Y}...) = var(\mu + \bar{R}. + \bar{S}.. + \bar{C}...) = \frac{\sigma_R^2}{I} + \frac{\sigma_S^2}{IJ} + \frac{\sigma_C^2}{IJK} \quad (3)$$

where the dots indicate summation over i, j, or k index and the bar denotes average values. For the example above (I=6, J=2, K=2), the estimate of the total variance is presented in Table 5.5. In this case the variability between runs (i.e., boulders) contributes the most to the overall variance, while the variabilities at the sequence and cycle levels are relatively less important. Therefore, to minimize the total variance, while keeping the total number of cycles constant (i.e., IxJxK=24), it is necessary to increase the number of runs (boulders) and decrease the number of cycles and sequences accordingly or to increase the number of sequences and decrease the number of cycles. Three hypothetical cases with increased number of runs (I) and sequences (J) are shown in Table 5.5. The three new overall variances are significantly smaller than the estimate in the original experiment, which indicates that a larger number of samples measured with lower precision (smaller number of sequences and/or cycles for each sample) is the most efficient means of minimizing the total variance associated with the mean and should give the best overall dating results.

In addition to improving the reliability of the dating, increasing the number of samples allows for more significant statistical analysis of the results, which may have important implications for unraveling postdepositional history of the landforms. In the next section, we discuss origins of the boulder-to-boulder variability and develop a mathematical model of soil erosion and gradual exposure of boulders at the surface of

the earth.

Table 5.5. Comparison of variances calculated for four nested experiments with different number of runs, sequences, and cycles. The variances σ_R^2, σ_S^2, σ_C^2 are calculated in text using the data from Table 5.3.

Experiment #	I	σ_R^2/I	J	σ_S^2/IJ	K	σ_C^2/IJK	$var(\bar{Y}...)$
1	6	23.2	2	6.0	2	2.6	31.8
2	12	11.6	1	6.0	2	2.6	20.2
3	12	11.6	2	3.0	1	2.6	17.2
4	24	5.8	1	3.0	1	2.6	11.4

Gradual exposure model - theoretical development

We model the process of gradual exposure by using the distribution of fast and thermal neutrons in the subsurface and a range of soil erosion rates (ϵ) and erosion depths (x_{max}). Both fast and thermal neutrons interact with certain target elements to produce ^{36}Cl (Phillips et al., 1986; Zreda et al., 1991). The production rates are functions of depth below the surface and on eroding surfaces are also functions of time. The conceptual model for gradual exposure of boulders to cosmic radiation is shown in Figure 5.3. We assume that at time $t=0$ boulder A was buried in soil with its top at depth x_0 below the ground surface (Figure 5.3a). With an erosion rate

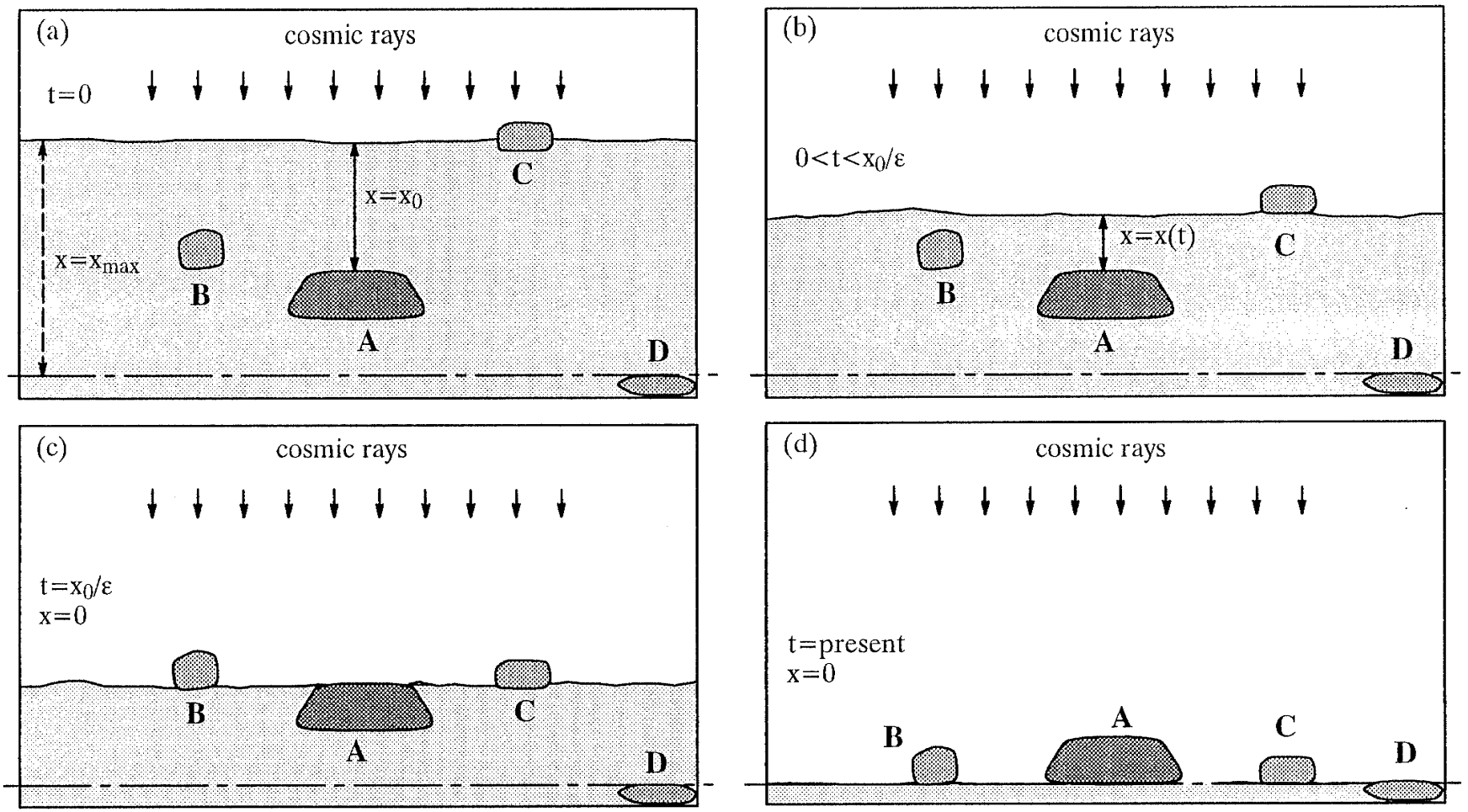

Fig. 5.3. Conceptual model of soil erosion and gradual exposure of boulders at the surface.

ϵ, it takes $t_e=x_0/\epsilon$ years for the covering soil to be removed and for the boulder to be exposed at the ground surface (Figure 5.3b,c). At any given depth x (g cm^{-2}), the production rate due to spallation can be calculated as the surface rate (P_s) multiplied by $exp(-x/\lambda_n)$, where λ_n is the attenuation length for the spallation component (Lal and Peters, 1967). The production of thermal neutrons below the surface is approximated by scaling of the surface production (P_n) using the formulation developed by Liu et al. (this issue) based on the experimental data of Fabryka-Martin et al. (1991). The depth profiles for both the spallation neutrons and thermal neutrons are graphed in Figure 3 in the paper by Liu et al. (this issue). After an exposure time t_e, buildup continues at the surface (Figure 5.3d) until the time of measurement. At present, boulders that started at different depths (boulders A, B, C, and D in our model) and were exposed at the surface at different times t_e are sitting on the surface and are macroscopically indistinguishable from one another. They contain, however, different amounts of cosmogenic ^{36}Cl and this property will be used in our attempt to unravel the time of the landform formation and its erosional history.

The differential equation describing buildup of cosmogenic ^{36}Cl in gradually exposed surfaces

$$\frac{dN_{36}}{dt} = P[x(t)] - \lambda_{36}N_{36} \qquad (5)$$

contains depth- and time-dependent production rates $P[x(t)]$

$$P(x(t)) = EL\left[P_s D_s(x(t)) + P_n D_n(x(t))\right] \quad (6)$$

where N_{36} is the number ^{36}Cl atoms, t is the time, P is the production rate of ^{36}Cl, $x(t)=x_0-\epsilon t$ before the time of exposure on the surface and $x(t)=0$ afterwards, x_0 is the initial burial depth of the boulder, ϵ is the erosion rate, λ_{36} is the decay constant of ^{36}Cl, D is the scaling factor for depth below the surface, the subscripts s and n indicate spallation and thermal neutron activation, and EL is the scaling factor for the elevation and geomagnetic latitude of the sampled location. The general solution to this linear first order differential equation is

$$N_{36} = e^{-\int \lambda dt} \int EL\left[P_s D_s(x(t)) + P_n D_n(x(t))\right] e^{\int \lambda dt} dt + Ce^{-\int \lambda dt} \quad (7)$$

The integration constant C is obtained from the initial condition $t=0$, $N_{36}=0$, which is appropriate for initially shielded material. Equation 7 will be used to model ^{36}Cl buildup between the time of landform formation ($t=0$) and the exposure of the boulder at the surface ($t_e=x_0/\epsilon$). After time t_e, buildup continues according to the following equation if the erosion of the rock surface is negligible

$$N_{36} = EL\left[N_e e^{-\lambda_{36} t} + \frac{P_s + P_n}{\lambda_{36}}\left(1 - e^{-\lambda_{36} t}\right)\right] \quad (8)$$

or according to Equation 7, with an appropriate erosion rate, if it cannot be neglected. In Equation 8, N_e is the number of ^{36}Cl atoms accumulated at time t_e in the subsurface due to cosmic radiation, calculated according to Equation 7 and the last term is new buildup at the surface since time t_e.

Different boulders will have different amounts of cosmogenic ^{36}Cl accumulated and yield different apparent cosmogenic ^{36}Cl ages due to two components. Firstly, because they started at different depths (x_0) below the surface and had been buried in the soil for different periods of time before exposure at the surface. Each of them, therefore, integrated a different part (the top x_0 g cm^{-2}) of the production profile of cosmogenic ^{36}Cl in the subsurface. Secondly, the boulders have different chemical compositions which results in different shapes of their production profiles and leads to variability of the apparent ages of even those boulders that were initially buried at the same depth. These two mechanisms are shown schematically in Figure 5.4a. The dotted lines represent depth profiles of production rates for different chemical compositions of boulders; the top line represents pure thermal neutron activation mechanism, the bottom line is for pure spallation, and the two intermediate lines are for 33% and 67%

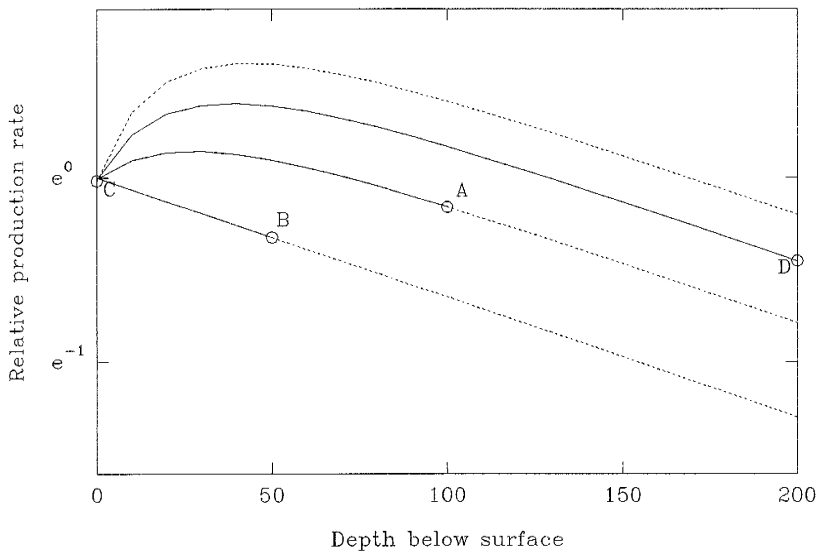

Fig. 5.4a. Dependence of cosmogenic ^{36}Cl production rates on depth below surface and chemical composition of the rock/soil matrix. The top line is for pure thermal neutron activation of ^{35}Cl, the bottom for pure spallation of ^{39}K and ^{40}Ca. Letters A, B, C, and D correspond to boulders in Figure 5.3.

contribution of thermal neutron activation to the total production rate of ^{36}Cl. The open circles show initial depths of the four boulders (A, B, C, and D) from Figure 5.3a and the solid lines show the production profiles integrated by these boulders as the surface is gradually lowered and the boulders become closer to the land surface.

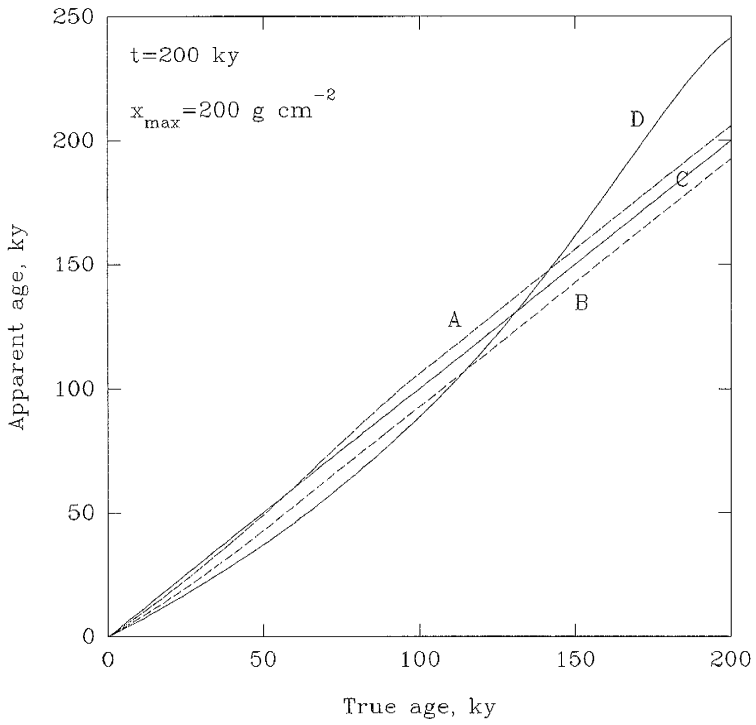

Fig. 5.4b. Chlorine-36 accumulation paths and resulting apparent ages for the same four boulders.

Figure 5.4b shows accumulation paths of the cosmogenic ^{36}Cl with time for the four boulders and the resulting apparent cosmogenic ^{36}Cl ages. The assigned age of the surface is 200 ky and the erosion depth x_{max} is 200 g cm^{-2}; the resulting erosion rate is thus 1 g cm^{-2} ky^{-1}. Because of the initial position of boulder C at the surface, the constant surface production rate has been integrated over 200 ky and the apparent age of boulder C is equal to the true age of the surface. Boulder B was buried for the first 50 ky and exposed for the last 150 ky at the surface. Its chemical composition is such

that almost 100% of the produced cosmogenic ^{36}Cl is due to spallation reactions with ^{39}K and ^{40}Ca. Because of its chemistry, during the first 50 ky the boulder integrated production rates lower than the surface rate. Therefore, the resulting production path is below the surface production path of boulder C and the apparent age is lower than the true age of the landform. Boulder A was buried for the first 100 ky and then exposed. Its chemical composition results in 67 % of the ^{36}Cl production due to spallation and 33 % due to thermal neutron activation of ^{35}Cl. The production profile starts below the surface production rate value, increases with time (and decreasing depth) to reach a maximum value at the depth of about 30 g cm^{-2}, and finally decreases back to the surface value. This history results in the accumulation path that initially goes below the surface path of boulder C. After some time, the boulder enters the shallow depth where the production rate is higher than at the surface. Buildup of cosmogenic ^{36}Cl is faster and the accumulation path steepens and continues above the path of boulder C. Because of this accelerated accumulation of the cosmogenic ^{36}Cl, the apparent age of boulder A is slightly older than the true landform age. Boulder D has been continuously buried in soil and just recently exposed at the surface. Its chemistry dictates that 33 % of the cosmogenic ^{36}Cl is produced by spallation of ^{39}K and ^{40}Ca and 67 % by thermal neutron activation of ^{35}Cl. Because of the large contribution of thermal neutron activation to the total production of ^{36}Cl, only the lowest third of the production profile has values lower than the surface value, whereas the top two thirds is positioned above the surface production rate value. This distribution of the production rates with depth results in the accumulation path that continues below the surface path of boulder C for about 140 ky.

At this time the boulder is at the shallow depth where the production rates are highest; the accumulation path thus steepens markedly and continues above the path of boulder C. The resulting apparent age is notably higher than the true landform age.

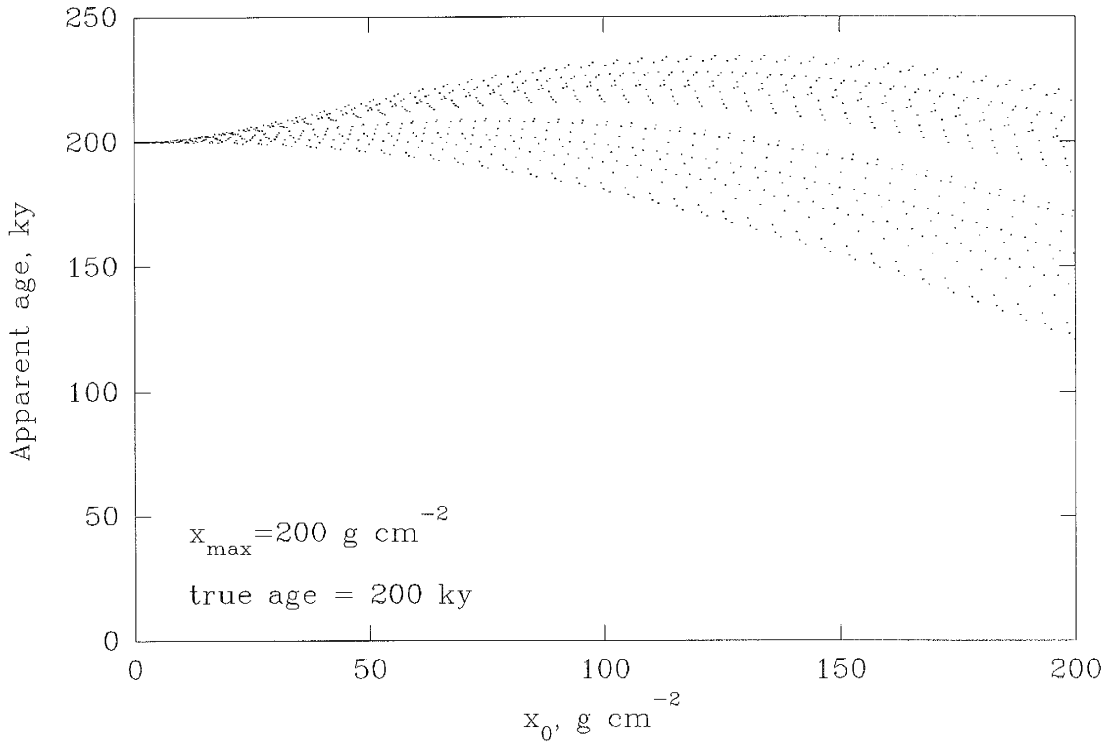

Fig. 5.4c. Example of Monte Carlo results showing the dependence of apparent ages on initial depth and chemical composition. We used 1000 samples with 26 different chemical compositions and initial burial depth sampled regularly from interval 0 to 200 g cm^{-2}. The points were generated deterministically to show the patterns, but their statistics is the same as for a uniform distribution on the same interval .

For the Monte Carlo calculations, we used 1000 boulders with different initial burial depths x_0 and variable chemical compositions. As an example, a landform with a true age of 200 ky and erosion depth of 200 g cm^{-2} yielded the 1000 apparent ^{36}Cl ages

shown in Figure 5.4c. We used 26 different chemical compositions and initial burial depths x_0 uniformly distributed between 0 and 200 g cm^{-2}. The lineations observed in Figure 5.4c (from left to right) depict samples of the same chemical composition, but of variable x_0. The uppermost points are for the samples with high Cl content and thus relatively high production rate of ^{36}Cl due to thermal neutron activation of ^{35}Cl, which leads to apparent ages older than the true landform age. On the other hand, the lowest points are for the samples with relatively high spallogenic ^{36}Cl resulting in younger apparent ages. The spread in the vertical direction for samples from the same depth is due to variable chemistry; it increases with increasing x_0. The apparent ages of these 1000 boulders are used to construct empirical distributions and calculate their first two moments. These distributions are graphed in Figure 5.5 for different values of the initial burial depth x_0 and true landform age t. An additional condition, boulder heights (sampled from a measured set of values), was added to the model to make the apparent age distributions more realistic.

The distributions of the apparent cosmogenic ^{36}Cl ages depend on the erosion depth of the landform. For small erosion depths, most apparent ^{36}Cl ages are equal to the true ages (Figure 5.5a, d, g). In the case 5.5a, a 50 ky old surface yielded ages from 49 to 54 ky with the majority very close to 50 ky. Surfaces that are 200 and 500 ky old

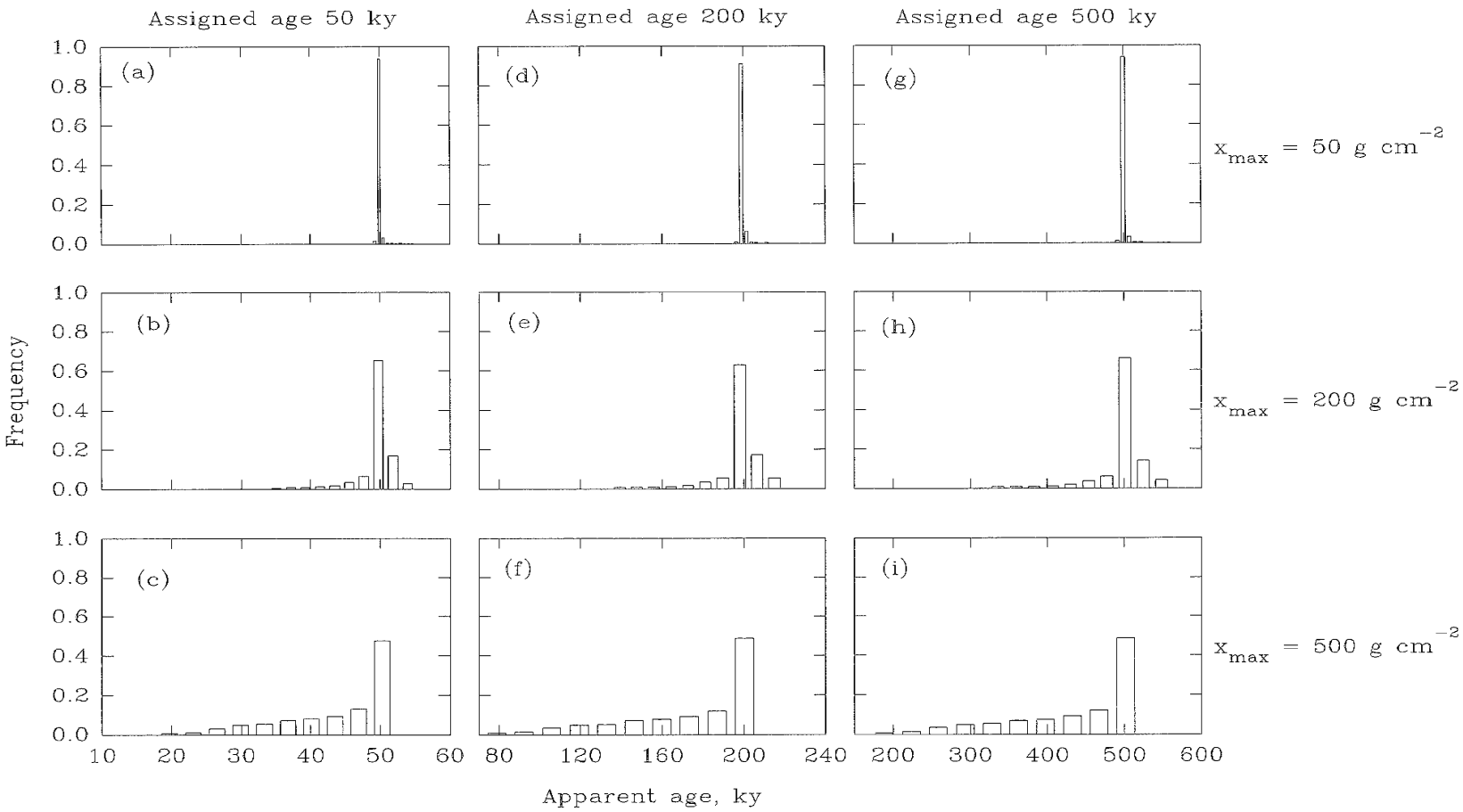

Fig. 5.5. Distribution of apparent surface exposure ages from nine Monte Carlo simulations with 1000 samples each. Columns have the same assigned true age and rows have the same erosion depth. The first moment of the distribution depends on both the true age and erosion depth while the shape of the distribution and its second moment depend on the erosion depth alone.

exhibited similar distributions of the apparent ages. If the erosion depth is increased to 200 g cm^{-2}, only about 60 % of samples have the same apparent age as the assigned true age (Figure 5.5b, e, h), about 20 % are overestimated by up to 10 % because the thermal neutron flux increases with depth down to about 45 g cm^{-2}, and the remaining samples form a tail towards younger ages. As in the case of smaller erosion depth, the mean of the apparent ages is very close to the assigned landform age and should be used to estimate the true age. For the erosion depth of 500 g cm^{-2}, the distribution becomes skewed towards the younger ages (Figure 5.5c, f, i) with a half of the samples close to the true age and few or no samples older than the true landform age. In this case, the oldest apparent ages are equal to the assigned age and they should be used to estimate the true age.

The model results lead to the following useful observations. First, the shapes of the apparent age distributions are not sensitive to the surface age, but are very sensitive to the erosion depth. For the same erosion depth, but different true ages, the shapes of the apparent age distributions are almost identical when they are scaled by their respective means. It is therefore possible to estimate the erosion depth by looking at the distribution of the apparent ages (as we did in Fig. 5.5) or, alternatively, at their first two moments (Fig. 5.6a). This age distribution and the mean apparent age (t_{app} in Figure 5.6a) are strongly inversely correlated and this correlation can be used to calculate the true landform age from the apparent ^{36}Cl ages. Another useful observation is made from a plot of apparent ages and property of the apparent age data set might be used to

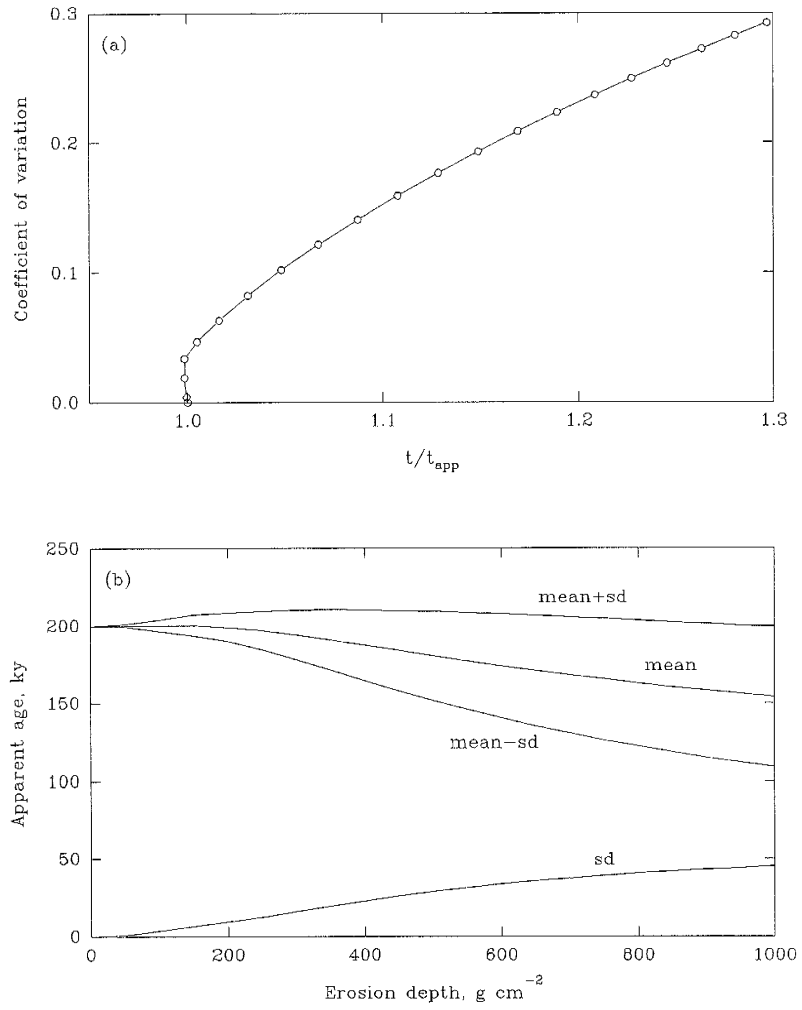

Fig. 5.6. (a) Apparent coefficient of variation vs. mean apparent age (t_{app}). The coefficient of variation defines the ratio t/t_{app}; the graph can therefore be used to estimate the true age and the erosion depth from a set of apparent ^{36}Cl ages. (b) The mean and standard deviation of apparent ages as functions of the erosion depth; based on Monte Carlo simulation with 1000 samples. The mean generally decreases and the standard deviation increases with increasing erosion depth; both are independent of the surface age.

reconstruct the erosional histories of landforms and calculate their formation ages. The coefficient of variation of the apparent standard deviations versus the erosion depth (Figure 5.6b). The line representing the mean plus one standard deviation is almost horizontal, i.e., does not change significantly with the erosion depth, and does not deviate markedly from the assigned age of 200 ky. This property might be used to

perform a first-cut estimation of landform age using the mean plus one standard deviation calculated for the apparent ^{36}Cl ages. We also observe that the mean decreases less rapidly as the erosion depth increases and in the limit would reach an asymptotic value of half of the true landform age. This is expected because of the distribution of fast and thermal neutrons in the subsurface. As the erosion depth increases, the maximum production rate at the depth of about 45 g cm^{-2} becomes progressively less consequential and eventually, for large erosion depth, is negligible. In this case, the boulders integrate a production profile essentially identical to that for pure spallation (Figure 5.4a, boulder B) and the resulting distribution of the apparent ^{36}Cl ages is approximately uniform with the maximum close to the true age and the mean close to half of that value.

The actual age and the erosion depth of a real landform can be estimated by executing a set of model calculations, each with a different value of the true age (which is the input variable) of the landform. In each calculation, the erosion depth (another input variable) is systematically changed and the first two moments of the apparent ^{36}Cl age distribution are calculated. These two moments can either be obtained directly, by treating N_{36} in Equation 6 as a random variable and taking appropriate expected values, or indirectly, using Monte Carlo simulations with initial boulder depth sampled from a desired distribution on the interval between 0 and the assigned erosion depth. In the case of morainal deposits, it is appropriate to sample x_0 from a uniform distribution because material of glacial till is usually very poorly sorted and large boulders are found at all locations within the finer matrix. The shape and/or the first two moments of the

simulated distribution can then be compared with those of the experimental distribution based on AMS measurements of cosmogenic ^{36}Cl in rock samples. The procedure is reiterated until good agreement is obtained between the theoretical and experimental distributions. For most conditions, the combination of the first two moments uniquely defines the distribution and allows determination of (1) the true age, which was the input variable in the model calculation that gave the correct first two moments, (2) the erosion depth, the other input variable that produced the correct first two moments, and (3) the erosion rate, which is the erosion depth divided by the true age. We use this procedure in the next section to calculate the age and erosion depth of a late Pleistocene moraine from the Sierra Nevada.

Gradual exposure model - comparison with data

The model calculations were tested using samples from boulders on an independently dated late Pleistocene glacial moraine from Bishop Creek, Sierra Nevada, California. We collected 26 samples, extracted Cl, measured ^{36}Cl, constructed the empirical distribution of the apparent cosmogenic ^{36}Cl ages, and calculated sample statistics for this data set. We then simulated exposure histories for this surface and found the moraine age and the erosion depth that best match the observed data. In addition, we measured ^{36}Cl in three surficial soil materials sampled and used them to independently calculate the erosion depth using a simple analytical erosion model.

Sample collection and preparation

The samples (Table 5.6) were collected from two transects along the crest of the "Older Bishop Creek" (PTi5) moraine (Phillips et al., 1993), at Bishop Creek, eastern Sierra Nevada, California. This particular moraine was chosen because it had been previously dated by cosmogenic ^{36}Cl accumulation and varnish cation-ratio (Phillips et al., 1993) and because a large number of medium-sized boulders were available on the moraine crest. The sampling criteria were as follows: (1) samples were arbitrarily collected at five meter intervals along two transects parallel to the moraine crest; (2) the minimum sample size was 10 cm; (3) only relatively fresh samples were collected (i.e., without major chemical alteration) in order to avoid samples that might contain meteoric chlorine in secondary weathering minerals; (4) rounded rather than sharp-edged samples were collected in order to increase the likelihood that they were not products of spalling. Large boulders were sampled from the tops, as close to the boulder center as possible, using a hammer and a chisel, whereas smaller ones were split into several pieces and the top parts were retained for the subsequent analysis.

Three soil samples from the top 1 cm of the soil (Table 5.7) were collected from the same location at the flat moraine crest. They were collected to a maximum of 1 cm depth and from about 20x20 cm area.

Table 5.6. Measured $^{36}Cl/Cl$ ratios, apparent boulder ages, their heights, target element concentrations and associated production rates of ^{36}Cl, macroscopic thermal neutron absorption cross sections, and fraction (FS) of cosmogenic ^{36}Cl produced due to spallation reactions with ^{39}K and ^{40}Ca for the samples from "Older Bishop Creek" moraine of Phillips et al. (1993).

Sample ID	$^{36}Cl/Cl$ 10^{-15}	Age ky	Height m	K_2O %	Ψ_K N $kg^{-1}y^{-1}$	CaO %	Ψ_{Ca} N $kg^{-1}y^{-1}$	Cl ppm	$\Sigma\sigma N$ cm^2	Ψ_{Cl} N $kg^{-1}y^{-1}$	FS
bpcr90-63	1464	83	0.7	4.76	8147	1.63	840	141	4.80	5214	0.63
bpcr90-64	1306	85	0.6	4.11	7036	2.07	1065	154	5.03	5429	0.60
bpcr90-65	1482	76	0.7	4.04	6916	2.03	1044	108	4.88	3924	0.67
bpcr90-66	4670	65	0.5	3.73	6386	2.36	1214	21	4.68	776	0.91
bpcr90-67	1461	80	0.8	4.03	6899	1.88	967	118	4.85	4292	0.65
bpcr91-1	731	31	0.3	1.61	2756	5.20	2674	63	4.63	2393	0.69
bpcr91-2	964	40	0.3	1.93	3304	5.50	2829	64	6.05	1758	0.78
bpcr91-3	2572	17	0.15	3.18	5444	1.44	741	8	4.27	336	0.95
bpcr91-4	754	42	0.25	4.04	6916	1.64	843	131	4.55	5106	0.60
bpcr91-5	3675	84	2	3.59	6146	1.51	777	32	4.64	1213	0.85
bpcr91-6	8503	76	0.15	3.78	6471	0.28	144	11	4.10	470	0.93
bpcr91-7	818	16	0.35	4.34	7430	1.24	638	35	4.25	1462	0.85
bpcr91-8	773	40	0.3	3.94	6745	1.31	674	109	4.78	4040	0.65
bpcr91-9	1010	82	1.5	2.30	3938	4.07	2093	131	7.24	3201	0.65

bpcr91-10	1387	21	0.3	4.32	7396	1.11	571	26	4.33	1054	0.88
bpcr91-11	633	36	0.2	3.84	6574	1.54	792	138	4.34	5619	0.57
bpcr91-12	850	43	0.3	4.02	6882	1.66	854	114	4.40	4592	0.63
bpcr91-13	988	49	0.2	3.95	6762	1.96	1008	108	4.49	4281	0.64
bpcr91-14	1294	30	0	1.69	2893	5.07	2608	28	4.45	1116	0.83
bpcr91-15	639	38	0.5	3.68	6300	1.95	1003	147	4.37	5939	0.55
bpcr91-16	1576	93	0.8	4.19	7173	1.44	741	139	4.18	5915	0.57
bpcr91-17	1315	43	0.3	1.38	2363	5.22	2685	39	4.60	1483	0.77
bpcr91-18	1556	49	0.2	4.75	8132	0.91	468	62	4.60	2497	0.78
bpcr91-19	1312	51	0.9	1.35	2311	5.29	2721	48	4.70	1698	0.75
bpcr91-20	733	33	0.1	4.11	7036	1.43	735	108	3.93	4856	0.62
bpcr91-21	1129	42	0.3	2.48	4246	4.23	2175	59	4.43	2362	0.73
AVG[1]	1677	52	0.49	3.43	5869	2.46	1265	82	4.68	3116	0.72
STDS[2]	1672	23	0.45	1.07	1826	1.61	828	49	0.66	1877	0.12

[1] Arithmetic mean

[2] Sample standard deviation

Table 5.7. Data for three soil samples from the "Older Bishop Creek" moraine at Bishop Creek, eastern Sierra Nevada, California. The apparent age is calculated assuming negligible erosion of the surface. The erosion depth is calculated using true surface age of 85 ky (Phillips et al., 1993) and constant erosion rate.

Sample ID	$\Sigma\sigma N$ ($cm^2\ kg^{-1}$)	K_2O (%)	CaO (%)	Cl (ppm)	$^{36}Cl/Cl$ (10^{-15})	Apparent age (ky)	Erosion depth ($g\ cm^{-2}$)
BCS92-2CR	5.03	3.65	2.90	46	1149±100	27.8±2.6	580±60
BCS92-3CR	4.95	3.58	2.75	45	1128±68	27.4±1.8	590±40
BCS92-4CR	5.04	3.67	2.45	46	1044±45	25.6±1.2	640±30

The samples were cleaned of any organic overgrowths by scrubbing with a wire brush and ground using a tungsten mill to fractions smaller than the smallest phenocrysts of quartz and feldspars. The fraction smaller than 45 μm was discarded to remove any clay minerals present. The remaining sample material was leached in 5 % HNO_3 for 24 hours to remove meteoric chlorine and any secondary carbonates from the grain boundaries and the microfractures within the rock matrix. Samples for ^{36}Cl measurements were obtained by dissolution of approximately 100 g of sample in a hot mixture of concentrated HF and HNO_3 and precipitation of chlorine as AgCl. About 10 g of powdered sample was used for determination of major elements, chlorine, boron, and gadolinium. Chlorine-36 was measured by accelerator mass spectrometry (Elmore et al., 1979) at the Purdue University PRIME Laboratory, major elements by XRF spectrometry, chlorine by the ion-selective electrode (Aruscavage and Campbell, 1987; Elsheimer, 1988), and boron and gadolinium by prompt gamma emission spectrometry. The details of analytical procedures can be found in our earlier publications (Zreda et al., 1990, 1991, 1993; Phillips et al., 1990, 1991) and will not be discussed here.

Analytical results and comparison with model calculations

The analytical results are reported in Table 5.6, along with the apparent ^{36}Cl ages. These apparent ages were calculated in the usual way, i.e., assuming negligible erosion of soil and boulder surfaces.

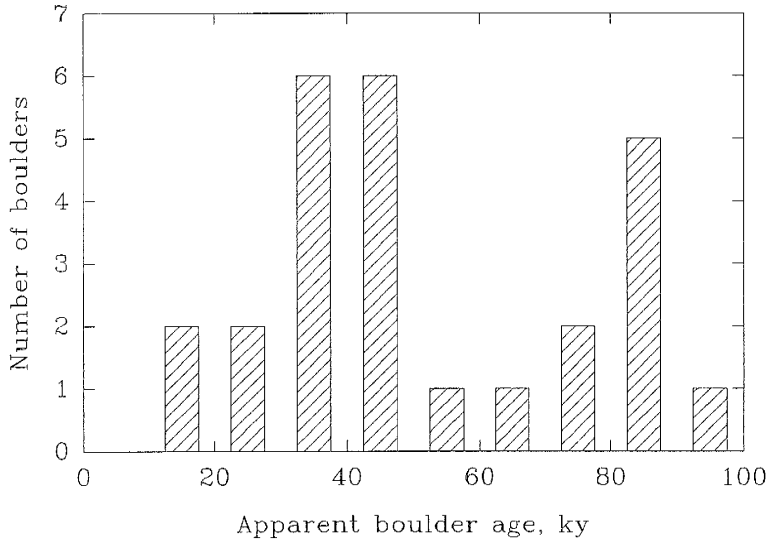

Fig. 5.7a. Observed distribution of apparent ^{36}Cl ages for 26 samples from Bishop Creek.

The ages range from 16 to 93 ky and are characterized by a bi-modal distribution with modes at 85 and 40 ky (Figure 5.7a). The older mode of the distribution has a characteristic skew towards the younger ages which is indicative of a surface that has undergone erosion of about 500 g cm^{-2} (see Figure 5.5c, f, i). For this value of the erosion depth, the true age is close to the upper limit of the distribution. We can thus conjecture that the true moraine age is about 90 ky and values close to this number will be used as input in the model calculations. The younger mode of the distribution does not correspond to any distribution predicted for simple continuous erosion and will be discussed further below.

Model calculations were performed with the assigned true age from 60 to 100 ky and the assigned erosion depth from 200 to 1000 g cm^{-2} and the resulting theoretical distributions of the apparent ages compared with the observed distribution. The best agreement between the calculated statistics and those based on the older part of the experimental distribution (upper part of Figure 5.7b) was obtained for the following parameters: assigned age of 85 ky, erosion depth of 570 g cm^{-2}, and erosion rate of 6.7 g cm^{-2} ky^{-1}; these erosion parameters refer to removal of loose till, not rock erosion. The theoretical distribution based on these parameters is shown as the lower part in Figure 5.7b. The strong correspondence between the experimental and modeled distribution indicates that the model successfully simulates the basic effects of moraine erosion and offers additional support for its use in estimating landform ages and erosion rates.

To test the above results using a different approach, we analyzed three surficial soil materials from the moraine crest. Because the moraine has been modified by erosion since its formation, the collected soil particles have been exposed only recently at the surface. The amount of accumulated ^{36}Cl, and thus the apparent age, is a function of the true age and erosion depth and therefore *a priori* knowledge of either one permits calculation of the other. The moraine age has been established by cosmogenic ^{36}Cl buildup and varnish cation-ratio, both of which yielded an age of 85 ky. We now use a simple, analytical, constant rate erosion model to calculate the erosion depth which results in the observed apparent ages. The model is essentially the same as the

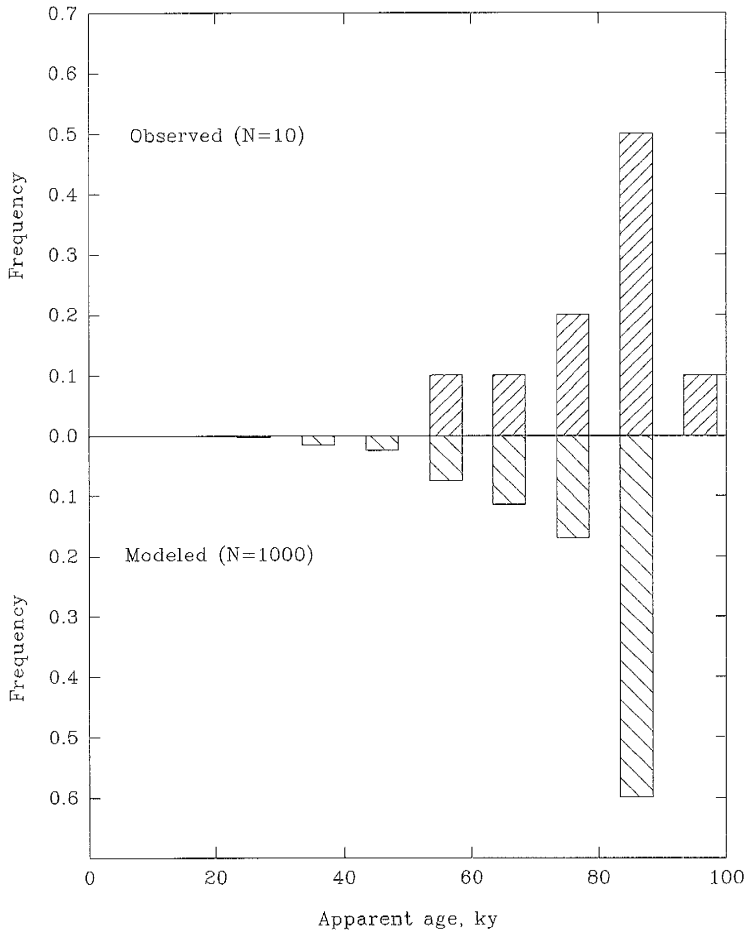

Fig. 5.7b. Observed vs. modeled distribution of ^{36}Cl ages.

"subsurface" part of our gradual exposure model (Equation 6) applied to a single sample. It is also similar to the published model of eroding bedrock (Lal, 1991); the paper by Lal (1991) should be consulted for the details.

The three surficial soil materials have almost identical chemical composition (Table 5.7) which indicates that the soil material has been well homogenized. The apparent ages and calculated erosion depths are also very uniform. The average erosion

depth of 603±32 g cm $^{-2}$ corresponds well with that of 570 g cm $^{-2}$ calculated earlier from the gradual exposure model. This close agreement supports our gradual exposure model, indicates that the model can indeed produce reasonable estimates of the true landform age and erosion depth, and supports its use in surface exposure dating.

We believe that the younger mode of the experimental distribution results from geomorphic processes other than simple soil erosion. One clue can be obtained from the relation of boulder height to age. Virtually all of the young "second mode" boulders are shorter than 0.4 m. In order to further examine possible controls on the distribution, in Figure 5.8 we plotted boulder heights above the soil surface versus the apparent boulder ages (data from Table 5.6). Most boulders that are relatively low (less than 0.4 m above the soil surface) group closely and yield ages younger than 50 ky; these samples are inside the small ellipse in Figure 5.8 and constitute the younger mode of the empirical

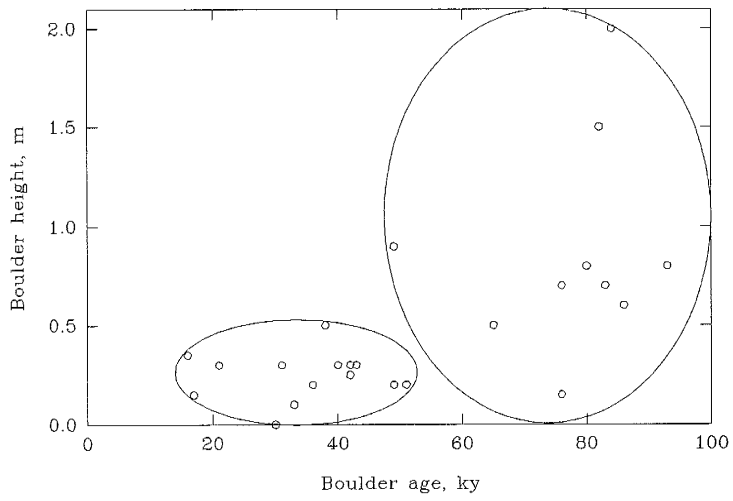

Fig. 5.8. Relationship between boulder size and measured ^{36}Cl age. Small ellipse encircles the samples that form the younger mode of the distribution, large ellipse contains the samples forming the older mode.

distribution. On the other hand, boulders that yielded ages close to the moraine age (85 ky) are relatively taller; they are inside the large ellipse in Figure 5.8 and form the older mode of the distribution.

The very young age of such a large number of samples can best be explained by the process of spalling, which is common in periglacial climate and also in areas with frequent forest fires. When a boulder experiences internal stress (e.g., due to sudden temperature changes) it may respond by spalling off smaller fragments or breaking into two or more pieces; fresh surfaces are thus exposed to cosmic radiation. These pieces initially have sharp edges and their origin can be easily recognized from their shape. With time they weather into rounded cobbles and eventually may no longer be recognizable. Although we avoided obviously spalled samples, we now believe that many of the low boulders we randomly collected are derived from weathered spall fragments. The grouping of the younger ages close to 40 ky may indicate that the spalling processes were climate controlled. Previous studies (Dorn et al., 1991; Phillips et al., 1990, 1993) indicate that the most severe glaciations of the past 85 ky were at about 60-70 ky (mid-Wisconsin glaciation) and 15-20 ky (late Wisconsin glaciation). The older advance could not have been responsible for the observed younger mode of the apparent ^{36}Cl ages because of the following consideration. Cosmogenic ^{36}Cl accumulates throughout rock mass, not only at the surface. If a boulder splits or a fragment is spalled off of it, the freshly exposed surface will already have had some ^{36}Cl present. Therefore, if significant spalling had occurred during the mid-Wisconsin glaciation, it would have

resulted in ^{36}Cl ages older than 60-70 ky. On the other hand, the Late Wisconsin glaciation would have resulted in ages older than 20-25 ky, possibly close to the observed younger mode of the experimental distribution at about 40 ky. The route of the late Wisconsin glacier passed within 2 km of the sample site (Phillips et al., 1993) and intense periglacial spalling might be expected under these conditions.

Summary and conclusions

Numerical dating of boulders from late Pleistocene moraines in Bishop Creek, Sierra Nevada, California provided valuable details about the sampling and analytical requirements for cosmogenic nuclide dating as well as about the nature of postdepositional processes that modify landforms. Accuracy and precision of the cosmogenic ^{36}Cl landform age estimates depend on two major components: the analytical uncertainty and the natural variability among boulders. For all but very young glacial landforms, the natural variability is the critical component and it determines how well a surface can be dated by the accumulation of cosmogenic ^{36}Cl. Because of this, we recommend that very young geomorphic surfaces be sampled sparingly (approximately five samples) and the samples analyzed with high precision. On the other hand, as many as 10-20 samples should be collected from older landforms and they should be analyzed with lower precision in order to minimize AMS costs. This arrangement should produce the best overall dating results and allow for useful statistical evaluation of the data sets.

The natural variability of the apparent ^{36}Cl ages among boulders from a moraine is due to soil erosion and gradual exposure of boulders at the surface. Two mechanisms are responsible for the resulting distributions of the apparent ^{36}Cl ages. The variability of the initial burial depth among boulders leads to different production rates of ^{36}Cl because of attenuation of cosmic rays by the soil material. The variability in the chemical composition of boulders from the same depth also results in different ^{36}Cl ages due to the dependence of the depth production profile on the boulder chemistry. The distributions of the apparent ^{36}Cl ages provide information on the erosion depth and rate and on the formation time of landforms. For small erosion depths, the apparent ages are clustered together and their mean age is the best estimate of the true landform age. In contrast, for greater erosion depths, the apparent ages form distributions with long tails towards younger ages and the oldest apparent age is the best estimate of the true age. Ideally, one would need a large number of samples to perform such statistical analysis, but even with only a few samples from a surface one may attempt to calculate the first two moments of the experimental distribution and estimate the true age and erosion parameters.

We tested the above theoretical results by measuring cosmogenic ^{36}Cl in boulders from a late Pleistocene moraine. The distribution of the calculated apparent ages allowed us to calculate the "true" age of 85 ky and the erosion rate of 570 g cm^{-2} which are in excellent agreement with independently estimated values of 87 ky (by cation-ratio dating, Phillips et al., 1993) and 600 g cm^{-2} (from a conceptually different model of soil erosion)

for the same parameters. These results demonstrate that the model satisfactorily simulates effects of erosion processes and can thus aid in surface exposure dating of eroding landforms.

Acknowledgements. Funding for this research was provided by NSF grant SES-8901437. We thank R. Dorn and A. Bach for help in sample collection.

References

Aruscavage, P.J., and E.Y. Campbell, An ion-selective electrode method for determination of chlorine in geological materials, *Talanta, 28*, 745-749, 1987.

Bentley, H.W., F.M. Phillips, and S.N. Davis, Chlorine-36 in the terrestrial environment, in *Handbook of environmental isotope geochemistry*, Volume 2, The terrestrial environment, B, edited by P. Fritz and J.-Ch. Fontes, p. 427-480, Elsevier, New York, 1986.

Davis, R., Jr. and O.A. Schaeffer, Chlorine-36 in nature, *Annals of New York Academy of Science, 62*, 105-122, 1955.

Dorn, R.I., F.M. Phillips, M.G. Zreda, E.W. Wolfe, A.J.T. Jull, P.W. Kubik and P. Sharma, Glacial chronology of Mauna Kea, Hawaii, as constrained by surface-exposure dating, *National Geographic Research and Exploration, 7*, 456-471, 1991.

Elmore D., B.R. Fulton, M.R. Clover, J.R. Marsden, H.E. Gove, H. Naylor, K.H.

Purser, L.R. Kilius, R.P. Beukins and A.E. Litherland, Analysis of ^{36}Cl in environmental water samples using an electrostatic accelerator, *Nature, 277*, 22-25, 1979.

Elsheimer, H.N., Application of an ion-selective electrode method to the determination of chloride in 41 international geochemical reference materials, *Geostandards Newsletter, 11*, 115-122, 1987.

Fabryka-Martin, J.T., *Production of radionuclides in the earth and their hydrologic significance, with emphasis on chlorine-36 and iodine-129,* 400 pp., Ph.D. dissertation, University of Arizona, 1988.

Fabryka-Martin, J.F., M.M. Fowler, and R. Biddle, *Study of neutron fluxes underground: Los Alamos National Laboratory Isotope and Nuclear Chemistry Division Quarterly Report October 1 - December 31,* 82-85, 1990

Imbrie, J., J.D. Hays, D.G. Martinson, A. McIntyre, A.C. Mix, J.J. Morley, N.G. Pisias, W.L. Prell, and N.J. Shackleton, The orbital theory of Pleistocene climate: Support from a revised chronology of the marine $\delta^{18}O$ record, in *Milankovitch and Climate, Understanding the Response to Orbital Forcing*, Part 1, edited by A. Berger, J. Imbrie, J. Hays, G. Kukla, and B. Salzman, p. 269-305, Reidel, Norwell, Massachusetts, 1984.

Lal, D., and B. Peters, Cosmic ray produced radioactivity on earth, in *Encyclopedia of Physics*, edited by S. Fluegge, vol. 46/1, *Cosmic Rays II*, edited by K. Sitte, p. 551-612, Springer-Verlag, Berlin, 1967.

Liu, B., F.M. Phillips, J.T. Fabryka-Martin, M.M. Fowler, and R.S. Biddle,

Cosmogenic ^{36}Cl accumulation in unstable landforms: I. Effects of the thermal neutron distribution, This issue.

Martinson, D.G., N.G. Pisias, J.D. Hays, J. Imbrie, T.C. Moore, Jr., and N.J. Shackleton, Age dating and the orbital theory of the ice ages: Development of a high-resolution 0 to 300,000-yr chronostratigraphy, *Quaternary Research, 27*, 1-29, 1987.

Phillips, F.M., B.D. Leavy, N.O. Jannik, D. Elmore, and P.W. Kubik, The accumulation of cosmogenic chlorine-36 in rocks: A method for surface exposure dating, *Science, 231*, 41-43, 1986.

Phillips, F.M., M.G. Zreda, S.S. Smith, D. Elmore, P.W. Kubik and P. Sharma, A cosmogenic chlorine-36 chronology for glacial deposits at Bloody Canyon, eastern Sierra Nevada, California, *Science, 248*, 1529-1532, 1990.

Phillips, F.M., M.G. Zreda, S.S. Smith, D. Elmore, P.W. Kubik, R.I. Dorn, and D.J. Roddy, Dating the impact at Meteor Crater: Comparison of ^{36}Cl buildup and varnish ^{14}C with thermoluminescence, *Geochimica et Cosmochimica Acta, 55*, 2695-2698, 1991.

Phillips, F.M., M.G. Zreda, R.I. Dorn, T. Liu, D. Elmore and J. Clark, Glacial geology of Lower Bishop Creek, eastern Sierra Nevada: I. Cosmogenic ^{36}Cl and rock varnish chronology, *Geological Society of America Bulletin*, Submitted, 1993.

Snedecor, G.W., and W.D. Cochran, *Statistical Methods*, 594 pp., Iowa State University Press, Ames, Iowa, 1967

Winograd, I.J., T.B. Coplen, J.M. Landwehr, A.C. Riggs, K.R. Ludwig, B.J. Szabo, P.T. Kolesar, and K.M. Revesz, Continuous 500,000-year climate record from vein calcite in Devils Hole, Nevada, *Science, 258*, 255-260, 1992.

Zreda, M.G., F.M. Phillips, and S.S. Smith, *Cosmogenic ^{36}Cl dating of geomorphic surfaces: New Mexico Tech Hydrology Program Report 90-1*, 104 pp., 1990.

Zreda, M.G., F.M. Phillips, D. Elmore, P.W. Kubik, P. Sharma, and R.I. Dorn, Cosmogenic 36Cl production rates in terrestrial rocks, *Earth and Planetary Science Letters, 105*, 94-109, 1991.

Zreda, M.G., F.M. Phillips, P.W. Kubik, P. Sharma and D. Elmore, Eruption age at Lathrop Wells, Nevada from cosmogenic chlorine-36 accumulation, *Geology*, 21, 57-60, 1993.

Appendix A. Balanced three-level nested ANOVA table for the sample setup in Figure 5.1.

Source	SS	DF	MS	E[MS]
Factor I = run	SS1	DF1 = I-1	SS1/DF1	$\sigma_C^2 + K\sigma_S^2 + JK\sigma_R^2$
Factor J = sequence	SS2	DF2 = I(J-1)	SS2/DF2	$\sigma_C^2 + K\sigma_S^2$
Factor K = cycle	SS3	DF3 = IJ(K-1)	SS3/DF3	σ_C^2
TOTAL	SST	DFT = IJK-1	---	---

SS is sum of squares, DF is degrees of freedom, MS is mean square, E[MS] is expected value of mean square, I, J, K are numbers of cycles, sequences, and runs, respectively. σ_C^2, σ_S^2, and σ_R^2 are variances at cycle, sequence, and run level, respectively, and are calculated by equaling MS and E[MS] at each level. Sum of squares and other relevant quantities are calculated as:

$$SS1 = \frac{1}{JK}\sum_{i=1}^{I} Y_{i..}^2 - \frac{1}{IJK}Y_{...}^2$$

$$SS2 = \frac{1}{K}\sum_{i=1}^{I}\sum_{j=1}^{J} Y_{ij.}^2 - \frac{1}{JK}\sum_{i=1}^{I} Y_{i..}^2$$

$$SS3 = \sum_{i=1}^{I}\sum_{j=1}^{J}\sum_{k=1}^{K} Y_{ijk}^2 - \frac{1}{K}\sum_{i=1}^{I}\sum_{j=1}^{J} Y_{ij.}^2$$

$$SST = SS1 + SS2 + SS3 = \sum_{i=1}^{I}\sum_{j=1}^{J}\sum_{k=1}^{K}\left(Y_{ijk} - \bar{Y}_{...}\right)^2$$

$$Y_{ij.} = \sum_{k=1}^{K} Y_{ijk}$$

$$Y_{i..} = \sum_{j=1}^{J}\sum_{k=1}^{K} Y_{ijk}$$

$$Y_{...} = \sum_{i=1}^{I}\sum_{j=1}^{J}\sum_{k=1}^{K} Y_{ijk}$$

Appendix B. Balanced two-level nested ANOVA table for the sample setup in Figure 5.1, with sequences and cycles combined into one level, "analytical" component.

Source	SS	DF	MS	E[MS]
Factor I = natural (run)	SS1	DF1 = I-1	SS1/DF1	$\sigma_S^2 + J\sigma_R^2$
Factor J = analytical (sequence)	SS2	DF2 = I(J-1)	SS2/DF2	σ_S^2
TOTAL	SST	DFT = IJK-1	---	---

I and J are numbers of boulders and analyses on each boulder, respectively. σ_S^2 and σ_R^2 are variances at analytical and natural (boulder) level, respectively, and are calculated by equaling MS and E[MS] at each level. Sum of squares and other relevant quantities are calculated as follows:

$$SS1 = \frac{1}{J}\sum_{i=1}^{I} Y_{i.}^2 - \frac{1}{IJ}Y_{..}^2$$

$$SS2 = \sum_{i=1}^{I}\sum_{j=1}^{J} Y_{ij}^2 - \frac{1}{J}\sum_{i=1}^{I} Y_{i.}^2$$

$$SST = SS1 + SS2 = \sum_{i=1}^{I}\sum_{j=1}^{J}\left(Y_{ij} - \bar{Y}_{..}\right)^2$$

$$Y_{i.} = \sum_{j=1}^{J} Y_{ij}$$

$$Y_{..} = \sum_{i=1}^{I}\sum_{j=1}^{J} Y_{ij}$$

6. Cosmogenic ^{36}Cl dating of a young basaltic eruption complex, Lathrop Wells, Nevada

Marek G. Zreda and Fred M. Phillips

Geoscience Department, New Mexico Tech, Socorro, New Mexico 87801

Peter W. Kubik* and Pankaj Sharma

Nuclear Structure Research Laboratory, University of Rochester, Rochester, New York 14627

* Present address: Institut Für Mittelenergiephysik, ETH-Hönggerberg, CH-8093 Zürich, Switzerland

David Elmore

Department of Physics, Purdue University, West Lafayette, Indiana 47907

Abstract

It has been proposed that the Lathrop Wells volcanic center, a late Quaternary basaltic complex in southern Nevada, has erupted more than once. In common with most Quaternary basalts, this volcanic center has proved difficult to date by K/Ar and other commonly employed methods. We have measured the accumulation of ^{36}Cl in 11 samples from lava flows and volcanic bombs and obtained a combined average age of 81 $\pm$7.9 ka, with no systematic differences between

Published in 1993, Geology 21, 57-60.

sample subsets collected from different volcanic features. The ^{36}Cl dates do not support a history of multiple eruptions, but neither do they completely preclude the possibility.

Introduction

Quaternary basaltic eruptives are common in many parts of the world and provide important information on tectonic activity, crust and mantle geochemistry, and geomorphic history. Although volcanic rocks have commonly been dated by K/Ar and $^{40}Ar/^{39}Ar$ methods, young basaltic rocks can be difficult to date by these methods because of low K content, unsuitable mineral content, and contamination by atmospheric Ar. The development of alternative methods for dating young basalts would, therefore, aid several branches of the earth sciences.

In this paper, we report results from ^{36}Cl dating at the Lathrop Wells volcanic center in southern Nevada. The Lathrop Wells center is a typical late Quaternary basaltic cinder cone complex. The proximity of the cinder cone to the proposed high-level nuclear waste repository at Yucca Mountains, Nevada, has stimulated interest in the chronology of its activity. As a result, numerous K/Ar and $^{40}Ar/^{39}Ar$ measurements have been performed there (Turrin et al., 1991). Many other dating approaches either have been attempted or are in progress. The variety of methods employed at the Lathrop Wells center make it a valuable site for the intercomparison of dating methods.

The approach described herein is fundamentally different from conventional radiometric dating methods. The underlying assumption for both K/Ar and $^{40}Ar/^{39}Ar$ methods is that the system is closed chemically and isotopically at the time of crystallization, and the concentrations of relevant isotopes change with time owing to radioactive decay of the parent and formation of daughter nuclides. In contrast, the dating method based on accumulation of cosmic-ray-induced ^{36}Cl assumes negligible initial concentration of ^{36}Cl and an "open" system with respect to accumulation of cosmic-ray-induced ^{36}Cl. This assumption is valid because energetic cosmic-ray particles easily penetrate crystal lattices of minerals in surficial rocks, interact with certain target nuclides, and produce cosmogenic ^{36}Cl, even though no chemical transfer of species occurs. While open to cosmogenic ^{36}Cl, the system is closed chemically and isotopically with respect to other, noncosmogenic sources of ^{36}Cl. The concentration of cosmogenic ^{36}Cl, after accounting for decay of ^{36}Cl to ^{36}Ar, is thus a predictable function of time and is the basis of this geochronometer.

Eruptive deposits of the Lathrop Wells volcanic area

The Lathrop Wells cone belongs to a group of five isolated late Cenozoic basaltic eruptives in the Crater Flat, Nevada, volcanic field (Wells et al., 1990). At Lathrop Wells, the volcanic eruptives are represented by aa and block lava flows, scoria deposits, and volcanic bombs (Vaniman et al., 1982; Crowe et al., 1983; Turrin et al., 1991). The lava flows, located south and east of the rim, are composed of vesicular basalts with

olivine and plagioclase phenocrysts in a finely crystalline matrix. They are usually only slightly weathered and exhibit original flow structures at the surface. The scoria deposits are found in the area immediately around the cone and in isolated patches southeast of the rim. The bombs are present in the rim area and immediately to the northwest of the rim, as well as in several isolated locations on a small alluvial plateau west of the rim (Fig. 6.1).

The oldest of the Crater Flat cones was dated by K/Ar at ~ 1.5 Ma (Vaniman et al., 1982), whereas the age of the youngest, the Lathrop Wells cone, is uncertain. It has been intensively studied in connection with the proposed high-level radioactive waste repository at the southwest margin of the Nevada Test Site. The eruption age was bracketed by U/Th ages of 345 and 25 ka obtained for underlying and overlying carbonate sedimentary units (Szabo et al., 1981). U-trend dates of 240 and 145 ka were obtained for associated Quaternary deposits in the nearby Yucca Mountains area (Swadley et al., 1984). Initial studies based on K/Ar analysis reported an age "much younger" than 270 ka which was later reduced to < 100 and possibly < 50 ka (Crowe et al., 1988) based on new K/Ar dates and soil studies. This conclusion was supported by Wells et al. (1990), who used surface modification criteria to compare the Lathrop Wells cinder cone with K/Ar-dated cinder cones from the Cima volcanic field, California, and found evidence for polycyclic volcanic activity at Lathrop Wells, with the youngest episode as recent as 20 ka. A contrasting view was proposed by Turrin et al. (1991), who reported whole-rock $^{40}Ar/^{39}Ar$ ages of several lava flows and scoria units and combined these

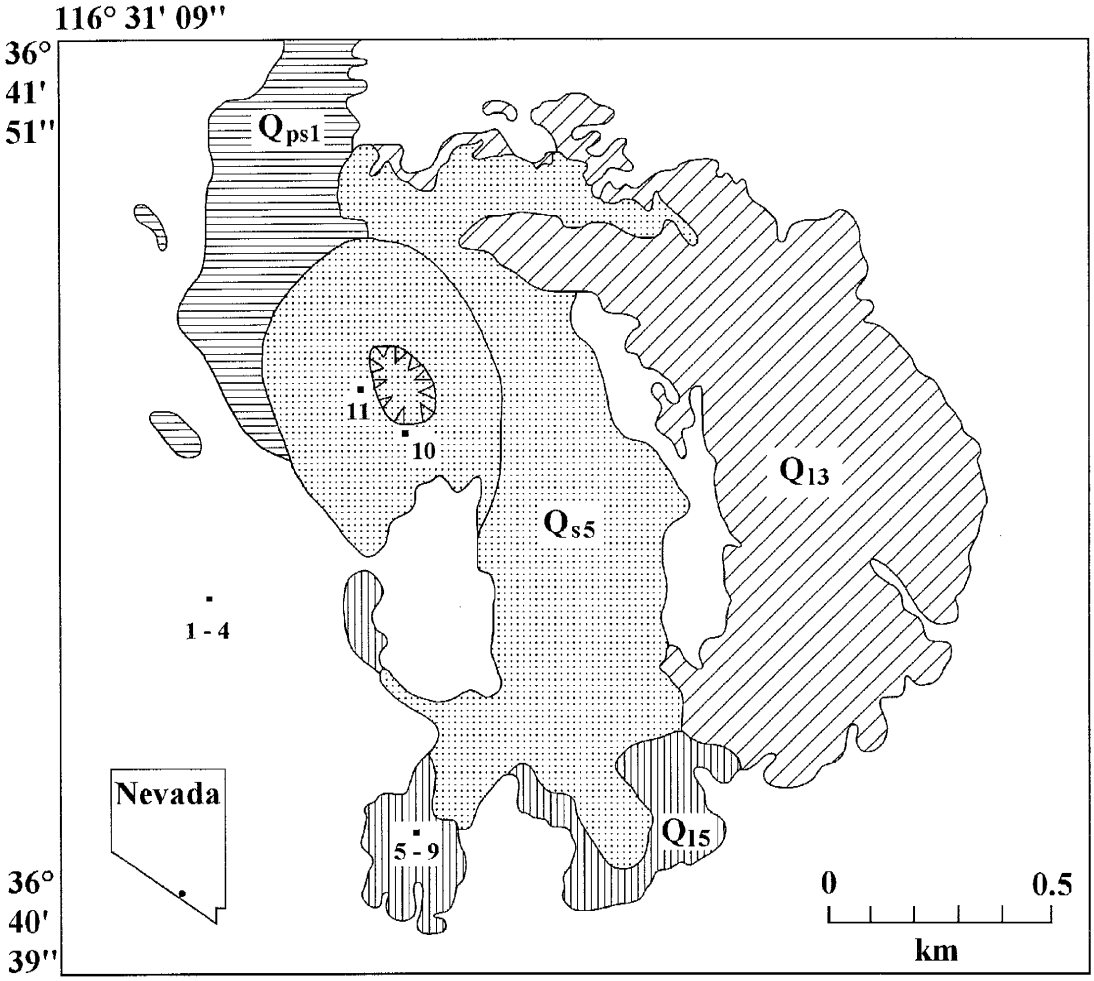

Fig. 6.1. Geologic map of Lathrop Wells volcanic center (modified from Turrin et al., 1991) and locations of samples for ^{36}Cl. Numbers correspond to those in Table 6.1. Patterns and letter designations indicate major stratigraphic units: Q_{l5} - stratigraphically older lava flow; Q_{s5} - scoria deposits contemporary with Q_{l5}; Q_{l3} - stratigraphically younger lava flow; Q_{ps1} - pyroclastics; blank space indicates undifferentiated alluvial deposits surrounding the volcanic center. Toothed pattern indicates the rim area.

results with the existing K/Ar dates to obtain weighted means of 136 $\pm$8 ka for the older unit and 141 $\pm$9 ka for the younger one. Although several age determinations have been attempted, the existing age estimates are discordant, and the problem of the eruption history at Lathrop Wells remains controversial.

Surface exposure dating by cosmogenic ^{36}Cl accumulation

The cosmogenic ^{36}Cl method (Davis and Schaeffer, 1955; Phillips et al., 1986) is based on the fundamental difference between high surface (cosmogenic) and low subsurface (radiogenic or background) production rates of ^{36}Cl. In the subsurface, ^{36}Cl forms almost exclusively due to thermal neutron activation of ^{35}Cl by slow neutrons associated with radioactive decay of U and Th (Bentley et al., 1986). In rocks exposed at the surface, ^{36}Cl is produced primarily by spallation reactions on ^{39}K and ^{40}Ca due to fast secondary neutrons and by thermal neutron activation of ^{35}Cl (Phillips et al., 1986; Zreda et al., 1990, 1991). The subsurface ^{36}Cl concentration is in secular equilibrium between radiogenic production and decay, i.e., it is constant over time. The radiogenic ^{36}Cl can thus be subtracted from the measured ^{36}Cl to yield the cosmogenic component, which is subsequently used to calculate surface-exposure ages. In this study, we used the dating equations, scaling factors for latitude and altitude, and ^{36}Cl production parameters presented in Zreda et al. (1991).

Evaluation of accuracy and precision of ^{36}Cl age determination is based on the following considerations. (1) Accuracy of the method is primarily dependent on uncertainty in the production rates which are estimated to be less than 10% (Zreda et al., 1991) in the Great Basin area. These production rates have already been applied to date Meteor Crater, Arizona (Phillips et al., 1991) and yielded an average age within 2% of that from independent age estimates. Potential problems with temporal variations in cosmogenic nuclide production rates that affect young samples ($\sim$10 ka) are probably negligible for older samples because these variations are averaged over time. (2) Analytical errors associated with determination of major and trace elements, stable Cl, and ^{36}Cl are on the order of a few percent and lead to similar uncertainties in ^{36}Cl ages. Precision of ^{36}Cl ages depends mainly on rates of postdepositional processes occurring on sampled surfaces. Erosional removal of <80 cm of soil (since the surface formation) results in a small overestimation of the age, whereas removal of thicker material will have an opposite result. These two effects can be recognized based on statistical analysis of ^{36}Cl data sets. The cosmogenic ^{36}Cl method has been shown to yield accurate and precise ages for surfaces with negligible erosion (Phillips et al., 1990; Zreda et al., 1991; Phillips et al., 1991), but its applicability to fast eroding landforms remains to be confirmed. In this study, we therefore concentrated our sampling on relatively stable surfaces, such as basalt flows.

Experimental methods

Using a hammer and a chisel we collected samples from the top 5 cm of carefully selected rocks. We then extracted Cl from all samples and measured ^{36}Cl by accelerator mass spectrometry.

Sample collection

Samples LWC88-1, YM88-5, YM88-6L, YM88-6M, and YM88-8 were taken from pressure ridges on the tops of the lava flow south of the cone (unit Q_{l5} of Turrin et al., 1991), which is stratigraphically the oldest unit in the volcanic center (Turrin et al., 1991). Field observations indicated a possibility that parts of the lava flow were covered by eolian sand deposits, which would have provided shielding from cosmic rays and temporarily decreased the cosmic-ray flux reaching the rock surface if the sand dunes had migrated over the rocks sampled. This would result in underestimation of the calculated eruption age. To minimize this possibility, we selected the highest pressure ridges we could find for sample collection. We also explored deep fractures in the higher parts of the lava flow for remnants of eolian deposits but could not find any. We consider it unlikely that the high points on the floor which we sampled were ever covered by sand.

A small alluvial plateau west of the cone contains isolated pyroclastics (unit Q_{ps1} of Turrin et al., 1991), which are considered the youngest volcanics in this area. Bombs were sampled from this relatively flat alluvial surface because we considered it less subject to erosional modification than the loose and steeply sloping cone surfaces. We collected four small volcanic bombs (LWC88-3 through LWC88-6) lying on top of the soil. The sampled bombs are ellipsoidal and range in size from 40 to 80 cm in length. The rocks are dense, contain no vesicles, and are lightly weathered. The bombs did not have the thick weathering rinds that are typical of buried basaltic cobbles.

Finally, we analyzed two samples (LWC89-S and LWC89-W) of volcanic bombs from the top of the very rim of the cinder cone (unit Q_{s5} of Turrin et al., 1991). Although sample LWC89-W was relatively fresh-looking, sample LWC89-S was brick-red and clearly was strongly chemically altered. Although the rim area is geomorphically less stable and thus less suitable for dating than the other two locations, we analyzed the two samples for comparison with the flow and volcanic bomb samples.

Sample preparation and analyses

The samples were cleaned of any organic material present at the surfaces, ground, and leached in 5% nitric acid to remove any meteoric Cl from the grain boundaries and to dissolve any secondary carbonates present in the vesicles and micropores within the rock matrix. Samples for ^{36}Cl were obtained by dissolution of powdered rocks in hot

mixture of concentrated nitric and hydrofluoric acids and precipitation of Cl as AgCl (Zreda et al., 1990, 1991). The samples were measured by accelerator mass spectrometry (Elmore et al., 1979) at either the University of Rochester or Purdue University. Major element composition was determined by X-ray fluorescence on fused disks, boron and gadolinium by prompt gamma emission spectrometry, and chlorine by combination ion-selective electrode.

Determination of ^{36}Cl ages

The lava-flow samples (LWC88-1 and YM88-5 through YM88-8; Table 6.1) collected from the tops of pressure ridges required correction for surface geometry. The thermal-neutron absorption rate calculated by Zreda et al. (1990, 1991) is valid for smooth, flat, and broad surfaces where thermal neutrons are lost from the rock only in the vertical direction. If the surface geometry is rough (e.g., basalt flows with pressure ridges), thermal neutrons will leak out of the rock not only upwards, but also sideways. This added outflux of thermal neutrons reduces the thermal neutron capture rate and lowers the production rate of ^{36}Cl from ^{35}Cl, thus leading to underestimation of the apparent ^{36}Cl ages.

The required correction depends on the surface geometry, particularly on the height of those parts that protrude above the base level, and calculating it on the basis of principles of cosmic-ray physics is rather difficult. Fortunately, experimental data for

Table 6.1. Target element concentrations, macroscopic cross sections (Σ), $^{36}Cl/Cl$ ratios, and ^{36}Cl surface-exposure ages for samples from Lathrop Wells, Nevada.

Map no.	Sample ID	K_2O (%)	CaO (%)	Cl (ppm)	Σ^* (cm^2/kg)	$^{36}Cl/Cl^\dagger$ (10^{-15})	Sample age (ka)	Surface age (ka)	Eruption age (ka)
1	LWC88-3	1.67	7.48	268	7.54	344 ±15	79 ±3.4		
2	LWC88-4	1.44	7.41	255	7.49	417 ±19	96 ±4.5	84 ±8.1	
3	LWC88-5	1.64	7.57	272	7.44	371 ±20	85 ±4.6		
4	LWC88-6	1.67	7.40	105	7.39	600 ±35	78 ±4.6		
5	LWC88-1	1.75	7.33	270	7.53	335 ±26	93§ ±7.2		
6	YM88-5	1.72	7.14	268	7.43	270 ±25	73§ ±6.8		81 ±7.9
7	YM88-6L	1.84	7.06	308	7.07	281 ±19	81§ ±5.4	81 ±7.3	
8	YM88-6M	1.88	7.19	292	7.67	270 ±21	77§ ±6.0		
9	YM88-8	1.98	7.48	217	6.96	352 ±27	79§ ±6.1		
10	LWC89-S	1.59	7.51	1164	8.45	263 ±29	83# ±9.2	76 ±10	
11	LWC89-W	1.61	7.32	233	7.27	326 ±27	68 ±5.7		

Note: The sample ages are for single rock samples, the surface ages are arithmetic averages of the sample ages, and the eruption age is the overall arithmetic mean. All samples are from the surface, at elevation 914 m above sea level, lat 36.4°N, long 243.4°E; the elevation-latitude-depth (ELD) scaling factor (equation 1 in Zreda et al., 1991) for all samples is 1.89.

* Macroscopic absorption cross section of the rock (Zreda et al., 1991).

† After subtraction of the radiogenic $^{36}Cl/Cl$ of 11×10^{-15}.

§ Corrected for surface geometry (see text for details). Uncorrected surface age is 67 ± 6.1 ky.

Corrected for meteoric $^{36}Cl/Cl$ (see text for details).

thermal neutron behavior at and below the solid-air interface have recently been made available for various geometries (Fabryka-Martin et al., 1990). Specifically, for a pyramidlike construction above a base-level surface, which was geometrically closest to pressure ridges on lava flows, Fabryka-Martin et al. (1990) observed a 30% decrease in the thermal neutron flux, relative to the flux at the flat surface. Therefore, for the samples from the lava flow, we reduced by 30% the production rate of ^{36}Cl due to thermal neutron absorption by ^{35}Cl. We note that this correction is simply empirical and probably represents a maximum estimate of neutron leakage. The production rates due to spallation reactions remain unchanged because the energetic neutrons that are responsible for these reactions are relatively unaffected by the rock-air interface.

The five lava-flow samples yielded corrected cosmogenic ^{36}Cl ages ranging from 73 to 93 ka, with the mean of 81 $\pm$7.3 ka (Table 6.1; Fig. 6.2). The ages are approximately uniformly distributed in this interval. Their scatter can be attributed to analytical errors of ^{36}Cl determination, which range from 6.8% to 10.7%, and to errors associated with the other geochemical parameters. The standard deviation of the sample mean is similar to the individual standard deviations, which indicates that there are probably not any random factors, other than analytical uncertainties, that significantly affect these dates.

The group of four "alluvial" volcanic bombs (samples LWC88-3 through LWC88-6) yielded surface-exposure ages ranging from 78 to 96 ka, with an average value of 84

±8.1 ka (Table 6.1; Fig. 6.2). The sample standard deviation of 9.6% is somewhat higher than the individual analytical errors, that range from 4.3% to 5.8%. This discrepancy may result from erosional processes occurring on the surface where the samples are collected. Because of the distribution of thermal neutrons below the surface, erosion may result in either too old or too young apparent ages, depending on erosion rates. In this case, since the spread of the data points is very small, and the number of samples is very limited, the sample mean is the best estimate of the eruption time. Furthermore, these dates are in very good agreement with those calculated above for the lava flow.

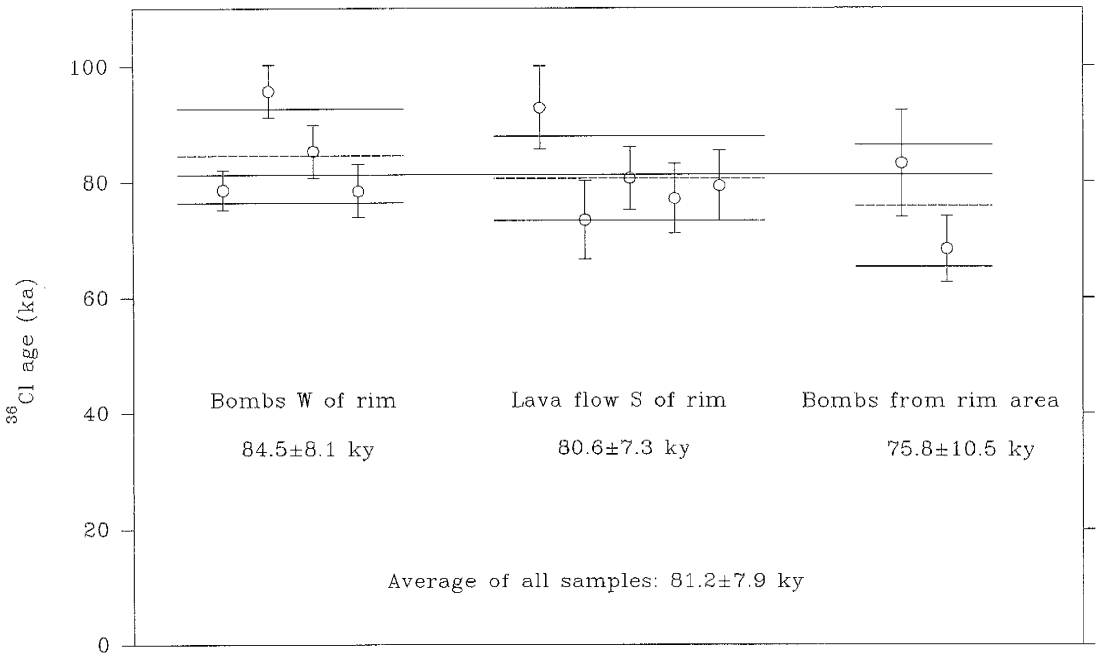

Fig. 6.2. ^{36}Cl ages of samples from Lathrop Wells. Error bars represent ^{36}Cl measurement errors. Long dashes are means of three groups of samples; short dashes represent intervals within one standard deviation calculated for each group; solid line is mean of all 11 samples.

The last two samples we measured (LWC89-S and LWC89-W) are less suitable for dating than the remaining nine because of their location in the rim area and because of the presence of inseparable secondary minerals in one of them. They were collected from the geomorphically unstable rim area, where the effects of erosion are particularly profound. We consider it likely that both of them could have been initially covered by some loose volcanic material and then gradually exposed by erosion. Full evaluation of this hypothesis would require a much more complete data set and will not be attempted here.

In addition to its possibly complex exposure history, sample LWC89-S has undergone extensive chemical and mineralogical changes; olivines have been replaced by iddingsite and micropores have been filled with secondary carbonates. The carbonates are easily separable from the rock matrix by leaching in nitric acid. However, iddingsite is not separable from the rest of the rock, and, therefore, the measured ^{36}Cl content and total concentration of Cl in the weathered sample are essentially composite components that make these samples unsuitable for dating in a straightforward fashion. However, it is possible to decompose this combined information into two parts, cosmogenic and meteoric, if one of them is known beforehand. We discuss the procedure in a separate paper (in preparation) and focus here on the dating.

The calculated age for sample LWC89-S is 83 $\pm$9.2 ka, which is in acceptable agreement with the age of 68 $\pm$5.7 ka obtained for the second sample from the rim area.

The average value of 76 $\pm$10 ka is slightly below the average values for the lava flow and the four volcanic bombs described above. This small discrepancy may be explained by faster erosion on the cone rim than in other areas, but may also be a result of analytical uncertainty.

Comparison of the ^{36}Cl data from the three surfaces studied indicates that the three average ages are statistically indistinguishable. We therefore combine them to obtain an overall average of 81 $\pm$7.9 ka as our best estimate of the eruption time (Table 6.1; Fig. 6.2). Our age estimate appears to be in reasonable agreement with independent methods. It falls between the bracketing U/Th dates of 345 and 25 ka from Szabo et al. (1981). In Figure 6.3, we compare the cumulative distribution of the ^{36}Cl dates with the distribution of $^{40}Ar/^{39}Ar$ dates reported by Turrin et al. (1991). Although the medians of the two distributions differ by about 60 ka, the two distributions do overlap. The younger median age by the ^{36}Cl method could possibly be attributed to the effects of erosion, which would bias cosmogenic nuclide methods toward younger (in this case) than actual apparent ages. However, erosion should produce a wide scatter in apparent ages from samples collected from different locations, and the close grouping of the ^{36}Cl dates argues strongly that the effects of erosion have been minimal.

Turrin et al. (1992) presented a result of incremental heating $^{40}Ar/^{39}Ar$ analysis. The sample from unit Q_{l3} yielded a plateau age of 142 $\pm$19 ka, which agrees with the earlier total fusion estimates, and which is statistically different than the ^{36}Cl ages

reported herein. However, the same sample gave an isochron age of 107 ±31 ka (Turrin et al., 1992) that appears to be in better agreement, within 1σ, with our estimates. Additional analyses will be required to adequately compare the results of the two methods.

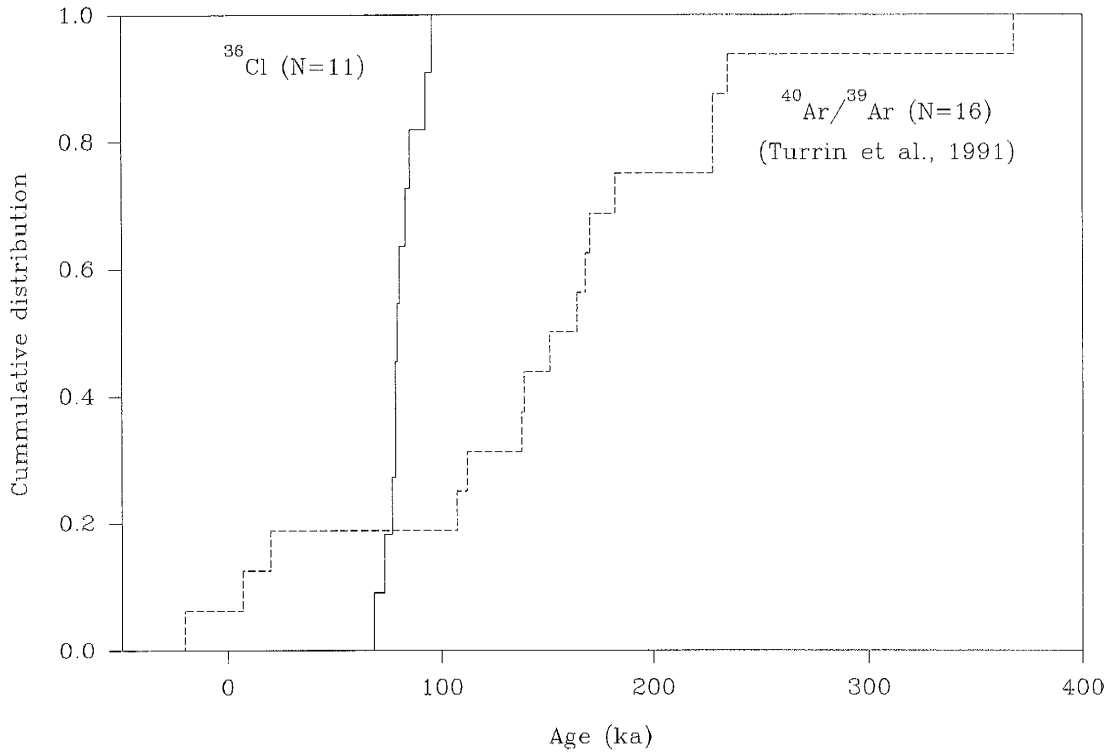

Fig. 6.3. Cumulative distributions of ^{36}Cl ages and total fusion ^{40}Ar/^{39}Ar and K/Ar ages of Turrin et al. (1991). Two distributions overlap, but respective means differ by ~60 ka. For comparison, recently reported incremental heating ^{40}Ar/^{39}Ar plateau age is 142 ±19 ka, while isochron age is 107 ±31 ka (Turrin et al., 1992).

As demonstrated by Figure 6.2, there are no statistically significant differences between the ^{36}Cl dates from the various sample groups. Our data, therefore, do not support a hypothesis of multiple eruptions at the Lathrop Wells center. However, neither

do the data preclude multiple eruptions. The following considerations must be acknowledged when evaluating the possibility of multiple eruptions. (1) Not all mapped eruptive units have been dated. (2) The one-standard-deviation statistics of the combined data would permit a 16 ka interval within which the center could have erupted more than once. (3) The empirical neutron leakage correction for samples from flow Q_{l5} could be too large. The limiting minimum case would be no excess neutron leakage, in which case the mean age for the Q_{l5} samples would be 67 $\pm$6.1 ka. This age is different at 1σ level than the age of the four bombs and would support the possibility of multiple eruptions. This possibility might be evaluated by sampling Q_{l5} at other, flatter locations. (4) There is some possibility that a recent, minor scoria eruption could have deposited only a thin layer of cinders on the cone rim. If such a thin layer were then rapidly eroded off the rim, the ^{36}Cl dates on previously erupted bombs might possibly be little affected, and thus still agree with the dates from the flow and bombs away from the cone. This possibility could readily be evaluated by measuring profiles of cosmogenic nuclide accumulation with depth through the scoria near the base of the cone.

Acknowledgments

Supported by the National Science Foundation grants EAR-8603440, EAR-8916667, SES-8901437, PHY-8818281. We thank R. Dorn for supplying samples LWC89-S and LWC89-W and W. McIntosh for helpful discussions on the $^{40}Ar/^{39}Ar$ dating method.

References cited

Bentley, H.W., Phillips, F.M., and Davis, S.N., 1986, Chlorine-36 in the terrestrial environment, *in* Fritz, P. and Fontes, J.-Ch., eds., Handbook of environmental isotope geochemistry, Volume 2, The terrestrial environment, B: New York, Elsevier, p. 427-480.

Crowe, B., Self, S., Vaniman, D., Amos., R., and Perry, F., 1983, Aspects of potential magmatic disruption of a high level radioactive waste repository in southern Nevada: Journal of Geology, v. 91, p. 259-276.

Crowe, B., Harrington, C., McFadden, L., Perry, F., Wells, S., Turrin, B., and Champion, D., 1988, Preliminary geologic map of the Lathrop Wells volcanic center: Los Alamos Report LA-UR-88-4155, p. 7.

Davis, R., Jr. and Schaeffer, O.A., 1955, Chlorine-36 in nature: Annals of New York Academy of Science, v. 62, p. 105-122.

Elmore D., and nine more, 1979, Analysis of ^{36}Cl in environmental water samples using an electrostatic accelerator: Nature, v. 277, p. 22-25.

Fabryka-Martin, J.F., Fowler, M.M., and Biddle, R., 1990, Study of neutron fluxes underground: Los Alamos National Laboratory Isotope and Nuclear Chemistry Division Quarterly Report October 1 - December 31, 1990, p. 82-85.

Phillips, F.M., Leavy, B.D., Jannik, N.D., Elmore D., and Kubik, P.W., 1986, The accumulation of cosmogenic chlorine-36 in rocks: A method for surface exposure dating: Science, v. 231, p. 41-43.

Phillips, F.M., Zreda, M.G., Smith, S.S., Elmore, D., Kubik, P.W., Dorn, R.I., and Roddy, D.J., 1991, Dating the impact at Meteor Crater: Comparison of ^{36}Cl buildup and varnish ^{14}C with thermoluminescence: Geochimica et Cosmochimica Acta, v. 55, p. 2695-2698.

Swadley, W.C., Hoover, D.L., and Rosholt, J.N., 1984, Preliminary report on late Cenozoic faulting and stratigraphy in the vicinity of Yucca Mountain, Nye County, Nevada: U.S. Geological Survey Open-File Report 84-788, p. 42.

Szabo, B.J., Carr, W.J., and Gottschall, W.C., 1981, Uranium-thorium dating of Quaternary carbonate accumulations in the Nevada Test Site region, southern Nevada: U.S. Geological Survey Open-File Report 81-119, p. 35.

Turrin, B.D., Champion, D., and Fleck, R.J., 1991, $^{40}Ar/^{39}Ar$ age of the Lathrop Wells volcanic center, Yucca Mountains, Nevada: Science, v. 253, p. 654-657.

Turrin, B.D., Champion, D., and Fleck, R.J., 1992, Measuring the age of the Lathrop Wells volcanic center at Yucca Mountain: Response to comment on $^{40}Ar/^{39}Ar$ age of the Lathrop Wells volcanic center, Yucca Mountains, Nevada: Science, v. 257, p. 556-558.

Vaniman, D.T., Crowe, B.M., and Gladney, E.S., 1982, Petrology and geochemistry of Hawaiite lavas from Crater Flat, Nevada: Contributions to Mineralogy and Petrology, v. 80, p. 341-357.

Wells, S.G., McFadden, L.D., Renault, C.E., and Crowe, B.M., 1990, Geomorphic assessment of late Quaternary volcanism in the Yucca Mountain area, southern Nevada: Implications for the proposed high-level radioactive waste repository:

Geology, v. 18, p. 549-553.

Zreda, M.G., Phillips F.M., and Smith, S.S., 1990, Cosmogenic ^{36}Cl dating of geomorphic surfaces: New Mexico Tech Hydrology Program Report 90-1, p. 104.

Zreda, M.G., Phillips, F.M., Elmore, D., Kubik, P.W., Sharma, P., and Dorn, R.I., 1991, Cosmogenic ^{36}Cl production rates in terrestrial rocks: Earth and Planetary Science Letters, v. 105, p. 94-109.

7. Age and geomorphic history of Meteor Crater, Arizona, from cosmogenic ^{36}Cl and rock varnish ^{14}C

FRED M. PHILLIPS[1], MAREK G. ZREDA[1], STEWART S. SMITH[1], DAVID ELMORE[2*], PETER W. KUBIK[2#], RONALD I. DORN[3] and DAVID J. RODDY[4]

[1]Geoscience Department, New Mexico Tech, Socorro, NM 87801

[2]Nuclear Structure Research Laboratory, University of Rochester, Rochester, NY 14627

[3]Geography Department, Arizona State University, Tempe, AZ 85287

[4]U.S. Geological Survey, Flagstaff, AZ 86001

[*]Present address: Physics Department, Purdue University, West Lafayette, IN 47907

[#]Present address: Institut Für Mittelenergiephysik, ETH-Hönggerberg, CH-8093 Zürich, Switzerland

Abstract - Using cosmogenic ^{36}Cl buildup and rock varnish radiocarbon, we have measured the exposure age of rock surfaces at Meteor Crater, Arizona. Our ^{36}Cl measurements on four dolomite boulders ejected from the crater by the impact yield a mean age of 49.7 $\pm$ 0.85 ka, which is in excellent agreement with an average age of 49 $\pm$ 3 ka obtained from thermoluminescence studies on shock-metamorphosed dolomite and

Published in 1991, Geochimica et Cosmochimica Acta 55, 2695-2698.

quartz. These ages are supported by undetectably low ^{14}C in the oldest rock varnish sample.

THE AGES OF TERRESTRIAL impact structures yield important information on meteorite fluxes. Young meteorite craters are difficult to date by conventional means, but may be amenable to recently-developed surface exposure dating techniques such as rock varnish dating or cosmogenic nuclide accumulation methods. For an initial application of surface exposure dating to meteorite craters we selected Barringer Meteor Crater in northern Arizona, U.S.A.. Barringer Crater is the largest terrestrial crater (1.2 km diameter and 170 m depth) whose impact origin is proven by meteorite fragments (comparison with other craters in GRIEVE, 1979). The crater was originally estimated to be 25,000 $\pm$ 5,000 years old (SHOEMAKER, 1983; SHOEMAKER and KIEFFER, 1979), based on soil development within the crater and on the ejecta blanket and on the stratigraphy of lacustrine sediments in the crater. However, a recent thermoluminescence study on impact-shocked dolomite and sandstone yielded an average age of 49,000 $\pm$ 3,000 years (SUTTON 1985a, 1985b). The considerable discrepancy between these dates motivated further research into the crater chronology, using cosmogenic ^{36}Cl (half-life 301,000 years) and varnish ^{14}C (half-life 5,730 years).

Chlorine-36 is produced in rocks at the surface of the earth by cosmic-ray spallation, mainly of K and Ca, and by activation of ^{35}Cl by cosmic-ray neutrons (PHILLIPS et al., 1986; FABRYKA-MARTIN, 1988). Cosmogenic ^{36}Cl significantly

above subsurface concentrations is produced only to depths of a few meters below the earth's surface (FABRYKA-MARTIN, 1988; LAL, 1987), and its buildup has been shown to be a regular function of time (PHILLIPS et al., 1986). Zreda et al. (1990, in press) have determined ^{36}Cl production rates (normalized to sea level and 90° N latitude) of 4,160 $\pm$ 310 atoms ^{36}Cl (mole $^{39}K)^{-1}$ yr^{-1} and 3,050 $\pm$ 210 atoms ^{36}Cl (mole $^{40}Ca)^{-1}$ yr^{-1}, and a thermal neutron capture rate of $(3.07\pm0.24)*10^5$ neutrons (kg rock)$^{-1}$ yr^{-1}. Meteor Crater is an excellent subject for cosmogenic nuclide accumulation dating because we can identify and sample one geological unit (the Kaibab Formation) that was virtually completely shielded from cosmic rays by 10 m of Moenkopi Sandstone prior to the impact (RODDY, 1978). Boulders of Kaibab Formation were nearly instantaneously exposed to cosmic radiation when they were ejected from the crater by the impact. The date of the impact can be determined by measuring the amount of cosmogenic ^{36}Cl that has accumulated, provided that the boulder surfaces are not strongly eroded. Erosion rates in the range of millimeters per thousand years will have little effect on cosmogenic ^{36}Cl dates, but loss of decimeter, or greater thickness, slabs would reduce the apparent age.

For ^{36}Cl dating we sampled five large boulders of siliceous dolomite of the Kaibab Formation, ranging in height from 1 to 7 meters above the land surface. We attempted to select boulders that would have stood above the surface of the post-impact ejecta blanket. Boulder surfaces were examined for visual evidence of weathering and erosion and only surfaces that appeared stable were sampled. Three of the boulders were from

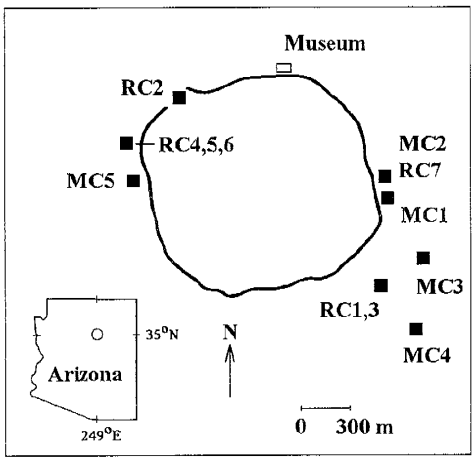

Fig. 7.1. Carbon-14 and chlorine-36 sample locations at Barringer Meteor Crater, Arizona

the crater rim and two from the ejecta blanket surrounding the crater (Fig. 7.1). Samples were obtained by chiseling pieces from the top 2 cm of the centers of the boulder tops. The samples were ground and leached in deionized water to remove any meteoric chlorine. Chlorine was extracted from approximately 100 g samples by dissolution in nitric and hydrofluoric acid and precipitated as AgCl. Details of the extraction and analytical methods can be found in ZREDA et al. (1990, in press). The $^{36}Cl/Cl$ ratio of the AgCl precipitate was measured by accelerator mass spectrometry (ELMORE et al., 1979) at the University of Rochester. Major elements and chlorine were measured by x-ray fluorescence and rare earth elements and boron by inductively-coupled argon plasma atomic emission (WALSH et al., 1981). Results are given in Table 7.1. Exposure ages were then calculated using recently determined ^{36}Cl production rates (ZREDA et al., 1990, in press) and the cosmic-ray altitude/latitude dependence of LAL (In press), using the ^{36}Cl production equation solved for time:

$$t = \frac{-1}{\lambda}\ln\left[1-\frac{(R-R_0)\lambda N}{E_n L_n D_n\left[\psi_K C_K+\psi_{Ca}C_{Ca}+\phi_n\frac{\sigma_{35}N_{35}}{\Sigma\sigma_i N_i}\right]}\right]$$

where:

t - exposure time (years),

λ - decay constant for ^{36}Cl (2.30×10^{-6} yr^{-1}),

R - measured $^{36}Cl/Cl$ ratio,

R_0 - background $^{36}Cl/Cl$ ratio in equilibrium with the U and Th derived neutrons,

N - total number of chlorine atoms per kg of rock,

E_n, L_n and D_n - scaling factors for elevation above sea level (E), latitude and longitude (L), and depth below surface (D),

ψ_K, ψ_{Ca} - production rates of ^{36}Cl from ^{39}K and ^{40}Ca, in atoms of ^{36}Cl (kg rock)$^{-1}$ yr^{-1} (unit concentration of K and Ca)$^{-1}$,

C_K and C_{Ca} - concentrations of K and Ca,

ϕ_n - thermal neutron capture rate, in neutrons (kg rock)$^{-1}$ yr^{-1},

σ_{35} - thermal neutron absorption cross-section for ^{35}Cl, in cm^2,

N_{35} - number of ^{35}Cl atoms per kg of rock,

σ_i - thermal neutron absorption cross-section for element i in the sample, in cm^2,

N_i - number of atoms of element i per kg of rock.

Rock varnish is a thin coating of manganese and iron oxides and clays that accumulates on exposed rocks in arid and semi-arid environments (DORN and

OBERLANDER, 1982). Organic matter that has been encapsulated by rock varnish provides a minimum-limiting age for the exposure of the underlying rock surface, as long as organic matter is not found in the rock underlying varnish. This conclusion is supported by dozens of AMS radiocarbon measurements on varnish organic matter, sampled from sites with independent age control (DORN et al., 1989). The stable carbon isotope composition of this organic matter is similar to adjacent vegetation (DORN and DENIRO, 1985), and images of varnish organic matter in cross-section suggest it consists of fragments of pollen, lichens, cyanobacteria, and other organic matter.

Light and electron microscope observations of varnish in cross-section reveal that most of the organic fragments are sandwiched between the basal varnish and the underlying rock. The organic matter was extracted with HF, HCl, hydroxylamine hydrochloride, and dithionite. Details of the method can be found in DORN et al. (1989, 1986). Rock varnish does not accumulate on relatively soluble lithologies such as limestone (DORN and OBERLANDER, 1982) and the only ^{36}Cl sample with a silicified limestone surface that retained varnish was MC-2 (same as RC-7 in Table 7.2). The other six samples in Table 7.2 are from surfaces that record the geomorphic evolution of Barringer Meteor Crater. Microscopic examination of varnish cross-sections indicated that all varnishes except RC-3 displayed suitable characteristics for dating, according to criteria outlined by DORN (1989) and KRINSLEY et al. (1990).

Table 7.1. Chemical and ^{36}Cl data for ejected material at Barringer Meteor Crater Arizona. All ages were computed using a subsurface $^{36}Cl/Cl$ ratio of 11 x 10^{-15}.

Sample[a]	CaO [%]	K_2O [%]	Cl [ppm]	$^{36}Cl/Cl$ [10^{-15}]	Sigma[b] [cm^2/kg]	Altitude [m]	Boulder age [years]
MC-1	21.1	0.47	143	1462 ± 44	2.38	1,730	49,700 ± 1,500
MC-2	23.4	0.47	131	1194 ± 39	2.37	1,730	36,500 ± 1,150
MC-3	29.2	0.43	217	1280 ± 57	2.65	1,700	50,400 ± 2,200
MC-4	23.8	0.78	132	1469 ± 71	2.73	1,700	48,500 ± 2,350
MC-5	28.2	0.44	259	1207 ± 38	2.50	1,730	50,300 ± 1,600
Mean[c]							47,100 ± 6,000
Mean without MC-2[c]							49,700 ± 850

[a] Correlation with Nishiizumi et al. (1991) sample numbers: MC-1 = M-8, MC-2 = M-9, MC-4 = M-10, MC-5 = M-7.

[b] Macroscopic absorption cross-section of rock sample calculated as $\Sigma\sigma_i N_i$, where σ_i is the thermal neutron absorption cross-section for element i and N_i is the number of atoms of element i per kg of rock.

[c] Standard deviation of individual sample ages, not from analytical uncertainties.

Four of the five boulders sampled for ^{36}Cl have exposure ages that are in excellent agreement. The mean and standard deviation of samples MC-1 and MC-3 through MC-5 is 49,700 ± 850 years. In contrast, MC-2 yielded an exposure age of 36,500 years. This age differs from the mean of the other four samples by 15 standard deviations and thus the discrepancy seems unlikely to be due to analytical variation. This inference is supported by comparison with the ^{10}Be data from the same boulders, reported by NISHIIZUMI et al. (1991); they found that MC-2 exhibited a relative ^{10}Be deficit very similar to the relative ^{36}Cl deficit that we measured. We conclude that some surficial material was removed from MC-2 subsequent to its emplacement on the crater rim, and that the mean age of 49,700 years (excluding MC-2) is preferred as our best estimate for the date of the meteorite impact.

Table 7.2. AMS Radiocarbon analyses of varnish from Barringer Meteor Crater, Arizona.

Sample	^{14}C age (radiocarbon years)	Lab Numbers	
		Beta (target)	ETH (^{14}C)
RC-1 Meteorite Fragments*	24,470 ± 470	17179	2416
RC-2 Moenkopi Fracture*	24,130 ± 710	18874	2611
RC-3 Coconino Nodules+*	26,610 ± 360	19889	2805
RC-4A Kaibab Boulder 1*	17,210 ± 180	20572	2944
RC-4B Kaibab Boulder 1#	17,220 ± 180	20571	2943
RC-5 Kaibab Boulder 2#	22,990 ± 290	22210	3196
RC-6 Kaibab Boulder 3#	21,830 ± 250	22212	3198
RC-7 Kaibab Boulder 4#	>37,300	26686	4290

+ Control sample contaminated, age probably older than date of varnish formation.

* Varnish sample prepared by D. Tanner

Varnish sample prepared by R. Dorn

There is a remote possibility that the boulders were initially covered by some material, and then gradually exposed. However, the consistency of the ^{36}Cl data indicates that in such a case a unique set of conditions, including thickness of the covering materials and erosion rates, would have to be present to explain the observed $^{36}Cl/Cl$ ratios. In one potential scenario all four boulders would be covered by the same amount of material and the erosion rates at all locations would be uniform; in another scenario the cover would be of different thickness at each boulder and the erosion rates would have to be such that they would result in simultaneous exposure of all boulders. None of these circumstances seems reasonable; we therefore conclude that the four older boulders were exposed at the surface virtually instantaneously after the impact. The

close agreement between samples MC-1 and MC-3 through MC-5 also indicates that the boulders' surfaces have experienced little degradation, since it is unlikely that they would all erode at the same rate.

The mean ^{36}Cl date is supported by the ^{14}C results. Given that the basal varnish ^{14}C dates provide limiting minimum ages, the oldest ages should provide the best estimate of the date of crater formation. The oldest age (RC-7) is greater than 37,400 years, reasonably consistent both with the individual ^{36}Cl age for that boulder (36,500 years, sample MC-2) and with the preferred date for the impact (49,700 years). One sample, RC-3, was suspected of being contaminated because the subvarnish rock from the control sample showed organic matter that could have been incorporated into the basal varnish, resulting in an apparent age older than the basal varnish.

RC-1 is an aggregate sample collected from 26 meteorite fragments on a pediment surface on the southeast flank of the crater; the ^{14}C age indicates that the pediment formed and stabilized before about 24-25 ka. This is in excellent agreement with geomorphologic interpretation that the pediment stabilized about 25 ka ago, based on correlations with radiocarbon dates in the region (SHOEMAKER, 1983; SHOEMAKER and KIEFFER, 1979). The remaining four varnish samples were taken from small boulders on the ejecta sheet and a fracture in the crater wall. Because of their small size, these boulders were probably deeply buried in the loose ejecta sheet that surrounded the crater shortly after the impact. Their ^{14}C ages range between 17,000 and 25,000 years.

These ages reflect the geomorphologic evolution of the crater; they probably indicate a period of geomorphic instability due to major and rapid climatic fluctuations accompanying (and following) the last glacial maximum (FORESTER, 1987).

Our study and the parallel one by NISHIIZUMI et al. (1991) offer one of the first opportunities to compare ^{36}Cl buildup ages with those from the ^{10}Be-^{26}Al pair. The comparison is quite favorable. NISHIIZUMI et al. (1991) sampled four of the same boulders we sampled. In agreement with our result, MC-2 (their number M-9) gives a younger age (30,700) than the other three. The average of MC-1, MC-4, and MC-5 (their M-7, M-8, and M-10) is 42,200 $\pm$ 7,600, that of M-7 and M-10 is 48,500 years. The very close agreement may be somewhat fortuitous, but the consistency does support the fundamental assumptions of cosmogenic nuclide accumulation dating.

Our results indicate that ^{36}Cl buildup and other cosmogenic nuclide accumulation techniques should be applicable to the dating of Quaternary meteorite impact features, and could thus contribute to quantifying the rate of meteorite impacts. The individual ^{36}Cl ages were satisfactorily reproducible (one standard deviation of 1.7 percent) for samples from stable surfaces. This reproducibility is very close to the theoretical optimum value calculated from the ^{36}Cl analytical uncertainties: 1.9 percent. This standard deviation provides a realistic empirical estimate of the method reproducibility, including sample-to-sample variability. It does not address systematic sources of error (for example, in the production rate estimates), which will cause greater uncertainty in

the accuracy of the age estimate. Further testing will be necessary to provide the data for realistic estimation of the systematic uncertainties. However, the mean ^{36}Cl age of 49,700 $\pm$ 850 is supported by the absence of measurable ^{14}C in basal rock varnish from one of the boulders and by the agreement of the mean ^{36}Cl age with both the thermoluminescence dates of SUTTON (1985b) and the ^{10}Be-^{26}Al dates of NISHIIZUMI et al. (1991). All these methods indicate that the meteorite impact was indeed about 25,000 years earlier than previously thought.

Acknowledgements - This work was supported by NSF grants EAR-8603440, SES-8901437, and PHY-8515908 and by a grant from the Barringer Crater Company for radiocarbon dating that was matched by NSF grant EAR-86507041. We thank D. Dorn and D. Tanner for field and laboratory assistance and M. Tamers, J. Stipp and W. Wolfli for AMS ^{14}C analyses.

References

DORN R.I. (1989) Cation-ratio dating: A geographic perspective. *Prog. Phys. Geogr.* **13**, 559-596.

DORN R.I. and OBERLANDER T.M. (1982) Rock varnish. *Prog. Phys. Geogr.* **6**, 317-367.

DORN R.I., JULL A.J.T., DONAHUE D.J., LINICK T.W. and TOOLIN L.J. (1989) Accelerator mass spectrometry radiocarbon dating of rock varnish. *Geol. Soc.*

Amer.Bull. **101**, 1363-1372.

DORN R.I., BAMFORTH D.B., CAHILL T.A., DOHRENWEND J.C., TURRIN D.B.,DONAHUE D.J., JULL A.T.J., LONG A., MACKO M.E., WEIL E.B., WHITLEY D.S. and ZABEL T.H. (1986) Cation-ratio and accelerator radiocarbon dating of rock varnish on Mojave artifacts and landforms. *Science* **231**, 830-833.

DORN R.I. and DENIRO M.J. (1985) Stable carbon isotope ratios of rock varnish organic matter: A new paleoenvironmental indicator. *Science* 227, 1472-1474.

ELMORE D., FULTON B.R., CLOVER M.R., MARSDEN J.R., GOVE H.E., H.NAYLOR H., PURSER K.H., KILIUS L.R., BEUKINS R.P. and LITHERLAND A.E. (1979) Analysis of ^{36}Cl in environmental water samples using an electrostatic accelerator. *Nature* **277**, 22-25.

FABRYKA-MARTIN J.T. (1988) Production of radionuclides in the earth and their hydrogeologic significance, with emphasis on chlorine-36 and iodine-129. Ph.D. dissertation, University of Arizona.

FORESTER R.M. (1987) Late Quaternary paleoclimate fluctuations from lacustrine ostracods. In *North America and Adjacent Oceans During the Last Deglaciation* (eds. Rudiman W.F. and Wright H.E. Jr.), Geol. Soc. Amer. (Boulder) K-3, 261-276.

GRIEVE R.A.F. and ROBERTSON P.B. (1979) The terrestrial cratering record: I. Current status of observations. *Icarus* **38**, 211-229.

KRINSLEY D.H., DORN R.I. and ANDERSON S.W. (1990) Factors that interfere with

the age determination of rock varnish. *Phys. Geogr.* **11**, 97-119.

LAL D. (1987) Cosmogenic nuclides produced in situ in terrestrial solids. *Nucl. Instr. Meth. Phys. Res.* **B29**, 238-245.

LAL D. (1991) Cosmic ray lebeling of erosion surfaces: in situ production rates and erosion models. *Earth Planet. Sci. Lett.* 104, 424-439.

NISHIIZUMI K., KOHL C.P., SHOEMAKER E.M., ARNOLD J.R., KLEIN J., FINK D. and MIDDLETON R. (1991) ^{10}Be-^{26}Al exposure ages at Meteor Crater, Arizona. *Geochim. Cosmochim. Acta.*

PHILLIPS F.M., LEAVY B.D., JANNIK N.D., ELMORE D. and KUBIK P.W. (1986) The accumulation of cosmogenic chlorine-36 in rocks: a method for surface exposure dating. *Science* **231**, 41-43.

RODDY D.J. (1978) Pre-impact geologic conditions, physical properties, energy calculations, meteorite and initial crater dimensions and orientations of joints, faults and walls at Meteor Crater, Arizona. *Proc. Lunar Planet. Sci. Conf. 9th*, 3891-3930.

SHOEMAKER E.M. (1983) Asteroid and comet bombardment of the earth. *Ann. Rev. Earth Planet. Sci.* **11**, 461-494.

SHOEMAKER E.M. and KIEFFER S. (1979) *Guidebook to the Geology of Meteor Crater.* Arizona State Univ.

SUTTON S.R. (1985a) Thermoluminescence measurements on shock-metamorphosed sandstone and dolomite from Meteor Crater, Arizona: 1. Shock dependence of thermoluminescence properties. *J. Geophys. Res.* **90**, 3683-3689.

SUTTON S.R. (1985b) Thermoluminescence measurements on shock-metamorphosed sandstone and dolomite from Meteor Crater, Arizona: 2. Thermoluminescence age of Meteor Crater. *J. Geophys. Res.* **90**, 3690-3700.

WALSH J.N., BUCKLEY F. AND BAKER J. (1981) The simultaneous determination of the rare-earth elements in rocks using inductively coupled plasma source spectrometry. *Chem. Geology* 33, 141-153.

ZREDA M.G., PHILLIPS F.M. and SMITH S.S. (1990) Cosmogenic ^{36}Cl dating of geomorphic surfaces. *Hydrology Program Rept. 90-1*, New Mexico Tech.

ZREDA M.G., PHILLIPS F.M., ELMORE D., KUBIK P.W., SHARMA P. and Dorn R.I. (1991) Cosmogenic ^{36}Cl production rates in terrestrial rocks. *Earth Planet. Sci. Lett.* 105, 94-109.

8. Glacial chronology of the eastern White Mountains, California-Nevada by the cosmogenic ^{36}Cl method

Marek G. Zreda and Fred M. Phillips

Geoscience Department, New Mexico Tech, Socorro, New Mexico 87801

Peter W. Kubik* and Pankaj Sharma

Nuclear Structure Research Laboratory, University of Rochester, Rochester, New York 14627

* Present address: Paul Scherrer Institut, c/o Institut Für Mittelenergiephysik, ETH-Hönggerberg, CH-8093 Zürich, Switzerland

Cosmogenic ^{36}Cl was measured in boulders on lateral and terminal moraines at Chiatovich Creek and nearby canyons, eastern White Mountains. The chronology developed from the ^{36}Cl data indicates glacial episodes at ~150,000, ~100,000(?), 18,000-19,000, 13,000-14,000, and 12,000 yr. The previously mapped Early Middle Creek, Late Perry Aiken, and Early Perry Aiken all apparently date to the last glacial maximum (18,000-19,000 yr). The ^{36}Cl chronology generally confirms previous age estimates, with the exception of the Perry Aiken glaciation (18,000-19,000 yr) which was previously thought to be as old as 150,000 yr. The chronology indicated much more extensive glaciation at ~150,000 yr (Indian glaciation) than during any subsequent glaciations. This may have been due to unique climatic

Submitted to Quaternary Research, November 1993.

conditions at that time, or due to uncertainties regarding the actual extent of glaciations.

Introduction

The White Mountains are an eastward tilted block composed of Precambrian and Cambrian sedimentary rocks intruded in their northern part by granitic plutons. The block is uplifted to a maximum elevation of more than 4.3 km above sea level. The range rises ~ 3 km above the valley floor in its northern part and ~ 1.5 km in the south. The White Mountains are separated from the tectonically similar Sierra Nevada (a westward tilted and uplifted block) by the Owens Valley graben. Because of their position east of the Sierra Nevada, the White Mountains are in the rain shadow of the Sierra Nevada and receive much less precipitation.

In the Pleistocene, the northeastern part of the range was intensively glaciated. The glaciations may have become progressively less extensive with time because continuous uplift of the Sierra Nevada block resulted in intensification of the rain shadow and decreasing precipitation. The deposits of the oldest glaciations are found at low elevations of < 2.0 km, while the lower limit of the late Wisconsin moraines is at ~ 3.0 km (Elliott-Fisk, 1987).

The glacial deposits in the canyons on the northeastern side of the range were described by Blackwelder (1934), LaMarche (1965), Elliott-Fisk (1987) and Swanson et al. (1993), and mapped by Krauskopf (1971), Crowder et al. (1972) and Swanson et al. (1993). It has been postulated that although the glacial units correspond chronologically with those from the Sierra Nevada, the magnitudes of successive glaciations were different largely due to tectonic uplift of the White Mountain block and changing climatic conditions (Elliott-Fisk, 1987). While in the Sierra Nevada the late Pleistocene glaciers extended far down the valleys and obliterated older deposits, in the White Mountains early glaciations are thought to have been more extensive than later ones and thus evidence of a larger number of glaciations preserved.

Table 8.1. Glacial chronostratigraphy for the White Mountains and its Sierra Nevada equivalents (after Elliott-Fisk, 1987). The ages for the deposits in South Chiatovich Creek were assigned by Swanson et al. (1993) based on weathering rind thickness.

Glaciation	Assigned age (10^3 yr)		Proposed Sierra Nevada equivalent
	White Mountains	Chiatovich Creek	
Chiatovich Cirque	10	10	Hilgard
Late Middle Creek	14	14	Late Tioga
Early Middle Creek	20	20	Early Tioga
Perry Aiken	140	55-150	Tahoe
Indian	400-600	220-328	pre-Tahoe
Dyer	1000	611-2532	Sherwin
Chiatovich Flats	2000-2500	-------	McGee

An attempt to assign ages to the glacial deposits from the White Mountains and correlate them with those in the Sierra Nevada was made by Elliott-Fisk (1987) who used morphostratigraphic and relative-dating criteria, supported by ^{14}C dating of rock varnish from the youngest deposits (Dorn et al., 1990), to develop a glacial chronology. She found evidence of seven glaciations to which she assigned ages ranging from 10,000 yr to 2.5 myr, and related them to the major Sierran glaciations (Table 8.1). A detailed study of soils in South Chiatovich Creek by Swanson et al. (1993) confirmed the stratigraphy of the first-order glaciations proposed by Elliott-Fisk (1987) and allowed for development of a refined chronology (Table 8.1) for the older glacial deposits, based on semi-quantitative rind thickness data.

Only a limited number of numerical ages for glacial deposits in the White Mountains have been obtained. Varnish ^{14}C ages obtained for the youngest moraines in Chiatovich Creek and Middle Creek indicate glaciations at 10,000, 13,000-14,000, and 18,000-20,000 yr (Dorn et al., 1990); these ages are the basis for the chronology of the youngest glacial units listed in Table 8.1. No older deposits have been systematically dated yet and only a few single ^{26}Al-^{10}Be surface exposure ages have been reported by Nishiizumi et al. (1993).

In this paper, we report 42 new ^{36}Cl surface exposure ages from 14 glacial surfaces in South Chiatovich Creek (Figs. 8.1 and 8.2) and develop a local glacial chronology. Thirteen other samples from Middle Creek, immediately north of

Chiatovich Creek, Perry Aiken Creek, below White Mountain Peak, and Cottonwood Creek, below Sheep Mountain (Fig. 8.1) were also analyzed to extend the results from Chiatovich Creek and place them in a regional context.

Cosmogenic ^{36}Cl dating of moraines

Mountain glaciers erode bedrock and previously accumulated deposits, transport the debris down the valley, and deposit some of the material in the form of moraines. The surface of the moraine is bombarded by energetic cosmic particles which interact with ^{40}Ca, ^{39}K, and ^{35}Cl to produce cosmogenic ^{36}Cl. Since the production rates of ^{36}Cl from these target nuclei are known, its accumulation in surficial rocks can be used to calculate surface exposure ages (Phillips et al., 1990; Zreda et al., 1991). The production rates determined by Zreda et al.(1991) and reevaluated in chapter 4 are: 2910 atoms ^{36}Cl (mol Ca)$^{-1}$ yr^{-1}, 7520 atoms ^{36}Cl (mol K)$^{-1}$ yr^{-1}, and 313500 thermal neutrons (kg rock)$^{-1}$ (calendar year)$^{-1}$, all at sea level and high geomagnetic latitudes. We note that although the original data set used by Zreda et al. (1991) for estimating the ^{36}Cl production rates was calibrated in part on varnish ^{14}C ages from Chiatovich Creek glacial boulders, the new data set used in chapter 4 does not contain any samples from Chiatovich Creek.

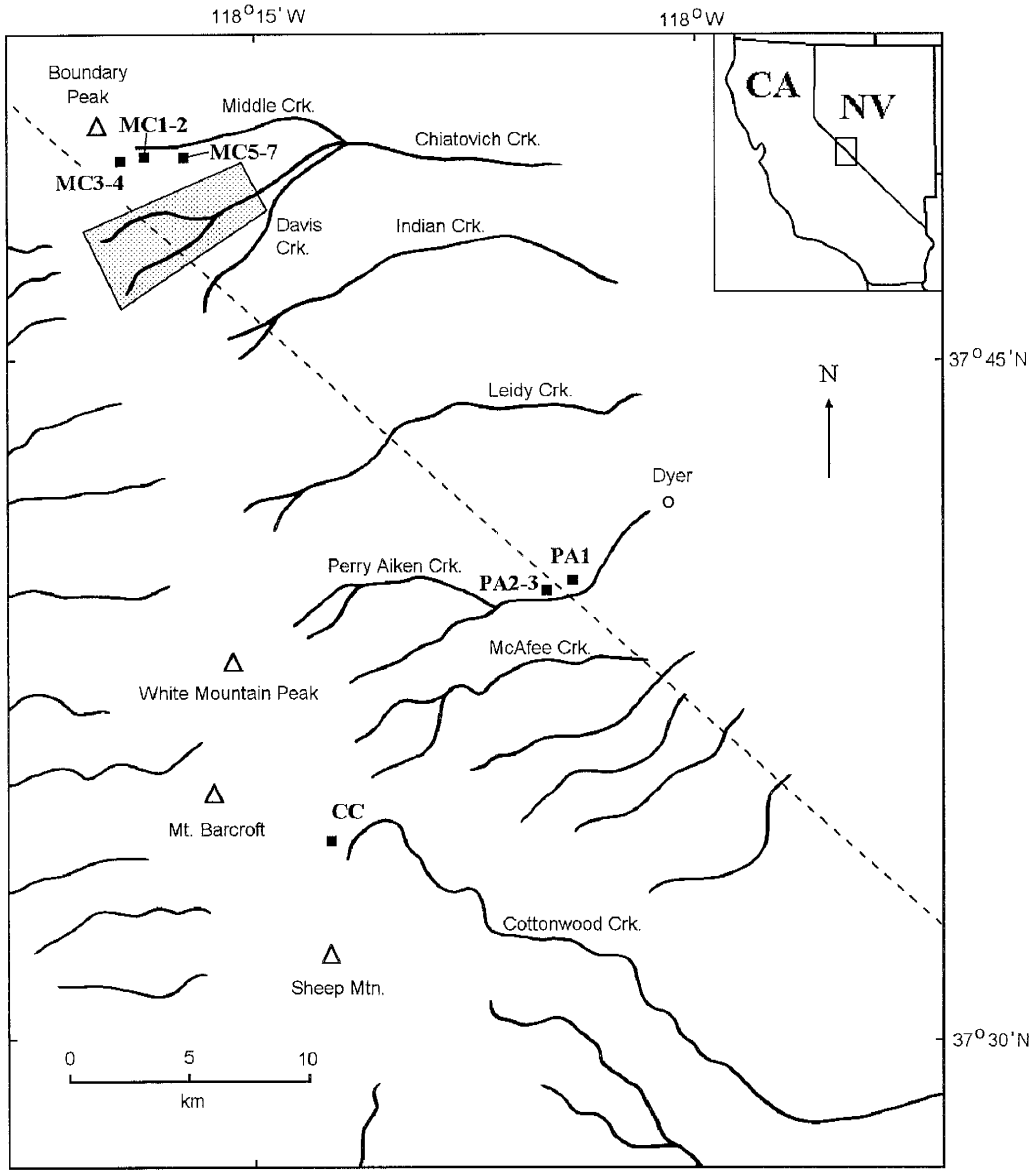

Fig. 8.1. Study areas in the eastern White Mountains (adapted from Elliott-Fisk, 1987). Shaded area is enlarged in Figure 8.2.

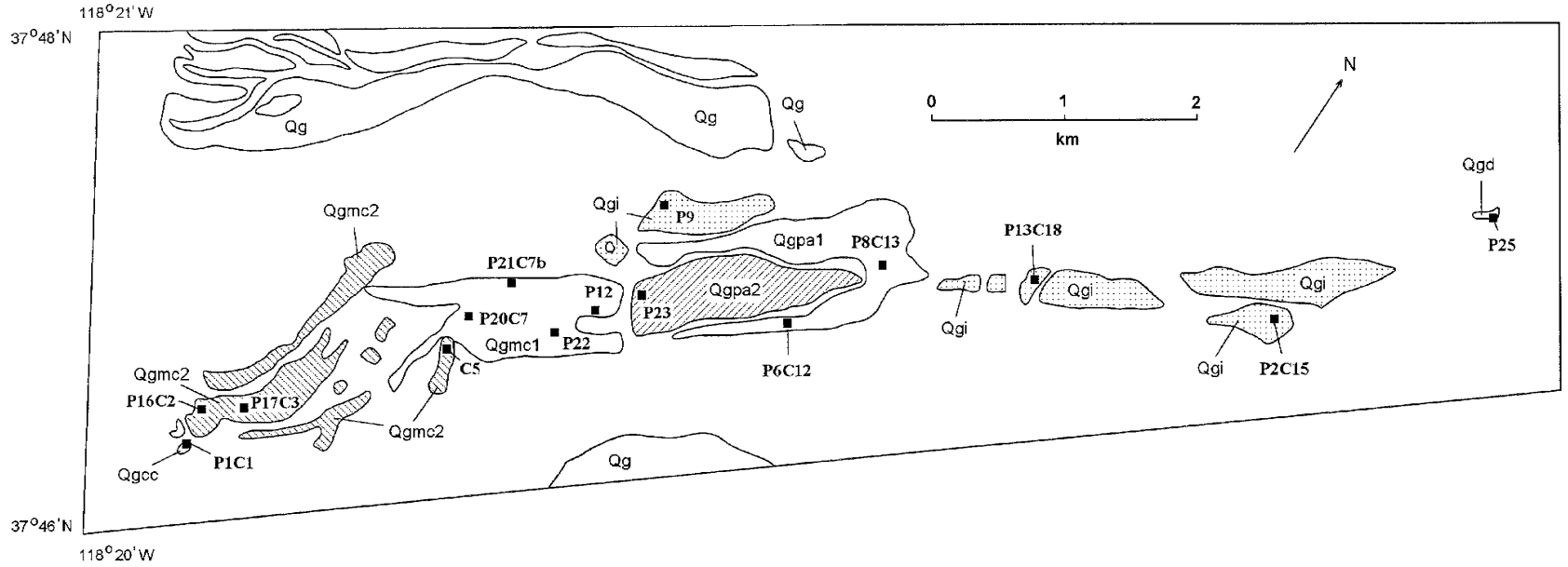

Fig. 8.2. Glacial deposits at Chiatovich Creek (modified from Swanson et al., 1993).

Uncertainties in the exposure time calculation result from a combination of (a) analytical errors associated with isotopic and chemical analyses; (b) temporal variability of the production rates; (c) spatial variability of the production rates; and (d) uncertainty in the determination of the current production rates. The analytical error is on the order of five to ten percent and is mainly due to analytical uncertainty of ^{36}Cl measurements by accelerator mass spectrometry; this error is routinely reported as the uncertainty of the age determination (Phillips et al. 1990, 1991; Zreda et al. 1990, 1991, 1993). The uncertainties in the assessment of the temporal and spatial distribution of the cosmic-ray intensity and also the production rates of cosmogenic ^{36}Cl may perhaps add another ten or twenty percent to the estimated error of the exposure time. The error associated with temporal variability of the production rates may be on the order of 15-20% for surfaces younger than 15,000 yr and becomes negligible for older surfaces (Cerling and Craig, submitted). In addition to these uncertainties, the calculated age from a single boulder can vary from the actual landform age because the individual boulder may have had an exposure history differing from the "model" history of the landform. The most common source of variation is that individual boulders may have eroded out of the landform subsequent to its deposition, yielding younger ages than that for the formation of the surface.

Samples

The samples were collected using the field criteria described by Phillips et al. (1990) and Zreda et al. (1990), except that only three samples, instead of the usual minimum of five, were collected at most individual sample locations; instead, more locations were sampled. This sampling strategy was employed because of the following two considerations. Firstly, numerous glacial landforms exist in Chiatovich Creek and field evidence indicates that there are groups of deposits made during single glaciations. Secondly, some of these landforms have been modified more than others by postdepositional surficial processes and such modifications result in apparent ^{36}Cl ages usually younger than the true age. To minimize the likelihood of dating only a strongly modified surface, multiple landforms were sampled and the oldest surface ages used in construction of the glacial chronology. The sample locations and the stratigraphic units from which the samples were collected are in Figures 8.1 and 8.2 and Table 8.2.

The samples were prepared as described by Phillips et al. (1990, 1991) and Zreda et al. (1990, 1991, 1993). Chlorine-36 was measured by accelerator mass spectrometry (Elmore et al., 1979) at the University of Rochester, major element composition was determined by X-ray fluorescence on either fused disks or pressed pellets, boron and gadolinium by prompt gamma emission spectrometry, and chlorine by combination ion-selective electrode.

Results and discussion

The geochemical and isotopic data and calculated cosmogenic ^{36}Cl exposure ages are presented in Table 8.2. The exposure ages for single boulders are also graphed in Figure 8.3. The results are discussed below in the stratigraphic order from the youngest deposits to the oldest.

Glacial deposits at Chiatovich Creek

Chiatovich Cirque (Qcc)

A very small terminal moraine (samples C87-1 through 4) just below the cirque in South Chiatovich Creek at an elevation of ~3.75 km is the youngest glacial deposit in this area. Two out of the four samples have an average ^{36}Cl surface exposure age of 12,000 $\pm$ 1100 yr, while the other two ages are close to 5500 yr. It is likely that the younger ages are due to surface modifications and the moraine age is closely approximated by the older samples. This age is in agreement with the result of Dorn et al. (1990) who reported a rock varnish ^{14}C age of 9740 yr (~11,500 calendar yr) for a boulder from this moraine.

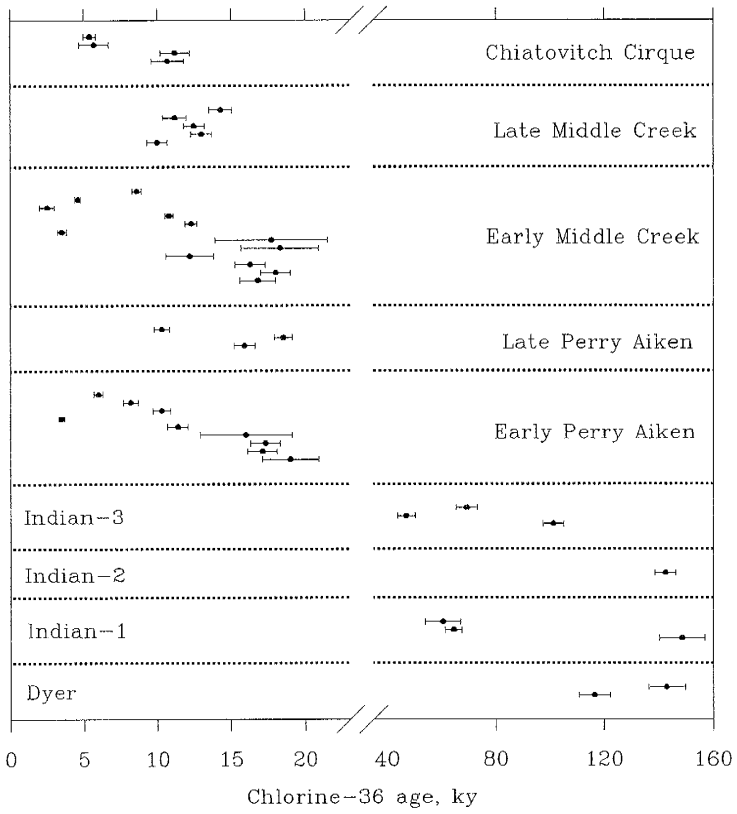

Fig. 8.3. Cosmogenic ^{36}Cl ages for the glacial deposits in the Chiatovich Creek basin.

Late Middle Creek (Qmc2)

The deposits of Late Middle Creek glaciations occupy the area below the cirque at an elevation ~3.7 km. Five samples from two morainal ridges (samples C287-5 and 6, and C387-1 through 3) gave a mean age of 12,900 ± 700 yr, with the oldest age 14,300 yr. The maximum age agrees with the varnish radiocarbon age of 12,700 yr B.P. (~14,000 calendar yr) for deposits in similar stratigraphic position in Middle Creek, few km north of this location (Elliott-Fisk, 1987).

Table 8.2. Locations, target element concentrations, $^{36}Cl/Cl$ ratios, and calculated ^{36}Cl ages for samples from Chiatovich Creek. Mean, median and maximum ages are reported for some surfaces; for other, only the maximum age is reported.

Unit	Sample	Cl ppm	K_2O %	CaO %	$\Sigma\sigma N$ cm^2/kg	Elev. km	ELD	$^{36}Cl/Cl$ 10^{-15}	Age, 10^3 yr	
									Boulder	Surface
	C87-1	126	3.21	0.74	4.76	3.75	12.22	762 ± 76	12.7 ± 1.3	
Chiatovich	C87-2	56	2.48	0.24	4.50	3.75	12.46	953 ± 77	11.2 ± 1.0	12.0 ± 1.1
Cirque	C87-3	123	5.44	0.21	4.97	3.75	12.46	473 ± 74	5.7 ± 1.0[a]	12.0
	C87-4	140	2.91	0.38	4.59	3.75	12.46	320 ± 21	5.2 ± 0.4[a]	12.7
	C287-5	117	5.16	3.77	5.96	3.72	12.38	879 ± 62	10.0 ± 0.7	
Late	C287-6	149	2.53	0.43	4.66	3.72	12.38	652 ± 35	13.0 ± 0.7	12.2 ± 1.7
Middle	C387-1	134	5.37	0.65	5.08	3.67	12.13	910 ± 50	12.5 ± 0.7	12.5
Creek	C387-2	97	4.76	1.19	5.16	3.67	12.13	972 ± 65	11.2 ± 0.8	14.3
	C387-3	74	2.89	0.22	4.56	3.67	12.13	1065 ± 54	14.3 ± 0.8	
	C587-1	152	3.78	0.83	4.79	3.29	9.83	788 ± 51	16.8 ± 1.2	
	C587-2	121	2.77	0.83	4.64	3.29	9.83	834 ± 43	18.0 ± 1.0	
	C587-3	65	0.15	0.25	4.40	3.29	9.83	458 ± 27	16.3 ± 1.0	
	C787-1	160	5.43	0.49	6.44	3.24	9.51	595 ± 74	12.2 ± 1.6[a]	17.4 ± 0.8
Early	C7b87-1	72	3.04	0.66	6.00	3.17	9.51	1059 ± 144	18.3 ± 2.6	17.7
Middle	C787-2	88	2.31	0.73	4.56	3.24	9.51	861 ± 176	17.7 ± 3.8	18.3
Creek	C787-3	46	2.60	0.46	4.44	3.24	9.51	294 ± 19	3.5 ± 0.3[a]	
	CH89-P12	87	6.27	0.30	5.57	3.05	8.41	927 ± 29	12.3 ± 0.4[a]	
	CH89-P12-1	43	4.70	2.41	5.48	3.05	8.41	1283 ± 33	10.8 ± 0.3[a]	

	CH89-P22-1	58	0.10	0.46	3.58	3.14	8.87	103 ± 14	2.5 ± 0.5[a]	
	CH89-P22-2	42	4.42	0.26	4.48	3.14	8.87	533 ± 26	4.6 ± 0.2[a]	
	CH89-P22-3	50	3.68	0.88	4.42	3.14	8.87	769 ± 27	8.6 ± 0.3[a]	
Late	CH89-P23-1	124	5.11	0.86	5.80	2.95	7.92	759 ± 33	15.9 ± 0.7	17.2 ± 1.8
Perry	CH89-P23-2	94	3.98	0.47	4.99	2.95	7.92	925 ± 27	18.5 ± 0.6	17.2
Aiken	CH89-P23-3	82	5.05	1.05	6.03	2.95	7.92	670 ± 28	10.3 ± 0.5[a]	18.5
	C1187-1	151	4.36	1.00	4.91	3.02	8.20	680 ± 125	16.0 ± 3.1	
	C1187-2	99	1.90	0.42	4.58	3.02	8.20	418 ± 22	11.4 ± 0.7[a]	
	C1187-3A-W	104	2.87	0.22	4.48	3.02	8.20	575 ± 79	13.6 ± 2.0[a]	
Early	C1287-1A-W	144	5.30	0.51	4.57	2.84	7.24	565 ± 78	13.2 ± 1.9[a]	17.4 ± 1.2
Perry	C1287-2	79.0	2.22	0.47	4.44	2.84	7.24	336 ± 19	8.2 ± 0.5[a]	17.2
Aiken	C1287-3	105	0.05	9.74	6.93	2.84	7.24	218 ± 13	6.0 ± 0.3[a]	19.0
	CH89-P8-C13-1	41	4.76	0.44	5.28	2.81	7.27	1837 ± 184	19.0 ± 1.9	
	CH89-P8-2	66	5.12	0.48	5.58	2.81	7.27	1170 ± 67	17.1 ± 1.0	
	CH89-P8-3	122	5.15	0.70	6.26	2.81	7.27	753 ± 42	17.3 ± 1.0	
Indian-3	CH89-P2-C15	84	5.22	0.47	5.96	2.36	5.48	5225 ± 115	143 ± 3.8	143
	CH89-P3-C18-1	54	3.97	0.60	4.97	2.49	5.95	5073 ± 162	101 ± 3.7	
Indian-2	CH89-P3-2	58	5.24	0.37	5.28	2.49	5.95	2858 ± 183	47.0 ±3.2	101
	CH89-P3-3	42	4.45	0.28	4.97	2.49	5.95	4721 ± 245	69.3 ± 3.9	
	CH89-P9-1	97	4.66	0.71	6.61	3.05	8.41	6732 ± 312	149 ± 8.3	
Indian-1	CH89-P9-2	123	5.15	0.72	6.17	3.05	8.41	2965 ± 129	64.5 ± 3.1	149
	CH89-P9-4	35	4.71	1.01	5.30	3.05	8.41	7430 ± 738	60.6 ± 6.5	

Dyer	CH89-P25-1	54	5.22	0.60	5.49	2.26	5.12	6019 ± 259	116 ± 5.8	143
	CH89-P25-2	126	5.20	0.38	5.37	2.26	5.12	3729 ± 145	143 ± 6.7	
	MC87-1	71	4.24	1.51	4.58	2.7	6.68	5889 ± 604	116 ± 14	
	MC87-2	81	4.92	2.04	5.29	2.7	6.68	3844 ± 153	73.1 ± 3.2	
	MC87-3	32	0.77	1.91	4.50	2.8	7.07	1982 ± 405	45.2 ± 10	116
Indian	MC87-4	38	3.45	1.94	4.50	2.8	7.07	2928 ± 94	34.2 ± 1.2	
(Middle Creek)	MC87-5	152	5.05	2.22	5.38	2.6	6.48	1708 ± 46	49.4 ± 1.4	
	MC87-6	108	5.48	1.34	5.36	2.6	6.48	5607 ± 604	142 ± 19	140 ± 11
	MC87-7	101	2.70	2.37	4.87	2.6	6.48	4114 ± 330	138 ± 13	
Dyer	PA87-1	6	3.23	3.02	4.73	1.66	3.38	10677 ± 255	47.8 ± 1.2	46.0 ± 2.5
(Perry Aiken	PA87-2	5	4.00	1.78	4.51	1.76	3.63	6191 ± 412	18.2 ± 1.1[a]	44.2
Creek)	PA87-3	6	4.12	2.32	4.83	1.76	3.63	12156 ± 412	44.2 ± 1.6	47.8
Cottonwood	CC87-1	402	5.32	3.68	6.20	3.60	11.42	3505 ± 150	106 ± 5.2	
Creek	CC87-2	445	4.98	4.24	6.24	3.60	11.42	2389 ± 104	73.9 ± 3.6	106
	CC87-3	379	3.35	0.82	4.92	3.60	11.42	1144 ± 71	33.2 ± 2.2	

[a] Young outlier, not used in the calculation of the mean surface age.

Early Middle Creek (Qmc1)

The Early Middle Creek moraines extend 1-2 km down the valley to an elevation of 3.0 km. Seven samples from three ridges in the upper part of this moraine complex (samples C587-1 through 3, C787-1 through 3, and C7B87-1) and five samples from the lower part (CH89-P12, CH89-P12-1 and CH89-P22-1 through 3) gave discordant results. The upper moraines have maximum boulder ages of ~18,000 yr, while the lower part of the complex has apparent ages no older than 12,000 yr. A boulder from site C7 has a varnish ^{14}C age of 17,800 yr B.P., i.e., ~19,800 calendar yr (Dorn et al., 1990) and similar deposits in Middle Creek a varnish age of 18,500 yr B.P., i.e., ~20,500 calendar yr (Elliott-Fisk, 1987). The probable Sierran equivalent of the Early Middle Creek, the Tioga, has been dated at ~19,000 yr B.P. by varnish ^{14}C (Dorn et al., 1987).

Late Perry Aiken (Qpa2)

Only one terminal moraine (samples CH89-P23-1 through 3) was sampled from this unit and a maximum age of 18,500 yr was calculated. This age is older than the single ^{26}Al-^{10}Be age of 13,300 ± 500 obtained for a different boulder from this site by Nishiizumi et al. (1993). It is approximately equal to the maximum ^{36}Cl ages from the Early Middle Creek deposits which may indicate that both moraine complexes were deposited during the same glaciation. However, more samples from this site would be necessary to closely constrain the moraine age.

Early Perry Aiken (Qpa1)

Two lateral moraines (samples C1187-1 through 3 and C1287-1 through 3) and a terminal moraine (samples CH89-P8-1 through 3) were sampled. The boulders having the oldest surface exposure ages are 16,000, 10,000, and 19,000 yr. Because the stratigraphically younger deposits of the Late Perry Aiken glaciation date to 18,500 yr, these deposits must be older and thus the age of 19,000 $\pm$ 1900 yr is preferred. It is in good agreement with the minimum exposure age of 17,500 $\pm$ 800 yr calculated for a boulder from the terminal moraine (site P23) using the ^{26}Al-^{10}Be pair (Nishiizumi et al., 1993).

Both Early and Late Perry Aiken have significantly younger surface exposure ages than the ages obtained using relative dating methods (Elliott-Fisk, 1987; Swanson et al., 1993). Swanson et al. (1993) notes that the Perry Aiken moraines exhibit evidence of deep stream dissection. This process may result in erosion of the moraine surfaces and thus exposure of new surfaces to cosmic rays. In such a case, apparent ^{36}Cl ages depend on the erosion depth and the true landform age. For very deep erosion at constant rate, the mean of the apparent ages approaches one half of the true landform age (chapter 5). If the moraine surfaces have been lowered by as much as 15 m, as suggested by Swanson et al. (1993), the mean ^{36}Cl age of all boulders from this unit, 11,900 yr, would indicate a true age of no more than 24,000 yr, still much younger than the age estimates by Elliott-Fisk (1987) and Swanson et al. (1993). Both our ^{36}Cl ages and the ^{26}Al-^{10}Be age

of Nishiizumi et al. (1993) indicate that the Perry Aiken moraines were deposited approximately 20,000 yr ago and are therefore correlative with the Tioga moraines in the Sierra Nevada (Dorn et al., 1987).

Indian (Qi)

The Indian deposits are preserved as subdued moraines down valley at elevations of 2.49 (samples CH89-P3-1 through 3) to 2.36 km (sample CH89-P2) and as a left lateral moraine remanent perched ~100 m above the Perry Aiken deposits at an elevation of 3.05 km (samples CH89-P9-1, 2, and 4). The oldest ^{36}Cl boulder age for site P3 was 101,000 ± 10,000 yr, while the other two surfaces yielded similar oldest boulder ages of 143,000 ± 3800 and 149,000 ± 8300 yr, for P2 and P9, respectively. Nishiizumi et al. (1993) obtained an ^{26}Al-^{10}Be surface exposure age of 51,000 ± 4,000 yr for a boulder from site P9. This young age as well as the other younger ^{36}Cl ages must be due to erosion of the moraine surface. The oldest ^{36}Cl surface age, 149,000 yr, was obtained for a 5-m tall boulder (sample CH89-P9-1) whose top surface had presumably been continuously exposed to the cosmic radiation since deposition. This age is therefore our best estimate for the minimum age of the Indian glaciation. It is stratigraphically consistent with the ^{36}Cl ages of the Early Perry Aiken glaciation, but numerically inconsistent with previously assigned ages in the range 400,000-600,000 yr (Elliott-Fisk, 1987) and 220,000-328,000 yr (Swanson et al., 1993).

Dyer (Qd)

The oldest glacial deposits in Chiatovich Creek were found along a lower valley sidewall, approximately 50 m above the valley floor, at an elevation of 2.26 km (samples CH89-P25-1 and 2). They consisted of a few large plutonic erratics perched on Tertiary andesite outcropping on the valley wall. These samples gave ^{36}Cl ages of 116,000 $\pm$ 5800 (P25-1) and 143,000 $\pm$ 6700 yr A split of sample P25-1 was also dated by the cosmogenic ^{26}Al-^{10}Be pair and gave a minimum exposure age of 116,000 $\pm$ 11,000 yr (Nishiizumi et al., 1993). Both P25 samples are from geomorphically unstable side wall of the valley and they may have eroded out of the moraine matrix some time after the deposition of this moraine. In that case, even the maximum boulder age may considerably underestimate the true formation age. More than one cosmogenic nuclide can be useful in unraveling complex exposure histories and particularly in determining whether a surface has undergone significant lowering due to erosion. Significant erosion at a constant rate should result in different ages for nuclides having different half lives, while stable surfaces should give similar exposure ages. Thus, the good agreement between ^{26}Al-^{10}Be and ^{36}Cl ages for the younger sample supports a model of a stable surface. However, these two consistent ages are younger than the older ^{36}Cl age (sample P25-2) from this surface, which indicates that some surface modification other than erosion at a constant rate has occurred. One possible explanation is episodic erosion of the moraine surface during which a thick layer was removed in relatively short time and the cosmogenic nuclide clock was set for the younger boulder, but not for the older one.

This scenario is supported by the larger size of the older boulder (height $\sim$2 m) than of the younger one (only $\sim$1 m tall).

Other glacial deposits in the White Mountains

Middle Creek is north of Chiatovich Creek (Fig. 8.1) and contains a glacial sequence similar to that in Chiatovich Creek (Elliott-Fisk, 1987). We collected seven samples from two lateral moraines (samples MC87-1 through 4 and MC87-5 through 7) at elevations between 2.6 and 2.8 km on the south side of Middle Creek. These moraines are in a similar stratigraphic position to the moraines of the Indian glaciation in Chiatovich Creek (sample sites P2 and P3) and have been assigned to the Indian glaciation by Elliott-Fisk (1987). The oldest sample from the upper, stratigraphically younger moraine (sample MC87-1) has a ^{36}Cl age of 116,000 $\pm$ 14,000 yr, while the other samples from this location are much younger. The lower glacial deposit (MC87-5 through 7) yielded two ages close to 140,000 yr and one younger age. The oldest ages are also similar to the oldest age from the Indian moraines in Chiatovich Creek (site P2), 143,000 $\pm$ 4000 yr. The consistency of these ages indicates a similar timing and extent of glaciation in both valleys.

Three samples (PA87-1 through 3) were collected from large boulders on the surface of an uplifted diamicton near the mouth of Perry Aiken Creek, west of Dyer (Fig. 8.1) at an elevation of $\sim$1.7 km. This is the type site for the proposed Dyer

glaciation (Elliott-Fisk, 1987), although the subdued morphology and tectonic modification render difficult unambiguous distinction between tills and debris flow deposits at this site. Two out of three samples have a mean ^{36}Cl age of 46,000 $\pm$ 2500 yr, while the third sample is considerably younger. For comparison, the ^{26}Al-^{10}Be age of a different sample from the same surface is 71,000 $\pm$ 3000 yr (Nishiizumi et al., 1993). Neither the ^{36}Cl nor the ^{26}Al-^{10}Be ages correlate with any of our ages assigned to glacial episodes in this area. All of the cosmogenic nuclide accumulation ages are much younger than the $\sim$1 myr age estimated by Elliott-Fisk (1987) for the Dyer glaciation. These younger ages may result from fluvial deposition or reworking between 50,000 and 100,000 yr, or may reflect erosion associated with uplifting. In any case, it is highly unlikely that the ages have any but an indirect connection to glacial events in the White Mountains.

The last three samples described here (CC87-1 through 3) are from the Cottonwood Creek basin (Fig. 8.1). The samples were collected from Barcroft Granodiorite erratics perched on an interfluvial ridge of Reed Dolomite near the headwater of the basin, at an elevation of $\sim$3.6 km. The site is illustrated in Figure 5 of Elliott-Fisk (1987), who tentatively assigned deposition of the erratics to the Dyer glaciation. The oldest of the three erratics collected from this surface yielded an age of 106,000 $\pm$ 5000 yr which is younger than the age of 155,000 $\pm$ 5000 yr reported by Nishiizumi et al. (1993). The discrepancy may be explained by natural exposure variability between samples, since the ^{36}Cl and ^{26}Al-^{10}Be measurements were performed

on samples from different boulders. Both of these ages are similar to those obtained from Indian till in Chiatovich and Middle Creeks and suggest that the Cottonwood erratics were deposited during that glaciation.

Conclusions

We have measured cosmogenic ^{36}Cl accumulated in boulders on glacial deposits in four canyons on the eastern side of the White Mountains. The surface exposure ages calculated from these measurements can be compared to independent surface exposure age estimates from varnish ^{14}C and/or ^{10}Be-^{26}Al. The resulting chronology is, in all cases except one, in agreement with the relative age chronologies inferred by Elliott-Fisk (1987) and Swanson (1993).

The oldest glaciation for which we have been able to obtain reliable ages is the Indian. Maximum ages of about 150,000 yr have been measured at two of three Indian till sampling sites from Chiatovich Creek and one of two sites from Middle Creek. The younger maximum ages (101,000 and 116,000 yr) at the two remaining sites are probably due to erosion, although it is possible that they were actually deposited during a less extensive glaciation between 100,000 and 120,000 yr. The similar age distribution (including ^{10}Be-^{26}Al ages reported by Nishiizumi et al., 1993) for erratics from near the headwaters of the Cottonwood Creek drainage suggests that much of the crest of the range was covered by an ice cap during this glaciation. The presence of an ice cap

during the Indian glaciation, but not during the subsequent Perry Aiken glaciation, would be consistent with the much greater extent inferred for the Indian glaciation. Elliot-Fisk (1987) reported that the average terminal moraine elevation for the Indian glaciation deposits was 2.5 km, compared to 2.75 km for the Perry Aiken deposits, and the calculated equilibrium line altitude was 2.7 km, compared to over 3.0 km for the Perry Aiken glaciation.

We have also measured ^{36}Cl buildup in deposits attributed to the Dyer glaciation. These have yielded ages much younger than the 1 myr estimate of Elliot-Fisk (1987). We attribute the young ages to a combination of possible non-glacial origin (especially for the Perry Aiken Creek samples) and possible surface modification (especially for the P25 samples at the mouth of Chiatovich Creek). Although the oldest ages from the P25 site are similar to those for the oldest Indian deposits we think it more likely that these reflect major surface modification by downstream fluvial processes than that they are a result of glacial deposition at the site during the Indian glaciation.

The next three glacial deposits (in stratigraphically ascending order: the Early Perry Aiken, the Late Perry Aiken, and the Early Middle Creek) all yielded maximum ^{36}Cl buildup ages of about 19,000 yr. These ages are generally in good agreement with independent varnish ^{14}C and ^{10}Be-^{26}Al age estimates. All of these data suggest that the Perry Aiken and Early Middle Creek deposits resulted from different phases of a major glacial advance and subsequent retreat between about 20,000 and 17,000 yr, the period

of the Wisconsin glacial maximum.

The Late Middle Creek ^{36}Cl ages are significantly younger than those from the stratigraphically older deposits; the oldest ages are about 14,300 yr. The oldest ages of the diminutive Chiatovich Cirque moraines are about 12,700 yr. Both of these ages are supported by varnish radiocarbon data. These data indicate that the Late Middle Creek and Chiatovich Cirque moraines were deposited during the terminal phase of the Late Wisconsin glaciation.

The ages we have determined for the Late Middle Creek and Chiatovich Cirque deposits are in good agreement with previous estimates by Elliot-Fisk (1987) and Swanson et al. (1993). However, the ages we have measured for the Indian and Perry Aiken glaciations are both significantly younger than those estimated by the same authors. The previous age estimates were largely by correlation with other glacial deposits, based on surficial modification and soil development data. In effect, by introducing the "Early Middle Creek", an extra glacial stage was added which caused the older glaciations to be miscorrelated by one age step. Our age data are consistent with the soil profile development index data of Swanson et al. (1993), which show marked increases in the index between the Late Middle Creek and Early Middle Creek deposits, and between the Early Perry Aiken and Late Indian deposits, but little difference between the Early Middle Creek and Late and Early Perry Aiken deposits. We suggest that the glacial sequence be consolidated by combining the Early Middle Creek, the Late Perry

Aiken, and the Early Perry Aiken into a single Perry Aiken unit, and that the Late Middle Creek be termed simply Middle Creek.

Swanson et al. (1993) have argued that gradual erosion of the older moraine crests may produce anomalously young ages for the older moraines. Although we agree that erosion does play a significant role, we find it unlikely that gradual erosion would consistently produce maximum ages between 140,000 and 150,000 yr at three different sites. This consistency points to either a depositional or an erosional origin for these landforms at that time.

One surprising implication of this chronology is the marked difference in glacial extent between the last glacial maximum and the penultimate one. The Indian till, as mapped by Swanson et al. (1993), reaches 3.5 km further down-canyon and 500 m lower in elevation than the Early Perry Aiken till. This magnitude of difference is not reflected in the nearby Sierra Nevada moraines, where the last glacial maximum terminal moraines (Tioga) are typically less than 1 km shorter and 100 m higher than the maximum preceding mid-to-late Pleistocene (Tahoe) terminal moraines. We hypothesize two possible explanations for this discrepancy. (1) Some climatic anomaly at 150,000 yr may have affected the White Mountains differently than the Sierra Nevada. For example, if at that time most storms approached the western Great Basin from the south or southeast, rather than the west, the Sierra Nevada would have been in the rain shadow of the White Mountains, rather than the reverse. (2) The down-canyon Indian deposits may actually

be either erosional remanents of much older moraines, or else pro-glacial constructional features, whose present form is a result of major geomorphic modification during the extensive glaciation attested by the up-canyon glacial deposits dating to 150,000 yr (P9 and the Cottonwood erratics). In this case, the glaciers themselves need not have extended to very low elevations as recently as 150,000 yr and the glacial history therefore need not be markedly different from the Sierra Nevada. Additional work is necessary to address this important question.

Acknowledgments

Supported by National Science Foundation grants EAR-8603440, EAR-8916667, SES-8901437 and PHY-8818281. We thank R.I. Dorn, D.L. Elliott-Fisk and T.W. Swanson for sharing their knowledge of glacial geology of the White Mountains and for assistance in the field.

References

Blackwelder, E. (1934). Supplementary notes on Pleistocene glaciation in the Great Basin. Journal of the Washington Academy of Sciences 24, 217-222.

Cerling, T.E. and Craig, H. (Submitted). Cosmogenic ^{3}He production rates from 39°N to 46°N latitude. Geochimica et Cosmochimica Acta.

Crowder, D.F., Robinson, P.F., and Harris, D.L. (1972). Geologic map of the Benton

quadrangle, Mono County, California and Esmeralda and Mineral Counties, Nevada, USGS Map GQ-1013.

Dorn, R.I., Jull, A.J.T., Donahue, D.J., Linick, T.W., and Toolin, L.J. (1990). Latest Pleistocene lake shorelines and glacial chronology in the western Basin and Range province, USA:Insights from AMS radiocarbon dating of rock varnish and paleoclimatic implications. Palaeogeography, Palaeoclimatology, Palaeoecology 78, 315-331.

Elliott-Fisk, D.L. (1987). Glacial geomorphology of the White Mountains, California and Nevada: Establishment of a glacial chronology, Physical Geography 8, 299-323.

Elmore, D., Fulton, B.R, Clover., M.R., Marsden, J.R., Gove, H.E., Naylor, H., Purser, K.H., Kilius, L.R., Beukins, R.P., and Litherland, A.E. (1979). Analysis of ^{36}Cl in environmental water samples using an electrostatic accelerator. Nature 277, 22-25.

Gibbons, A.B., Megeath, J.D., and Pierce, K.L. (1984). Probability of moraine survival in a succession of glacial advances. Geology 12, 327-330.

Krauskopf, K.B. (1971). Geologic map of the Mt. Barcroft quadrangle, California-Nevada, USGS Professional Paper GQ-960.

LaMarche, V.C., Jr. (1965). Distribution of Pleistocene glaciers in the White Mountains of California and Nevada, USGS Professional Paper 525-C, 144-146.

Nishiizumi, K., Kohl, C.P., Arnold, J.R., Dorn, R.I., Klein, J., Fink, D., Middleton, R., and Lal, D. (in press). Role of *in situ* cosmogenic nuclides ^{10}Be and ^{26}Al in

the study of diverse geomorphic processes. Earth Surface Processes and Landforms 18.

Phillips, F.M., Zreda, M.G., Smith, S.S., Elmore, D., Kubik, P.W., and Sharma, P. (1990). A cosmogenic chlorine-36 chronology for glacial deposits at Bloody Canyon, Eastern Sierra Nevada, California. Science 248, 1529-1532.

Phillips, F.M., Zreda, M.G., Smith, S.S., Elmore, D., Kubik, P.W., Dorn R.I., and Roddy, D.J. (1991). Age and geomorphic history of Meteor Crater, Arizona, from cosmogenic ^{36}Cl and ^{14}C in rock varnish. Geochimica et Cosmochimica Acta 55, 2695-2698.

Swanson, T.W., Elliott-Fisk D.L., and Southard, R.J. (1993). Soil development parameters in the absence of a chronosequence in a glaciated basin of the White Mountains, California-Nevada. Quaternary Research 39, 186-200.

Zreda, M.G, Phillips F.M., and Smith, S.S. (1990). "Cosmogenic ^{36}Cl dating of geomorphic surfaces." Unpublished Hydrology Program Rept. 90-1, New Mexico Tech.

Zreda, M.G., Phillips, F.M., Elmore, D., Kubik, P.W., Sharma P., and Dorn, R.I. (1991). Cosmogenic chlorine-36 production rates in terrestrial rocks. Earth and Planetary Science Letters 105, 94-109.

Zreda, M.G., Phillips, F.M., Kubik, P.W., Sharma P., and Elmore, D. (1993). Eruption age at Lathrop Wells, Nevada from cosmogenic chlorine-36 accumulation. Geology 21, 57-60.

9. Cosmogenic ^{36}Cl chronology for glacial deposits in the eastern Sierra Nevada, California

Abstract

Using the cosmogenic ^{36}Cl method, I obtained a chronology of late Pleistocene glaciations in the eastern Sierra Nevada, California. The combined records from Bloody Canyon, Little McGee Creek and Bishop Creek indicate glaciations at 150, 120-90, 70-60, 45, 20, 14-12, 8, 7, and <1 ky. These events correlate well with the marine stages 6, 5b and d, 4 and 2 and with glaciations in the nearby White Mountains.

Two periods, the earliest and latest Wisconsin, are characterized by fast deposition of multiple moraines. In either case, they indicate instability of the climate during the transition from glacial to interglacial, or vice versa, conditions. While the early Wisconsin moraines are found only in the piedmont setting at Bishop Creek, the deglacial deposits (~ 14 ky) are ubiquitous and almost as extensive as the moraines deposited during the glacial maximum. The most complete sequence of late glacial and deglacial moraines was found at Little McGee Creek where the ^{36}Cl ages indicate rapid deglaciation progressing through several oscillations between 14 and 12 ky.

A fragmentary character of alpine glacial records is apparent from the ^{36}Cl ages. No single location contains deposits of all glaciations and some glaciations are recorded

in only one valley. The apparent gaps bracketed by younger and older ages may be due to either obliterative overlap or unfavorable conditions for glacier development. This incompleteness of the record has important implications for glacial correlations, which are based on stratigraphic relationships and other relative dating techniques. Surprising miscorrelations were revealed by the absolute ages reported herein. They lead to the conclusion that although the stratigraphic units commonly used in the Sierra Nevada imply certain chronologic relationships, they have no meaning unless accompanied by numerical ages. Glacial correlations should, therefore, be based more on absolute ages and less on stratigraphic correlations. The usage of the commonly employed names must be reevaluated and put in the context of numerical chronologies.

Introduction

The Sierra Nevada is a westward-tilted fault block composed of deformed Paleosoic and Mesosoic metamorphic rocks intruded by a granitic batholith. The block is uplifted to elevations of 2,500 to 4,400 m above sea level. Its eastern side is a wall rising 750 to 3,100 m at a slope of 15%. Volcanic rocks of Miocene to Holocene age are present locally and provide limited radiometric control for associated glacial deposits.

The range forms a natural barrier to the eastward flow of maritime air masses off the Pacific Ocean. Precipitation is highest on the western slopes (up to 1,600 mm/yr) and drops to 400-500 mm/yr to the east of the crest and to <200 mm/yr in the Owens

Valley. Snowfall may amount to 11.5 m per season at altitudes 2,300 to 2,600 m and remains for significant periods at elevations above 1,300 m.

In the Pleistocene, the snow line was about 750 m lower than it is now. A region 55 km wide along the crest was intensively glaciated. Ice was most abundant in the southern and central Sierra between latitudes 37 and 38° N. To the north, the lower elevation of the range resulted in smaller volume of ice; to the south, the higher temperature kept the volume small. The largest glaciers were 100 km long on the western slope and only 16 km on the eastern one (Wahrhaftig and Birman, 1965). This difference reflects the topography and spatial distribution of precipitation in the range. Main glaciers descended to altitudes of 1,300 to 2,200 m on the eastern slope of the Sierra Nevada (Blackwelder, 1931).

Stratigraphy of glacial sequences

The lateral and terminal moraines in canyons along the eastern front of the Sierra Nevada are relatively well studied because they are well preserved and not hidden from view by forest vegetation. They have been a focus of modern geological investigations since the early 1930's. Blackwelder (1931) first used semiquantitative criteria, such as granite weathering ratios and boulder frequency counts, for differentiation of glacial advances. He recognized deposits of four glaciations: the Tioga (youngest), Tahoe, Sherwin, and Mc Gee, and a possible advance between the Sherwin and Tahoe.

Blackwelder correlated these glaciations with glacial events in the Basin Ranges and Rocky Mountains and with the standard mid-continent stratigraphy. He assigned the Tioga and Tahoe to the Wisconsin, the Sherwin to the Kansan, and the Mc Gee to the Nebraskan of the standard mid-continent section. In addition, he closely estimated the time of the Tioga maximum at 25 ky by correlating it with the Würm stage dated by using varve-clay lake deposits in Sweden (De Geer and Antevs, 1925, cited by Blackwelder, 1931). Blackwelder was also aware of the fact that the lengths of the established glacial periods were different; he believed that the Tahoe was deposited between 90 and 150 ky, and the Sherwin about 1.4 ma ago.

Investigations in the 1950's and 1960's provided evidence for two additional advances in the Sierra Nevada (Sharp and Birman, 1963). The Tenaya was found between Tioga and Tahoe and was correlated with the Wisconsin. Tenaya moraines were found "distinctly fresher, sharper, and topographically more ragged than Tahoe" (Sharp and Birman, 1963) and more weathered than the Tioga moraines. The Mono Basin, tentatively assigned to the Illinoian, preceded the Tahoe and was also less extensive. It is usually obscured by the Tahoe and can be found only in areas where the Tahoe glaciers did not follow the Mono Basin path. The Tenaya and Mono Basin were described in Bloody Canyon where "one of the most clean-cut and spectacular sets of lateral moraines of the east Sierra Nevada" can be found (Sharp and Birman, 1963).

Burke and Birkeland (1979), however, suggested that the Tenaya is not a distinct glaciation but an early phase of the Tioga. The authors used multiparameter relative dating techniques in four valleys along the eastern Sierra Nevada and normalized the data to similar vegetation conditions. They concluded that there were only two major post-Sherwin glaciations - the Tahoe and Tioga. They grouped the Mono Basin till with the Tahoe, and the Tenaya with Tioga in some drainages but with the Tahoe in others.

The postglacial Holocene is characterized by small glacial advances separated by warmer periods. The Hilgard glaciers produced moraines extending a few km from the cirque areas, while the deposits of younger advances (Recess Peak Glaciation, Neoglacial and Little Ice Ages) are restricted to the highest locations located within 1-2 km from the cirques (Birman, 1964).

Glacial chronology

The Sherwin till was bracketed by underlying basalt dated at 3.26 ma, and overlying Bishop Tuff dated at 738 ky (Dalrymple, 1964). Both dates were obtained by means of K-Ar method. Based on development of the paleosol, Sharp (1968) and Birkeland et al. (1980) estimated that the till is at least 50 ky older than the tuff. This relative age was confirmed by the cosmogenic ^{26}Al-^{10}Be studies of Nishiizumi et al. (1989) who found that the time between the deposition of the till and the tuff was 53-67 ky. The till was also correlated with reversed-polarity continental till that was deposited

800-890 ky ago (Hallberg, cited in Fullerton, 1986).

Numerical ages bracketing younger glacial deposits were obtained in Sawmill Canyon (near Independence, California) by Dalrymple (1964). An olivine basalt flow between two tills was dated at 93 $\pm$ 116 and 58 $\pm$ 73 ky. The till below the flow was considered pre-Tahoe and correlated with the Mono Basin by Dalrymple (1964) and with the Tahoe by Burke and Birkeland (1979) and Dalrymple et al. (1982). The same volcanic rocks were redated by means of more precise ^{39}Ar-^{40}Ar technique at 119 $\pm$ 7 ky (Gillespie et al., 1984), and the underlying flow at 463 $\pm$ 40 ky (Gillespie, 1982). The author concluded that the lower till was deposited before 119 ky ago and thus is pre-Tahoe or pre-Wisconsin; the upper till is younger than 119 ky and is thus correlative with the Tahoe (early Wisconsin). Pre-Wisconsin and early Wisconsin moraines at Bloody Canyon gave ^{36}Cl ages of $\sim$65, 100-120 and 140-200 ky (Phillips et al., 1990).

The Tioga glaciation, commonly represented by multiple end moraines, has been bracketed by ^{14}C dates on associated lacustrine sediments. A maximum constraining age, 26 ky, was obtained from basal lake sediments at Tulare Lake (Atwater et al., 1986) and a minimum age, 10-11 ky, from peat overlying the Tioga till and basal lake sediments (Fullerton, 1986; Mezger and Burbank, 1986). Smith and Anderson (1992) studied sediments from Swamp Lake and documented Tioga stage deglaciation between $>$16 and 13.7 ky. Late Wisconsin terminal and lateral moraines at Bloody Canyon were dated by cosmogenic ^{36}Cl at 20-25 ky (Phillips et al., 1990), and moraines in similar stratigraphic

positions at Pine Creek, 60 km south of Bloody Canyon, were directly dated at 19 ky by rock varnish ^{14}C (Dorn et al., 1987). A constraining maximum age for Tioga moraines in the Mono Basin is 25.2 thousands calibrated years (Bursik and Gillespie, 1993) based on stratigraphic relationships between glacial deposits and interbedded ash layers dated by ^{14}C (Benson et al., 1990).

The Hilgard moraines were assigned to the early Holocene (Curry, 1969, 1971; Burke and Birkeland, 1983) or latest Pleistocene (Fullerton, 1986; Anderson, 1990) based on limited ^{14}C ages of associated lake deposits. The later advances are considered significantly younger, but their absolute ages are uncertain. The Recess Peak Glaciations of Birman (1964) were dated by lichenometry (Curry, 1969, 1971) at 2.6, 2.1, and 1.1 ky. However, the recent work by Burbank (1989) shows that the outermost Recess Peak moraines in the type area are >7 ky old and may thus represent recessional Hilgard deposits. The youngest advance, the Little Ice Age, occurred within the last 1 ky (Birman, 1964).

Chlorine-36 dating results and discussion

In this chapter, I report the use of the ^{36}Cl method to date glacial moraines in three drainages of the eastern Sierra Nevada: Bloody-Sawmill Canyon, near Mono Lake, Little McGee Creek, and Bishop Creek, both near Bishop (Fig. 9.1). These areas were selected for cosmogenic ^{36}Cl studies because of the large number of previous

investigations, the large number of morphologically distinct moraines that are preserved, and the clear-cut relative age sequence that can be inferred from the geometries of the moraines (Phillips et al., 1990). Bloody Canyon contains the type locality of the Mono Basin and one of the first Tenaya tills described east of the Sierra Nevada crest (Sharp and Birman, 1963). Little McGee Creek contains several fresh recessional moraines, which should provide information on late Wisconsin deglaciation. A unique sequence of 14 nested moraines, representing several (perhaps up to nine) different glaciations, is present in Bishop Creek. In the next three sections, I describe glacial deposits in the three study areas and present chronologies based on cosmogenic ^{36}Cl accumulation in morainal boulders. In the final section of this chapter, I briefly discuss the glacial history of the eastern Sierra Nevada and compare the ^{36}Cl chronologies obtained herein with the global glacial chronology.

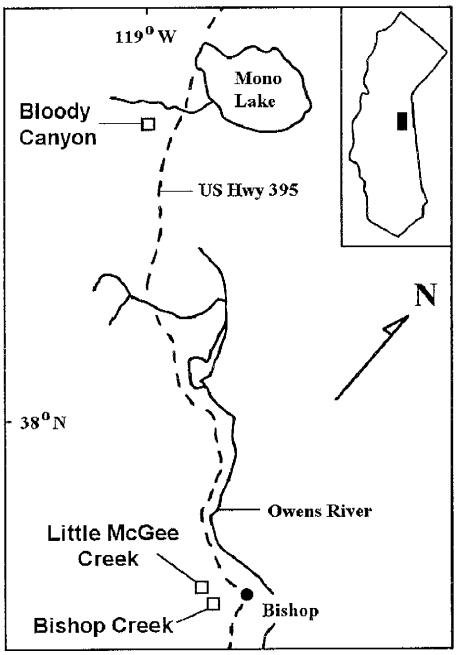

Fig. 9.1. Study areas in the eastern Sierra Nevada, California.

The time of exposure for single boulders was calculated using the production equation solved for time. Radiogenic ^{36}Cl component (see chapters 2 and 3) was assumed to be 30×10^{-15}, which is typical for granitic rocks (Bentley et al., 1986); this value was subtracted from the measured $^{36}Cl/Cl$ ratios. The production parameters and corrections are calculated and discussed above in chapters 3 and 4.

Bloody Canyon

Bloody Canyon is located west of Mono Lake (Fig. 9.1). It has been intensively glaciated and deposits of at least four glacial episodes are present (see for instance, Sharp and Birman, 1963). Although their stratigraphy and relative chronology have been established, absolute chronology was absent and cosmogenic ^{36}Cl dating was therefore attempted to provide age control for these deposits.

The samples were collected from the largest boulders that could be located along the crest of each moraine. The crest itself is an almost horizontal surface on which boulders are not likely to roll or shift after deposition. Only large boulders were selected for dating because they were most likely to have been exposed at the surface before any degradation of the moraine crest, and because they are more likely to be snow-free due to projecting above the average snow depth. All samples were collected from the top 5 cm of rock, as close to the center of the boulder as possible, using a hammer and a chisel. This procedure should minimize any shielding effect by rock material present

above the sampling point (rocks attenuate cosmic rays) and any edge effect (due to anisotropy of the cosmic ray flux at the boundary between rock and air).

The samples were collected in 1986, 1987, 1988, and 1990 and those from Sawmill Canyon in 1986 and 1988. The last two letters in sample names designate moraine/glaciation as follows: Tioga (Ti), Tenaya (Te), Tahoe (Ta), and Mono Basin (MB) according to Sharp and Birman (1963). The sample locations are presented in Figure 9.2 and elevations given in Table 9.1. At least five samples were collected from each surface to assure that the true age of the moraines would be closely approximated.

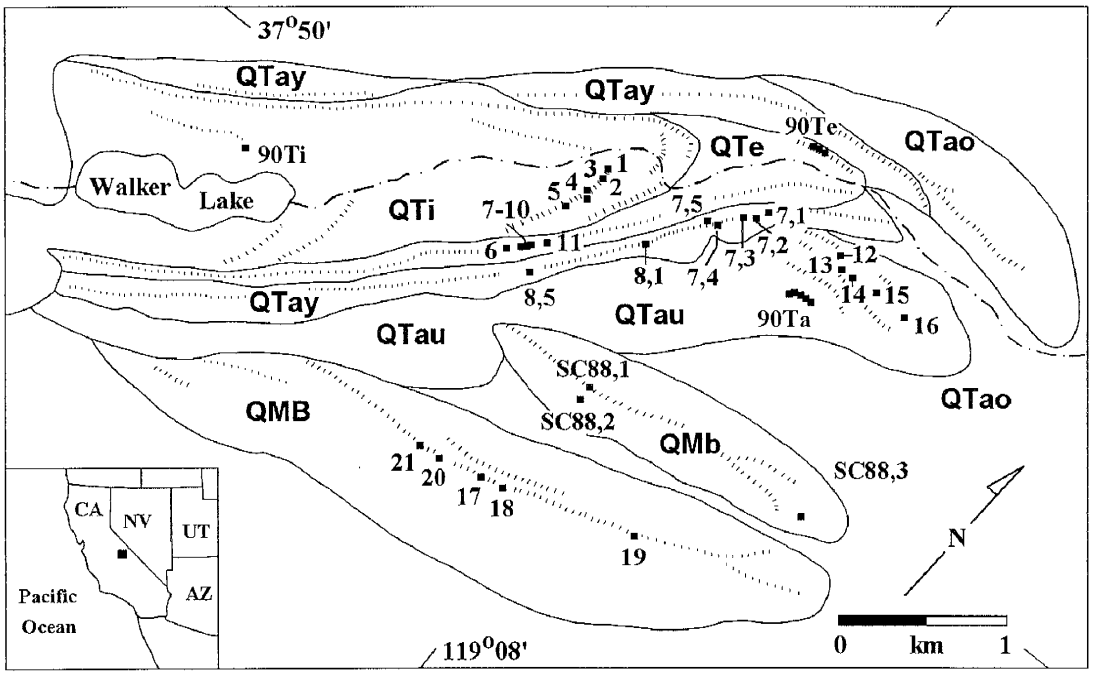

Fig. 9.2. Late Pleistocene glacial deposits at Bloody Canyon, eastern Sierra Nevada (from Phillips et al., 1990). Single numbers refer to year 1986, in entries separated by comma, the first number indicates the year, e.g., 7,1 is sample 87-1.

The results of chemical and isotopic analyses and the calculated ^{36}Cl surface exposure ages are in Table 9.1. The exposure ages are also graphed for each moraine in Figure 9.3. The names of moraines from Bloody Canyon correspond to those in Figure 9.2 and to those of Sharp and Birman (1963).

This is a second attempt to date these deposits; the first was by Phillips et al. (1990), who based their surface ages on ^{36}Cl production rates of Zreda et al. (1991). These production rates have recently been revised using new, well-dated surficial rocks (Chapter 4). While the production rates from ^{35}Cl and ^{40}Ca are unchanged (comparing to Zreda et al., 1991), the production rate from ^{39}K increased by a factor of two. Consequently, previously reported ^{36}Cl ages of high-potassium samples, such as those from Bloody Canyon, have changed. In this section, a revised chronology for Bloody Canyon moraines is developed.

Tioga (QTi)

The mean of the boulder ages from the Tioga moraine, 11.0 $\pm$ 2.2 ky, and the oldest age, 14.2 ky, are in good agreement with limiting maximum ^{14}C ages of $\sim$26 ky (Atwater et al., 1986; Bursik and Gillespie, 1993) and minimum ^{14}C age of 10-11 ky (Mezger and Burbank, 1986) for the corresponding lake sediments, but is considerably lower than a limiting minimum varnish ^{14}C age of 19 ky obtained for a Tioga moraine in the corresponding position at Pine Creek, 60 km south along the Sierra crest (Dorn

Table 9.1. Target element concentrations, macroscopic thermal neutron absorption cross sections, locations, ELD factors and measured $^{36}Cl/Cl$ ratios, and calculated surface ages for samples from Bloody Canyon.

Stratigraphic unit	Sample	Cl (ppm)	K_2O (%)	CaO (%)	$\Sigma\sigma_i N_i$ (cm^2/kg)	Elevation (km)	ELD	$^{36}Cl/Cl$	Age (ky)	
									Boulder	Surface[a]
	BC86-1-TI	20	5.09	0.84	4.89	2.38	5.56	1770 ± 13	11.8 ± 0.9	
Tioga	BC86-2-TI	60	2.96	2.27	4.13	2.38	5.56	402 ± 17	8.1 ± 0.4	11.0 ± 2.2
(QTi)	BC86-3-TI	78	4.38	2.12	4.72	2.38	5.56	536 ± 39	11.0 ± 0.9	11.0
	BC86-5-TI	122	3.44	2.89	5.02	2.38	5.56	455 ± 25	14.2 ± 0.7	14.2
	BC90-5TI	17	4.18	1.16	3.24	2.38	5.56	1660 ± 81	10.3 ± 0.5	
	BC86-6-TE	29	3.75	2.14	4.55	2.45	5.76	1350 ± 96	14.1 ± 1.0	
	BC86-7-TE	40	1.68	3.69	3.66	2.33	5.38	244 ± 37	4.1 ± 0.7[b]	
	BC86-8-TE	61	3.30	1.47	4.59	2.40	5.59	697 ± 38	14.9 ± 0.9	
Tenaya	BC86-9-TE	62	4.32	1.94	4.72	2.44	5.72	839 ± 54	14.7 ± 1.0	14.2 ± 1.3
(QTe)	BC86-10-TE	60	3.96	1.52	4.27	2.33	5.38	469 ± 28	8.7 ± 0.6[b]	14.5
	BC86-11-TE	20	5.34	0.98	4.97	2.43	5.69	1951 ± 16	11.8 ± 1.0	15.8
	BC90-1TE	42	4.47	1.94	4.55	2.37	5.50	1038 ± 66	13.4 ± 0.9	
	BC90-2TE	52	4.15	0.84	4.11	2.37	5.50	928 ± 55	15.8 ± 1.0	
	BC90-3TE	43	4.34	2.20	4.60	2.37	5.50	1088 ± 61	14.5 ± 0.9	

	BC87-1TA	68	4.05	2.02	4.69	2.34	5.36	1638 ± 211	35.9 ± 4.9	
Younger	BC87-2TA	30	5.57	0.79	4.64	2.34	5.36	3763 ± 133	34.8 ± 1.3	
Tahoe	BC87-3TA	56	3.88	2.04	4.34	2.37	5.47	1309 ± 87	23.9 ± 1.7[b]	39.0 ± 3.6
(QTy)	BC87-4TA	64	2.48	2.18	4.37	2.39	5.54	1461 ± 180	37.9 ± 5.0	37.9
	BC87-5TA	102	4.31	1.83	4.68	2.41	5.61	1699 ± 94	46.3 ± 2.7	46.3
	BC88-1	38	4.70	1.61	3.72	2.34	5.36	315 ± 18	3.4 ± 0.2[b]	
	BC88-5	81	4.41	2.72	5.31	2.34	5.36	1701 ± 162	40.1 ± 4.1	
	BC86-12TA	59	1.06	7.37	6.18	2.20	4.89	3155 ± 238	98.9 ± 8.5	
Older	BC86-13TA	64	4.37	2.20	5.79	2.24	5.02	4313 ± 248	103 ± 6.8	104 ± 9
Tahoe	BC86-14TA	38	3.74	1.19	4.64	2.24	5.02	5736 ± 256	102 ± 5.2	103
(QTo)	BC86-15TA	66	3.85	1.46	5.26	2.20	4.89	4211 ± 240	119 ± 8.0	118
	BC86-16TA	107	3.92	3.82	5.68	2.21	4.92	2790 ± 197	98.0 ± 7.9	
	SC86-17MB	57	3.93	0.56	4.39	2.29	5.24	3123 ± 223	69.7 ± 5.5	
	SC86-18MB	106	3.90	1.22	4.37	2.29	5.24	2001 ± 153	65.1 ± 5.5	
Mono	SC86-19MB	100	3.22	2.40	4.99	2.41	5.67	1959 ± 122	62.2 ± 4.2	
Basin	SC86-20MB	23	5.16	1.18	4.57	2.41	5.67	5289 ± 178	39.1 ± 1.4[a]	64.0 ± 9.0
(QMB)	SC86-21MB	22	5.52	0.66	4.69	2.41	5.67	7031 ± 250	48.7 ± 1.8[a]	65.1
	SC88-1	71	4.73	2.36	4.74	2.38	5.56	2848 ± 62	57.0 ± 1.3	77.1
	SC88-2	102	4.38	2.64	5.16	2.38	5.56	1916 ± 67	52.4 ± 2.0[a]	
	SC88-3	138	4.19	3.41	5.12	2.38	5.56	2266 ± 167	77.5 ± 6.4	

	BC90-1TA	53	3.30	1.95	4.05	2.23	5.00	1838 ± 94	39.3 ± 2.1	
Younger	BC90-2TA	58	4.93	0.67	4.13	2.23	5.00	1787 ± 111	33.6 ± 2.2	38.6 ± 9.8
Tahoe	BC90-3TA	31	3.22	2.03	4.20	2.23	5.00	2511 ± 182	36.6 ± 2.8	36.6
Shoreline	BC90-4TA	42	3.51	1.93	4.18	2.23	5.00	3053 ± 163	54.7 ± 3.2	54.7
	BC90-5TA	28	3.87	1.58	4.14	2.23	5.00	2410 ± 109	28.9 ± 1.4	

[a] The mean ± standard deviation, the median, and the maximum surface ages are reported.

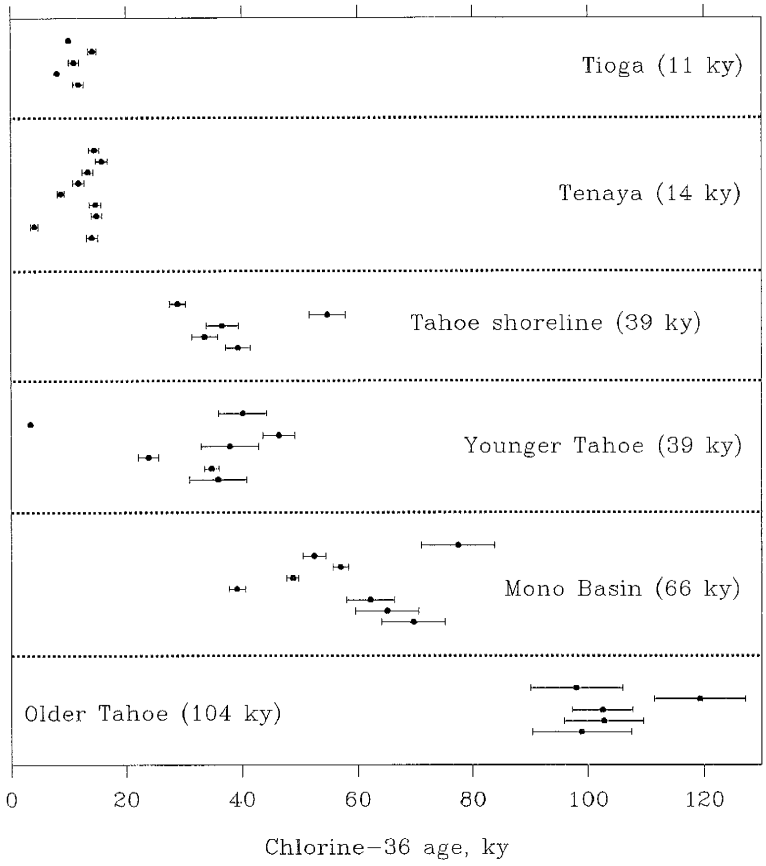

Fig. 9.3. Cosmogenic ^{36}Cl exposure ages for moraines at Bloody Canyon.

et al., 1987). This apparent discrepancy and absence of deposits correlative with the late Wisconsin maximum are most likely because of covering of 19-ky deposits by 14-ky advance at Bloody Canyon.

Tenaya (QTe)

The Tenaya moraine, although morphologically distinct from the Tioga, is less than 3 ky older. The mean age of 14.2 $\pm$ 1.3 ky place it with the Tioga in the latest Wisconsin. This is in line with conclusions of Burke and Birkeland (1979), who did not

detect any major differences between the two, and combined them in one unit, the Tioga. The slightly older age of the Tenaya crest can suggest an advance of the Tioga glaciation, followed by recession, and another advance <3 ky later. There is a concern, however, that the Tenaya age may be affected by fire shattering because the Tenaya crest lies between the highly forested Tioga and Tahoe moraines, and might have experienced more forest fires than other moraines (Burke and Birkeland, 1979). Intense fire shattering could result in a bias toward anomalously young ages of analyzed rocks. In such a case one would expect data points scattered over the entire interval since deposition of the moraine. However, there is evidence that the reported ages are unaffected by fire: (1) six out of nine Tenaya samples form a tight cluster between 13.4 and 15.8 ky, with three slightly younger outliers and (2) samples TE90 from unforested terminal moraines produced the same ages as those from forested lateral moraines. These observations lead to a conclusion that the six oldest samples accurately represent the glacial event.

Based on the ^{36}Cl ages, the Tioga and Tenaya moraines as mapped by Sharp and Birman (1963) are grouped together and correlated with the latest Wisconsin. Late Wisconsin glacial deposits have been identified in all the glaciated mountain ranges in the western United States. Although the maximum occurred between 23 and 25 ky in Alaska, about 23 ky ago in Colorado, and 24 ky ago in Wyoming (Richmond and Fullerton, 1986), younger advances between 15 and 10 ky also occurred. They correspond well with the ^{36}Cl dates presented in this study.

Tahoe (QTay and QTao)

Based on the ^{36}Cl dates, and following Gillespie (1984), the Tahoe moraine of Sharp and Birman (1963) was divided into an older and younger Tahoe (c.f., Phillips et al., 1990). The boulder dates for the younger Tahoe are clustered between 35-46 ky, whereas the older Tahoe dates group between 98 and 119 ky. In the case of Younger Tahoe, two anomalously young rocks were sampled. Their young ages can be explained by the same factors that affected the young outliers at the Tenaya crest. The younger and older Tahoe dates are very distinct and there is no overlap between the maximum of the younger Tahoe (46 ky) and the minimum of the older Tahoe (98 ky). The younger Tahoe is correlative with the middle Wisconsin, whereas the older Tahoe corresponds to the early Wisconsin of the standard mid-continent stratigraphy.

Mono Basin (QMB)

The Mono Basin boulder ages cluster in the range between 39.1 and 77.5 ky and have a mean age 64.0 $\pm$ 9.0 ky. The boulders on the Mono Basin moraine crests exhibit indications of advanced weathering and spalling (Phillips et al., 1990), which would result in removal of the original surface and thus in apparent ^{36}Cl ages differing from the actual moraine age. Slightly older ages due to erosion are expected in high Cl rocks, whereas in low Cl rocks the apparent ages can be younger (see Chapter 5). If the observed positive correlation between the Cl content and apparent age were due to

boulder erosion, the most likely age for the Mono Basin moraine should be the mean age, 64.0 $\pm$ 9.0 ky. The scatter in calculated ages may also indicate that the Mono Basin moraine is a product of multiple glaciations that occurred between 80 and 40 ky (cf. Gillespie, 1982; Gillespie et al., 1984). There is some evidence from moraine morphology to support this interpretation (Phillips et al., 1990). The Mono Basin moraine was deposited between the younger and older Tahoe and is correlative with the early Wisconsin. This age corresponds well with the maximum limiting age of 119 ky (Gillespie et al., 1984) obtained for a basalt flow between two tills at Sawmill Canyon (near Independence, California).

Little McGee Creek

Little McGee Creek is a small glaciated valley west of Bishop (Fig. 9.1) in which several moraines and glacially polished bedrock surfaces have been preserved. The glacial deposits extend from the elevation of 3.9 km (youngest) down to 2.4 km (oldest). Good preservation of the glacial deposits in Little McGee Creek may be attributed to the local topography that favors frequent changes of direction of glaciers coming out from the valley and onto the piedmont. These changes of glacier direction help preserve older glacial deposits that would have otherwise been destroyed by younger ice.

The samples from Little McGee Creek were collected over several years, from 1986 through 1991. Besides multiple boulders from several lateral and terminal moraines

at elevations between 2.4 and 3.9 km, glacially polished bedrock surfaces from the upper part of the valley were sampled to determine the last time these surfaces were glacially abraded. The cirque area is still glaciated and a recent deposit is present in front of the glacier. Two samples were collected from this deposit to test the assumption of a negligible amount of inherited ^{36}Cl in typical moraine boulders. The samples are presented in Table 9.2 and in Figure 9.4.

The results of chemical and isotopic analyses and the calculated ^{36}Cl surface exposure ages are in Table 9.2. The exposure ages are also graphed for each moraine in Figure 9.5. The names of moraines from Little McGee Creek are based on field designations. They may or may not correspond to those at Bloody Canyon or elsewhere and absolute ages will be used to correlate deposits at different locations.

Neoglacial (NG)

The ages of the two youngest samples (LMC87-1NG and -2NG) from the recent deposit in the cirque area are 0.3 and 0.9 ky. These boulders were found at the present ice margin and their freshness indicates that they were eroded out of the cirque wall quite recently. The calculated ages reflect the cosmogenic ^{36}Cl accumulated either after the boulders had been deposited or while they were still exposed in the cirque wall. In either case, the low concentrations of ^{36}Cl prove that boulders at this location do not have appreciable amounts of previously accumulated cosmogenic ^{36}Cl when they are deposited

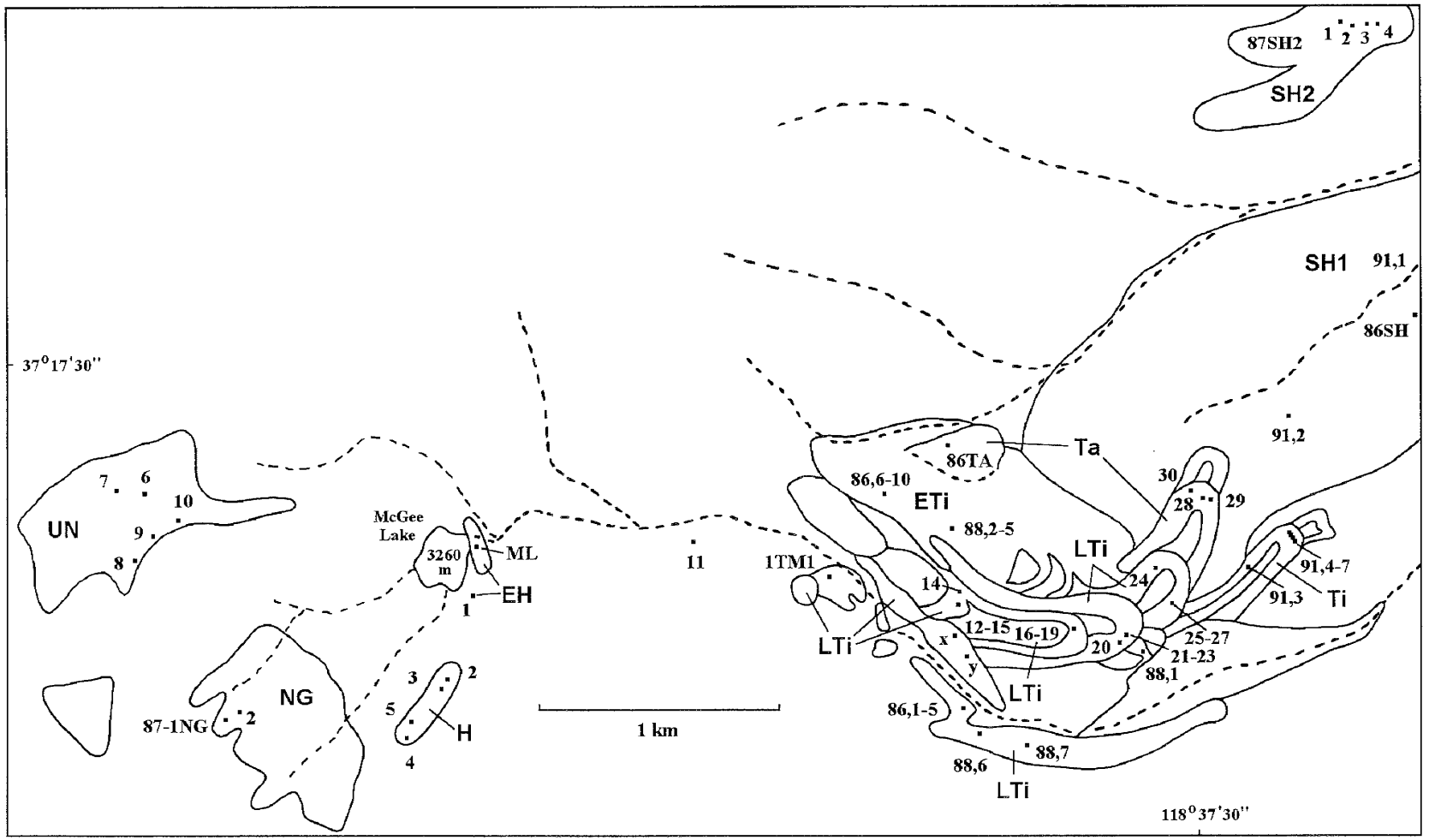

Fig. 9.4. Glacial deposits at Little McGee Creek.

Table 9.2. Target element concentrations, macroscopic thermal neutron absorption cross sections, elevations, $^{36}Cl/Cl$ ratios, and calculated ^{36}Cl ages for samples from Little McGee Creek.

Unit	Sample ID	Cl (ppm)	K_2O (%)	CaO (%)	$\Sigma\sigma N$ (cm^2/kg)	Elevation (km)	ELD	$^{36}Cl/Cl$ (10^{-15})	Age (ky)	
									Boulder	Surface
Neoglacial	lmc87-1ng	39	4.34	1.34	4.51	3.70	11.95	188 ± 23	0.9 ± 0.1	<1
(NG)	lmc87-2ng	54	4.42	1.36	4.58	3.70	11.95	68 ± 15	0.3 ± 0.1	
	lmc90-2	12	4.42	1.35	4.40	3.41	10.27	3070 ± 193	7.1 ± 0.5	6.8 ± 0.7
Hilgard	lmc90-3h	50	4.00	1.70	4.36	3.43	10.34	777 ± 91	6.6 ± 0.8	6.7
(H)	lmc90-4h	12	4.57	1.55	4.36	3.48	10.66	2967 ± 345	6.5 ± 0.8	7.1
	lmc90-5pbrh	34	4.25	1.51	5.97	3.47	10.59	1117 ± 126	6.8 ± 0.8	
	lmc87-1ml	25	4.26	1.30	4.84	3.27	9.44	1525 ± 99	8.0 ± 0.5	
Early	lmc87-2ml	34	4.29	1.16	4.63	3.27	9.44	1206 ± 28	8.3 ± 0.2	8.2 ± 0.3
Hilgard	lmc87-3ml	29	4.53	1.21	4.52	3.27	9.44	779 ± 61	4.4 ± 0.4[a]	
(EH)	lmc90-11ti	17	3.90	2.13	4.70	3.07	8.43	1884 ± 138	7.9 ± 0.6	8.2 ± 0.6
	lmc87-1tm1	21	4.04	2.24	4.60	2.97	7.90	1639 ±	8.5 ±	
	lmc90-1ml-pbr	13	0.88	4.06	4.21	3.34	9.85	2017 ± 101	11.2 ± 0.6[a]	11.2
	lmc87-1x	28	4.1	1.51	4.61	2.92	7.60	1528 ± 82	11.1 ± 0.6	11.5 ± 0.7
Late	lmc87-1y	44	4.60	1.68	4.62	2.92	7.60	1248 ± 81	12.2 ± 0.8	
Tioga	lmc90-12	115	1.49	6.48	5.06	2.93	7.72	455 ± 24	11.1 ± 0.6	10.6 ± 1.6
(LTi)	lmc90-13ti	15	4.34	1.49	4.79	2.93	7.72	2637 ± 135	10.5 ± 0.5	10.8
	lmc90-14ti	181	1.60	8.16	6.27	2.93	7.72	435 ± 20	13.7 ± 0.7	13.7
	lmc90-15ti	17	2.56	2.54	4.65	2.93	7.72	1477 ± 73	8.9 ± 0.5	

	lmc90-16ti	20	3.82	1.51	4.48	2.87	7.44	2114 ± 97	13.3 ± 0.6	13.0 ± 0.9
	lmc90-17ti	308	2.11	6.84	6.08	2.87	7.44	293 ± 13	12.2 ± 0.6	13.3
	lmc90-19ti	162	1.60	8.08	6.22	2.87	7.44	455 ± 26	14.0 ± 0.9	14.0
Late	lmc90-21	15	3.95	2.25	4.81	2.83	7.28	7320 ± 250	33.2 ± 1.2	?
	lmc90-23ti	10	4.44	1.18	4.32	2.83	7.28	3346 ± 215	9.5 ± 0.6	
	lmc90-24	9	3.18	1.59	4.17	2.81	7.19	3684 ± 170	13.0 ± 0.6	13.0
	lmc90-25ti	16	4.73	1.54	4.68	2.82	7.22	3243 ± 128	13.3 ± 0.6	13.6 ± 0.8
Tioga	lmc90-26	6	4.63	0.60	4.22	2.82	7.22	8236 ± 360	13.8 ± 0.7	13.8
	lmc90-27ti	6	4.43	0.55	4.24	2.82	7.22	8187 ± 775	14.1 ± 1.4	14.1
	lmc88-6	14	2.16	1.55	3.89	2.90	7.55	2179 ± 115	13.6 ± 0.7	13.7 ± 0.9
(LTi)	lmc88-7	33	4.69	1.69	5.14	2.90	7.55	1803 ± 168	14.0 ± 1.4	
	lmc86-1ti	111	4.30	1.60	5.03	2.91	7.61	562 ± 48	11.5 ± 1.0[a]	
	lmc86-2ti	53	4.12	1.56	4.58	2.91	7.61	1079 ± 71	13.4 ± 0.9	13.8 ± 0.7
	lmc86-3ti	84	4.40	4.47	4.80	2.91	7.61	920 ± 39	13.6 ± 0.6	13.6
	lmc86-4ti	22	4.17	1.79	4.57	2.91	7.61	1862 ± 93	10.8 ± 0.6[a]	14.3
	lmc86-5ti	41	4.11	1.61	4.38	2.91	7.61	1415 ± 80	14.3 ± 0.8	
	lmc91-ta3	10	3.53	1.36	4.12	2.72	6.80	3370 ± 168	13.2 ± 0.7[a]	
	lmc91-ta4	8	3.14	1.64	4.06	2.68	6.65	4991 ± 358	15.7 ± 1.2[a]	20.4 ± 0.7
Tioga	lmc91-ta5c	9	3.51	1.30	4.16	2.68	6.65	5443 ± 292	19.8 ± 1.0	20.2
(Ti)	lmc91-ta6	182	0.99	7.42	4.95	2.68	6.65	352 ± 29	12.7 ± 1.2[a]	20.6
	lmc91-ta7	8	3.35	1.56	4.13	2.68	6.65	6242 ± 186	20.6 ± 0.6	
	lmc91-ta8	229	1.36	7.69	5.71	2.68	6.65	378 ± 28	15.6 ± 1.3[a]	

	lmc86-6ti	26	3.47	1.48	4.52	3.01	8.19	3372 ± 310	25.2 ± 2.4	
Early	lmc86-7ti	23	3.97	1.71	4.41	3.01	8.19	478 ± 55	2.6 ± 0.3[a]	26.2 ± 1.4
Tioga	lmc86-8ti	67	4.41	1.47	4.42	3.01	8.19	1992 ± 79	26.6 ± 1.1	25.8
(ETi)	lmc86-9ti	24	4.31	1.48	4.40	3.01	8.19	2858 ± 300	16.3 ± 1.8[a]	26.6
	lmc86-10ti	37	4.06	1.90	4.67	3.01	8.19	2956 ± 158	25.8 ± 1.4	
Early	lmc88-2	17	2.67	2.06	4.31	2.98	7.95	2660 ± 190	16.1 ± 1.2	
Tioga	lmc88-3	33	2.48	2.03	4.24	2.98	7.95	2248 ± 116	25.1 ± 1.4	?
or	lmc88-4	37	2.63	2.26	4.40	2.98	7.95	4095 ± 251	49.4 ± 3.2	
Tahoe	lmc88-5	42	4.00	2.35	4.88	2.98	7.95	663 ± 24	6.2 ± 0.2	
	lmc86-11ta	19	4.86	0.62	4.59	2.93	7.89	2187 ± 100	10.3 ± 0.5[a]	
	lmc86-12ta	26	4.60	1.08	4.58	2.93	7.89	3696 ± 163	23.7 ± 1.1[a]	47.7 ± 4.7
	lmc86-13ta	123	2.64	3.30	4.79	2.93	7.89	1133 ± 40	28.7 ± 1.1[a]	49.1
	lmc86-14ta	29	4.56	1.01	5.38	2.93	7.89	6135 ± 338	45.8 ± 2.7	52.4
Tahoe	lmc86-15ta	25	4.28	1.86	4.62	2.93	7.89	8206 ± 611	52.4 ± 4.2	
(Ta)	lmc90-28ta	11	5.00	0.60	4.44	2.80	7.17	14559 ± 511	47.3 ± 1.8	55.0 ± 7.8
	lmc90-29ta	14	5.08	0.70	4.43	2.80	7.17	14133 ± 1555	53.1 ± 6.3	55.8
	lmc90-30	12	4.36	0.68	4.32	2.80	7.17	14667 ± 1613	58.5 ± 7.0	65.5
	lmc90-31	8	5.11	0.83	4.45	2.80	7.17	28582 ± 853	65.5 ± 2.1	
	lmc86-16sh	23	4.63	1.50	4.68	2.48	5.85	4985 ± 429	38.4 ± 3.5	
	lmc86-17sh	56	3.99	2.40	4.55	2.48	5.85	2122 ± 170	36.3 ± 3.1	
Sherwin-1	lmc86-18sh	32	4.75	0.72	4.75	2.48	5.85	3155 ± 243	32.6 ± 2.6	109 ?
(SH1)	lmc86-19sh	13	4.31	1.42	4.52	2.48	5.85	5732 ± 651	27.0 ± 3.2	
	lmc91-sh1	110	0.85	6.95	5.09	2.46	5.78	2653 ± 277	109 ± 13.3	
	lmc91-sh2	106	1.44	6.31	5.20	2.65	6.49	1655 ± 111	52.0 ± 3.8	

	lmc87-1sh2	30	4.53	0.67	4.51	2.44	5.67	4906 ± 282	52.5 ± 3.2	49.7 ± 5.4
Sherwin-2	lmc87-2sh2	46	4.55	1.03	4.82	2.43	5.63	2839 ± 262	43.4 ± 4.3	52.5
(SH2)	lmc87-3sh2	39	4.68	0.84	4.58	2.41	5.58	4012 ± 503	53.1 ± 7.2	53.1
	lmc87-4sh2	35	4.15	0.74	4.35	2.40	5.54	2471 ± 159	32.0 ± 2.2[a]	
	lmc90-6	26	4.61	1.53	4.68	3.88	13.23	12767 ± 282	49.1 ± 1.2	
	lmc90-7	236	1.74	6.44	5.57	3.88	13.23	1381 ± 62	31.0 ± 1.5	
Unnamed	lmc90-8	152	2.24	6.04	5.72	3.88	13.23	1155 ± 64	19.6 ± 1.1	?
(UN)	lmc90-9	7	3.71	1.35	4.31	3.88	13.23	14323 ± 744	17.9 ± 1.0	
	lmc90-10	22	3.23	1.97	4.33	3.86	13.14	5121 ± 177	20.8 ± 0.7	

[a] Not used in determination of the surface mean, median, and maximum ages.

by ice. This result validates one of the principal assumptions of the method, that samples have no inherited ^{36}Cl at the time of landform construction.

Hilgard (H)

The highest right lateral moraine (samples LMC90-2H, 3H, 4H) and polished bedrock at the high end of the moraine (sample LMC90-5PBRH) are at elevations between 3.3 and 3.5 km. The moraine is very steep, which indicates its freshness, but boulders are well weathered and oxidized. These features are typical of Hilgard moraines found elsewhere in the eastern Sierra Nevada. The samples yielded consistent ^{36}Cl ages between 6.5 and 7.1 ky with a mean age of 6.8 $\pm$ 0.3 ky. The ages are compatible with the much younger age of the Neoglacial deposits above and slightly older deposits below this moraine.

Early Hilgard (EH)

Three early Holocene moraines (samples LMC87-1 through 3 ML, LMC90-11, LMC87-1TM1) and polished bedrock (sample LMC90-1ML-PBR) are at and below McGee Lake at elevations between 3.3 and 3.0 km . The samples gave surface exposure ages close to 8 ky, except one older age of $\sim$11 ky for the polished bedrock, consistent with the younger ages above the elevation of 3.3 km and older below that of 3.0 km. The age of $\sim$8 ky reflects the early advance of the Hilgard glacier and indicates

existence of early Holocene glaciers that descended at least 0.6 km, in the vertical direction, from the cirque area at ~3.6 km down to ~3.0 km. This early advance of the Hilgard glacier was followed by rapid deglaciation during which the Hilgard moraine above the lake was deposited. The older age of the bedrock may result from exposure before 8 ky. The elevation of the bedrock surface is higher than that of the moraines and it is possible that the bedrock was abraded 11 ky ago, but not covered by ice during the Hilgard advance.

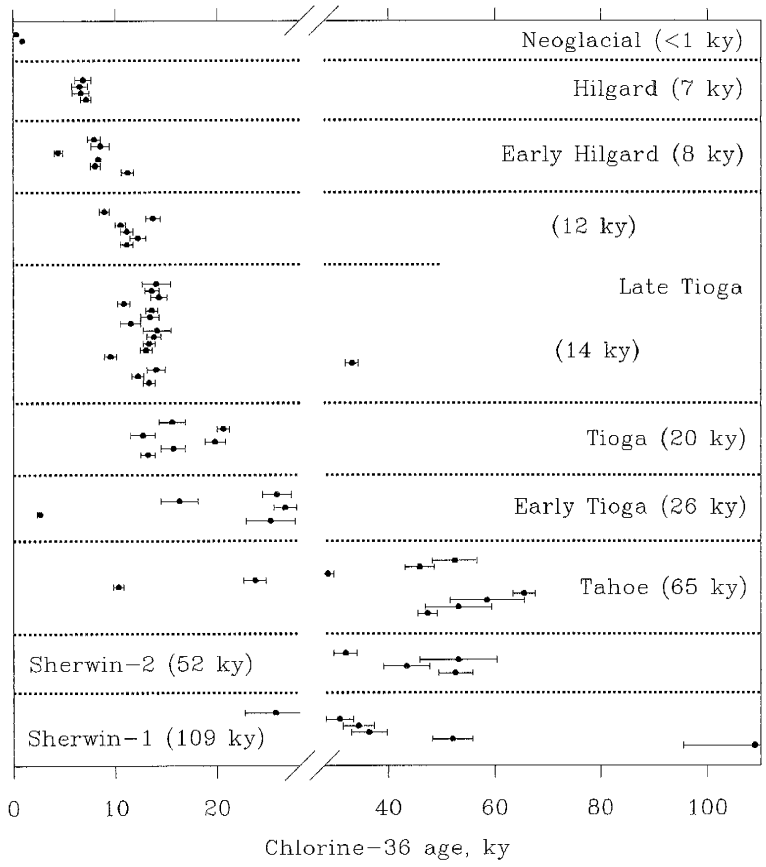

Fig. 9.5. Distribution of exposure ages at Little McGee Creek.

Late Tioga (LTi)

Several distinct moraines are present at the bottom of the valley at elevations between 3.0 and 2.6 km. They have different sizes, shapes, and lithology and have different degrees of surface preservation. Twenty-one samples from eight morphologically different glacial landforms were collected. The sample designations of the eight surfaces are as follows: LMC90-12 through 15, LMC90-16 through 19, LMC90-21 and 23, LMC90-24, LMC90-25 and 26, LMC88-6 and 7, LMC87-X and Y, and LMC86-1 through 5 (see the map in Figure 9.3 for the details). All samples, except LMC90-21, yielded cosmogenic ^{36}Cl ages closely grouped between 9 and 14 ky, with majority in the interval between 13 and 14 ky (Table 9.2). Sample LMC90-21 has an older exposure age of 33.2 ky. Because this is the only sample with a distinctly older age, I treat it as an outlier and explain it by cosmogenic ^{36}Cl from some previous exposure episode; this scenario is possible if the boulder originated from an older moraine or a talus deposit in the upper part of the valley, or from a slowly eroding outcrop.

This suite of samples gives clues about rates of glacial advances and following deglaciation. Eight different moraines were constructed in a relatively short time. The most extensive lateral and terminal moraines in this complex date to 13-14 ky, at which time the glacier reached its maximum size. The following deglaciation resulted in construction of several recessional moraines with maximum boulder ages between 13 and

14 ky again. The whole process of glacier advance and retreat, which proceeded in several steps, took only about a thousand years, and possibly less than that. Unfortunately, the resolution of the cosmogenic ^{36}Cl method is not fine enough to distinguish surfaces with exposure ages different by less than a thousand years and we are therefore unable to say with great certainty how fast the deglaciation really was. It can be however speculated, based on the number of moraines and the range of exposure ages, that the average rate of moraine formation in this complex was approximately one per 100-200 years. This figure represents the time scale of glacier development and retreat and suggests that local environmental conditions were changing very rapidly in that period.

One moraine in this group (samples LMC90-12 through 15) and an incision surface (samples LMC87-1X and 1Y) may actually be slightly younger than the other deposits described as late Tioga. Samples 1X and 1Y are from a deposit representing a major incision in the older moraine complex and have exposure ages 11.1 and 12.2 ky. This event thus postdates by ~ 2 ky the deposition of the 14 ky old moraines and corresponds to the Younger Dryas. The age of the moraine with samples LMC90-12 through 15 may be either 11 ± 2 ky (the mean age) or 13.7 (the maximum age). Both ages are stratigraphically correct as the moraine cuts the main 14 ky old complex and is itself cut by the 11-12 ky incision (samples 1X and 1Y).

Tioga (Ti)

Down the valley from the moraine complex described above, there is a well-developed morainal loop with large and relatively unweathered boulders (samples LMC91-4 through 7). The age of ~ 20 ky obtained for the two oldest samples is taken as the surface age, while the two younger samples must be due to erosion or other postdepositional processes that might affect surface exposure ages. This age corresponds with the timing of the late Wisconsin maximum in both marine (e.g., Martinson et al., 1987) and terrestrial (e.g., Richmond and Fullerton, 1986) records. This terminus marks the maximum extent of the Tioga glaciation in Little McGee Creek. The extensive glacial deposits found below the terminal Tioga exhibit much more extensive surface modifications and must therefore be substantially older than the Tioga.

Early Tioga (ETi)

Samples LMC86-6 through 10 were collected from a left lateral moraine at elevation ~3.0 km. Three out of five ages are clustered around 26 ky, which is the most likely age of this surface. This age is consistent with the stratigraphic position of this moraine between The Tioga complex dated at ~14 ky and the Tahoe ridge dated at ~50 ky. It represents the earliest advance of the Tioga glaciation. This advance was smaller than that of the Tioga maximum and the moraine is preserved only because it is perched high on the valley wall, out of the way of the Tioga maximum glacier.

Tahoe (Ta)

The Tahoe crests are located to the north and east of the Tioga deposits, at elevations 2.9 and 2.7 km. Two Tahoe moraines were sampled (samples LMC86-TA11 through 15, and LMC90-28 through 31). The oldest ages on the two ridges were 52 and 66 ky, respectively. The spread of the ^{36}Cl ages indicates strong surface modification on the LMC86 moraine and therefore the age of 52 ky should only be a minimum age. The other Tahoe moraine yielded more consistent results in the range between 47 and 66 ky and the age of 66 ky is probably closest to the true surface age. This age fits well in the local stratigraphy; the sampled moraine is located between the overlying Tioga moraines with the age of $\sim$14 ky, and the underlying Sherwin-2 moraine with the oldest boulder age of $\sim$109 ky (described below).

"Sherwin" (SH1 and SH2)

The "Sherwin" moraines are the most extensive moraines in the valley and descend to the elevation of $\sim$2.4 km. Two different crests were sampled: Sherwin-1 (samples LMC86-16 through 19 and LMC91-1 and 2) in the main Little McGee Creek valley and Sherwin-2 (samples LMC87-1 through 4 -SH2) in a small valley N of Little McGee Creek, descending from Basin Mountains. The oldest surface exposure age on the Sherwin-1 moraine is 109 ky, but all other ages are in the interval between 26 and 52 ky. It is likely that the oldest age is closest to the true age, but it almost certainly

underestimates the true moraine age because of the subdued morphology of the Sherwin moraines and strong modifications of boulders. The Sherwin-2 moraine gave more consistent, but young, ages between 32 and 53 ky. This moraine was deposited by a small glacier that descended from Basin Mountain and should reflect the time of the maximum extent of this glacier. Based on the moraine morphology and surface preservation, which are similar to those on the Sherwin-1 moraine, the two ridges can be correlated, but it is hard to assess with certainty their chronological equivalence.

Bishop Creek

Bishop Creek is a large drainage basin west of Bishop and south of Little McGee Creek (Fig. 9.1). Because of the large size of the drained area, water is abundant and during glaciations large alpine glaciers developed and descended from the valley and onto the piedmont area down to the elevation of ~1.5 km. In the piedmont area, the glaciers were no longer constrained by the valley walls and took many different paths. As a result, many older moraines survived subsequent glaciations and form a unique and well-preserved morainal complex deposited during at least six or seven different glacial episodes. These moraines were studied using ^{36}Cl and a chronology of glaciations was developed. About 100 samples were collected from 19 different surfaces to provide information for detailed glacial chronology in the area. Table 9.3 contains sample locations, chemical and isotopic data, and calculated ^{36}Cl ages for the samples from Bishop Creek. Figure 9.6 shows the sample locations and the geomorphic units

described in detail below; the names of these units are after local geographical names. The calculated ages are graphed in Figure 9.7.

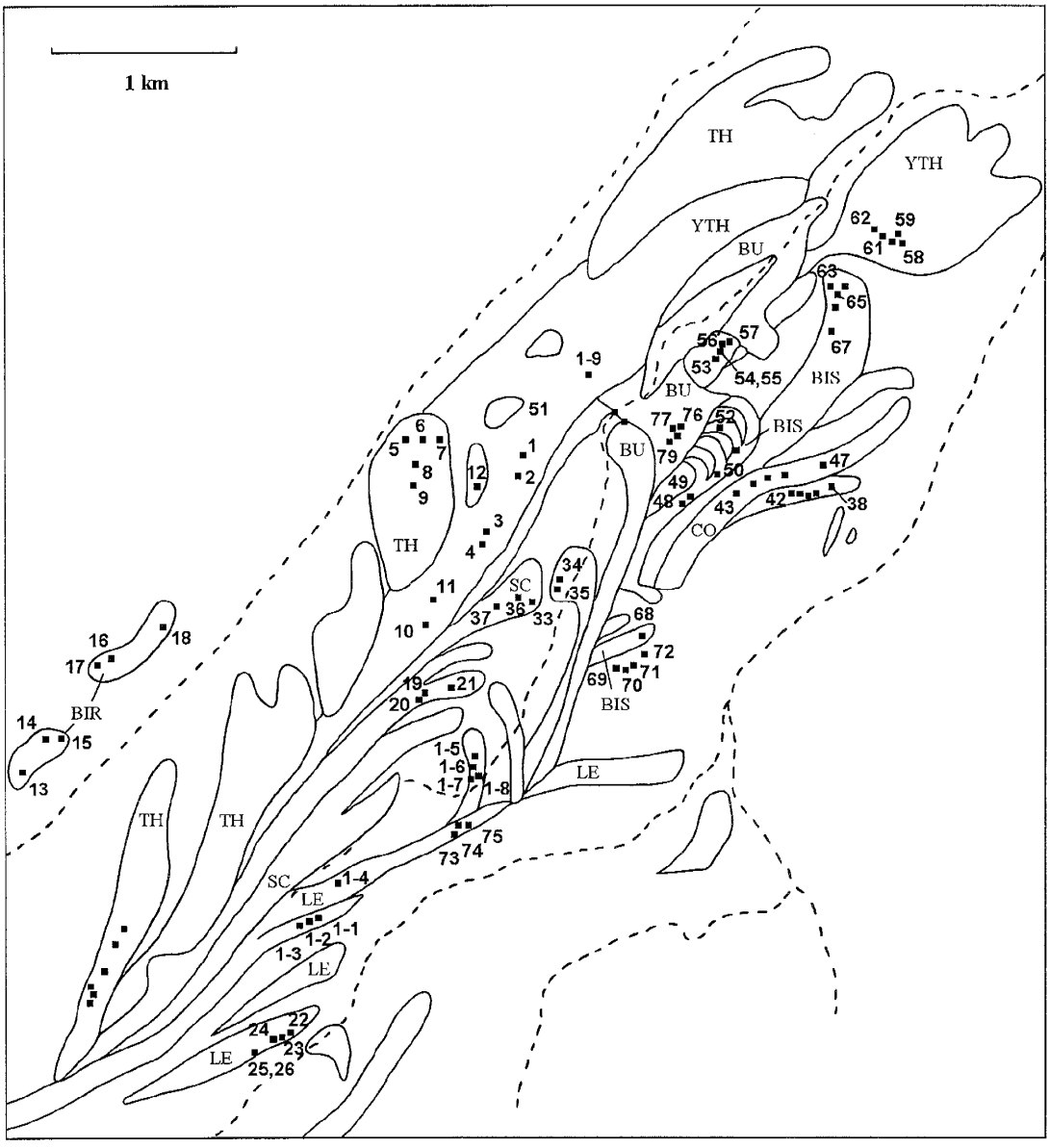

Fig. 9.6. Glacial deposits at Bishop Creek.

Shreve

One sample (BPCR91-11LTi) was collected from a glacially polished bedrock on the bottom of the Middle Fork canyon, just upstream of the moraines. The ^{36}Cl surface exposure age of 18 ky thus dates the deglaciation and shows that any younger glacial events were less extensive and never reached these low elevations. It agrees with the data set from Little McGee Creek, where deposits of this and younger ages were found at higher elevations. This is the youngest surface in this valley dated by the cosmogenic ^{36}Cl accumulation.

Little Egypt (LE)

Three different lateral moraines (BPCR90-22 through 26, BPCR90-73 through 75, and BPCR91-1 through 4) were deposited at elevations 1.9-1.95 km at the junction of Bishop and Coyote Creek. Ten out of twelve samples have ^{36}Cl ages between 16 and 18 ky, with two younger outliers. The samples at the upper end of the moraines are slightly younger (16 ky) than those down the valley (18 ky). The older set was deposited during the glacial maximum, while the younger ones may be a result of glacial retreat and subsequent readvance.

Table 9.3. Target element concentrations, macroscopic thermal neutron absorption cross sections, elevations, $^{36}Cl/Cl$ ratios, and calculated ^{36}Cl ages for samples from Bishop Creek.

Unit	Sample ID	Cl (ppm)	K_2O (%)	CaO (%)	$\Sigma\sigma N$ (cm^2/kg)	Elevation (km)	ELD	$^{36}Cl/Cl$ (10^{-15})	Age (ky)	
									Boulder	Surface
Shreve	bpcr91-11-lti	59	3.84	2.03	5.79	2.47	5.63	937 ± 36	18.3 ± 0.7	18.6 ± 0.7
	bpcr91-11-lti	59	3.84	2.03	5.79	2.47	5.63	966 ± 40	18.9 ± 0.8	
	bpcr90-22-ti2	9	4.16	1.13	4.19	1.87	3.76	2940 ± 261	16.2 ± 1.5	
	bpcr90-23-ti2	30	6.02	1.35	4.94	1.87	3.76	781 ± 53	8.9 ± 0.6[a]	15.8 ± 1.3
	bpcr90-24-ti2	117	3.69	2.02	4.50	1.88	3.80	373 ± 17	15.7 ± 0.8	15.5
	bpcr90-25-ti2	14	4.43	0.68	4.41	1.88	3.80	1963 ± 235	15.5 ± 1.9	16.2
Little	bpcr90-26-ti2	8	3.60	0.39	4.52	1.88	3.80	2697 ± 375	16.1 ± 2.3	
	bpcr91-1-ti1	64	1.81	5.41	5.23	1.99	4.09	496 ± 31	15.9 ± 1.1	16.3 ± 1.1
Egypt	bpcr91-2-ti1	144	3.77	1.90	4.23	1.99	4.09	158 ± 21	5.9 ± 1.0[a]	16.4
	bpcr91-3-ti1	83	3.17	4.03	5.18	1.99	4.09	504 ± 29	16.6 ± 1.0	16.6
(LE)	bpcr91-4-ti1	72	2.05	4.88	5.42	1.98	4.06	467 ± 39	16.4 ± 1.5	
	bpcr90-73-pti8	78	2.46	5.21	5.23	1.85	3.71	452 ± 19	16.5 ± 0.8	17.2 ± 0.9
	bpcr90-74-pti8	123	2.03	5.88	5.47	1.85	3.71	350 ± 38	17.8 ± 2.2	17.8
	bpcr90-75-pti8	71	3.08	4.34	4.96	1.85	3.71	555 ± 24	17.9 ± 0.8	17.9

	bpcr91-5-ti1	67	3.83	2.02	4.28	1.89	3.83	480 ± 58	13.6 ± 1.8[a]	19.1 ± 1.0
	bpcr91-6-ti1	93	1.96	4.96	5.50	1.89	3.83	430 ± 26	19.4 ± 1.3	19.2
Sand	bpcr91-7-ti1	226	1.77	5.84	5.18	1.89	3.83	410 ± 39	28.9 ± 3.1[a]	19.4
Canyon	bpcr91-8-ti1	6	4.74	0.95	4.35	1.89	3.83	6032 ± 262	19.0 ± 0.8	
(SC)	bpcr90-19-ti	18	4.33	2.60	4.84	1.82	3.65	1960 ± 116	18.6 ± 1.1	17.0 ± 1.6
	bpcr90-20-ti	11	3.88	0.46	4.15	1.82	3.65	2303 ± 141	16.7 ± 1.1	16.7
	bpcr90-21-ti	9	3.71	0.70	4.29	1.82	3.62	2364 ± 200	15.3 ± 1.3	18.6
	bpcr90-33-pti1	58	3.68	3.80	4.88	1.76	3.50	3496 ± 158	110 ± 5.7	
Younger	bpcr90-34-pti1	48	2.34	4.24	5.04	1.76	3.50	2771 ± 95	92.3 ± 3.6	96.6 ± 16.3
Buttermilk	bpcr90-35-pti1	6	3.91	0.59	4.12	1.76	3.50	15714 ± 127	70.7 ± 6.3	99.1
(BU)	bpcr90-36-pti1	19	4.35	0.54	4.20	1.76	3.50	7800 ± 487	99.1 ± 7.0	111
	bpcr90-37-pti1	75	2.68	5.00	5.35	1.76	3.53	2579 ± 113	111 ± 5.6	
Older	bpcr90-76-pti3	95	2.35	5.35	5.51	1.74	3.44	1300 ± 70	66.5 ± 4.0	55.5 ± 10.1
Buttermilk	bpcr90-77-pti3	56	2.14	5.02	5.30	1.74	3.44	1699 ± 103	62.8 ± 4.2	56.6
(BU)	bpcr90-78-pti3	64	5.55	0.62	4.51	1.74	3.44	1592 ± 49	44.2 ± 1.5	66.5
	bpcr90-79-pti3	139	4.12	1.87	4.83	1.74	3.44	910 ± 98	50.4 ± 6.0	

	bpcr90-48-pti4	74	2.67	4.75	5.42	1.76	3.50	2580 ± 138	113 ± 7.0[a]	
	bpcr90-49-pti4	122	2.80	5.01	5.55	1.77	3.51	1140 ± 68	64.1 ± 4.3	58.4 ± 6.9
	bpcr90-50-pti4	56	4.94	0.60	4.45	1.74	3.44	1949 ± 119	54.4 ± 3.6	59.2
Younger	bpcr90-51-pti4	145	2.83	4.87	5.39	1.71	3.38	1703 ± 110	117 ± 8.9[a]	64.1
Bishop	bpcr90-52-pti4	32	4.20	1.67	4.67	1.71	3.37	4930 ± 228	101 ± 5.3[a]	
(BIS)	bpcr90-68-pti8	137	3.89	1.91	4.75	1.81	3.63	1246 ± 91	68.2 ± 5.6	69.5 ± 5.0
	bpcr90-69-pti8	168	4.28	1.74	4.97	1.81	3.63	1168 ± 66	70.4 ± 4.5	
	bpcr92-1-pti4	278	0.81	8.86	6.00	1.74	3.44	770 ± 70	78.5 ± 8.2	78.3 ± 9.7
	bpcr92-2-pti4	92	1.75	5.34	5.19	1.74	3.44	1402 ± 200	77.7 ± 12.6	
	bpcr90-63-pti5	141	4.76	1.63	4.80	1.63	3.19	1464 ± 74	86.7 ± 5.0	
	bpcr90-64-pti5	154	4.11	2.07	5.03	1.62	3.16	1306 ± 67	89.1 ± 5.2	76.0 ± 9.2
Older	bpcr90-65-pti5	108	4.04	2.03	4.88	1.63	3.19	1482 ± 73	79.7 ± 4.4	83.6
Bishop	bpcr90-66-pti5	20	3.73	2.36	4.68	1.63	3.19	4670 ± 164	68.6 ± 2.6	89.1
(BIS)	bpcr90-67-pti5	118	4.03	1.88	4.85	1.64	3.20	1461 ± 44	83.6 ± 2.8	
	bpcr90-70-pti8	142	4.24	1.79	4.86	1.81	3.63	1530 ± 146	84.8 ± 9.2	81.3 ± 5.2
	bpcr90-71-pti8	185	2.32	6.06	5.65	1.79	3.57	1378 ± 82	107 ± 7.5[a]	83.6
	bpcr90-72-pti8	72	5.29	0.75	4.52	1.79	3.57	2387 ± 122	75.2 ± 4.3	84.8

	bpcr90-43-pti6	79	3.54	3.98	5.19	1.71	3.37	2569 ± 78	109 ± 3.8	
	bpcr90-44-pti6	78	4.18	1.38	4.48	1.70	3.36	1458 ± 113	56.9 ± 4.8	75.2 ± 24.0
	bpcr90-45-pti6	36	4.72	1.32	4.62	1.63	3.19	3632 ± 104	77.3 ± 2.5	77.3
	bpcr90-46-pti6	60	5.00	1.25	4.88	1.63	3.19	2668 ± 89	85.2 ± 3.2	109
Coyote	bpcr90-47-pti6	132	4.33	1.65	5.19	1.63	3.19	824 ± 45	47.8 ± 2.9	
(CO)	bpcr90-38-pti7	64	3.53	3.99	5.24	1.62	3.17	2889 ± 409	113 ± 18.8	
	bpcr90-39-pti7	14	4.95	0.69	4.46	1.64	3.20	7498 ± 438	67.5 ± 4.3	87.4 ± 16.5
	bpcr90-40-pti7	26	4.48	0.58	4.29	1.65	3.22	5120 ± 203	89.5 ± 4.0	85.4
	bpcr90-41-pti7	131	4.01	1.48	4.87	1.66	3.25	1319 ± 107	80.8 ± 7.4	113
	bpcr90-42-pti7	170	4.18	1.38	4.44	1.66	3.25	1273 ± 96	85.4 ± 7.3	
	bpcr90-ta-1	79	3.37	4.26	5.13	1.79	3.57	2831 ± 99	116 ± 4.7	
	bpcr90-ta-2	63	2.10	4.71	5.04	1.79	3.58	2829 ± 140	119 ± 6.9	109 ± 12
Younger	bpcr90-ta-3	78	3.16	4.22	5.24	1.81	3.62	2241 ± 95	89.9 ± 4.3	114
Tungsten	bpcr90-ta-4	19	4.32	0.57	4.32	1.81	3.63	7983 ± 458	99.3 ± 6.5	119
Hills	bpcr90-ta-10	68	2.29	8.70	7.20	1.85	3.73	3183 ± 262	112 ± 10.8	
(YTH)	bpcr90-ta-11	71	3.21	4.09	5.08	1.84	3.70	3079 ± 432	116 ± 19.3	
	bpcr90-58-opb	29	4.63	0.67	4.42	1.61	3.13	4816 ± 257	92.3 ± 5.6	
	bpcr90-59-opb	82	3.02	4.19	4.98	1.61	3.13	2399 ± 106	122 ± 6.3	100 ± 14
	bpcr90-60-opb	26	3.41	0.56	3.96	1.61	3.13	4389 ± 271	98.2 ± 6.9	98.2

	bpcr90-61-opb	77	2.55	4.82	5.24	1.62	3.16	1726 ± 102	83.9 ± 5.6	122
	bpcr90-62-opb	138	3.06	4.58	5.17	1.62	3.16	1538 ± 55	105 ± 4.3	
	bpcr90-pta1-5	96	2.04	5.65	5.61	1.75	3.47	2101 ± 116	121 ± 7.9	
	bpcr90-pta1-6	7	4.48	0.43	4.26	1.75	3.47	14106 ± 660	69.3 ± 3.5	91.8 ± 33.1
	bpcr90-pta1-7	48	3.62	3.60	4.91	1.75	3.46	3155 ± 132	86.2 ± 4.0	86.2
Older	bpcr90-pta1-8	15	4.38	0.52	4.13	1.75	3.47	5306 ± 370	52.7 ± 3.9	130
	bpcr90-pta1-9	171	2.17	5.44	5.58	1.77	3.51	1633 ± 117	130 ± 11.3	
	bpcr90-53-pti3	294	2.50	5.63	5.81	1.71	3.37	1302 ± 60	139 ± 7.8	
Tungsten	bpcr90-54-pti3	67	2.43	4.75	5.19	1.69	3.33	1383 ± 84	56.9 ± 3.8[a]	114 ± 11
	bpcr90-55-pti3	50	4.74	0.67	4.41	1.69	3.33	2367 ± 141	64.4 ± 4.2[a]	109
	bpcr90-56-pti3	38	4.90	1.44	4.68	1.69	3.32	4953 ± 155	106 ± 3.8	139
Hills	bpcr90-57-pti3	24	3.98	1.07	4.53	1.69	3.33	6143 ± 182	109 ± 3.7	
	bpcr90-27-pta3	24	4.54	0.56	4.33	1.97	4.04	11195 ± 653	158 ± 11.1	
	bpcr90-28-pta3	12	4.42	0.65	4.30	1.98	4.07	15978 ± 158	111 ± 12.7	124 ± 23
(TH)	bpcr90-29-pta3	15	4.60	0.55	4.32	2.01	4.14	13991 ± 785	115 ± 7.5	115
	bpcr90-30-pta3	13	4.44	1.77	4.60	2.03	4.20	16410 ± 622	115 ± 5.0	158
	bpcr90-31-pta3	22	3.94	2.53	4.69	2.03	4.21	8452 ± 464	97.7 ± 6.1	
	bpcr90-32-pta3	67	2.26	5.11	5.40	2.03	4.21	3875 ± 219	144 ± 9.8	

Birch (BIR)	bpcr90-13-sh	40	4.61	7.21	6.37	1.88	3.81	2082 ± 121	30.9 ± 1.9	
	bpcr90-14-sh	28	4.28	1.50	4.61	1.88	3.79	3573 ± 173	54.2 ± 2.8	70.7 ± 32.9
	bpcr90-15-sh	10	5.30	0.56	4.41	1.88	3.79	8723 ± 527	45.1 ± 2.9	69.6
	bpcr90-16-sh	58	2.03	4.69	5.09	1.83	3.67	3138 ± 122	125 ± 5.7	125
	bpcr90-17-sh	65	2.55	4.52	5.08	1.83	3.67	2261 ± 139	85.1 ± 5.9	
	bpcr90-18-sh	43	4.46	0.54	4.42	1.80	3.59	3723 ± 199	90.4 ± 5.4	
Other Samples	bpcr91-9-ss	54	2.59	4.33	4.75	1.79	3.57	77.4 ± 25	1.4 ± 0.8	
	bpcr91-10-ow	19	4.09	1.51	4.55	1.51	2.93	7284 ± 651	110 ± 11.4	
	bcr89-ta1	18	4.33	0.52	4.24	2.35	5.20	18643 ± 967	163 ± 10.4	
	bpcr90-12-pta2	9	3.32	0.64	4.09	1.75	3.47	7050 ± 357	57.0 ± 3.1	

[a] Not used in determination of the surface mean, median, and maximum ages.

Sand Canyon (SC)

Two small terminal moraines (samples BPCR90-19 through 21 and BPCR91-5 through 8) from the bottom of Sand Canyon record a glacial advance older and slightly less extensive than that of the Little Egypt moraines. The Sand Canyon moraines are preserved because the Little Egypt glacier did not follow the same path. Most of the ^{36}Cl ages are just under 20 ky, except sample BPCR91-7, which gave an age of 29 ky. This oldest age is in reasonable agreement with the varnish ^{14}C age of ~37 ky obtained for the same sample (Phillips et al., 1993). However, the close grouping of other samples

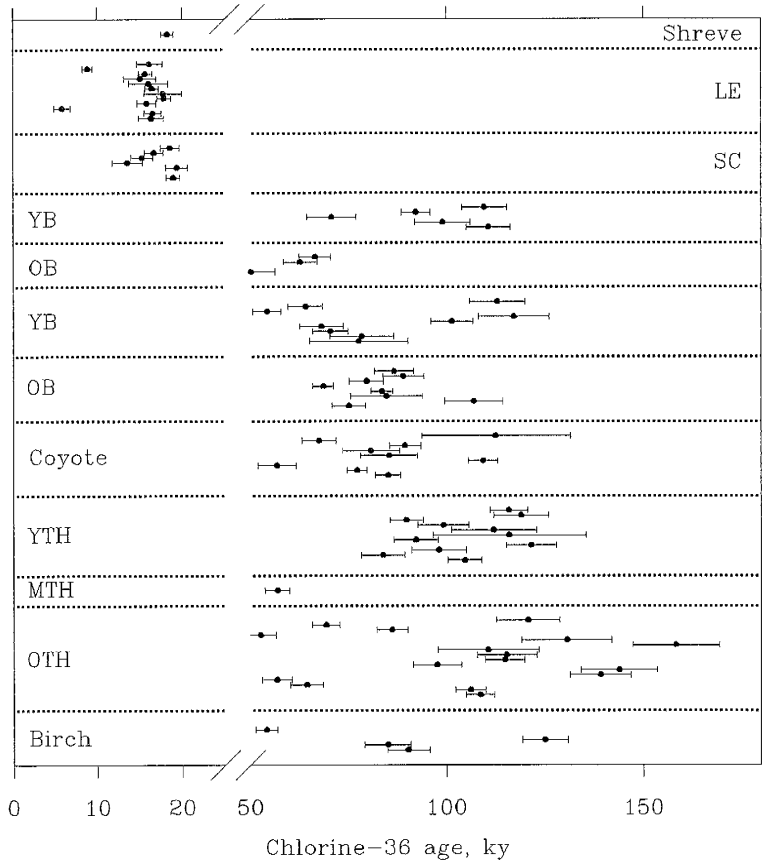

Fig. 9.7. Distribution of exposure ages for moraines from Bishop Creek.

indicates that the age 29 ky could be due to prior exposure and the age ~20 ky is preferred for these deposits. These moraines are stratigraphically between the younger Little Egypt moraines and older Buttermilk moraines and either of the two ages (20 and 29 ky) would fit in the local stratigraphy.

Buttermilk (BU)

Below the terminal moraines described above, there is an extensive set of older moraines descending along Sand Canyon down to the elevation of ~1.6 km. Two moraines were sampled: Younger Buttermilk (samples BPCR90-33 through 37) and Older Buttermilk (samples BPCR90-76 through 79). The ^{36}Cl ages are inconclusive; the Younger Buttermilk moraines have ages between 71 and 111 ky, while the Older Buttermilk moraines yielded ages from 44 to 65 ky. The older apparent ages for the stratigraphically younger deposits must be due to prior exposure. The age of the Older Buttermilk deposit is probably close to the oldest boulder age of 65 ky, whereas the Younger Buttermilk glacial episode must have occurred between the Older Buttermilk and Sand Canyon advances, i.e., between 20 (or 29) and 65 ky.

Bishop (BIS)

The Bishop moraines border the Buttermilk complex on the southeast. They form several terminal loops as well as right laterals. Two sets of moraines designated as the

Younger Bishop (samples BPCR90-48 through 52, BPCR90-68 and 69, and BPCR92-1 and 2) and the Older Bishop (samples BPCR90-63 through 67 and 70 through 72) were sampled. Three out of nine boulders in the younger set (samples 48, 51, and 52) gave ages older than the age of the Older Bishop moraines and are therefore considered to have resulted from prior exposure. The remaining ages form a close group with the maximum age of 78 ky, which is the best age estimate for this surface. The Older Bishop moraines yielded consistent ages clustered in the interval between 75 and 89 ky, with one younger age at 69 ky and one older outlier dated to 116 ky. The older sample was described in the field as least suitable for dating because of its weathered appearance. The surface age is then best estimated by the oldest boulder in the cluster dated at 89 ky; this age is consistent with the local stratigraphy.

Coyote (CO)

Ten samples from two right lateral moraine ridges to the southeast of the Older Bishop moraine gave ^{36}Cl ages distributed approximately uniformly between 50 and 110 ky. This scatter of the apparent ages is due to erosion of at least several meters of soil and the oldest apparent boulder age is the best estimate of the surface age. The age of 110 ky is stratigraphically consistent as the moraine must be older than the 89-ky-old Older Bishop moraine.

Tungsten Hills (YTH and TH)

The Tungsten Hills moraines are three older moraines that bound the entire terminal moraine complex on the west and north. The Younger Tungsten Hills (samples BPCR90-1 through 4, BPCR90-10, and 11, and BPCR90-58 through 62) yielded the ages from 84 to 122 ky. The Older Tungsten Hills (samples BPCR90-5 through 9, BPCR90-27 through 32, and BPCR90-53 through 57) gave much less consistent ages between 53 and 158 ky. In both cases the maximum boulder ages are likely to be the best estimates of the surface ages. The Younger and Older Tungsten Hills moraines are thus ~120 and ~160 ky old, respectively.

Birch (BIR)

The Birch moraines (samples BPCR90-13 through 18), preserved only in isolated patches to the west of the main moraine complex gave ages between 31 and 119 ky. Even the maximum age of 119 ky is clearly too young because these deposits are stratigraphically older than the Older Tungsten Hills moraines described above. At this point, the age of these surfaces cannot be estimated with any certainty and further work is needed to constrain the age of the glaciation that produced these deposits.

Other samples

Sample BPCR91-9SS was collected from a road cut in the Younger Tungsten Hills moraine. The sample has been shielded from cosmic radiation by approximately 15 m of soil. At this depth the intensity of cosmic rays is negligible and all ^{36}Cl is produced by neutrons derived from U and Th in the rocks. This sample was collected to test whether deeply buried samples have low $^{36}Cl/Cl$ ratios in conformity with the assumptions of the conceptual model. The measured ratio of 77×10^{-15} is higher than the assumed value of 30×10^{-15}, but it is negligible comparing with the cosmogenic component ($\sim3000\times10^{-15}$) in surficial samples from this moraine.

Sample BPCR91-10OW was collected from an outwash deposit northeast of the main moraine complex. Its age of 110 ky is consistent with the age of the Younger Tungsten Hills moraine, from which it might have been derived.

One sample (BCR89-1) was collected from a lateral moraine above the main complex. The exposure age of 162 ky is similar to that of the Older Tungsten Hills moraine, which suggests that the two moraines may have been deposited by the same glacier.

Conclusions

The ^{36}Cl glacial chronologies developed above for the three basins in the Sierra Nevada offers an opportunity to test the synchroneity of the late Pleistocene glaciations in this region. The size of the ^{36}Cl data set is sufficiently large to support this comparison and provide meaningful results. Beyond intercomparison of the ^{36}Cl ages, the obtained chronologies are also compared with the global marine ^{18}O record to establish whether there is a link between development of small mountain glaciers and the global climate change.

Table 9.4 shows the inferred ages for all surfaces reported in this chapter. I report for each surface the exposure age that I believe most closely estimates its true constructional age. Where boulder ages are grouped closely together, I use the mean surface age; where there is a large spread in the exposure ages, I use the maximum boulder age obtained for the surface. This methodology was adopted based on the study of effects of erosion on ^{36}Cl surface exposure ages (this work and Zreda et al., submitted) which shows that stable surfaces, with small erosion depth, yield consistent exposure ages, while eroding moraines have boulder ages exhibiting a wide uniform distribution with its upper limit very close to the true surface age.

Table 9.4. Comparison of ^{36}Cl chronologies for late Pleistocene glacial surfaces from Bloody Canyon, Little McGee Creek and Bishop Creek, eastern Sierra Nevada and eastern White Mountains.

^{18}O stage	Bloody Canyon		Little McGee Creek		Bishop Creek		White Mountains	
	Unit	Age	Unit	Age	Unit	Age	Unit	Age
1			Neoglacial	<1				
			Hilgard	7				
			Early Hilgard	8				
2	Tioga	11-14	Late Tioga	12			Chiatovich	12
	Tenaya	14		14			Y. Middle Creek	14
					Little Egypt, Shreve	18	O. Middle Creek	18
			Tioga	20	Sand Canyon	19	Perry Aiken	19
			Early Tioga	26				
3	Younger Tahoe	45						
4	Mono Basin	65	Tahoe	65	Buttermilk	65		
					Younger Bishop	75		
5					Older Bishop	90		
	Older Tahoe	100						
			Sherwin	110	Coyote	110		
					Y. Tungsten Hills	120		
6					Tungsten Hills	158	Indian	150
?					Birch	>150	Dyer	>150

The compilation presented in Table 9.4 indicates that many glacial deposits correlate well with deposits in other drainages, which is due to simultaneous development of glaciers in all three areas. This is especially apparent in the case of young, late Wisconsin deposits that have identical ages throughout the study area. The most noticeable correlation is observed for deposits dated to 11-12, 14 and 18-20 ky. The older deposits are less well correlated because of moraine crest erosion and obliterative overlap. The first process leads to gradual exposure of boulders and results in (usually) underestimation of the true age; the second process removes evidence of older glaciations and may lead to false interpretation regarding climatic conditions.

The oldest studied deposits date to ~150 ky (found only at Bishop Creek) and correlate with the penultimate glaciation of the marine stage 6. Moraines of similar ages were reported from the eastern White Mountains (see the chapter on the White Mountains, this work) and Pine Creek in the eastern Sierra Nevada (Dorn et al., 1990) as well as from the Rocky Mountains (e.g., Pierce et al., 1976; Hall and Michaud, 1988).

Early Wisconsin deposits are present in all three valleys and are dated at 90-120 ky, correlative with the stage 5 (b and d) of the marine ^{18}O record. While at Little McGee Creek and Bloody Canyon only single deposits of this age are found, a sequence of several distinct moraines deposited between 120 and 90 ky is preserved at Bishop Creek. At this age range, the method's accuracy may be affected by geological processes

modifying the surface and it may be difficult to reliably distinguish moraines constructed 10 ky apart. My interpretation of the ^{36}Cl ages shows that the last interglacial-to-glacial transition was characterized by recurring environmental changes, from glacial to interglacial, to glacial again, and so on. These climate changes were global in scope, which is apparent from the ^{18}O record (Martinson et al., 1987).

Glacial deposits correlative with the stage 4 of the marine record ($\sim$65 ky) are present at all three locations. This local maximum in the global ice volume was followed by a period of average climatic conditions during which glaciers might have developed locally, but the global ice volume was smaller than that at 65 ky. One moraine from this period, dated at 45 ky, is preserved at Bloody Canyon. Its substantial size is in apparent conflict with the warm climate inferred from the small global ice volume and may indicate that local conditions, such as increased precipitation, controlled glacier development at this time and location.

The late Wisconsin maximum that occurred at 18-20 ky is recorded in the Little McGee and Bishop Creek areas, but not at Bloody Canyon, while deglacial deposits, dated at $\sim$14 ky, are ubiquitous and almost as extensive as the moraines deposited during the glacial maximum. Presumably, at Bloody Canyon, deposits that would have correlated with the last glacial maximum (18-20 ky) were obliterated by glaciers about 14 ky ago.

The most complete sequence of late glacial and deglacial moraines was found at Little McGee Creek. The ^{36}Cl ages indicated deglaciation progressing in several steps that all lasted only about 1-2 ky. The ice disappeared quickly and a warm climate dominated until ~ 8 ky ago.

The youngest deposits in Little McGee Creek indicate that the Holocene climate was variable and at least three cold periods were present. The oldest glacial deposits (designated here as early Hilgard and Hilgard) are 7-8 ky old and thus predate the Holocene climatic optimum (the Hypsithermal). They are correlative with the oldest Recess Peak advances at Mills Creek (as mapped by Birman, 1964) dated by ^{14}C at >7 ky (Burbank, 1989), but not with the Hilgard deposits from Barrett Lake ^{14}C dated at 12 ky (Anderson, 1990). The age 7-8 ky also coincides with the period of worldwide expansion of alpine glaciers and high latitude ice caps that occurred between 7.5 and 8.5 ky (Beget, 1983 and references therein). The following period of a warmer climate (the Hypsithermal) separates the early Holocene (Hilgard) advances from the post-Hypsithermal (Neoglacial) ones. The Neoglacial deposits at Little McGee Creek gave ages 0.3 and 0.9 ky and thus correspond with the Matthes (Matthes, 1942) advances of the last several hundred years (Curry, 1969, 1971).

The ^{36}Cl glacial chronologies generally support synchroneity of glacial events in the Sierra Nevada with those in the White Mountains (this work) and with the global ice volume record (e.g., Martinson et al., 1987), although there also are some discrepancies.

The major maxima in the ice volume record at ~150 ky (stage 6), 90-120 ky (stage 5b, d), 65-75 ky (stage 4) and 18-20 ky (stage 2) also show in the ^{36}Cl glacial record. In addition to this positive correlation, there are glacial deposits whose ages correlate with small global ice volume. One of them is the Younger Tahoe moraine in Bloody Canyon dated at 45 ky and thus correlative with the warmer, interstadial stage 3 of the marine record. It is likely that this moraine was deposited during a short pulse of cold climatic conditions, perhaps similar to the Younger Dryas of ~12 ky ago. The other moraines that do not correlate with increased global ice volume are those of the Hilgard and Little Ice Age glaciations. Both occurred during the interglacial Holocene and probably represent changes in climatic conditions too short to be reflected in the global ice record.

An interesting characteristic of the information presented in the correlation chart is the fragmentary character of all three glacial records. None of the three drainages contains deposits of all glacial events and some events are recorded only in one valley (e.g., the 45-ky old moraine at Bloody Canyon). Some missing ages are due to incomplete sampling, which is especially true in the case of youngest moraines. For instance, Holocene deposits were sampled only at Little McGee Creek (Neoglacial and Hilgard) and their apparent absence at other locations does not necessarily mean that they are absent there. The chronostratigraphic hiatuses bracketed by younger and older ages are probably due to obliterative overlap (Gibbons et al., 1984). The most significant gap is observed at Bloody Canyon where deposits corresponding to the late Wisconsin maximum (~20 ky) are missing. It is difficult to accept that at Bloody Canyon there

was no glaciation at 20 ky, while in the other two valleys as well as in the White Mountains this glacial advance was among the most pronounced. This absence of potentially correlative deposits must thus be due to their destruction by younger, latest Wisconsin glaciers.

This incompleteness of the terrestrial glacial record in the Sierra Nevada has important implications for glacial stratigraphy, chronology and correlations. Historically, glacial deposits in the Sierra Nevada were correlated with the mid-continent stratigraphy, which was, in turn, made to match the fourfold division developed for the European Alps. Coincidentally, deposits of three to four out of ten glaciations are typically preserved in alpine settings because of obliterative overlap (Gibbons et al., 1984). In consequence, three or four glacial units commonly found in individual valleys were assumed to be correlative with deposits at other locations. They were given common names, such as Tioga, Tahoe, or Sherwin, based either on their relative stratigraphic position or on other relative dating techniques. The problem inherent in this approach is that deposits of different ages are correlated and those of the same age assigned to two different units.

To illustrate this point, I consider the Tioga, Tenaya and Tahoe deposits at Bloody Canyon (BC) and Little McGee Creek (LMC). The Tioga (BC), as mapped by Sharp and Birman (1963) correlates with the younger Tioga (LMC), although its stratigraphic position is the same as that of the older Tioga (LMC). The Tenaya (BC)

has the same age as the Tioga (LMC). The term Tahoe is even more confusing. Its age at Little McGee Creek is 65 ky, which correlates with the Mono Basin (BC). The Tahoe (BC) is subdivided into two parts, older and younger, neither of which corresponds to the Tahoe (LMC). The younger Tahoe does not have a temporal equivalent at Little McGee Creek, while the older Tahoe is correlated with the Sherwin.

Miscorrelation of glacial deposits from the Sierra Nevada with those from the White Mountains was even more marked (see the chapter on the White Mountains, this work). The Perry Aiken deposits from Chiatovich Creek were correlated by Elliott-Fisk (1987) with the stage 6 Tahoe at Pine Creek, eastern Sierra Nevada and thus assigned an age of ~ 150 ky. The ^{36}Cl ages for these moraines are < 19 ky and indicate that they are deposits of the late Wisconsin maximum rather than of the penultimate glaciation.

The above observations lead to the conclusion that the existing correlations are often in error. Although the stratigraphic units commonly used in the Sierra Nevada imply certain chronologic relationships, they have no meaning unless accompanied by numerical ages. In other words, the terms like Tioga or Tahoe mean different things at different locations; when one says "Tahoe" one need not mean a unit correlative with the Tahoe in the type area. One solution to this problem might be giving local lithostratigraphic names to glacial deposits. It would eliminate the ambiguities associated with the common names like Tioga, but would introduce new names that would make correlation charts incomprehensible. Therefore, glacial correlations should be based

more on absolute ages and less on stratigraphic relationships. The usage of the commonly employed names must be reevaluated and put in the context of numerical chronologies.

References

Anderson, R.S., 1990, Holocene forest development and paleoclimates within the central Sierra Nevada, California, Journal of Ecology 78, 470-489.

Atwater, B. F., D. P. Adam, R. M. Bradbury, R. K. Forester, W. R. Mark, W.R. Lettis, G. R. Fisher, K. W. Gobalet, and S. W. Robinson, 1986, A fan dam for Tulare Lake, California, and implications for the Wisconsin glacial history of the Sierra Nevada, Geological Society of America Bulletin 97, 97-109.

Beget, J.E., 1983, Radiocarbon-dated evidence of worldwide early Holocene climatic change, Geology 11, 389-393.

Benson, L.V., D.R. Currey, R.I. Dorn, K.R. Lajoie, C.G. Oviatt, S.W. Robinson. G.I. Smith and S. Stine, 1990, Chronology of expansion and contraction of four Great Basin lake systems during the past 35,000 years, Paleogeography, Paleoclimatology, Paleoecology 78, 241-286.

Bentley, H. W., F. M. Phillips, and S. N. Davis, 1986, Chlorine-36 in the terrestrial environment. In Handbook of Environmental Isotope Geochemistry, Vol. 2, The Terrestrial Environment, B, edited by P. Fritz and J.-Ch. Fontes, pp. 427-480.

Birkeland, P.W., R.M. Birke and A.L. Walker, 1980, Soils and subsurface rock-

weathering features of Sherwin and pre-Sherwin glacial deposits, eastern Sierra Nevada, California, Geological Society of America Bulletin 91, 238-244.

Birman, J.H., 1964, Glacial geology across the crest of the Sierra Nevada, California, Geological Society of America, Special Paper 75, pp. 1-80.

Blackwelder, E., 1931, Pleistocene glaciation in the Sierra Nevada and Basin ranges. Geological Society of America Bulletin 42, 865-922.

Burbank, D.W., 1989, Late Quaternary snowline reconstructions for the southern and central Sierra Nevada, California and a reassessment of the "Recess Peak Glaciation", Quaternary Research 36, 294-306.

Burke, R.M., and P.W. Birkeland, 1979, Reevaluation of multiparameter relative dating techniques and their application to the glacial sequences along the eastern escarpment of the Sierra Nevada, California, Quaternary Research 11, 21-51.

Burke, R.M., and P.W. Birkeland, 1983, Holocene glaciation in the mountain ranges of the western United States, In Late-Quaternary Environments of the United States, Vol. 2, The Holocene, H.E. Wright (ed.), 3-11, University of Minnesota Press.

Bursik, M. and A.R. Gillespie, 1993, Late Pleistocene glaciation of Mono Basin, California, Quaternary Research 39, 24-35.

Curry, R.R., 1969, Holocene climatic and glacial history of the central Sierra Nevada, California, Special Paper - Geological Society of America 123.

Curry, R.R., 1971, "Glacial and Pleistocene History of the Mammoth Lakes Area, California: A Geologic Guidebook", Vol. II, University of Montana Department of Geology Geological Series Publication.

Dalrymple, G.B., 1964, Potassium-argon dates of three Pleistocene interglacial basalt flows from the Sierra Nevada, California, Geological Society of America Bulletin 75, 753-758.

Dalrymple, G.B., R.M. Burke and P.W. Birkeland, 1982, Concerning K-Ar dating of a basalt flow from the Tahoe-Tioga interglaciation, Sawmill Canyon, southeastern Sierra Nevada, California, Quaternary Research 17, 120-122.

Dorn R. I., B. D. Turrin, A. J. T. Jull, T. W. Linick, and D. J. Donahue, 1987, Radiocarbon and cation-ratio ages for rock varnish on Tioga and Tahoe morainal boulders of Pine Creek, eastern Sierra Nevada, California, and their paleoclimatic implications, Quaternary Research 28, 38-49.

Dorn, R.I., T.A. Cahill, R.A. Eldred, T.E. Gill, B.H. Kusko, A.J. Bach and D.L. Elliott-Fisk, 1990, Dating rock varnishes by the cation ratio method with PIXE, ICP, and the electron microprobe, International Journal of PIXE 1, 157-195.

Elliott-Fisk, D.L., 1987, Glacial geomorphology of the White Mountains, California and Nevada: Establishment of a glacial chronology, Physical Geography 8, 299-323.

Fullerton, D.S., 1986, Chronology and correlation of glacial deposits in the Sierra Nevada, California, In Quaternary Glaciations in the Northern Hemisphere - Report of the International Geological Correlation Programme Project 24, V. Sibrava, D.Q. Bowen and G.M. Richmond (eds.), 161-169, Pergamon Press.

Gibbons, A.B., Megeath, J.D., and Pierce, K.L. (1984). Probability of moraine survival in a succession of glacial advances, Geology 12, 327-330.

Gillespie, A.R., 1982, Quaternary glaciation and tectonism in the southern Sierra

Nevada, Inyo County, California, 695 p., Ph.D. dissertation, California Institute of Technology.

Gillespie, A.R, J.C. Huneke and G.J. Wasserburg, 1984, Eruption age of a ~100,000-year-old basalt from ^{40}Ar-^{39}Ar analysis of partially degassed xenoliths, Journal of Geophysical Research 89, 1033-1048.

Hall, R.D. and D. Michaud, 1988, The use of hornblende etching, clast weathering, and soils to date alpine glacial and periglacial deposits: A study from southwestern Montana, Geological Society of America Bulletin 100, 458-467.

Hallberg, G.R., 1986, Pre-Wisconsin glacial stratigraphy of the Central Plains region in Iowa, Nebraska, Kansas, and Missouri, In Quaternary Glaciations in the Northern Hemisphere - Report of the International Geological Correlation Programme Project 24, V. Sibrava, D.Q. Bowen and G.M. Richmond (eds.), 11-15, Pergamon Press.

Mezger, L. and D. Burbank, 1986, The glacial history of the Cottonwood Lakes area, southeastern Sierra Nevada, Geological Society of America Abstracts with Programs 18, 157.

Phillips, F.M., M.G. Zreda, S.S. Smith, D. Elmore, P.W. Kubik and P. Sharma, 1990, A cosmogenic chlorine-36 chronology for glacial deposits at Bloody Canyon, Eastern Sierra Nevada, California, Science 248, 1529-1532.

Pierce, K.L., J.D. Obradovich and I. Friedman, 1976, Obsidian hydration dating and correlation of Bull Lake and Pinedale glaciations near West Yellowstone, Montana, Geological Society of America Bulletin 87, 703-710.

Richmond, G.M. and D.S. Fullerton, 1986, Introduction to Quaternary glaciations in the United States of America, In Quaternary Glaciations in the Northern Hemisphere - Report of the International Geological Correlation Programme Project 24, V. Sibrava, D.Q. Bowen and G.M. Richmond (eds.), 3-10, Pergamon Press.

Sharp, R.P. and J.H. Birman, 1963, Additions to classical sequence of Pleistocene glaciations, Sierra Nevada, California, Geological Society of America Bulletin 74, 1079-1086.

Sharp, R.P., 1968, Sherwin Till-Bishop Tuff geological relationships, Sierra Nevada, California, Geological Society of America Bulletin 83, 2233-2260.

Smith, S.J. and R.S. Anderson, 1992, Late Wisconsin paleoecologic record from Swamp Lake, Yosemite National Park, California, Quaternary Research 38, 91-102.

Wahrhaftig, C. and J.H. Birman, 1965, The Quaternary of the Pacific mountain system in California, In The Quaternary of the United States, H.E. Wright, Jr. and D.G. Frey (eds.), 299-340, Princeton University Press.

Zreda, M. G., F. M. Phillips and D. Elmore, In press, Cosmogenic ^{36}Cl accumulation in unstable landforms: II. Simulations and measurements on eroding moraines, Water Resources Research.

10. Cosmogenic ^{36}Cl chronology for glacial deposits at Bull Lake, eastern Wind River Range, Wyoming

Abstract

Cosmogenic ^{36}Cl ages of boulders from late Pleistocene moraines and outwash terraces in the eastern Wind River Range indicate major glacial episodes at 190, 150, 90-110, and 14-18 ky, correlative with stages 6, 5, and 2 of the marine ^{18}O record. The most important feature of this chronology is the apparent absence of deposits correlative with stage 4 which may indicate either obliteration of these deposits by later glaciers or non-glacial local climatic conditions at that time, although the global climate was in the glacial mode. Eowisconsin (stage 5) moraines are more extensive than the late Wisconsin (stage 2) deposits which shows that the conditions for glacier development were more favorable at the beginning of the last glacial cycle than at its end.

Introduction

Glacial deposits in the Wind River Range have been found in both western and eastern parts of the range, where Blackwelder (1915) described moraines of three glaciations: Buffalo (the oldest), Bull Lake, and Pinedale (the youngest). The Pinedale area on the western side of the range and the Bull Lake area on its eastern side are the type localities of the last two glaciations. While the Pinedale glaciation is correlated with

the late Wisconsin (last 30 ky; Porter et al., 1983), and the Bull Lake glaciation is considered pre-Wisconsin (>100 ky) in age (Richmond, 1986), there is also evidence of glaciations intermediate in age, i.e., early Wisconsin (Richmond, 1986). The Bull Lake area contains, among others, deposits of both above glaciations (Richmond, 1976). At Washakie Point, north rim of the lake, five different tills are exposed; the youngest two are believed to be of the Bull Lake age. Immediately to the east of Washakie Point and in stratigraphic position above the Bull Lake deposits, moraines of the early and middle Pinedale glaciation are found. Five nested Pinedale moraines occur at Bull Lake. The oldest one is the most extensive, whereas the later three advances are limited in extent. The youngest moraine, located in the upper valley much higher than the other moraines, resulted from the last glacier advance just before the final deglaciation.

In this paper, 49 cosmogenic ^{36}Cl ages for samples from the Bull Lake area are reported and a cosmogenic ^{36}Cl chronology is developed. This chronology is preliminary since about 35 more samples are still in preparation and will be measured in the next year or so. The glacial record contained in these deposits is compared with those from the Sierra Nevada and White Mountains, both located close to the Pacific Ocean and thus having a different precipitation pattern, to evaluate synchroneity of glaciations in the Great Basin and the Rocky Mountains. This information will help assess whether the mountain glaciations are closely linked to the global climate change or perhaps are a result of regional or local environmental conditions.

Samples

The samples were collected using the usual sampling criteria outlined above and in the previous publications by our group (Phillips et al., 1990; Zreda et al., 1990, 1991). The major emphasis was placed on the moraine complex in the Bull Lake area (Figure 10.1) where three Pinedale and five Bull Lake moraines were sampled. Besides the above, samples from the Sacagawea Ridge moraine at Dinwoody Lake and from two outwash terraces south of Dubois were collected. More than five samples were obtained from most older surfaces to constrain landform age in case of strong surface modification (cf. Chapter 5).

Results and discussion

Table 10.1 shows the geochemical and isotopic data, locations and ELD factors, calculated ^{36}Cl boulder ages and inferred surface ages. The boulder ages are also graphed in Figure 10.2. The results are discussed in the order from the youngest deposits to the oldest. In the moraines from the Bull Lake area, the Roman and Arabic numerals indicate the Bull Lake and Pinedale moraines, respectively, with lower numbers given to stratigraphically older units. The numbering of the stratigraphic units at Bull Lake is different from the numbering scheme used for the samples because the geological map by Robert Hall used during sampling in 1992 has been refined by Hall in 1993 and many new stratigraphic units appeared.

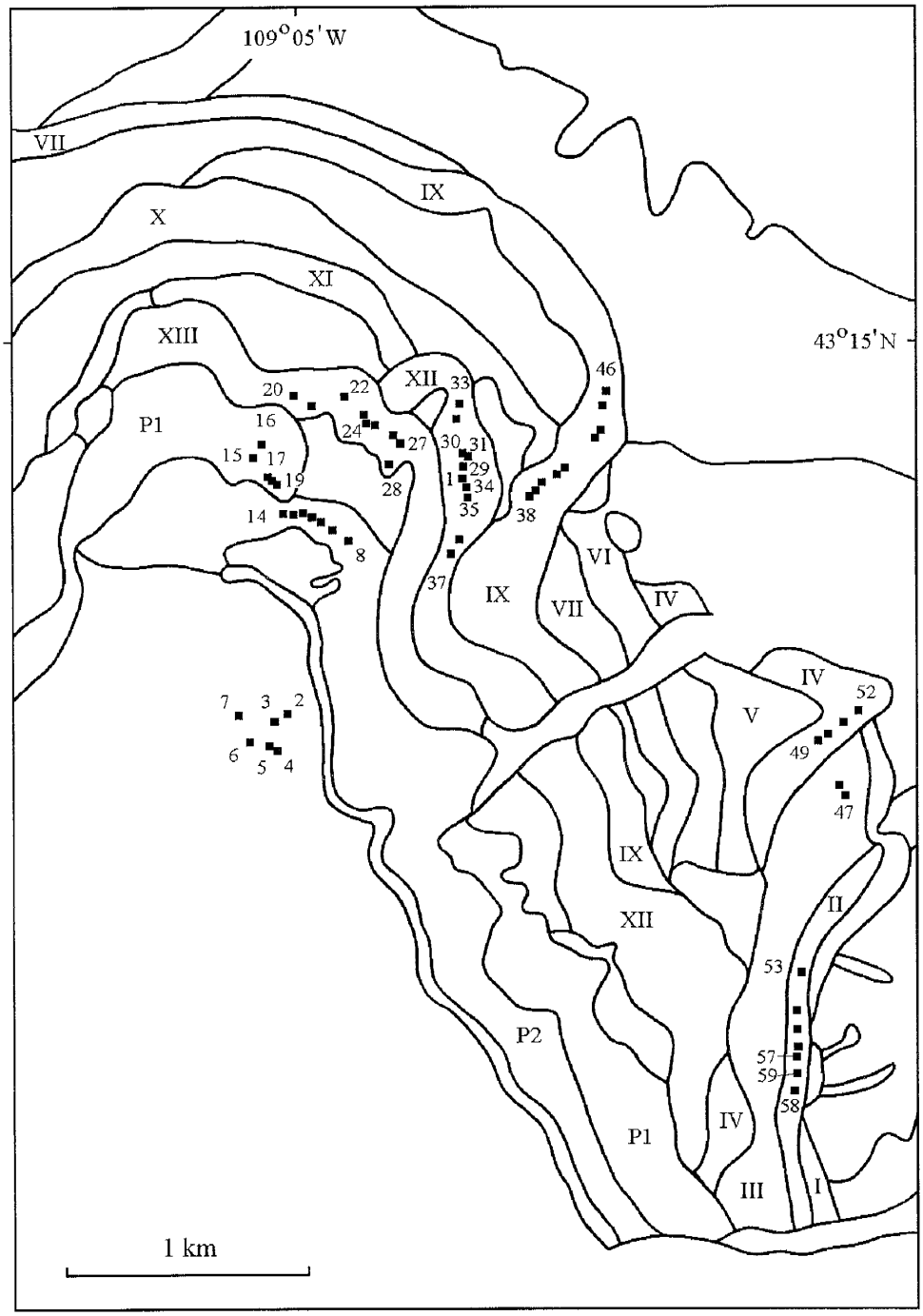

Fig. 10.1. Glacial deposits at Bull Lake, Wind River Range, Wyoming.

Table 10.1. Locations, geochemistry and ^{36}Cl ages of samples from the Bull Lake area, Wind River Range, Wyoming.

Stratigraphic unit[a]	Sample ID[b]	Cl (ppm)	K_2O (%)	CaO (%)	$\Sigma\sigma N$ (cm^2 kg^{-1})	Elev. (km)	ELD	$^{36}Cl/Cl$ (10^{-15})	Age (ky)	
									Boulder	Surface
	BL92-2-PN3	53	0.35	5.20	3.09	1.90	4.43	474 ± 44	14.5 ± 1.5	
Pinedale 3	BL92-5-PN3	154	0.93	6.01	5.01	1.90	4.45	211 ± 20	10.7 ± 1.2	16.0
(P3)	BL92-6-PN3	78	4.27	1.80	3.31	1.91	4.48	586 ± 37	13.9 ± 0.9	
	BL92-7-PN3	93	3.87	1.08	3.26	1.90	4.45	553 ± 19	16.0 ± 0.6	
	BL92-8-PN2	862	0.25	11.20	7.24	1.89	4.42	70 ± 7	4.9 ± 0.9	
Pinedale 2	BL92-10-PN2	203	1.73	4.97	6.12	1.90	4.44	256 ± 23	15.9 ± 1.6	
(P2)	BL92-11-PN2	183	1.50	4.82	4.73	1.90	4.44	428 ± 113	24.3 ± 7.1	18.1
	BL92-12-PN2	48	0.74	3.88	2.76	1.90	4.44	640 ± 40	18.1 ± 1.2	
	BL92-14-PN2	71	0.69	4.73	2.80	1.90	4.44	468 ± 32	15.0 ± 1.1	
Pinedale 1	BL92-15-PN1	124	0.31	5.61	4.61	1.87	4.35	275 ± 22	14.7 ± 1.3	
(P1)	BL92-16-PN1	85	1.46	1.94	2.87	1.87	4.35	311 ± 26	11.0 ± 1.0	15
	BL92-17-PN1	60	0.56	4.14	2.83	1.87	4.35	438 ± 40	14.3 ± 1.4	
	BL92-22-BLVI	97	2.01	2.67	3.20	1.87	4.35	2159 ± 218	89.1 ± 10.2	
Bull Lake XIII	BL92-24-BLVI	65	0.89	3.11	2.89	1.88	4.39	1778 ± 110	67.4 ± 4.6	88
	BL92-25-BLVI	78	0.15	10.30	4.82	1.88	4.39	2235 ± 130	86.2 ± 5.7	
	BL92-26-BLVI	55	1.42	3.72	3.06	1.88	4.37	2776 ± 86	87.3 ± 3.0	

	BL92-29-BLV	170	0.82	3.55	3.38	1.86	4.33	1384 ± 58	81.8 ± 3.9	
	BL92-30-BLV	102	0.23	11.50	7.04	1.86	4.33	1822 ± 281	88.7 ± 15.7	
	BL92-31-BLV	98	3.39	1.55	3.29	1.86	4.33	1488 ± 70	51.6 ± 2.6	
Bull Lake XII	BL92-32-BLV	73	1.26	2.97	2.85	1.86	4.33	1477 ± 62	54.3 ± 2.5	88
	BL92-34-BLV	537	1.85	1.79	4.11	1.88	4.38	1010 ± 56	82.6 ± 5.2	
	BL92-35-BLV	260	1.52	2.36	4.28	1.88	4.38	1392 ± 47	107.0 ± 4.2	
	BL92-36-BLV	101	0.99	5.68	4.26	1.89	4.44	1736 ± 102	82.6 ± 5.5	
	BL92-37-BLV	143	0.99	3.55	4.04	1.90	4.46	1260 ± 86	74.9 ± 5.8	
	BL92-39-BLIV	89	3.51	1.86	3.26	1.86	4.32	2046 ± 224	66.4 ± 8.0	
	BL92-40-BLIV	96	1.92	5.91	4.13	1.86	4.32	1644 ± 84	63.7 ± 3.6	
Bull Lake IX	BL92-42-BLIV	84	0.96	4.15	3.05	1.85	4.30	2184 ± 117	92.2 ± 5.6	100
	BL92-44-BLIV	220	1.11	4.24	4.45	1.83	4.22	1403 ± 75	107.2 ± 6.7	
	BL92-46-BLIV	139	1.46	2.40	3.44	1.83	4.21	1723 ± 122	98.5 ± 8.0	
Bull Lake IV	BL92-49-BLIVB	209	5.66	1.39	5.43	1.83	4.23	1976 ± 141	111.3 ± 9.3	111
Bull Lake III	BL92-47-BLIII	831	0.28	11.70	7.18	1.83	4.23	1091 ± 71	155.1 ± 12.7	155
	BL92-53-BLII	101	3.00	2.08	3.93	1.90	4.44	1739 ± 88	68.2 ± 3.8	
Bull Lake II	BL92-54-BLII	223	0.28	11.30	5.86	1.90	4.44	1977 ± 73	149.9 ± 6.8	150
	BL92-56-BLII	133	0.33	12.30	5.19	1.90	4.44	1385 ± 179	64.6 ± 9.3	
	BL92-57-BLII	128	3.33	1.29	4.26	1.90	4.44	1358 ± 240	61.5 ± 12.1	

	BL92-60-SR	84	2.92	1.93	3.37	2.08	5.05	5462 ± 163	187.4 ± 7.1	
Sacagawea	BL92-62-SR	108	0.52	12.30	5.57	2.08	5.06	3670 ± 221	145.3 ± 10.6	
Ridge	BL92-63-SR	94	0.12	13.00	4.54	2.09	5.09	3479 ± 141	115.6 ± 5.4	190
(SR)	BL92-64-SR	82	4.60	0.52	3.55	2.09	5.09	6609 ± 264	189.1 ± 9.6	
	BL92-67-SR	71	3.32	1.34	3.26	2.14	5.28	4277 ± 133	110.9 ± 4.0	
	BL92-68-SR	65	4.76	0.64	3.56	2.14	5.28	3746 ± 292	75.4 ± 6.5	
Bull Lake	BL92-70-BLT	180	4.29	1.44	4.42	2.03	4.89	2133 ± 95	98.9 ± 5.0	
Terrace	BL92-71-BLT	191	4.18	1.37	5.01	2.03	4.89	1908 ± 45	98.1 ± 2.6	
(BLT)	BL92-72-BLT	197	3.66	1.67	4.61	2.03	4.89	1832 ± 58	95.9 ± 3.5	100
	BL92-73-BLT	216	4.59	1.36	4.45	2.03	4.89	4265 ± 134	250.2 ± 10.8	
Pinedale	BL92-75-PNT	91	3.51	1.81	3.44	2.08	5.08	496 ± 24	12.8 ± 0.7	
Terrace	BL92-76-PNT	126	3.77	1.39	3.94	2.08	5.08	504 ± 25	16.4 ± 0.9	18
(PNT)	BL92-78-PNT	92	5.05	0.93	3.64	2.08	5.08	874 ± 127	20.3 ± 3.1	
	BL92-79-PNT	96	4.05	1.16	3.26	2.08	5.08	444 ± 44	10.9 ± 1.2	

[a] Stratigraphic units from the geological map by Chadwick et al. (1993).

[b] Sample designations as given in the field in 1992, based on an earlier version of the geological map by Chadwick et al. (1993).

Pinedale moraines

Three nested moraines (samples BL92-2, 5, 6 and 7 PN3, BL92-8, 10, 11, 12 and 14 PN2, and BL92-15 through 17 PN1) are stratigraphically the youngest deposits in this glacial complex. Three oldest boulders from the youngest (PN3) moraine gave a mean ^{36}Cl exposure age of 14.8 $\pm$ 1.1 ky and the maximum age of 16 ky; one younger outlier dated to 11 ky.

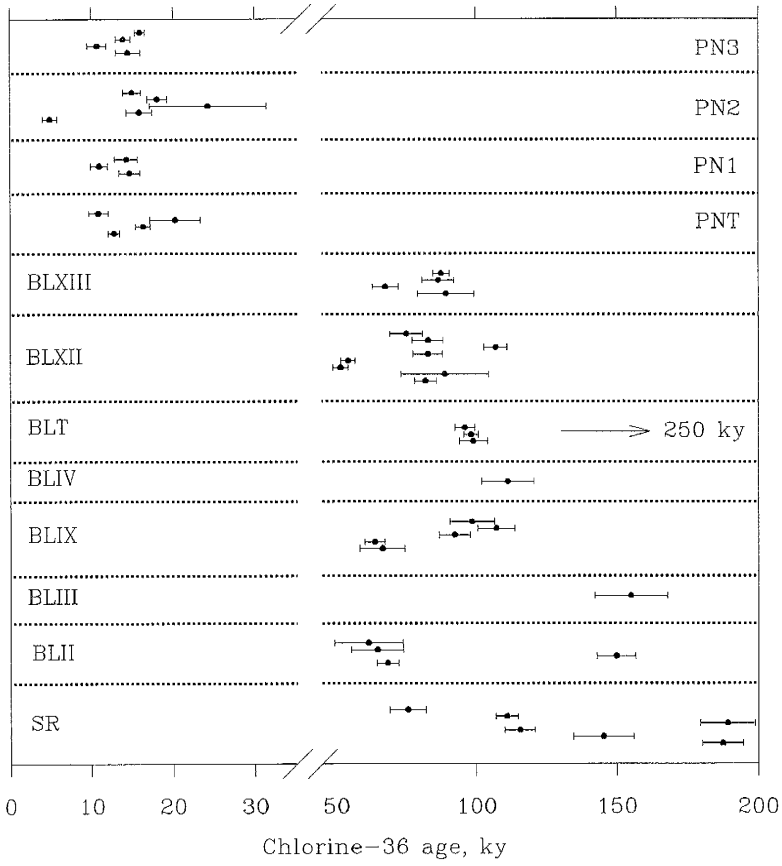

Fig. 10.2. Age distributions for moraines in the Bull Lake area.

The middle moraine has two outliers: one is considerably younger than the rest of the samples whereas the older outlier has large uncertainty associated with the measurement of ^{36}Cl. The age of the older moraine is therefore best approximated by the three samples grouped between 15 and 18 ky that gave a mean age of 16.3 $\pm$ 1.6 ky. This mean age is statistically indistinguishable from that of the younger moraine and it is likely that both moraines were deposited during the same glacial advance.

The outermost Pinedale moraine (PN1) is in the stratigraphic position below moraine PN2. Its mean ^{36}Cl exposure age, 14.5 $\pm$ 0.5 ky, is similar to the ages of the two stratigraphically younger moraines. The age distribution on all three Pinedale moraines suggests that they were formed during the same glaciation. The three distinct morainal loops resulted from multiple readvances of the late Wisconsin glacier just before the final deglaciation.

The reported ages exhibit certain inconsistencies that do not allow a definitive chronology to be established. The oldest boulder age on the PN2 moraine, 24.1 ky, may closely estimate the construction age of this moraine. The age of PN1 would then have to be older than 24 ky, but this is not supported by the ^{36}Cl ages. However, we measured only three samples from PN1 and it is possible that they underestimate the moraine age. In either case, all three moraines are no older than the late Wisconsin maximum and they possibly record the subsequent deglaciation.

Bull Lake moraines

Five distinct Bull Lake terminal moraines (from the oldest BLII through the youngest BLXIII) were studied. They are all nested, younger inside the older, and their stratigraphy can be easily inferred in the field. The youngest moraine (BLXIII) yielded three consistent ^{36}Cl ages with the mean of 87 $\pm$ 2 ky and the oldest age of 89 ky. This moraine is in direct contact with the late Wisconsin Pinedale moraines that are nested inside it and there are no glacial deposits intermediate in age between 18 and 88 ky.

The ages for the stratigraphically older moraine (BLXII) are more scattered with two youngest boulder ages close to 55 ky and the oldest age of 107 ky. The remaining five samples form a cluster around 80 ky with a mean age of 82 $\pm$ 5 ky and the oldest age of 89 ky. This surface exposure age is my best estimate of the moraine age, although it is possible that the true age is as old as the oldest sample dated, i.e., 107 ky. Both dates are consistent with the ages of stratigraphically younger and older deposits and future samples will be necessary to assess which of the two ages, 89 or 107 ky, better estimates the moraine age.

Two older moraines, designated as BLIX and BLIV, were sampled and the ^{36}Cl ages group at $\sim$65 and $\sim$100 ky, with two oldest samples at 110 ky. These moraines are stratigraphically below the moraines BLXII described above and must therefore be older, possibly as old as the two oldest boulders, i.e., 110 ky.

One sample from moraine BLIII gave an age 155 ky. The underlying deposits (unit BLII) gave a similar oldest age of 150 ky, although three out of the four measured samples are considerably younger. The young age of most samples is due to erosion of the moraine surface. The age of 150 ky is consistent with the younger ages obtained for the overlying deposits of unit BLIX. The BLII moraines are the oldest sampled glacial deposits in the Bull Lake area.

Sacagawea Ridge moraine

In the area near Dinwoody Lake, north of Bull Lake, there exists an even older moraine deposited during the Sacagawea Ridge (SR) glaciation (Richmond, 1975, 1976). This moraine is very high and broad and has subdued morphology, which is a manifestation of an old age. Two oldest samples gave an age of $\sim$190 ky, while the remaining four samples were younger. This distribution is characteristic of an eroded surface, one on which the oldest sample is closest to the true age. For such an old age, however, even the oldest exposure age must be considered only a minimum age.

Outwash terraces

Two outwash terraces near highway 26, about 10 and 18 km SE of Dubois were studied. The older terrace (BLT, Bull Lake terrace) is almost perfectly flat and contains many large boulders. Three samples gave almost identical ages close to 100 ky, while

the fourth sample yielded an age of 250 ky. This extremely old age can be explained by prior exposure of the boulder surface to cosmic radiation, e.g., in the original outcrop or in a moraine that supplied the material for this outwash deposit. The most likely age of this surface is then 100 ky; this age correlates well with the younger Bull Lake moraines in the Bull Lake area.

Four samples from the younger terrace (PNT, Pinedale terrace) yielded ^{36}Cl ages between 11 and 20 ky, with the oldest age having large analytical uncertainty. It is thus likely that the true age is less than 20 ky. In either case, these deposits are correlative with the Pinedale moraines in the Bull Lake area. An additional sample to be analyzed in the future will help further constrain the age of this deposit.

Discussion and summary

The preliminary cosmogenic ^{36}Cl chronology developed for glacial deposits in the eastern Wind River Range shows that the major glaciations occurred at ≥ 190, ~ 150, 100-110, 90 and 14-18 ky. Deposits of the Sacagawea Ridge glaciation (≥ 190 ky) are the oldest dated by the ^{36}Cl method and probably represent an early stage 6 advance. The Bull Lake moraines were deposited during at least two different glacial episodes. The 150-ky-old Bull Lake moraines are correlative with marine stage 6 and with glacial deposits at Bishop Creek and Chiatovich Creek (Table 10.2). They are among the most extensive glacial deposits in this area. Nestled within that complex are the younger Bull

Table 10.2. Correlation of cosmogenic ^{36}Cl glacial chronologies in the western Great Basin area and the eastern Wind River Range. Shading indicates no deposits of this age and dashes indicate that no samples were collected from possible deposits of this age.

^{18}O stage	Great Basin	Wind River
1	<10	---
2	11-20	14-18
3	45	
4	65-75	
5	90-120	90-110
6	150	150
?	>150	≥ 190

Lake moraines with surface exposure ages not exceeding 110 ky. A similar age was obtained for the Bull Lake outwash terrace near Dubois. Both glacial and glaciofluvial deposits of this age can be correlated with the marine stage 5 and with extensive moraine complexes in all studied drainages of the eastern Sierra Nevada, particularly the Bishop Creek area. Richmond (1972) discussed a similar chronologic duality of Bull Lake deposits from the Yellowstone area. He assigned an age 105-125 ky to the early Bull Lake and 80-105 ky to the younger deposits. Two distinct Bull Lake advances were also reported from the Wind River Range by Shroba and Hall (1992), who considered the younger deposits to be intermediate in age between the 140-ky Bull Lake and the Pinedale glaciations.

The next younger glacial deposits (Pinedale moraines) have surface ages 14-18 ky. They are correlative with the stage 2 of the marine record and with glacial deposits in both eastern Sierra Nevada and eastern White Mountains. Three distinct moraines were deposited within a short period of time (<4 ky) and indicate generally unstable climate in the interval between 18 and 14 ky ago.

An interesting feature of this glacial record is the apparent absence of deposits between 20 and 80 ky, which would have been correlated with the stage 4 of the marine record. Deposits of this age are present in all Sierran drainages (this work) and on Mauna Kea (Dorn et al., 1991) where they record an important climatic event. Their absence here may suggest that despite global "glacial" conditions, local or regional environmental components were unfavorable for glacier development, and that those conditions are more critical for small mountain glaciers than is the global climate. Another important observation is that the earliest Wisconsin deposits extend beyond those of the late Wisconsin, which demonstrates that the early advances in the last glacial cycle were more extensive than the so called late Wisconsin maximum.

References

Blackwelder, E., 1915, Post-Cretaceous history of the mountains of central Western Wyoming, Journal of Geology 23, 307-340.

Chadwick, O.A., R.D. Hall and J.E. Conel, 1993, Revised mapping and chronology for

glacial and glaciofluvial deposits in Wind River Basin, Wyoming, Third International Geomorphological Conference, Hamilton, Ontario.

Dorn, R.I., F.M. Phillips, M.G. Zreda, E.W. Wolfe, A.J.T. Jull, P.W. Kubik and P. Sharma, 1991, Glacial Chronology of Mauna Kea, Hawaii, as Constrained by Surface-Exposure Dating, National Geographic Research and Exploration 7, 456-471.

Porter, S. C., K. L. Pierce and T. D. Hamilton, 1983, Late Wisconsin mountain glaciation in the western United States, In: Late-Quaternary Environments of the United States, H. E. Wright, Jr., editor, Vol. 1: The Late Pleistocene, S. C. Porter, editor, pp. 71-114, University of Minnesota Press, Minneapolis.

Richmond, G. M., 1972, Appraisal of the future climate of the Holocene in the Rocky Mountains, Quaternary Research 2, 315-322.

Richmond, G. M., 1975, A partial Quaternary chronology from Yellowstone National Park, In: V. Sibrava (ed.), Quaternary Glaciations in the Northern Hemisphere, pp. 144-147.

Richmond, G. M., 1976, Pleistocene stratigraphy and chronology in the mountains of Western Wyoming, In: Quaternary Stratigraphy of North America, W. C. Mahaney, ed., pp. 353-380, Dowden, Hutchinson and Ross, Stroudsburg, Pennsylvania.

Richmond, G. M., 1986, Stratigraphy and correlation of glacial deposits of the Rocky Mountains, the Colorado Plateau and the ranges of the Great Basin, In: Quaternary Glaciations in the Northern Hemisphere, V. Sibrava et al., eds., pp.

99-128, Pergamon Press.

Shroba, R. R. and R. D. Hall, 1992, Soil development in the type Pinedale, Bull Lake, and Sacagawea Ridge glacial deposits, Wind River Range, Wyoming, 12th Meeting of American Quaternary Association, Program and Abstracts, 77.

11. Cosmogenic ^{36}Cl ages of late Pleistocene shorelines in Panamint and Death Valleys, California

Abstract

Cosmogenic ^{36}Cl surface exposure ages of paleolake deposits in Panamint and Death Valleys indicate high paleolake stands at 50-60, 85-95, $< \sim 120$ and $< \sim 200$ ky. They are correlative with the ^{36}Cl ages of glacial deposits in the eastern Sierra Nevada. The most prominent shorelines in both valleys date to the early Wisconsin. This early pluvial maximum is similar in its extent to the early Wisconsin glaciations in the Sierra Nevada. Both indicate that the regional climate was more glacial at the beginning of the cycle than at its end.

Shoreline deposits are difficult to date by the cosmogenic ^{36}Cl method because of ^{36}Cl inherited from previous exposure episodes. The best material for cosmogenic surface exposure dating are tufa deposits that are precipitated directly from the lake water. In absence of tufa deposits, clastic material can be used, but the inherited ^{36}Cl must be independently determined, e.g., from subsurface samples.

The vertical displacement of the shorelines and their ^{36}Cl ages, permitted calculation of an average uplift rate of 0.7 m ky^{-1}, in agreement with other estimates in this region. This value is valid for the last ~ 200 ky.

Introduction

The Great Basin consists of about 150 subbasins, many of which have been internally drained and a few had occasionally overflowed during the wettest (pluvial) periods in the Pleistocene. Pluvial lakes (paleolakes) and their relation to alpine glaciations have been a focus of geological interest for over a century. Russell (1895) identified two deep-lake units, each of which he ascribed to a wetter and colder climate, separated by a shallow-lake gravel representing drier and warmer conditions. Russell (1885) and Gilbert (1890) correlated high lake levels with terminations of alpine glaciations. The possibility of correlation between pluvial and glacial records was further explored by Blackwelder (1931) who correlated the first pluvial interval with the Tahoe glaciation in the Sierra Nevada and the second deep-water interval with the Tioga glaciation. The studies conducted in the 1960's indicated that single pluvials of Russell (1885) consisted of two or more cycles separated by short intervals of low lake levels. Further dating (mainly by radiocarbon) confirmed this duality of pluvials (Smith and Street-Perrot, 1983) and indicated much more complex history of lake levels. It also drew the attention to the possibility of correlation of the lake pluvial records with the global marine ^{18}O and continental glacial record. Such comparisons indicated that pluvials were asynchronous with the "global" climate, but the relationships between mountain glaciations and pluvials could not be unequivocally established (Smith, 1984; Morrison, 1991).

In this work, I present the results of numerical dating of paleolake shorelines in Panamint and Death Valleys, California. Shorelines are formed during high stands of the lake and their ages should reflect the time when the lakes started regressions from these high stands. The high lake levels are associated with substantial increases in precipitation, which in turn are believed to have caused glaciations (Seltzer, 1990). The shoreline chronology developed here is based on cosmogenic ^{36}Cl surface exposure ages of boulders and tufa deposits from the most prominent shorelines. I compare it with the ^{36}Cl chronologies of mountain glaciations in the Sierra Nevada and the White Mountains to assess synchroneity of pluvial and glacial periods in the late Pleistocene. Cosmogenic ^{36}Cl ages of some uplifted shorelines, with the vertical offset between them, yield the uplift rate along the fault zone separating the shorelines.

Methods

My colleagues and I collected several rock samples from five shorelines in Panamint Valley, and two shorelines and an ancient beach bar in Death Valley. The samples were prepared and analyzed as before and all cosmogenic ^{36}Cl ages, with one exception, calculated according to the standard production equation. The age of the beach bar sample was corrected for ^{36}Cl accumulated before the shoreline construction.

Samples collected for cosmogenic ^{36}Cl age determination of paleoshorelines are of two different genetic types. The first type includes boulders and cobbles that

originated in the nearby mountains, were transported by streams and deposited at the lake shore. These samples may have complex exposure histories, e.g., inherited ^{36}Cl from exposures in outcrops or during fluvial transport (Nishiizumi et al., 1993). The second group includes tufas that precipitated *in situ*, directly from the lake water. This category should have a simpler exposure history than the first group had, but may have more complex geochemistry. Ideally, both types of samples should be collected from each surface, but while boulders and cobbles are present everywhere, tufas are scarce and were found at only two shorelines.

Most samples reported herein are from Pleasant Canyon where several distinct lake deposits are present (Smith, 1976, 1978). The samples are from five most prominent shorelines preserved at elevations from 735 m (oldest) down to 579 m (youngest). Additional samples are from two shorelines at Mormon Point and from the Beatty beach bar, ~3 km north of highway 190, Death Valley. These deposits formed when Panamint lake overflowed to Death Valley and should thus record the highest lake levels in this lake system. A study area map is shown in Figure 11.1.

Model for dating shorelines in presence of inherited ^{36}Cl

The standard ^{36}Cl buildup differential equation can be used for surfaces made of previously exposed material, but a different boundary condition, one that accounts for both radiogenic and inherited cosmogenic ^{36}Cl, must be used. This prior exposure

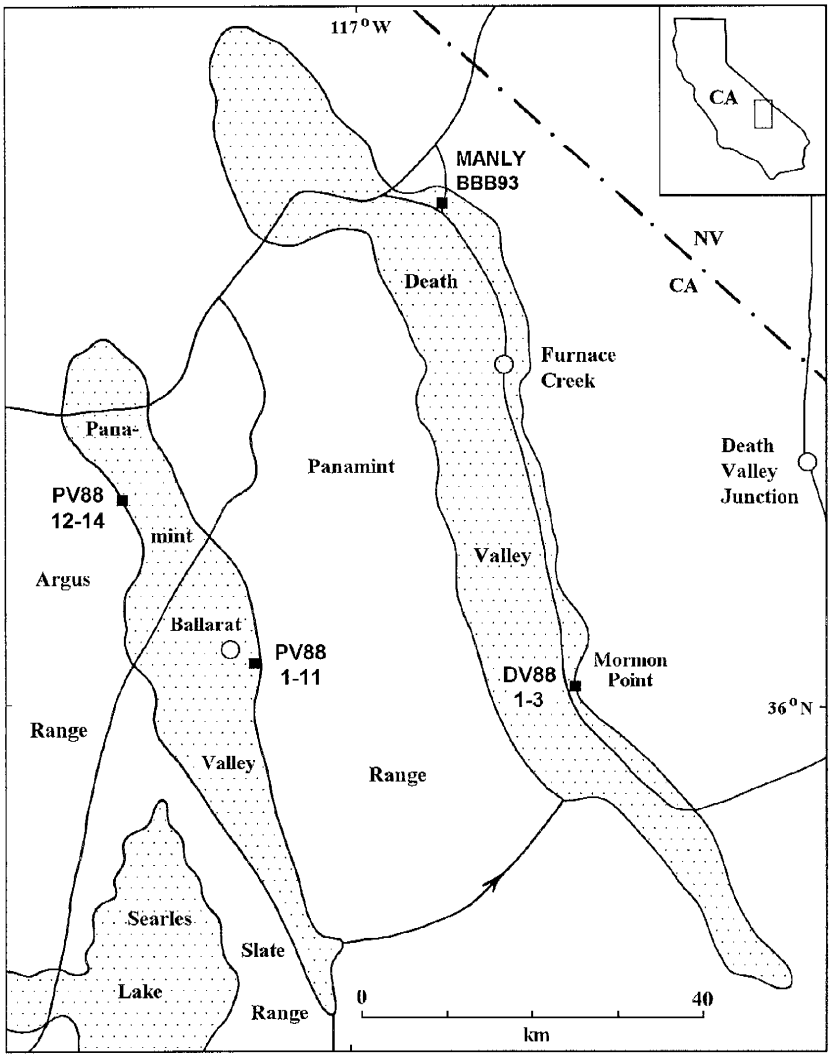

Fig. 11.1. Study areas in Panamint and Death Valleys, California.

might have been a combination of exposures in the outcrops or during the fluvial transport and lasted until time t=0 when the samples were deposited on the lake shore. The model assumes that since time t=0, the samples have been in a geomorphically stable position; the surface samples have remained at the surface until the present, while the samples that were buried at t=0 have remained in the subsurface. The measured ^{36}Cl

reflects both exposure episodes and one has to separate this composite signal into two parts.

In the model, the standard form of the ^{36}Cl buildup equation is used

$$\frac{dN_{36}}{dt} + \lambda_{36}N_{36} = P \tag{1}$$

where N_{36} is the number of ^{36}Cl atoms, t is the time, λ_{36} is the decay constant for ^{36}Cl, and P is the total production rate of cosmogenic ^{36}Cl from all target elements. A general solution to this equation is

$$N_{36} = \frac{P}{\lambda_{36}} + Ce^{-\lambda_{36}t} \tag{2}$$

where C is the integration constant. The initial condition appropriate for this situation in our model is

$$IC: \quad t=0, \quad N_{36} = N_b + N_i \tag{3}$$

where N_b is the radiogenic or background ^{36}Cl (a constant) and N_i is the initial or inherited cosmogenic ^{36}Cl present in the material at the time of its deposition. From the initial condition, the integration constant is

$$C = N_b + N_i - \frac{P}{\lambda_{36}} \tag{4}$$

and the particular solution becomes

$$N_{36} - N_b = N_i\, e^{-\lambda_{36}t} + \frac{P}{\lambda_{36}}\left(1 - e^{-\lambda_{36}t}\right) \quad (5)$$

The first term represents decay of the initial condition and the second term is new buildup at the surface. The last equation is divided by the total Cl concentration N_{Cl} to give the solution in terms of ratios R

$$R_{36} - R_b = R_i e^{-\lambda_{36}t} + \frac{P}{\lambda_{36}N_{Cl}}\left(1 - e^{-\lambda_{36}t}\right) \quad (6)$$

This equation in two unknowns, R_i and t, requires two samples for solution: one from the surface, another shielded from cosmic rays.

Shoreline ages

The analytical results, exposure ages of single samples and inferred landform ages are presented in Table 11.1. These results are discussed below separately for the two valleys and in chronological order from the youngest to the oldest.

Death Valley

Two low shorelines (5-m and Blackwelder shoreline) at Mormon Point and a fossil beach bar (Beatty beach bar) near the road to Beatty were sampled. They record overflow events from Panamint Valley through Wingate Pass and indicate wet climate.

Table 11.1. Concentrations of Cl, K_2O and CaO, macroscopic cross sections, $^{36}Cl/Cl$ ratios and calculated surface exposure ages for samples from Panamint and Death Valleys, California. Background ratio $R_0=6\times10^{-15}$ was used for all samples.

Unit	Sample	Cl ppm	K_2O %	CaO %	$\Sigma\sigma N$ cm^2kg^{-1}	Elev. km	ELD	$^{36}Cl/Cl$ 10^{-15}	Age, ky	
									Sample	Surface
1st prominent	PV88-1	222	3.29	1.35	5.30	0.617	1.493	953 ± 77	229 ± 25	?
shoreline	PV88-2	245	0.06	7.78	7.46	0.617	1.493	1151 ± 76	577 ± 88	
2nd prominent	PV88-3	72	4.33	1.38	5.80	0.648	1.530	1111 ± 100	100 ± 10	86 ± 20
shoreline	PV88-4A	268	0.94	1.29	4.75	0.648	1.530	279 ± 26	72 ± 8	
3rd prominent	PV88-5	58	0.40	54.48	3.85	0.664	1.550	4183 ± 68	94 ± 2	
(Gale)	PV88-6	83	0.49	57.08	4.06	0.664	1.550	3180 ± 173	94 ± 6	94 ± 5
shoreline	PV88-7	180	2.39	1.27	5.53	0.664	1.550	722 ± 43	165 ± 12	
	PV88-8	137	0.19	6.01	6.10	0.664	1.550	682 ± 31	164 ± 9	
2nd above Gale	PV88-10	87	4.17	4.22	6.10	0.735	1.640	1729 ± 126	163 ± 15	204 ± 58
	PV88-11	79	2.98	5.07	6.42	0.735	1.640	2204 ± 111	245 ± 17	
1900-ft shoreline	PV88-13	45	0.12	55.56	3.82	0.579	1.448	3244 ± 400	59 ± 8	59 ± 8
Beatty	MANLY	61	1.23	1.28	4.80		0.945	532 ± 34	138 ± 11	50
beach bar	BBB93-1	80	0.86	0.04	3.69		0.945	264 ± 85	77 ± 29	
15-ft	DV88-1	182	1.12	13.19	6.33	5	0.888	361 ± 26	101 ± 8	111 ± 14
shoreline	DV88-2	269	4.92	1.77	5.73	5	0.888	357 ± 31	121 ± 13	
Blackwelder sh.	DV88-3	341	1.93	7.06	6.60	87	0.888	264 ± 27	121 ± 15	121 ± 15

5-m shoreline

This shoreline is among the lowest (and the youngest) in the valley and its age should indicate the recession from a high lake level during the last pluvial stage. Two boulder samples (DV88-1 and 2) gave consistent ^{36}Cl surface exposure ages with a mean age 111 $\pm$ 14 ky. The ^{36}Cl ages are much older than a varnish ^{14}C age of $\sim$13 $\pm$ 0.2 ky reported by Dorn et al. (1990) from the same location. Inherited ^{36}Cl in sampled boulders can account for this discrepancy. Redistribution of boulders resets the varnish clock, which is sensitive to millimeter-scale erosion, but not the cosmogenic nuclide clock, which requires erosion on the order of meters to be completely reset.

Beatty beach bar

A fossil beach bar is preserved near the road to Beatty, Nevada, at an elevation $\sim$73 m. One surface sample (MANLY) and one from $\sim$2.5 m depth (BBB93-1) were collected and the model described above used to obtain the exposure age of this deposit. Both samples consisted of several tens of small cobbles so that exposure histories of individual cobbles would be averaged. The apparent ^{36}Cl ages are 138 $\pm$ 11 ky for the surface sample and 77 $\pm$ 29 ky for the buried sample. To use the model, the measured values of $^{36}Cl/Cl$ are normalized to the same chemical composition using the formula in Phillips et al. (1986). While measured, raw ratios reflect variabilities in both exposure time and sample chemistry, normalized ratios show how much $^{36}Cl/Cl$ a sample would

have if it had a given chemistry, i.e., they are functions of the exposure time alone. The normalized ratios of the two samples are 258×10^{-15} and 431×10^{-15} for the subsurface and surface sample, respectively. In these ratios, the background ratio (R_b) of 6×10^{-15}, based on U and Th concentration of 0.8 and 2.9 ppm, respectively, was already subtracted. Using equation 6 and the above ratios, we obtain the initial (inherited) ratio R_i = 289×10^{-15} and the true surface exposure time t $\approx$ 50 ky. This result shows that although the apparent age appears very old due to inherited ^{36}Cl, the surface age of the beach bar is only $\sim$50 ky. This deposit is thus correlative with the 579-m shoreline in Panamint Valley (sample PV88-13) and with a glacial advance in the eastern Sierra Nevada (Younger Tahoe at Bloody Canyon).

Blackwelder shoreline

Material on this 87-m shoreline is very weathered and eroded by wind. A sample collected from the top of a 0.6-m tall boulder yielded an age 121 $\pm$ 15 ky. This age is in a reasonable agreement with cation-ratio ages of 120 to 130 ky for abandonment of this shoreline (Dorn et al., 1988, 1990). It must be noted here that this agreement may be coincidental because the measured ^{36}Cl may include some inherited ^{36}Cl (like in the Beatty beach bar case). At present, this component cannot be quantified because of lack of subsurface samples from this deposit. On the other hand, the good agreement between the two ^{36}Cl dates and between the ^{36}Cl and independent age estimates suggests that this inherited component may be negligible at this location and the age 121 ky is close to the

formation age of this shoreline.

Panamint Valley

Samples from five major shoreline deposits were collected at Pleasant Canyon on the eastern side of the valley. The stratigraphic position of the shorelines clearly follows from their elevations; the highest are the oldest and vice versa. The most prominent is the Gale shoreline (named after Gale who investigated the Mono-Death Valley paleolake system in the early 1900's) preserved at an elevation ~664 m above sea level. Two older shorelines above the Gale, at elevations ~690 and 735 m, and three younger below it, at ~617, 648, and 579 m, were also studied. Smith (1976, 1978) designated the oldest five of these shorelines by capital letters E (oldest), F, G (Gale), H, and I (youngest).

579-m shoreline

This shoreline is probably related to events of overflow to Death Valley through Wingate Pass, when the lake level was temporarily stabilized at the elevation of the pass. One tufa sample (PV88-13) collected from this deposit gave an age 59 ± 8 ky. The construction of this shoreline is correlative with glacial advances in the eastern Sierra Nevada recorded at Bloody Canyon, Bishop Creek and Little McGee Creek (Chapter 9) and with the marine stage 4.

1st prominent shoreline (I)

This deposit is preserved in small benches at an elevation ~617 m. It contains neither tufas nor rounded gravels and thus its origin is unclear. Two boulders (PV88-1 and 2) yielded very old and inconsistent ages 229 and 577 ky. These ages are clearly too old because the next older shoreline has surface exposure ages not exceeding ~100 ky. One likely scenario is that this surface is not of lacustrine origin, but represents a mud flow event that moved boulders from outcrops above or from older shorelines. This interpretation is supported by absence of tufa deposits and rounded gravel on this surface (Smith, 1976, 1978).

2nd prominent shoreline (H)

Two boulders (samples PV88-3 and 4A) collected from an elevation ~648 m gave surface exposure ages 100 ± 10 and 72 ± 7 with a mean age 86 ± 20 ky. Both boulder ages and the mean agree with a limiting minimum ^{14}C age of 34.3 ± 1 ky obtained for a snail shell (Smith, 1976, 1978). They are also stratigraphically correct as this deposit must be older than the 579-m shoreline below (dated to 59 ky) and younger than the Gale shoreline above. The mean age corresponds well to surface ages of glacial deposits at Bishop Creek and to the late stage 5 or early stage 4 of the marine record. It is, however, difficult to ascertain which of the two sample ages is correct. In a glacial setting, the older age would more closely approximate the true age. In the

pluvial setting, however it is not so obvious because shoreline materials may contain inherited ^{36}Cl and the younger age may be more appropriate.

3rd prominent shoreline (Gale)

Two boulder samples (PV88-7 and 8) and two tufa samples (PV88-5 and 6) were collected from this shoreline. The boulder samples yielded a mean age 164 ± 8 ky, while the tufa samples indicate a much younger age of 94 ± 5 ky. The same factors that controlled the apparent ages of the Beatty beach bar are probably responsible for the older age of the boulders. The correct exposure age of 94 ky is obtained from the tufa samples, which do not have any inherited ^{36}Cl problem. This age agrees with a minimum radiocarbon age of 33.7 ± 0.5 ky obtained for a snail shell sample found in the sand underlying the gravel (Smith, 1976, 1978).

2nd shoreline above Gale (E)

Two samples (PV88-10 and 11) collected from the highest shoreline studied herein yielded exposure ages 163 and 245 ky and a mean age 204 ± 58 ky. This age is stratigraphically correct because the next younger shoreline (the Gale) dates to 94 ky. It may, however, overestimate the true age because of likely problem with inherited ^{36}Cl and therefore I consider it a maximum age.

Uplift rate

All shorelines described above were formed when the Panamint Lake overflowed to Death Valley through Wingate Pass, elevation ~600 m. Today, most shorelines are at higher elevations because of continuing uplift. The vertical offsets of shorelines with respect to the elevation of Wingate Pass are known and so are their ages. Both are plotted in Figure 11.2 for the following three shorelines: 2nd prominent, Gale and 2nd above Gale. In the figure, for each offset value, I used three ages, the mean, the minimum and the maximum, and fitted three lines through the origin. The average uplift

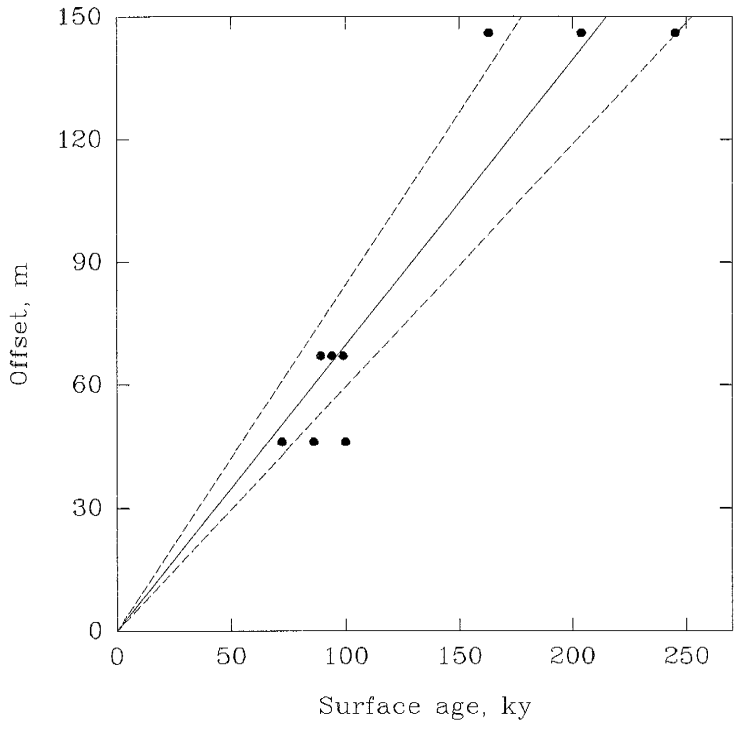

Fig. 11.2. Vertical offset vs. shoreline age for three shorelines at Pleasant Canyon. Three dots for each shoreline are for the mean, minimum and maximum ^{36}Cl age. The slopes of the lines are equal to the average uplift rate.

rate is ~0.7 m ky^{-1} and the bracketing values are 0.6 and 0.85 m ky^{-1} for the minimum and maximum age estimate, respectively. Uplift rates about 0.5 m ky^{-1} were reported

from other parts of the region (e.g., Bachman, 1978). For comparison, Smith (1976) reported higher uplift rates of 1.2 to 1.5 m ky^{-1}, but his estimates are largely based on nearly infinite ^{14}C ages, which are likely underestimated, and thus the rates are probably overestimated. The value 0.7 m ky^{-1} is my best estimate of the average vertical displacement during the last $\sim$200 ky.

Summary and conclusions

Cosmogenic ^{36}Cl surface exposure dating of paleolake shorelines and a beach bar deposit allowed development of a late Pleistocene local pluvial chronology in Panamint and Death Valleys. The obtained surface exposure ages indicate high paleolake stands at 50-60, 85-95, $< \sim 120$ and $< \sim 200$ ky. They can be correlated with the ^{36}Cl ages of glacial deposits in the eastern Sierra Nevada (Chapter 9), though this correlation may sometimes be fortuitous due to problems with inherited ^{36}Cl in shoreline deposits. The pre-Wisconsin ($\sim$120 ky) and early Wisconsin (85-95 ky) shorelines are the most prominent in both Panamint and Death Valley, which resulted from two factors: (1) the early lake cycle lasted longer and (2) in Death Valley, the lake was twice as deep in early than it was in the late Wisconsin (cf. Dorn et al., 1990). The early Wisconsin shoreline deposits are similar in their prominent character to early Wisconsin moraines in the eastern Sierra Nevada, which are among the most extensive. They indicate that the climate changed very rapidly to the full glacial/pluvial mode at the beginning of the glacial cycle. The glacial/pluvial conditions were reestablished at least two more times

during the Wisconsin, but the younger events had smaller extent in comparison with the early Wisconsin maximum.

In this study, I found that clastic shoreline deposits have a composite cosmogenic ^{36}Cl signal. Boulders and cobbles have ^{36}Cl from previous exposure episodes, for instance, in outcrops or during fluvial transport. This inherited ^{36}Cl must be subtracted from the total ^{36}Cl to yield the cosmogenic component accumulated since the shoreline construction. Assessment of previously accumulated ^{36}Cl is possible if samples shielded from cosmic rays are available besides surface samples. If subsurface samples are not available, correct shoreline ages can be obtained from tufa deposits. These carbonate deposits precipitate directly for the lake water and have simple exposure history.

The calculated ^{36}Cl ages gave means to estimate the uplift rate at Pleasant Canyon, Panamint Valley. Most shorelines that were established at $\sim$600 m are now at higher elevations. From the vertical offsets and the established ^{36}Cl ages, I calculated an average uplift rate of 0.7 m ky^{-1}, in agreement within a factor of two with other uplift rate estimates in the Mono Lake -Death Valley paleolake system.

References

Bachman, S.B., 1978, Pliocene-Pleistocene break-up of the Sierra Nevada - White - Inyo Mountains block and formation of Owens Valley, Geology 6, 461-463.

Blackwelder, E., 1931, Pleistocene glaciation in the Sierra Nevada and the Basin Ranges, Geological Society of America Bulletin 42, 865-922.

Dorn, R.I., A.J.T. Jull, D.J. Donahue, T.W. Linick and L.J. Toolin, 1988, Latest Pleistocene lake shorelines and glacial chronology in the western Basin and Range province, USA: Insights from AMS radiocarbon dating of rock varnish and paleoclimatic implications, Palaeogeography, Palaeoclimatology, Palaeoecology 78, 315-331.

Dorn R.I., 1988, A rock varnish interpretation of alluvial-fan development in Death Valley, California, National Geographic Research 4, 56-73.

Gilbert, G.K., 1890, Lake Bonneville, U.S. Geological Survey Monograph 1, 438 p.

Morrison, R.B., 1991, Quaternary stratigraphic, hydrologic, and climatic history of the Great Basin, with emphasis on Lakes Lahontan, Bonneville, and Tecopa, In: Morrison R.B. (Ed.), Quaternary non-glacial history - Conterminous U.S., Geological Society of America, Decade of North American geology, Vol. K-2, p. 283-320.

Nishiizumi, K., Kohl, C.P., Arnold, J.R., Dorn, R.I., Klein, J., Fink, D., Middleton, R., and Lal, D., 1993, Role of *in situ* cosmogenic nuclides ^{10}Be and ^{26}Al in the study of diverse geomorphic processes, Earth Surface Processes and Landforms

18, 407-425.

F.M. Phillips, B.D. Leavy, N.D. Jannik, D. Elmore and P.W. Kubik, The accumulation of cosmogenic chlorine-36 in rocks: a method for surface exposure dating, Science 231, 41-43, 1986.

Russell, I.C., 1885, Geological history of Lake Lahontan, a Quaternary lake of northwestern Nevada, U.S. Geological Survey Monograph 11, 287 p.

Seltzer, G.O., 1990, Recent glacial history and peleoclimate of the Peruvian-Bolivian Andes, Quaternary Science Review 9, 137.

Smith, R.S.U., 1976, Late-Quaternary pluvial and tectonic history of Panamint Valley, Inyo and San Bernardino Counties, California, Ph.D. dissertation, California Institute of Technology, 295 p.

Smith, R.S.U., 1978, Pluvial history of Panamint Valley, California, Guidebook for Friends of the Pleistocene, Pacific Cell, Geology Department, University of Houston.

Smith, G.I., 1984, Paleohydrologic regimes in the southwestern Great Basin, 0-3.2 my ago, compared with other long records of "global" climates, Quaternary Research 22, 1-17.

Smith, G.I and F.A. Street-Perrot, 1983, Pluvial lakes of the western United States, In: S.C. Porter (Ed.), The Late Pleistocene, University of Minnesota Press, Minneapolis, p. 190-212.

12. Summary of conclusions

The work presented in this dissertation consists of two major parts: (1) development of the surface exposure dating method by cosmogenic ^{36}Cl buildup and (2) establishment of ^{36}Cl chronologies of late Quaternary glaciations in the Western United States. Using independently dated samples, I calculated the production rates of ^{36}Cl from its three main target elements, estimated the precision and accuracy of the method, and investigated some factors influencing the buildup of ^{36}Cl. In the geochronological applications part, I developed local glacial chronologies at several locations in the Great Basin and the Wind River Range. These chronologies provided a basis for the regional correlations and for the comparison with the marine record of the global climate.

Several independently dated samples permitted adequate parametrization of the cosmogenic ^{36}Cl surface exposure dating method. All calibration samples were from landforms with simple exposure histories or from surfaces that are otherwise geomorphically well characterized. These conditions were necessary to assure that the cosmogenic signal has not been influenced by any postdepositional processes occurring at the landform surfaces. The calculated production rates are integrated over exposure periods of the calibration samples and thus average any temporal variabilities of the incident cosmic ray flux. As a result of this averaging, the temporal variabilities in the ^{36}Cl production rates are small or even negligible and constant values can be used for most geochronological applications. The reported sea-level and high geographic latitude ($>50°N$) production rates can be adjusted for applications at other locations. The

average absolute deviation associated with these production rates is $\sim 9\%$. The largest uncertainty is for the production rate from ^{39}K because of scarcity of K-rich samples; the other two production parameters are well constrained by several samples with high Ca and Cl content. Negative muon capture by ^{40}Ca contributes little to the total production of cosmogenic ^{36}Cl. The maximum sea-level production rate due to this process is less than 14% of that of spallation of calcium and becomes negligibly small at high (mountain) altitudes. Because both reaction paths use the same target element, the respective production rates can be combined into one "calciogenic" production rate. This rate is valid for surficial samples, but may not be applicable at greater depths because of different attenuation lengths for muons and neutrons.

Chlorine-36 ages of an impact crater at Meteor Crater, Arizona and volcanic deposits at Lathrop Wells, Nevada helped assess the accuracy and precision of the ^{36}Cl method. Excellent agreement with independent age estimates show that the ^{36}Cl method can produce accurate results. Similarly, internal consistency among samples from the same surfaces shows that the method has adequate precision. These demonstrated accuracy and precision results show that the method is capable of producing reliable surface exposure ages for late Quaternary landforms.

Surface exposure ages may be affected by postdepositional processes that modify landforms. I qualitatively discussed effects of these processes on calculated ^{36}Cl ages, and potential ways of minimizing of these effects. For a quantitative investigation, I

chose erosion, a major surface modifying process resulting in gradual exposure of fresh material to cosmic radiation. Its effects on surface exposure ages depend on the erosion depth and the fraction of the cosmogenic ^{36}Cl produced from thermal neutron activation of ^{35}Cl. For shallow erosion depth and high thermal neutron activation contribution, ^{36}Cl ages may slightly overestimate the true landform age while deeper erosion depth and/or low thermal neutron component result in an underestimation of the true age. Because the deviation of the apparent age from the true age is predictable, it can be helpful in interpreting ^{36}Cl ages of eroding surfaces.

The second part of the dissertation focused on applications of the cosmogenic ^{36}Cl method to dating late Quaternary glacial and pluvial deposits from the western United States. Moraines from three locations in the eastern Sierra Nevada, one in the eastern White Mountains, and two in the eastern Wind River Range provided data, which I used in an attempt to construct a regional record of glaciations. The comparison of local ^{36}Cl chronologies indicates that glaciations were generally synchronous at all locations with major glacial events at 150, 90-110, 60-70, and 14-20 ky. These glacial ages are correlative with the major peaks in the marine ^{18}O record and with ^{36}Cl dated glaciofluvial terraces from the Wind River Range and pluvial lake shorelines from Panamint Valley.

The local chronologies did not allow for straightforward interpretations and correlations because deposits of only three to four glacial advances are typically

preserved at single locations. The glacial records are fragmentary; no single location has deposits of all glaciations and no glacial advance is recorded at all locations. This is due to either unfavorable conditions for glacier development at some times or obliteration of existing deposits by later, more extensive glaciers. To obtain a full record of paleoenvironmental changes, it is necessary to combine absolute glacial chronologies from several locations.

This fragmentary nature of the terrestrial glacial record may lead to serious problems with glacial correlations. The ^{36}Cl data indicate that many deposits that were previously correlated, e.g., based on their stratigraphic positions, are not correlative; they represent different stadials and, sometimes, even different glaciations. Similarly, some previously uncorrelated deposits have the same exposure ages and are therefore correlative. Considering these results, it may become necessary to revise the existing correlation schemes. The new correlations should be based on numerical ages rather than on stratigraphic positions and other relative dating techniques. Development of absolute chronologies for terrestrial glacial records will also allow for their correlation with more continuous records of the global climate contained in marine and lake sediments and in polar ice cores.

At most locations, clusters of several distinct moraines of nearly the same age are present. One such cluster exists at Little McGee Creek and consists of eight different late Wisconsin (stage 2) moraines deposited within a period of one or two ky. Such a

large number of moraines deposited relatively fast suggests unstable climatic conditions at that time, perhaps accompanying the following final deglaciation. Clusters of similar nature, although on a different time scale, exist at Bishop Creek and in the Bull Lake area. Both consist of sets of moraines dating to 90-110 ky, i.e., correlative with the marine stage 5. Again, as in the Little McGee Creek area, they indicate unstable environmental conditions, here accompanying the transition from the interglacial to the glacial climate.

Appendix A: Laboratory procedures

Grinding and leaching

- Clean rock surfaces of any organic overgrowths using a wire brush.
- Crush the sample to pieces smaller than 1 cm using a jaw crusher.
- Grind the sample using a tungsten mill. Remove fraction $<75\mu$m and larger than average phenocryst size; the remaining material is the sample.
- Leach the sample overnight in 3% nitric acid to remove meteoric chlorine from grain boundaries and any secondary carbonates present.
- Rinse the sample repeatedly using deionized water until all acid is removed.
- Dry the sample in an oven at about 80°C.
- Take 10 grams of the sample for major and trace elements and place in a small, clean, labeled glass vial.
- Put the rest of the sample in a labeled plastic bag.

Total chlorine determination

- Clean the teflon diffusion cells using: (1) hot H_2SO4 + $K_2Cr_2O_7$; (2) deionized water; (3) hot HNO_3 + H_2O_2; (4) deionized water.
- Prepare reducing solution: 5.8 g KOH + 0.29 g Na_2SO_3 + 30 g H_2O.
- Prepare appropriate standards in clean teflon centrifuge tubes. For samples with low Cl content prepare four standards, for other samples two or three standards are sufficient.
- Write down cell numbers and sample names in the appropriate columns in the form designed for this experiment.
- Prepare blank by measuring 2.5 mL of reducing solution into the inner chamber of a teflon diffusion cell.
- Weigh 0.2 grams of a standard (or a sample) into the outer chamber of the teflon diffusion cell. Record the actual sample mass in the column "Initial mass".
- Measure 2.5 mL of the reducing solution into the inner chamber of each diffusion cell.
- Prepare oxidizing solution in a plastic beaker: 0.4 g $KMnO_4$ + 5.6 g H_2O + 1.9 mL of 50% H_2SO_4 + 32 mL of HF.
- Place the diffusion cells under the hood and add 3 mL of oxidizing solution to the outer chambers of the diffusion cells using an automatic pipette.
- Place all diffusion cells on the orbital shaker, set speed at less than 200, and shake the cells for 16 to 20 hours.

- Change filling solution in the ion selective electrode.
- Open the blank, pipette off the solution from the outer chamber using a small plastic pipette.
- Weigh the cell and calculate the mass of the solution left in the cell. Record the reducing solution mass in the column "Final mass".
- Put the electrode in the blank solution for 30 minutes. The bottom of the electrode should be fully immersed in the solution but should not touch the bottom of the diffusion cell. Record potential at the beginning and the end of this period in the column "mV".
- Open the diffusion cells (one at a time) and remove the solution from the outer chamber using a plastic pipette.
- Weigh the cell, calculate the mass of the solution left and record in the column "Final mass".
- Rinse the electrode (especially its sensing element at the bottom) in deionized water and shake off any droplets of water present.
- Put the electrode in the inner chamber of the diffusion cell so that it is fully immersed but does not touch the bottom of the diffusion cell.
- Observe potential readout and record it when it is stable in the column "mV". Stability is achieved after approximately 1 minute for samples containing more than 100 ppm of Cl, and after 2 to 5 minutes for samples with lower Cl concentrations.
- Rinse the diffusion cell using deionized water and put the cap on.

Chlorine extraction for ^{36}Cl

- Clean teflon bottles using "Fantastik" and soft sponge, rinse in tap water, then 3 times in deionized water, clean using hot HNO_3 + H_2O_2, rinse in deionized water.
- Weigh appropriate amount of sample; this amount depends on Cl concentration in the sample:

Cl concentration [ppm]	Sample mass [gram]
25 - 100	120-0.8*Cl concentration
> 100	40

- Put the sample in a teflon bottle. Label the bottle twice using tape and permanent marker.
- Add 10 cm^3 of 0.2M $AgNO_3$.
- Add HNO_3 in proportion 1 part of HNO_3 to 1 part of sample.
- Gradually add HF in proportion 2.5 parts HF to 1 part of sample. Add 20% first and wait 15-20 minutes, then add another 20% and so on. Keep the bottles closed (not very tight) except when adding HF.
- Close the bottle, put it in a hot bath at 80° C for 48 hours. Shake periodically. Chlorine is liberated from the rock matrix and precipitated as AgCl.
- After complete dissolution, move the content of the teflon bottle to a 250-mL teflon centrifuge tube. Label it twice.
- Centrifuge at 2500 rpm for at least 10 minutes.
- Decant the solution and repeatedly rinse the sediment in deionized water until it has

neutral pH.

- Add NH_4OH to dissolve AgCl. Make sure the solution has very basic pH.
- Centrifuge at 2500 rpm for 10 minutes to separate silicic acid from the solution.
- Transfer the clear solution to a 600-mL teflon beaker and carefully add concentrated HNO_3 to reprecipitate AgCl. AgCl will form a milky suspension in acidic solution.
- Put the beaker on a hot plate at 60°C for one day; AgCl will flocculate and settle at the bottom.
- Carefully remove the solution and rinse the remaining AgCl in deionized water.
- Transfer the sample to a 50-mL glass centrifuge tube.
- Dissolve the sample in concentrated NH_4OH and add 1 ml of Ba(NO3)2 to precipitate BaSO4. Leave the solution for at least 8 hours (but preferably longer).
- Centrifuge the glass tube at 2500 rpm for 10 minutes.
- Carefully remove the solution using clean glass pipette, place it in another glass centrifuge tube and label it twice.
- Add sufficient amount of HNO_3 to precipitate AgCl. Let it stand for 2 hours.
- Centrifuge, remove acidic solution and rinse the AgCl at least three times in deionized water. Make sure the pH of the final rinse is about 7.
- If samples may have high sulfur, repeat the last five steps once again.
- Transfer the AgCl onto a clean watch glass. Remove excess water using small glass pipette. Cover the glass with aluminum foil. Place two labels on the foil.
- Place the sample in the oven at about 60°C for 24 hours.

Appendix B: Geochemical data

Chapter 4: New calibration

Sample	SiO_2	TiO_2	Al_2O_3	Fe_2O_3	MgO	CaO	MnO	Na_2O	K_2O	P_2O_5	Cl	B	Gd
COM92-1	47.90	2.66	13.80	14.20	8.15	10.10	0.21	2.31	0.73	0.40	70		
COM92-2	47.60	2.68	13.70	14.60	8.22	10.10	0.21	2.32	0.70	0.41	72		
COM92-3	47.50	2.62	13.90	14.20	8.00	10.10	0.20	2.31	0.67	0.38	72		
COM92-4	49.70	4.06	13.50	17.00	3.27	5.86	0.25	2.88	1.65	0.74	207	5.7	8.1
COM92-5	48.60	4.00	13.10	17.50	3.59	6.19	0.25	2.83	1.65	1.14	236	8.9	10.4
COM92-6	47.60	4.07	12.80	18.20	4.07	6.63	0.27	2.83	1.68	1.43	258	5.6	12.7
COM92-7	50.90	2.89	13.10	16.80	3.09	5.93	0.27	3.34	2.24	1.33	347	7.3	17.7
COM92-8	50.70	3.01	13.00	16.80	3.05	6.16	0.27	3.27	2.26	1.52	348	5.5	19.6
COM92-9	51.50	2.96	13.20	16.40	2.95	5.85	0.26	3.34	2.31	1.29	334	6.4	18
COM92-11	50.30	3.47	13.70	17.00	3.04	5.85	0.26	3.22	2.10	1.00	334	7.4	11.8
COM92-12	50.10	3.44	13.70	17.50	3.29	5.85	0.27	3.27	2.09	1.04	343	4.2	13.6
COM92-13	51.20	3.45	13.50	17.30	3.17	5.14	0.27	3.11	2.09	0.52	311	7.4	8.1
COM92-14	46.70	3.46	12.70	19.10	4.08	6.23	0.30	3.14	2.03	1.67	350	6.1	18.4
COM92-15	47.80	3.54	13.20	18.40	3.92	6.02	0.28	3.13	2.09	1.50	340	4	14.5
COM92-16	47.20	3.41	12.80	18.80	4.06	5.79	0.29	3.15	2.00	1.35	322	6.3	15.8
COM92-18	48.00	2.89	14.70	14.20	7.18	9.51	0.21	2.40	0.84	0.58	80		
COM92-19	47.90	2.85	14.30	14.30	7.33	9.25	0.21	2.31	0.77	0.55	78		
COM92-20	48.10	2.95	14.50	14.10	7.14	9.50	0.20	2.49	0.84	0.74	99		
COM92-21	47.60	3.03	14.50	14.20	6.85	9.51	0.21	2.53	0.88	0.51	96		
COM92-22	48.10	2.97	14.20	14.50	7.29	9.35	0.21	2.41	0.88	0.70	87		
CW-3	73.02	0.24	15.07	2.53	0.45	0.03	0.02	4.01	3.20	0.01	18		
CW-7	77.30	0.26	11.47	1.97	0.42	0.20	0.02	0.95	5.30	0.03	6		
BI92-17-BML	50.30	1.69	12.70	15.20	6.38	11.60	0.23	1.94	0.29	0.02	218	9 4	
MC-1	28.78	0.13	2.52	0.33	17.16	21.13	0.05	0.16	0.47	0.23	143	3.5	0.2
MC-3	10.74	0.15	2.38	0.73	19.36	29.21	0.07	0.11	0.43	0.39	217	5.8	0.3
MC-4	27.00	0.24	4.97	0.60	16.19	23.78	0.03	0.17	0.78	0.19	132	7.6	0
MC-5	12.95	0.14	2.20	0.61	18.84	28.16	0.10	0.13	0.44	0.48	259	1.7	0.3
IN92-1-BR	0.91	0.00	0.01	0.06	4.43	50.50	0.01	0.01	0.03	0.07	74		
MK-AT3B-28	51.00	2.95	15.11	12.09	4.23	7.04	0.21	3.87	1.47	0.68	209		
9353	47.91	1.31	14.03	10.22	6.81	10.93	0.16	2.06	0.86	0.46	94	10	5.4
9354	46.13	1.42	14.84	11.65	6.75	10.69	0.17	2.37	0.78	0.42	111	10	5.7

Chapter 5: Gradual exposure model

bpcr90-63-pti5	72.55	0.26	13.94	1.78	0.84	1.63	0.06	3.18	4.76	0.07	141		
bpcr90-64-pti5	70.20	0.40	14.70	2.95	0.76	2.07	0.10	3.79	4.11	0.11	154		
bpcr90-65-pti5	71.00	0.31	15.10	2.48	0.58	2.03	0.07	3.88	4.04	2.03	108		
bpcr90-66-pti5	71.40	0.30	15.00	2.41	0.52	2.36	0.04	3.90	3.73	0.07	21		
bpcr90-67-pti5	72.30	0.32	14.20	2.63	0.67	1.88	0.07	3.66	4.03	0.20	118		
bpcr91-pti5-1	65.00	0.40	18.00	3.37	1.38	5.20	0.07	4.58	1.61	0.07	63	6.8	3.8
bpcr91-pti5-2	54.70	0.87	19.70	7.78	3.23	5.50	0.12	3.94	1.93	0.06	64	12.9	4.4
bpcr91-pti5-3	75.50	0.18	13.60	1.39	0.35	1.44	0.03	4.09	3.18	0.02	8		
bpcr91-pti5-4	73.20	0.18	14.10	1.45	0.24	1.64	0.03	3.62	4.04	0.04	131	6	3.9
bpcr91-pti5-5	73.70	0.29	13.50	2.21	0.47	1.51	0.09	4.03	3.59	0.07	32		
bpcr91-pti5-6	80.20	0.04	11.10	0.57	0.06	0.28	0.01	3.73	3.78	0.02	11		
bpcr91-pti5-7	77.90	0.08	12.60	0.43	0.11	1.24	0.02	3.07	4.34	0.02	35		
bpcr91-pti5-8	73.20	0.20	14.60	1.40	0.33	1.31	0.03	4.18	3.94	0.03	109	8.1	4.6
bpcr91-pti5-9	57.70	1.14	18.40	7.93	2.04	4.07	0.37	5.36	2.30	0.18	131	5.8	8.8

Sample	SiO_2	TiO_2	Al_2O_3	Fe_2O_3	MgO	CaO	MnO	Na_2O	K_2O	P_2O_5	Cl	B	Gd
bpcr91-pti5-10	77.80	0.13	12.40	0.85	0.20	1.11	0.03	3.00	4.32	0.02	26		
bpcr91-pti5-11	76.50	0.11	14.10	1.17	0.21	1.54	0.03	3.77	3.84	0.03	138	8.2	2.7
bpcr91-pti5-12	73.60	0.23	14.40	1.68	0.44	1.66	0.05	3.71	4.02	0.03	114	6.8	2.4
bpcr91-pti5-13	72.80	0.16	14.70	1.34	0.23	1.96	0.05	3.87	3.95	0.04	108	4.1	4
bpcr91-pti5-14	66.50	0.37	17.70	2.83	0.89	5.07	0.05	4.51	1.69	0.04	28		
bpcr91-pti5-15	72.50	0.24	14.80	1.68	0.43	1.95	0.06	3.92	3.68	0.04	147	6	2.6
bpcr91-pti5-16	74.20	0.17	13.60	1.28	0.20	1.44	0.04	3.68	4.19	0.03	139	6.1	1.8
bpcr91-pti5-17	65.10	0.52	17.70	3.59	1.41	5.22	0.07	4.57	1.38	0.05	39		
bpcr91-pti5-18	76.20	0.04	12.90	0.54	0.10	0.91	0.02	3.37	4.75	0.03	62	5.8	5
bpcr91-pti5-19	63.30	0.53	17.80	4.24	1.45	5.29	0.07	4.50	1.35	0.05	48		
bpcr91-pti5-20	74.80	0.16	13.40	1.04	0.23	1.43	0.03	3.70	4.11	0.03	108	4.7	1.3
bpcr91-pti5-21	66.10	0.43	16.50	4.22	1.55	4.23	0.08	3.92	2.48	0.05	59	3.1	2
BCS92-2CR	70.50	0.20	15.10	1.71	0.69	2.90	0.04	3.61	3.65	0.02	46		
BCS92-3CR	72.20	0.17	14.80	1.44	0.48	2.75	0.03	3.66	3.58	0.02	45		
BCS92-4CR	71.70	0.22	13.90	1.89	0.71	2.45	0.04	3.51	3.67	0.03	46		

Chapter 7: Meteor Crater

MC-1	28.78	0.13	2.52	0.33	17.16	21.13	0.05	0.16	0.47	0.23	143	3.5	0.2
MC-2	23.96	0.13	2.24	0.36	17.56	23.38	0.02	0.05	0.47	0.28	131	5.3	0.4
MC-3	10.74	0.15	2.38	0.73	19.36	29.21	0.07	0.11	0.43	0.39	217	5.8	0.3
MC-4	27.00	0.24	4.97	0.60	16.19	23.78	0.03	0.17	0.78	0.19	132	7.6	0
MC-5	12.95	0.14	2.20	0.61	18.84	28.16	0.10	0.13	0.44	0.48	259	1.7	0.3

Chapter 8: White Mountains

C87-1	71.54	0.24	14.54	1.26	0.04	0.74	0.05	8.00	3.21	0.01	126		
C87-2	74.74	0.28	12.57	0.90	0.02	0.24	0.03	8.54	2.48	0.01	56		
C87-3	75.00	0.21	13.80	1.22	0.14	0.21	0.03	4.26	5.44	0.02	123		
C87-4	74.85	0.30	12.94	1.15	0.04	0.38	0.03	7.31	2.91	0.01	140		
C287-5	66.95	0.77	14.11	5.06	0.09	3.77	0.11	3.51	5.16	0.33	117		
C287-6	73.67	0.26	12.62	0.86	0.01	0.43	0.03	9.41	2.53	0.01	149		
C387-1	73.80	0.22	14.20	1.77	0.22	0.65	0.06	4.29	5.37	0.02	134		
C387-2	68.48	0.33	16.91	1.66	0.11	1.19	0.05	6.22	4.76	0.04	97		
C387-3	74.39	0.33	12.99	1.11	0.03	0.22	0.02	7.65	2.89	0.01	74		
C587-1	73.25	0.25	14.08	1.43	0.06	0.83	0.06	6.25	3.78	0.02	152		
C587-2	72.74	0.29	13.63	1.11	0.05	0.83	0.03	8.43	2.77	0.01	121		
C587-3	70.88	0.29	13.18	0.45	0.02	0.25	0.02	15.13	0.15	0.01	65		
C787-1	73.50	0.21	14.00	1.35	0.12	0.49	0.02	4.83	5.43	0.05	160		
C7b87-1	74.88	0.22	13.30	1.21	0.03	0.66	0.05	7.26	3.04	0.01	72		
C787-2	74.57	0.25	12.60	0.78	0.03	0.73	0.04	9.69	2.31	0.01	88		
C787-3	75.86	0.20	12.21	1.03	0.02	0.46	0.04	7.61	2.60	0.02	46		
CH89-P12	72.92	0.16	14.73	0.74	0.02	0.30	0.96	3.68	6.27	0.03	87	4.3	2.1
CH89-P12-1	74.73	0.19	12.81	1.13	0.03	2.41	0.62	3.37	4.70	0.02	43		
CH89-P22-1	80.91	0.18	11.95	0.07	0.01	0.46	0.23	6.56	0.10	0.02	58		
CH89-P22-2	79.15	0.14	11.64	0.55	0.01	0.26	0.24	3.67	4.42	0.02	42		
CH89-P22-3	78.86	0.14	11.85	0.05	0.02	0.88	0.36	4.21	3.68	0.02	50		
CH89-P23-1	73.75	0.24	13.55	1.80	0.03	0.86	0.94	4.02	5.11	0.09	124		
CH89-P23-2	73.88	0.27	13.60	1.41	0.04	0.47	0.53	4.43	3.98	0.04	94		
CH89-P23-3	73.25	0.40	13.51	1.96	0.02	1.05	1.11	3.59	5.05	0.02	82		
C1187-1	72.68	0.29	15.03	1.58	0.09	1.00	0.04	5.61	4.36	0.03	151		
C1187-2	71.46	0.34	14.14	1.03	0.05	0.42	0.03	10.22	1.90	0.02	99		

Sample	SiO_2	TiO_2	Al_2O_3	Fe_2O_3	MgO	CaO	MnO	Na_2O	K_2O	P_2O_5	Cl	B	Gd
C1187-3A-W	75.20	0.28	13.90	0.65	0.20	0.22	0.02	6.24	2.87	0.05	104	7	4.5
C1287-1A-W	75.70	0.08	13.50	0.62	0.12	0.51	0.02	3.97	5.30	0.03	144	12	2
C1287-2	74.47	0.25	13.02	1.08	0.03	0.47	0.02	8.49	2.22	0.05	79		
C1287-3	55.27	1.53	13.00	15.37	1.15	9.74	0.25	2.97	0.05	0.10	105		
CH89-P8-C13-1	77.56	0.17	11.66	0.84	0.03	0.44	0.45	4.74	4.76	0.02	41		
CH89-P8-2	77.13	0.19	12.24	0.90	0.03	0.48	0.67	4.01	5.12	0.04	66		
CH89-P8-3	73.88	0.32	13.84	1.50	0.04	0.70	1.06	4.19	5.15	0.08	122	4.3	5.1
CH89-P2-C15	73.59	0.26	13.35	1.06	0.02	0.47	0.85	5.39	5.22	0.03	102	9.6	3.6
CH89-P3-C18-1	77.94	0.18	12.26	0.96	0.02	0.60	0.34	4.50	3.97	0.02	57		
CH89-P3-2	76.85	0.14	12.78	1.28	0.02	0.37	0.38	3.41	5.24	0.01	57		
CH89-P3-3	76.78	0.14	12.39	0.89	0.02	0.28	0.34	3.88	4.45	0.02	37		
CH89-P9-1	72.82	0.36	14.17	2.37	0.05	0.71	1.33	4.29	4.66	0.05	97		
CH89-P9-2	74.21	0.27	13.37	1.68	0.05	0.72	1.12	3.73	5.15	0.07	123	5.4	4.4
CH89-P9-4	77.02	0.12	11.47	0.86	0.02	1.01	0.43	5.19	4.71	0.02	35		
CH89-P25-1	74.68	0.24	13.23	1.32	0.05	0.60	0.77	3.75	5.22	0.08	54		
CH89-P25-2	75.59	0.24	13.34	1.27	0.03	0.38	0.63	3.83	5.20	0.02	126		
MC87-1	77.88	0.15	11.82	0.99	0.82	1.51	0.03	2.99	4.24	0.03	71		
MC87-2	71.45	0.37	14.34	2.31	1.42	2.04	0.10	3.73	4.92	0.09	81		
MC87-3	72.43	0.46	14.48	2.49	1.01	1.91	0.03	6.78	0.77	0.09	32		
MC87-4	75.19	0.33	13.23	0.47	1.23	1.94	0.02	4.28	3.45	0.04	38		
MC87-5	71.02	0.44	14.01	2.70	1.28	2.22	0.04	3.59	5.05	0.13	152		
MC87-6	71.72	0.40	14.01	2.57	1.26	1.34	0.03	3.40	5.48	0.11	108		
MC87-7	72.24	0.43	13.94	2.48	0.83	2.37	0.03	5.44	2.70	0.14	101		
PA87-1	68.86	0.28	16.59	2.09	3.29	3.02	0.04	3.24	3.23	0.12	6		
PA87-2	73.99	0.08	14.71	0.56	1.46	1.78	0.03	3.86	4.00	0.02	5		
PA87-3	70.05	0.14	15.97	1.69	2.70	2.32	0.05	3.76	4.12	0.05	6		
CC87-1	65.58	0.79	15.49	5.11	0.09	3.68	0.12	3.60	5.32	0.31	402		
CC87-2	65.62	0.86	14.85	5.27	0.13	4.24	0.12	3.62	4.98	0.24	445		
CC87-3	73.62	0.28	13.79	1.34	0.05	0.82	0.08	6.35	3.35	0.01	379		

Chapter 9: Bloody Canyon

BC86-1-TI	78.18	0.05	12.41	0.80	0.01	0.84	0.03	3.21	5.09	0.08	20	5	6
BC86-2-TI	65.66	0.18	12.74	1.82	0.78	2.27	0.03	3.54	2.96	0.38	60		
BC86-3-TI	74.77	0.31	15.42	2.66	1.24	2.12	0.08	3.92	4.38	0.25	78	8.6	1.8
BC86-5-TI	72.32	0.56	15.54	4.23	1.99	2.89	0.11	3.34	3.44	0.34	122	3.1	3.6
BC86-6-TE	76.88	0.17	14.18	1.82	0.41	2.14	0.10	3.37	3.75	0.09	29	5	3.9
BC86-7-TE	64.04	0.19	12.91	0.97	0.70	3.69	0.04	3.11	1.68	0.12	40		
BC86-8-TE	77.24	0.25	15.93	2.58	1.46	1.47	0.11	3.86	3.30	0.20	61		
BC86-9-TE	65.61	0.22	14.59	1.74	0.68	1.94	0.05	3.57	4.32	0.28	62	5	4.2
BC86-10-TE	73.19	0.18	12.73	1.97	0.41	1.52	0.09	3.54	3.96	0.12	60	5	2.2
BC86-11-TE	75.21	0.08	14.84	1.02	0.49	0.98	0.07	5.16	5.34	0.02	20	5	4.5
BC87-1TA	76.44	0.20	14.61	1.98	1.29	2.02	0.11	3.98	4.05	0.58	68		
BC87-2TA	73.80	0.09	14.40	0.78	0.25	0.79	0.04	4.85	5.57	0.28	30		
BC87-3TA	74.87	0.16	13.73	1.64	0.46	2.04	0.06	3.51	3.88	0.22	56		
BC87-4TA	75.62	0.18	13.24	1.97	0.54	2.18	0.08	3.10	2.48	0.36	64	5	4.8
BC87-5TA	69.60	0.23	14.90	2.25	0.87	1.83	0.11	3.47	4.31	0.29	102	5	3.3
BC88-1	75.64	0.12	13.64	0.63	0.27	1.61	0.04	3.01	4.70	0.06	38	0.9	1.1
BC88-5	68.80	0.54	15.09	3.03	1.05	2.72	0.07	3.09	4.41	0.44	81	5.6	5.1
BC86-12TA	63.40	1.29	9.41	8.56	3.95	7.37	0.25	3.41	1.06	0.48	59		
BC86-13TA	67.80	0.40	14.48	2.82	1.25	2.20	0.07	3.77	4.37	0.51	64	5	8.4
BC86-14TA	77.12	0.20	14.80	1.88	1.44	1.19	0.10	4.12	3.74	0.33	38		
BC86-15TA	75.30	0.51	9.40	3.41	3.13	1.46	0.06	3.07	3.85	0.95	66		

Sample	SiO_2	TiO_2	Al_2O_3	Fe_2O_3	MgO	CaO	MnO	Na_2O	K_2O	P_2O_5	Cl	B	Gd
BC86-16TA	72.16	0.58	16.18	4.18	2.82	3.82	0.09	4.38	3.92	0.64	107	5	5.7
SC86-17MB	75.20	0.15	11.40	1.36	0.95	0.56	0.07	3.24	3.93	0.94	57		
SC86-18MB	74.68	0.25	15.27	2.15	2.08	1.22	0.13	2.83	3.90	0.52	106	5	2.2
SC86-19MB	75.22	0.20	14.64	2.09	0.67	2.40	0.13	3.51	3.22	0.32	100		
SC86-20MB	74.68	0.10	14.65	1.06	0.48	1.18	0.05	3.43	5.16	0.17	22	5	3.4
SC86-21MB	72.30	0.05	13.30	0.47	0.00	0.66	0.03	3.85	5.52	0.18	12	5	4.4
SC88-1	70.75	0.43	14.64	2.73	0.89	2.36	0.07	3.14	4.73	0.30	71	1	3.2
SC88-2	69.48	0.50	14.67	3.13	1.06	2.64	0.07	3.27	4.38	0.34	102	6.7	4
SC88-3	67.24	0.60	15.76	3.17	1.24	3.41	0.08	3.74	4.19	0.30	138	4.8	3.6
BC90-5TI	76.62	0.06	12.23	0.54	0.30	1.16	0.04	3.09	4.18	0.02	17		
BC90-1TE	73.44	0.29	13.52	2.11	1.05	1.94	0.04	3.05	4.47	0.05	42		
BC90-2TE	75.49	0.09	11.86	0.85	0.37	0.84	0.03	3.16	4.15	0.03	52		
BC90-3TE	71.33	0.32	14.15	2.39	0.68	2.20	0.05	3.23	4.34	0.04	43		
BC90-1TA	76.30	0.09	13.00	1.33	0.49	1.95	0.04	3.43	3.30	0.04	53		
BC90-2TA	77.19	0.03	11.55	0.44	0.16	0.67	0.02	2.79	4.93	0.05	58		
BC90-3TA	73.36	0.17	13.51	2.09	0.97	2.03	0.08	3.23	3.22	0.22	31		
BC90-4TA	73.09	0.14	13.32	1.79	0.38	1.93	0.06	3.29	3.51	0.09	42		
BC90-5TA	74.45	0.11	12.89	1.35	0.35	1.58	0.06	3.00	3.87	0.11	28		

Chapter 9: Little McGee Creek

lmc87-1ng	72.06	0.23	13.58	1.71	0.65	1.34	0.08	4.12	4.34	0.16	39		
lmc87-2ng	73.06	0.22	14.57	1.80	0.74	1.36	0.08	3.95	4.42	0.12	54		
lmc90-2	73.00	0.27	14.20	1.69	0.48	1.35	0.06	4.17	4.42	0.05	12	4	2.5
lmc90-3h	73.96	0.26	13.90	2.16	0.58	1.70	0.07	3.50	4.00	0.06	50	4.3	2.4
lmc90-4h	74.45	0.24	14.01	1.76	0.53	1.55	0.06	3.14	4.57	0.05	12	4.0	2.5
lmc90-5pbrh	75.28	0.24	13.46	1.69	0.62	1.51	0.06	3.22	4.25	0.06	34	48.0	1.7
lmc87-1ml	73.50	0.25	14.30	2.19	0.31	1.30	0.08	5.38	4.26	0.03	25	5	3.5
lmc87-2ml	73.60	0.22	13.90	2.00	0.16	1.16	0.09	4.67	4.29	0.03	34		
lmc87-3ml	73.00	0.24	14.10	2.09	0.30	1.21	0.07	4.67	4.53	0.03	29	5	2.1
lmc90-11ti	71.26	0.31	15.21	2.20	0.73	2.13	0.08	3.99	3.90	0.08	17		
lmc87-1tm1	72.29	0.27	15.78	1.93	0.52	2.24	0.06	4.53	4.04	0.23	21		
lmc90-1ml-pbr	66.92	0.32	17.99	3.17	1.21	4.06	0.08	5.27	0.88	0.11	13		
lmc87-1x	72.59	0.28	13.68	1.92	0.84	1.51	0.08	4.85	4.13	0.19	28		
lmc87-1y	71.98	0.26	15.09	1.75	0.74	1.68	0.05	4.04	4.60	0.20	44		
lmc90-12	59.60	0.49	18.60	5.82	2.44	6.48	0.12	4.10	1.49	0.07	115	5.5	3.6
lmc90-13ti	69.73	0.23	13.66	2.00	0.39	1.49	0.07	3.15	4.34	0.06	15		
lmc90-14ti	51.10	1.00	19.24	9.61	4.35	8.16	0.15	3.23	1.60	0.27	181		
lmc90-15ti	70.26	0.37	14.58	3.64	1.74	2.54	0.11	3.79	2.56	0.09	17	5.5	3.6
lmc90-16ti	73.93	0.23	13.50	1.78	0.83	1.51	0.07	3.58	3.82	0.08	20		
lmc90-17ti	56.86	0.82	17.82	7.84	3.95	6.84	0.12	3.39	2.11	0.22	308	7.2	4.8
lmc90-19ti	52.23	0.90	19.50	10.60	5.84	8.08	0.16	3.48	1.60	0.20	162		
lmc90-21	69.80	0.33	15.20	2.55	0.70	2.25	0.07	4.37	3.95	0.08	15		
lmc90-23ti	78.32	0.11	12.81	0.72	1.17	1.18	0.04	2.92	4.44	0.02	10		
lmc90-24	76.00	0.12	13.40	1.22	0.16	1.59	0.03	3.97	3.18	0.02	9		
lmc90-25ti	72.74	0.23	14.57	1.65	2.37	1.54	0.07	3.18	4.73	0.05	16		
lmc90-26	78.80	0.05	12.00	0.39	0.10	0.60	0.02	3.04	4.63	0.02	6		
lmc90-27	79.80	0.10	11.20	0.78	0.10	0.55	0.03	2.80	4.43	0.02	6		
lmc88-6	83.12	0.17	10.07	0.95	0.01	1.55	0.15	2.70	2.16	0.00	14		
lmc88-7	70.83	0.53	12.85	3.83	0.65	1.69	0.23	1.27	4.69	0.14	33		
lmc86-1ti	73.00	0.24	14.20	2.00	0.75	1.60	0.07	4.30	4.30	0.20	111		
lmc86-2ti	73.42	0.24	13.84	1.81	0.66	1.56	0.07	4.32	4.12	0.17	53	5	3.3
lmc86-3ti	70.51	0.23	14.33	1.72	0.90	4.47	0.07	4.14	4.40	0.16	84	5	3.6

Sample	SiO_2	TiO_2	Al_2O_3	Fe_2O_3	MgO	CaO	MnO	Na_2O	K_2O	P_2O_5	Cl	B	Gd
lmc86-4ti	71.59	0.29	14.67	2.18	0.72	1.79	0.07	4.15	4.17	0.22	22	5	2.8
lmc86-5ti	72.23	0.24	14.25	1.94	0.55	1.61	0.07	4.65	4.11	0.17	41	5	2.0
lmc91-ta3	76.20	0.11	13.50	1.03	0.11	1.36	0.03	4.12	3.53	0.02	10		
lmc91-ta4	76.00	0.11	13.60	1.24	0.15	1.64	0.03	3.99	3.14	0.02	8		
lmc91-ta5c	76.40	0.13	13.30	1.25	0.22	1.30	0.04	3.89	3.51	0.02	9		
lmc91-ta6	59.20	0.55	18.20	6.74	2.53	7.42	0.12	3.61	0.99	0.05	182	4.5	2.8
lmc91-ta7	76.00	0.12	13.60	1.19	0.10	1.56	0.04	4.15	3.35	0.02	8		
lmc91-ta8	55.00	0.81	18.40	8.53	3.66	7.69	0.15	3.37	1.36	0.08	229	5.8	3.6
lmc86-6ti	74.50	0.27	13.71	2.44	0.07	1.48	0.09	4.52	3.47	0.07	26		
lmc86-7ti	72.01	0.27	14.49	2.13	0.62	1.71	0.08	4.58	3.97	0.23	23	4	2.3
lmc86-8ti	72.15	0.25	14.15	2.00	0.62	1.47	0.07	4.35	4.41	0.19	67	1.6	2.6
lmc86-9ti	71.89	0.24	16.07	1.83	0.35	1.48	0.06	4.60	4.31	0.10	24	1.6	2.6
lmc86-9ti	71.89	0.24	16.07	1.83	0.35	1.48	0.06	4.60	4.31	0.10	24	1.6	2.6
lmc86-10ti	72.00	0.28	14.29	2.01	0.86	1.90	0.07	4.70	4.06	0.50	37	5	3.3
lmc88-2	79.59	0.50	9.40	2.21	0.06	2.06	0.19	1.60	2.67	0.02	17		
lmc88-3	80.14	0.48	9.05	2.28	0.06	2.03	0.17	1.48	2.48	0.03	33		
lmc88-4	79.35	0.62	8.89	2.59	0.09	2.26	0.19	1.28	2.63	0.04	37		
lmc88-5	78.54	0.63	9.31	3.48	0.14	2.35	0.15	1.12	4.00	0.04	42		
lmc86-11ta	73.10	0.20	14.66	1.43	0.86	0.62	0.07	4.01	4.86	0.27	19		
lmc86-12ta	70.60	0.28	16.05	1.95	0.98	1.08	0.08	4.62	4.60	0.20	26	5	2.8
lmc86-13ta	58.72	0.98	15.85	5.82	0.88	3.30	0.29	5.27	2.64	0.56	123		
lmc86-14ta	71.17	0.26	15.43	1.91	1.42	1.01	0.07	4.07	4.56	0.42	29		
lmc86-15ta	71.22	0.29	15.65	2.08	0.38	1.86	0.06	4.42	4.28	0.42	25		
lmc90-28ta	78.58	0.09	12.59	0.76	1.32	0.60	0.05	2.70	5.00	0.02	11		
lmc90-29ta	76.28	0.09	12.61	0.73	2.04	0.70	0.05	2.80	5.08	0.04	14		
lmc90-30	78.60	0.09	11.40	0.87	0.14	0.68	0.04	3.57	4.36	0.07	12		
lmc90-31	77.90	0.08	12.00	0.71	0.14	0.83	0.03	3.19	5.11	0.03	8		
lmc86-16sh	72.03	0.25	15.00	1.80	0.28	1.50	0.06	4.10	4.63	0.81	23		
lmc86-17sh	72.86	0.32	14.74	2.85	0.04	2.40	0.16	3.04	3.99	0.30	56		
lmc86-18sh	74.87	0.20	14.53	1.52	0.46	0.72	0.07	3.18	4.75	0.28	32		
lmc86-19sh	72.07	0.21	15.17	1.59	0.07	1.42	0.06	4.77	4.31	0.06	13		
lmc91-sh1	62.60	0.42	17.60	5.93	2.43	6.95	0.13	3.74	0.85	0.07	110	7.3	4.3
lmc91-sh2	59.20	0.60	18.40	7.02	2.32	6.31	0.13	3.86	1.44	0.07	106	5.3	3.2
lmc87-1sh2	72.43	0.24	14.05	1.78	1.69	0.67	0.06	2.67	4.53	1.96	30	5	3.44
lmc87-2sh2	72.06	0.25	15.82	1.91	1.32	1.03	0.07	4.44	4.55	0.30	46	5	3.69
lmc87-3sh2	72.29	0.20	15.53	1.62	0.50	0.84	0.06	3.99	4.68	0.18	39	5	3.08
lmc87-4sh2	73.88	0.22	13.65	1.72	1.40	0.74	0.06	3.24	4.15	1.44	35	5	2.88
lmc90-6	73.03	0.23	14.30	1.71	0.58	1.53	0.07	3.46	4.61	0.05	26		
lmc90-7	59.07	0.77	17.61	7.56	3.47	6.44	0.12	3.37	1.74	0.15	236		
lmc90-8	58.50	0.75	17.36	7.67	3.20	6.04	0.12	3.46	2.24	0.21	152	3.9	4.5
lmc90-9	76.30	0.13	13.40	1.26	0.17	1.35	0.04	3.82	3.71	0.02	7	4	4
lmc90-10	74.81	0.19	14.16	1.68	2.08	1.97	0.05	3.62	3.23	0.05	22		

Chapter 9: Bishop Creek

bpcr91-11-lti	70.60	0.66	13.80	4.24	0.75	2.03	0.07	3.74	3.84	0.03	59	9.6	6
bpcr90-22-ti2	76.16	0.08	11.76	0.72	0.39	1.13	0.03	2.95	4.16	0.02	9		
bpcr90-23-ti2	74.17	0.20	12.50	2.06	1.30	1.35	0.04	2.06	6.02	0.05	30		
bpcr90-24-ti2	71.61	0.27	14.83	2.37	0.92	2.02	0.05	4.04	3.69	0.05	117		
bpcr90-25-ti2	79.29	0.13	12.49	0.92	1.66	0.68	0.04	3.12	4.43	0.06	14		
bpcr90-26-ti2	73.20	0.22	13.90	2.41	2.13	0.39	0.04	3.75	3.60	0.08	8		
bpcr91-1-ti1	60.70	0.67	18.60	5.46	2.14	5.41	0.10	4.41	1.81	0.07	64	8	3.7
bpcr91-2-ti1	75.50	0.13	14.70	1.49	0.26	1.90	0.04	3.75	3.77	0.04	144	5.4	2.3
bpcr91-3-ti1	66.40	0.42	16.00	4.14	1.53	4.03	0.07	3.48	3.17	0.06	83	8.2	4.3

Sample	SiO_2	TiO_2	Al_2O_3	Fe_2O_3	MgO	CaO	MnO	Na_2O	K_2O	P_2O_5	Cl	B	Gd
bpcr91-4-ti1	62.70	0.63	18.10	5.09	2.10	4.88	0.12	4.55	2.05	0.08	72	4.2	5.5
bpcr90-73-pti8	60.53	0.66	17.80	5.37	2.55	5.21	0.07	4.14	2.46	0.15	78		
bpcr90-74-pti8	57.74	0.77	18.35	6.76	3.41	5.88	0.11	3.92	2.03	0.17	123	5.7	3.8
bpcr90-75-pti8	64.52	0.46	15.80	4.25	2.05	4.34	0.08	3.23	3.08	0.14	71		
bpcr91-5-ti1	72.50	0.26	14.80	2.04	0.35	2.02	0.05	4.06	3.83	0.03	67	2.2	2.5
bpcr91-6-ti1	59.80	0.82	17.70	6.68	2.88	4.96	0.11	3.91	1.96	0.10	93	4.1	4.6
bpcr91-7-ti1	60.00	0.60	17.60	5.90	2.48	5.84	0.10	3.66	1.77	0.05	226		
bpcr91-8-ti1	77.50	0.07	12.30	0.64	0.14	0.95	0.02	3.08	4.74	0.02	6		
bpcr90-19-ti	71.33	0.30	15.20	2.56	1.60	2.60	0.06	3.12	4.33	0.06	18		
bpcr90-20-ti	79.00	0.05	12.02	0.35	0.89	0.46	0.01	4.07	3.88	0.03	11		
bpcr90-21-ti	75.12	0.17	12.12	1.07	0.38	0.70	0.07	3.96	3.71	0.03	9		
bpcr90-33-pti1	68.19	0.35	15.25	3.43	1.72	3.80	0.05	3.15	3.68	0.11	58		
bpcr90-34-pti1	64.58	0.54	15.80	5.17	2.33	4.24	0.10	3.80	2.34	0.23	48		
bpcr90-35-pti1	78.19	0.06	11.92	0.34	0.16	0.59	0.02	3.84	3.91	0.02	6		
bpcr90-36-pti1	76.58	0.06	11.89	0.51	0.14	0.54	0.01	3.41	4.35	0.02	19		
bpcr90-37-pti1	63.06	0.68	16.56	5.94	3.36	5.00	0.08	3.50	2.68	0.16	75		
bpcr90-76-pti3	60.58	0.77	18.55	6.45	3.59	5.35	0.10	3.92	2.35	0.21	95		
bpcr90-77-pti3	62.20	0.68	16.90	6.14	2.07	5.02	0.10	4.09	2.14	0.20	56		
bpcr90-78-pti3	77.53	0.13	11.41	0.54	0.43	0.62	0.02	2.49	5.55	0.03	64		
bpcr90-79-pti3	71.09	0.28	14.06	2.37	1.22	1.87	0.07	3.40	4.12	0.07	139	6.3	4
bpcr90-48-pti4	63.53	0.68	18.26	6.00	3.62	4.75	0.09	3.57	2.67	0.32	74		
bpcr90-49-pti4	62.71	0.58	16.25	5.68	2.57	5.01	0.09	3.44	2.80	0.20	122	11	4
bpcr90-50-pti4	79.06	0.12	11.62	0.84	0.54	0.60	0.03	2.70	4.94	0.03	56		
bpcr90-51-pti4	61.76	0.64	16.10	6.02	2.71	4.87	0.09	3.21	2.83	0.19	145	6.7	3.7
bpcr90-52-pti4	71.93	0.25	14.12	1.92	0.67	1.67	0.07	3.73	4.20	0.08	32		
bpcr90-68-pti8	70.96	0.33	14.75	2.21	1.23	1.91	0.07	3.61	3.89	0.13	137		
bpcr90-69-pti8	71.00	0.33	14.60	2.48	2.11	1.74	0.06	4.26	4.28	0.11	168		
BPCR92-1-PTI4	53.60	0.70	18.10	7.78	3.82	8.86	0.14	3.38	0.81	0.04	278		
BPCR92-2-PTI4	66.50	0.29	16.50	4.07	1.21	5.34	0.06	3.97	1.75	0.03	92		
bpcr90-63-pti5	72.55	0.26	13.94	1.78	0.84	1.63	0.06	3.18	4.76	0.07	141		
bpcr90-64-pti5	70.20	0.40	14.70	2.95	0.76	2.07	0.10	3.79	4.11	0.11	154		
bpcr90-65-pti5	71.00	0.31	15.10	2.48	0.58	2.03	0.07	3.88	4.04	2.03	108		
bpcr90-66-pti5	71.40	0.30	15.00	2.41	0.52	2.36	0.04	3.90	3.73	0.07	20		
bpcr90-67-pti5	72.30	0.32	14.20	2.63	0.67	1.88	0.07	3.66	4.03	0.20	118		
bpcr90-70-pti8	76.03	0.27	14.73	2.19	4.19	1.79	0.05	3.32	4.24	0.08	142		
bpcr90-71-pti8	61.06	0.64	17.47	7.40	5.18	6.11	0.12	3.18	2.13	0.18	185		
bpcr90-72-pti8	74.33	0.15	12.34	0.83	0.27	0.75	0.02	2.85	5.29	0.05	72		
bpcr90-43-pti6	66.49	0.45	15.44	4.81	2.00	3.98	0.08	3.22	3.54	0.15	79		
bpcr90-44-pti6	71.24	0.20	13.19	1.59	0.44	1.38	0.03	3.42	4.18	0.04	78		
bpcr90-45-pti6	75.64	0.20	12.95	1.30	0.87	1.32	0.09	2.91	4.72	0.05	36		
bpcr90-46-pti6	74.10	0.20	17.03	1.49	1.63	1.25	0.06	3.59	5.00	0.06	60		
bpcr90-47-pti6	77.38	0.28	14.33	1.89	0.83	1.65	0.06	3.57	4.33	0.06	132	9.5	4.8
bpcr90-38-pti	67.51	0.51	18.41	4.51	2.68	3.99	0.08	3.12	3.53	0.24	64		
bpcr90-39-pti7	77.26	0.18	11.91	0.62	0.39	0.69	0.05	2.93	4.95	0.04	14		
bpcr90-40-pti7	78.18	0.08	11.64	0.54	0.32	0.58	0.04	3.24	4.48	0.04	26		
bpcr90-41-pti7	73.04	0.35	13.74	2.06	0.71	1.48	0.06	3.61	4.01	0.07	131		
bpcr90-42-pti7	71.22	0.21	13.20	1.59	0.42	1.38	0.03	3.42	4.18	0.05	170		
bpcr90-ta-1	65.39	0.48	16.02	4.61	2.29	4.26	0.08	3.17	3.37	0.14	79		
bpcr90-ta-2	61.55	0.63	16.07	5.45	2.30	4.71	0.08	3.81	2.10	0.25	63		
bpcr90-ta-3	67.11	0.46	21.45	4.51	2.77	4.22	0.08	3.29	3.16	0.10	78		
bpcr90-ta-4	77.23	0.07	12.17	0.71	0.51	0.57	0.04	3.65	4.32	0.03	19		
bpcr90-ta-10	48.00	1.79	12.72	14.05	12.49	8.70	0.18	2.20	2.29	0.48	68		
bpcr90-ta-11	66.04	0.49	15.31	4.74	1.97	4.09	0.07	3.10	3.21	0.16	71		
bpcr90-58-opb	76.77	0.09	12.49	0.75	1.05	0.67	0.05	3.39	4.63	0.04	29		

Sample	SiO_2	TiO_2	Al_2O_3	Fe_2O_3	MgO	CaO	MnO	Na_2O	K_2O	P_2O_5	Cl	B	Gd
bpcr90-59-opb	66.16	0.42	15.59	4.43	2.12	4.19	0.07	3.29	3.02	0.11	82		
bpcr90-60-opb	76.57	0.06	11.37	0.38	0.33	0.56	0.02	3.77	3.41	0.02	26		
bpcr90-61-opb	62.59	0.67	16.20	5.56	2.85	4.82	0.08	3.84	2.55	0.23	77		
bpcr90-62-opb	64.54	0.51	16.08	4.84	2.34	4.58	0.09	3.37	3.06	0.15	138		
bpcr90-pta1-5	58.64	0.82	21.97	6.85	3.59	5.65	0.10	4.06	2.04	0.23	96		
bpcr90-pta1-6	76.53	0.07	11.64	0.76	0.38	0.43	0.04	3.09	4.48	0.02	7		
bpcr90-pta1-7	67.52	0.40	15.35	3.58	1.82	3.60	0.07	3.13	3.62	0.17	48		
bpcr90-pta1-8	81.05	0.07	10.61	0.33	0.61	0.52	0.01	2.52	4.38	0.04	15		
bpcr90-pta1-9	60.87	0.64	16.58	5.99	2.97	5.44	0.10	3.63	2.17	0.24	171	9.8	4.5
bpcr90-53-pti3	60.51	0.75	17.82	7.82	3.86	5.63	0.11	3.11	2.50	0.31	294		
bpcr90-54-pti3	61.96	0.66	16.59	5.50	2.33	4.75	0.09	3.88	2.43	0.19	67		
bpcr90-55-pti3	77.36	0.13	11.83	0.71	0.81	0.67	0.03	3.17	4.74	0.03	50		
bpcr90-56-pti3	75.74	0.20	13.46	1.42	0.58	1.44	0.04	3.10	4.90	0.06	38		
bpcr90-57-pti3	74.20	0.24	13.80	1.45	0.32	1.07	0.05	4.13	3.98	0.16	24		
bpcr90-27-pta3	76.03	0.09	12.32	0.70	0.24	0.56	0.03	3.41	4.54	0.03	24		
bpcr90-28-pta3	76.14	0.09	12.06	0.67	0.52	0.65	0.03	3.52	4.42	0.02	12		
bpcr90-29-pta3	77.53	0.07	11.78	0.70	0.44	0.55	0.03	3.07	4.60	0.03	15		
bpcr90-30-pta3	73.43	0.23	13.79	1.68	0.53	1.77	0.03	3.29	4.44	0.10	13		
bpcr90-31-pta3	71.21	0.29	13.78	2.64	1.62	2.53	0.06	3.03	3.94	0.13	22		
bpcr90-32-pta3	61.71	0.75	17.19	6.16	3.10	5.11	0.11	4.05	2.26	0.28	67		
bpcr90-13-sh	53.77	1.13	14.47	7.84	8.34	7.21	0.12	3.04	4.61	0.81	40		
bpcr90-14-sh	73.45	0.21	13.52	1.78	0.68	1.50	0.06	3.56	4.28	0.07	28		
bpcr90-15-sh	78.32	0.06	12.04	0.30	0.32	0.56	0.02	2.93	5.30	0.03	10		
bpcr90-16-sh	64.45	0.60	16.68	5.45	2.08	4.69	0.08	4.03	2.03	0.27	58		
bpcr90-17-sh	63.84	0.59	16.99	4.71	2.26	4.52	0.08	4.03	2.55	0.17	65		
bpcr90-18-sh	77.12	0.09	11.95	0.81	0.47	0.54	0.08	3.51	4.46	0.03	43		
bpcr91-9-ss	67.70	0.35	16.10	3.70	1.32	4.33	0.07	3.77	2.59	0.05	54		
bpcr91-10-ow	74.30	0.19	14.30	1.43	0.27	1.51	0.05	3.99	4.09	0.05	19		
bcr89-ta1	77.26	0.08	11.76	0.53	0.32	0.52	0.02	3.51	4.33	0.03	18		
bpcr90-12-pta2	78.42	0.09	12.20	0.65	0.52	0.64	0.02	4.23	3.32	0.03	9		

Chapter 10: Wind River Range

BL92-2-PN3	67.30	0.56	19.20	0.93	0.32	5.20	0.04	6.15	0.35	0.03	53		
BL92-5-PN3	62.10	0.51	18.20	4.69	1.94	6.01	0.09	5.06	0.93	0.02	154	5	4.9
BL92-6-PN3	77.70	0.11	12.30	0.50	0.20	1.80	0.02	2.77	4.27	0.02	78		
BL92-7-PN3	77.30	0.05	13.00	0.25	0.16	1.08	0.01	4.28	3.87	0.04	93		
BL92-8-PN2	49.10	1.53	12.70	16.10	6.97	11.20	0.23	1.72	0.25	0.03	862	5.6	2.7
BL92-10-PN2	63.40	0.77	16.50	5.48	1.58	4.97	0.08	4.51	1.73	0.03	203	11.4	7.4
BL92-11-PN2	61.30	0.47	17.30	4.71	2.23	4.82	0.08	4.24	1.50	0.02	183	12	2
BL92-12-PN2	73.80	0.07	14.90	0.96	0.18	3.88	0.02	5.04	0.74	0.05	48		
BL92-14-PN2	69.60	0.35	15.70	1.66	0.51	4.73	0.04	4.28	0.69	0.02	71		
BL92-15-PN1	65.70	TiO2	12.30	6.82	3.84	5.61	0.12	2.76	0.31	0.03	124	7	4
BL92-16-PN1	74.40	TiO2	14.20	0.85	0.25	1.94	0.02	5.58	1.46	0.04	85		
BL92-17-PN1	70.20	TiO2	15.50	1.91	0.46	4.14	0.03	4.82	0.56	0.03	60		
BL92-22-BLVI	71.80	0.18	14.70	1.66	0.24	2.67	0.02	4.86	2.01	0.02	97		
BL92-24-BLVI	69.80	0.17	16.20	0.91	0.33	3.11	0.02	6.13	0.89	0.03	65		
BL92-25-BLVI	50.40	0.52	6.55	13.70	15.50	10.30	0.20	0.32	0.15	0.02	78		
BL92-26-BLVI	71.20	0.22	15.00	1.61	0.47	3.72	0.03	4.65	1.42	0.02	55		
BL92-29-BLV	73.50	0.19	15.10	1.57	0.37	3.55	0.02	5.02	0.82	0.02	170		
BL92-30-BLV	46.90	1.33	10.80	20.70	7.36	11.50	0.30	0.97	0.23	0.02	102		
BL92-31-BLV	72.90	0.10	14.40	0.59	0.21	1.55	0.02	4.89	3.39	0.02	98		
BL92-32-BLV	74.40	0.11	14.50	0.87	0.40	2.97	0.03	4.74	1.26	0.02	73		

Sample	SiO_2	TiO_2	Al_2O_3	Fe_2O_3	MgO	CaO	MnO	Na_2O	K_2O	P_2O_5	Cl	B	Gd
BL92-34-BLV	71.20	0.26	15.40	1.66	0.39	1.79	0.03	6.78	1.85	0.02	537	9.5	0.5
BL92-35-BLV	71.00	0.29	14.10	2.44	0.78	2.36	0.04	4.82	1.52	0.02	260	9	3
BL92-36-BLV	64.10	0.46	18.10	3.74	1.28	5.68	0.06	5.16	0.99	0.03	101	8	1.5
BL92-37-BLV	67.90	0.28	16.50	3.06	1.00	3.55	0.06	5.87	0.99	0.03	143	12	0.5
BL92-39-BLIV	74.70	0.16	12.50	1.12	0.36	1.86	0.02	3.20	3.51	0.04	89		
BL92-40-BLIV	56.70	0.52	21.50	4.79	2.27	5.91	0.08	5.03	1.92	0.02	96		
BL92-42-BLIV	71.20	0.26	15.30	1.76	0.40	4.15	0.03	4.79	0.96	0.02	84		
BL92-44-BLIV	65.80	0.35	17.20	2.71	0.89	4.24	0.04	5.54	1.11	0.04	220	6	4
BL92-46-BLIV	74.00	0.16	14.00	1.62	0.29	2.40	0.02	4.99	1.46	0.17	139	6.5	0.5
BL92-49-BLIVB	70.70	0.32	15.20	2.39	0.65	1.39	0.03	3.34	5.66	0.03	209		
BL92-47-BLIII	48.70	1.46	11.00	15.60	8.19	11.70	0.23	1.47	0.28	0.05	831		
BL92-53-BLII	71.60	0.20	15.00	1.54	0.54	2.08	0.03	4.71	3.00	0.02	101	7.5	1
BL92-54-BLII	51.40	0.79	13.70	12.10	6.88	11.30	0.20	1.86	0.28	0.03	223	5	3
BL92-56-BLII	49.20	0.47	15.40	9.36	9.47	12.30	0.16	1.50	0.33	0.02	133	6	3
BL92-57-BLII	75.00	0.12	13.80	1.11	0.23	1.29	0.03	4.85	3.33	0.03	128		
BL92-60-SR	73.50	0.21	14.00	1.54	0.39	1.93	0.03	4.47	2.92	0.06	84		
BL92-62-SR	50.40	0.41	14.60	9.66	8.90	12.30	0.17	1.46	0.52	0.02	108	9	4
BL92-63-SR	50.80	0.44	13.10	10.70	9.23	13.00	0.19	1.16	0.12	0.03	94		
BL92-64-SR	74.70	0.16	12.80	1.17	0.22	0.52	0.02	3.61	4.60	0.03	82		
BL92-67-SR	73.90	0.13	13.30	0.93	0.24	1.34	0.02	4.37	3.32	0.04	71		
BL92-68-SR	74.80	0.12	13.10	1.05	0.24	0.64	0.02	3.61	4.76	0.04	65		
BL92-70-BLT	74.40	0.27	13.50	1.99	0.52	1.44	0.02	3.26	4.29	0.20	180		
BL92-71-BLT	74.00	0.24	13.60	2.01	0.36	1.37	0.03	3.79	4.18	0.09	191	7	5
BL92-72-BLT	73.40	0.17	13.90	1.27	0.39	1.67	0.02	3.73	3.66	0.05	197	5	5
BL92-73-BLT	73.30	0.24	13.60	1.84	0.54	1.36	0.02	3.13	4.59	0.08	216		
BL92-75-PNT	72.00	0.22	14.30	1.33	0.39	1.81	0.02	4.23	3.51	0.03	91		
BL92-76-PNT	74.90	0.24	13.40	1.56	0.40	1.39	0.03	3.80	3.77	0.03	126	7	0.5
BL92-78-PNT	74.50	0.18	12.90	1.02	0.28	0.93	0.02	3.31	5.05	0.04	92		
BL92-79-PNT	75.70	0.10	12.50	0.60	0.24	1.16	0.01	3.27	4.05	0.02	96		

Chapter 11: Panamint & Death Valleys

PV88-1	71.93	0.25	14.83	1.35	0.05	1.35	0.05	7.49	3.29	0.04	222	15	4.5
PV88-2	48.08	1.49	12.74	16.34	1.17	7.78	0.24	2.43	0.06	0.09	245		
PV88-3	72.43	0.42	13.22	5.11	0.20	1.38	0.09	2.57	4.33	0.09	72		
PV88-4A	75.73	0.20	10.83	0.58	0.02	1.29	0.04	10.24	0.94	0.02	268		
PV88-5	10.45	0.09	1.38	0.00	2.00	54.48	0.00	0.00	0.40	0.49	58	17	1.1
PV88-6	10.90	0.09	1.74	0.00	2.47	57.08	0.01	0.00	0.49	0.66	83	16	1.4
PV88-7	76.80	1.08	9.10	5.61	2.14	1.27	0.05	1.53	2.39	0.13	180	16	4.1
PV88-8	62.35	1.07	11.20	10.10	6.30	6.01	0.19	2.12	0.19	0.30	137	14	4.7
PV88-10	68.73	1.00	12.50	6.05	1.79	4.22	0.10	0.67	4.17	0.15	87		
PV88-11	67.37	1.26	11.79	8.32	1.34	5.07	0.11	1.50	2.98	0.18	79		
PV88-13	3.44	0.07	0.74	0.50	0.19	55.56	0.05	0.00	0.12	0.11	45		
MANLY	82.85	0.80	7.06	4.45	1.19	1.28	0.05	0.91	1.23	0.07	61		
BBB93-1	93.50	0.28	2.47	0.90	0.22	0.04	0.02	0.48	0.86	0.02	80		
DV88-1	54.59	1.20	17.33	8.04	1.60	13.19	0.14	2.18	1.12	0.24	182		
DV88-2	72.76	0.46	13.22	2.97	0.05	1.77	0.03	3.52	4.92	0.09	269		
DV88-3	59.38	1.11	15.79	7.94	0.82	7.06	0.16	4.70	1.93	0.22	341		

Author index

Anderson 206, 207, 249

Andrews 19, 22

Atwater 206, 211

Bachman 288

Barry 3

Beget 249

Benson 207

Bentley 17, 19, 146, 209

Berger 2

Birkeland 65, 205-207, 215, 216

Bishoff 4

Blackwelder 176, 203, 204, 258, 275, 280, 281, 283

Broecker 3

Burbank 206, 207, 211, 249

Burke 65, 205-207, 215, 216

Bursik 207, 211

Cerling 69, 84, 89, 181

Chadwick 264

Charalambus 39, 54

Conversi 16

Crowe 143, 144

Curry 207, 249

Dalrymple 205, 206

Davis 12, 14, 21, 22, 39, 97, 146

Dorn 80, 81, 130, 164, 165, 167, 177, 183, 188, 190, 207, 211, 247, 282, 283, 288

Elliott-Fisk 69, 175-177, 179, 184, 188-190, 192-194, 252

Elmore 12, 13, 125, 150, 163, 182

Emiliani 2, 3

Fabryka-Martin 14-17, 97, 110, 152, 161, 162

Feige 19

Forester 169

Fullerton 206, 207, 216, 229

Gibbons 250, 251

Gilbert 275

Gillespie 65, 206, 207, 211, 217, 218

Hallberg 206

Hendricks 22

Imbrie 2, 3, 99

Jannik 4

Krinsley 165

Kubik 200

Kuhn 19

Kuntz 84

Kurz 15

Lal 14-16, 59-61, 68, 97, 110, 128, 162, 163

Leavy 21

Lingenfelter 59, 60

Liu 110

Martinson 2, 3, 99, 229, 248, 249

Matthes 249

Mazaud 81

Mezger 206, 211

Mix 2

Montgomery 22

Morrison 275

Nishiizumi 67, 84, 166, 169, 177, 188-191, 193, 194, 205, 277

O'Brien 15

Oviatt 84

Phillips 3, 5, 12-14, 19-21, 39, 80, 85, 97-99, 101, 108, 122, 123, 125, 130-132, 146, 147, 161, 162, 178, 181, 182, 206, 208, 210, 211, 217, 218, 240, 260, 282

Porter 259

Reedy 54

Richmond 216, 229, 259, 268, 270

Roddy 93, 162

Rossi 16

Russell 275

Schlüchter 4

Seltzer 276

Shackleton 2, 5

Sharp 65, 122, 130, 204, 205, 208-211, 216, 217, 251

Shoemaker 161, 168

Simpson 22

Smith 4, 69, 206, 275, 277, 284-286, 288

Snedecor 100

Street-Perrot 275

Sutton 84, 161

Swanson 176, 177, 180, 189, 190, 194, 196, 197

Szabo 143, 155

Turrin 142-145, 148, 149, 155, 156

Vaniman 143

Wahrhaftig 203

Wolfe 63, 69, 84

Yamashita 15, 22

Yokoyama 14, 22, 39, 53, 59, 60

Zreda 3, 14-16, 19-21, 39, 80, 82, 87, 88, 91, 97, 98, 108, 125, 146, 147, 150, 151, 162, 163, 178, 181, 182, 211, 245, 260

Geographic index

Alaska 216

Arctic 1, 25, 28, 82, 85

Arizona 1, 35, 44, 64, 80, 84, 93, 147, 161, 163, 166, 167, 293

Banks Island 1, 80, 85

Barrett Lake 249

Barringer 161, 163, 165-167

Basin Mountain 231

Beatty 277, 280-283, 286

Bishop 96, 99, 101, 104-106, 121-123, 125, 126, 131, 205, 207, 208, 218, 231-234, 236, 240-242, 246-248, 269, 270, 284, 285, 296

Bishop Creek 96, 99, 101, 104-106, 121-123, 125, 126, 131, 207, 208, 231, 232, 234, 240, 246-248, 269, 270, 284, 285, 296

Bloody Canyon 65, 66, 99, 204, 206-212, 215, 219, 246, 247, 248, 250, 251, 283, 284

Bull Lake 259-265, 267-270, 296

California 1, 21, 35, 40, 44, 64, 66, 96, 99, 101, 104, 105, 106, 121, 122, 125, 131, 144, 206, 208, 218, 276, 278, 281

Canadian Arctic 1

Chiatovich Creek 40, 41, 78, 176-178, 180, 182-185, 191, 192, 194, 195, 252, 269

Cima 144

Colorado 216

Cottonwood Creek 178, 193, 194

Crater Flat 143

Craters of the Moon 1, 80

Death Valley 276-278, 280, 381, 284, 287-289

Dinwoody Lake 260, 268

Dubois 260, 268, 270

Great Basin 4, 26, 81, 147, 197, 259, 270, 275, 292

Great Britain 1

Hawaii 1, 40, 44, 57-59, 63, 78, 79, 81, 82

Idaho 1, 80, 82

Inuvik 1, 80, 85

Lathrop Wells 141-146, 151, 153, 156, 200, 293

Little McGee Creek 201, 207, 208, 218-221, 226, 229-231, 233, 246-252,

284, 295, 296

Mauna Kea 44, 57-59, 63, 67, 78, 79, 84

Meteor Crater 1, 35, 44, 64, 69, 83, 84, 147, 161-163, 165-167, 200, 293

Middle Creek 41, 43, 176, 177, 184, 187, 188, 192, 194-197, 246

Mormon Point 277, 280

Nevada 1, 4, 22, 35, 41, 43, 44, 64, 67, 69, 96, 99, 101, 104-106, 121, 122, 125, 131, 141-143, 151, 175-177, 190, 197, 202-205, 207, 208, 210, 225, 245-247, 249, 251, 252, 259, 270, 275, 276, 282-284, 288, 293, 294

Nevada Test Site 143

Owens River 4

Panamint 276-278, 280, 281, 283, 284, 287-289, 294

Panamint Valley 276, 280, 283, 284, 289, 294

Pine Creek 41, 65, 207, 211, 247, 252

Pleasant Canyon 277, 284, 287, 289

Puu Kee 79

Rocky Mountains 204, 247, 259

Sierra Nevada 1, 22, 35, 41, 43, 44, 64, 67, 69, 96, 99, 101, 104-106, 121, 122, 125, 131, 175-177, 190, 197, 202-205, 207, 208, 210, 211, 225, 245-247, 249, 251, 252, 259, 270, 275, 276, 283, 284, 288, 294

Tabernacle Hill 43, 64, 69, 80

Utah 35, 40, 43, 80, 84

Wales 1, 80, 85, 91

Washakie Point 259

White Mountains 1, 21, 35, 40-43, 67, 78, 175-177, 179, 192-194, 197, 246, 247, 249, 250, 252, 259, 276, 294

Wind River 2, 261, 262, 269, 270, 292, 294

Wingate Pass 280, 284, 287

Wyoming 2, 216, 261, 262

Yucca Mountains 142, 143

Subject index

^{10}Be 12, 25, 36, 54, 64, 82-84, 98, 166, 169, 177, 188, 189, 190, 191, 193-195, 205

^{14}C 12, 35, 36, 41-43, 49, 52, 53, 59-61, 63-65, 67-69, 78, 82-85, 99, 160, 167, 168, 177, 178, 183, 188, 194, 195, 206, 207, 211, 240, 249, 282, 285, 288

^{18}O 1-5, 99, 245-248, 270, 275, 294

^{26}Al 12, 25, 36, 64, 82-84, 98, 169, 177, 188-191, 193, 194, 195, 205

^{35}Cl 6, 12, 15, 18, 21, 36-40, 43, 44, 51, 52, 81, 91, 112, 114, 116, 146, 150, 152, 161, 164, 178, 211, 294

^{39}K 6, 12, 15, 22, 35-40, 43, 53, 54, 68, 80, 81, 85, 87, 88, 90, 91, 112, 114, 123, 146, 162, 164, 178, 211, 293

^{3}He 12, 36, 54, 89

^{40}Ar/^{39}Ar 141, 142, 144, 155, 156, 206

^{40}Ca 6, 12, 15, 16, 22, 35-40, 54-56, 68, 80, 81, 87, 88, 90, 91, 112, 114, 123, 146, 162, 164, 178, 211, 293

accelerator mass spectrometry 12, 18, 20, 36, 47, 99, 125, 148, 150, 163, 181, 182

altitude 49, 56, 59, 60, 62, 63, 146, 163, 166, 195

AMS 36, 45, 47, 48, 57-59, 62-64, 99, 101, 102, 105, 121, 131, 165, 167

ANOVA 100, 101, 137, 138

apparent age 11, 24, 25, 96, 98, 99, 112-116, 118, 119, 125-128, 132, 153, 155, 162, 168, 188, 189, 217, 241, 242, 283, 286, 294

ash 4, 25, 43, 67, 207

assumption 23, 98, 104, 142, 169, 219, 225, 244

attenuation 14-17, 55, 60, 67, 68, 110, 132, 293

background 19, 38, 39, 103, 146, 164, 279, 281, 283

Barringer 161, 163, 165-167

basalt 15, 35, 43, 45, 141, 143, 147, 150, 205, 206, 218

beach bar 276, 277, 280-283, 286, 288

Beatty beach bar 276, 277, 280-283, 286, 288

bi-modal 96, 126

Birch 239, 243, 246

Bishop Creek 96, 99, 101, 104-106, 121-123, 125, 126, 131, 201, 207, 208, 231, 232, 234, 240, 246-248, 269, 270, 284, 285, 296

Blackwelder shoreline 280, 283

bomb 141, 143, 149, 152, 155

boundary effect 15

Buffalo 258

Bull Lake 258-265, 267-270, 296

Buttermilk 235, 241, 246

calibration 1, 6, 42-44, 48, 49, 56, 57, 60, 61, 65, 67, 80, 81, 83, 84, 86, 88, 89, 292

carbonate 2, 15, 27, 35, 44, 45, 64, 125, 143, 149, 154, 289

cation ratio 59, 63, 78, 96, 99, 122, 127, 132, 283

Chiatovich Cirque 41, 43, 176, 183, 196

Chiatovich Creek 40, 41, 78, 174, 176-178, 180, 182-185, 191, 192, 194, 195, 252, 269

cirque 41, 43, 176, 183-185, 196, 205, 219, 226

correlation 4-6, 101, 118, 166, 168, 196, 202, 217, 247, 250-252, 270, 275, 288, 292, 294, 295

Cottonwood Creek 178, 193, 194

Coyote 233, 237, 242, 246

decay 11, 17, 19, 25, 37, 38, 64, 111, 142, 146, 164, 279, 280

deglaciation 171, 201, 206, 208, 226-228, 233, 248, 259, 266, 296

erosion 6, 11, 13, 23-25, 38, 64, 96-99, 107-121, 125-129, 132, 147, 153-155, 162, 167, 189, 190, 191, 193, 194, 197, 217, 218, 229, 242, 245, 247, 268, 282, 294

erosion depth 96, 98, 113, 115-121, 125-129, 132, 189, 245, 294

erosion rate 64, 96-98, 108, 111, 113, 121, 125, 127, 132, 153, 162, 167

exposure time 13, 17-20, 35, 36, 110, 164, 181, 282, 283

fault 12, 43, 202, 276

fault scarps 12

fault zone 43, 276

fission 39

fluid inclusions 45

fluvial 193, 195, 277, 278, 289

fluvial transport 278

Gale shoreline 281, 284, 285

geomagnetic latitude 13-15, 18, 35, 38, 44, 49, 52, 57, 59, 60, 69, 111, 178

geometry 28, 99, 150-152, 208

glacial stratigraphy 4, 251

glacially polished 78, 218, 219, 233

global ice 1, 2, 5, 248-250

gradual exposure 11, 23, 96, 107-109, 121, 128, 129, 132, 247, 294

gradual exposure model 96, 108, 121, 128, 129

granite 15, 203

grinding 45

half-life 10, 13, 20, 36, 98, 161

hawaiite 44, 57, 63, 78

heavy liquid 43

Hilgard 41, 176, 205, 207, 221, 225, 226, 246, 249, 250

Holocene 41, 202, 205, 207, 225, 226, 249, 250

Hypsithermal 249

impact crater 12, 98, 293

Indian 174, 176, 186, 187, 190, 192, 194-197, 246

inherited 219, 225, 274, 277, 279, 282, 283, 286, 288, 289

interglacial 2-4, 201, 247, 248, 250, 296

isostatic 27, 28

K/Ar 59, 68, 83, 84, 141-144, 146, 156

Kaibab 162, 167

lake level 275-277, 282, 284

lava flow 40, 59, 78-80, 82-84, 141, 143-145, 148, 152, 153, 155

leaching 45, 154

least squares 51, 60, 80, 85, 88

Levenberg-Marquardt 86

Little Egypt 233, 240, 241, 246

Little Ice Ages 205

Makanaka 78

marine stage 201, 247, 269, 270, 284, 296

meteoric 11, 23, 45, 122, 125, 149, 151, 154, 163

Middle Creek 41, 43, 174, 176, 177, 184, 187, 188, 192, 194-197, 246

mineral separation 43

minimization 80, 91, 105

Mono Basin 65, 204-208, 210, 217, 218, 246, 251

monzonite 21, 78

Neoglacial 205, 219, 221, 225, 246, 249, 250

nested analysis 95, 100-102, 104-106

obliteration 258, 295

obliterative overlap 202, 247, 250, 251

offset 43, 276, 287

Older Bishop Creek 122, 123, 125

outwash 244, 258, 260, 268-270

paleoclimatology 4

paleolake 1, 3-5, 274-276, 284, 288, 289

paleolake shorelines 1, 3, 276, 288

Perry Aiken 174, 176, 178, 187-192, 195-197, 246, 252

Pinedale 258-260, 262, 264-267, 269, 270

pluvial 6, 274-276, 282, 285, 288, 291, 294

polish 24

precipitation 27, 67, 125, 150, 175, 202, 203, 248, 259, 276

previous exposure 103, 227, 274, 289

prior exposure 241, 242, 269, 277

production equation 23, 35, 43, 50, 54, 56, 59, 86, 98, 163, 209, 276

production rate 10, 18-23, 35-44, 49-60, 64-69, 81-92, 96, 108-116, 120, 123, 146-152, 160, 162-164, 169, 178, 181, 211, 279, 292, 293

prominent shorelines 274, 276, 277

radiocarbon 41, 64, 160, 165, 167, 168, 184, 196, 275, 286

radiogenic 19, 146, 151, 209, 277, 279

random variable 106, 120

Recess Peak 205, 207, 249

run 50, 100-102, 105-108, 137, 138

Sacagawea Ridge 260, 268, 269

Sand Canyon 240, 241, 246

scaling 14, 18, 35, 38, 53, 56, 57, 60, 61, 63, 64, 66, 69, 110, 111, 146, 151, 164

scoria 143-145

Sherwin 176, 203-205, 223, 224, 230, 231, 246, 251, 252

shielding 11, 13, 65, 78, 148, 209

shoreline 1, 3, 214, 274, 276, 277, 280-289, 294

Shreve 233, 234, 246

snow 25, 67, 203, 209

soil 6, 23, 24, 96, 98, 99, 107-110, 112, 114, 121, 122, 125-129, 132, 144, 147, 149, 161, 177, 196, 242, 244

spallation 15, 16, 18, 19, 22, 34, 35, 37-39, 43, 44, 49, 50, 52-56, 68, 87, 90, 91, 110-112, 114, 120, 123, 146, 152, 161, 293

spalling 25, 99, 122, 130, 131, 217

spatial distribution 13, 20, 181, 203

stage 5, 36, 196, 201, 204, 206, 246-250,

252, 258, 269, 270, 282, 284, 285, 295, 296

steady state 11, 20

synchroneity 245, 249, 259, 276

Tahoe 176, 197, 203-206, 210, 213, 214, 216-218, 223, 229, 230, 246, 250, 251, 252, 275, 283

Tenaya 204, 205, 208, 210, 212, 215-217, 246, 251

termination 41, 275

terrace 258, 260, 264, 268-270, 294

thermoluminescence 64, 77, 82-84, 160, 161

till 120, 127, 193, 194, 197, 205, 206, 208, 218, 259

Tioga 41, 64-66, 176, 188, 190, 197, 203-207, 210-212, 215, 216, 221-223, 227-230, 246, 251, 252, 275

tufa 43, 274, 276, 277, 284-286, 289

U-Th 42, 143, 155

uplift 27, 43, 175, 176, 274, 276, 287-289

uplift rate 43, 274, 276, 287, 289

variance 95, 96, 99-108, 137, 138

varnish 12, 24, 41, 42, 52, 53, 59, 60, 63-65, 67, 69, 78, 82, 93, 99, 122, 127, 160, 161, 164, 165, 167, 168, 177, 178, 183, 184, 188, 194-196, 207, 211, 240, 282

vegetation 26, 165, 203, 205

vertical displacement 274, 288

volcanic 25, 43, 67, 80, 98, 141, 143-145, 148, 149, 152, 154, 155, 202, 206, 293

Waihu 78

weathering 11-13, 26, 27, 122, 149, 162, 176, 203, 217

Younger Dryas 228, 250